SOME ENGINEERING ASPECTS OF THE HYDROGEN-OXYGEN FUEL CELL

F. T. Bacon

Consultant to Energy Conversion Ltd.

Introduction

There is no doubt that the hydrogen-oxygen cell possesses a number of important characteristics which have made it much easier to develop into practical units capable of generating a useful amount of power, compared with hydrocarbon-air cells. It is perhaps worthwhile briefly to recapitulate these characteristics, and this will make plain the reasons for the choice of the particular system which was developed at Cambridge, England.

First of all, it is well known that hydrogen reacts electrochemically much more easily than any hydrocarbon fuel; this of course makes electrode design much easier.

Secondly, the use of pure hydrogen and oxygen makes it possible to use an alkaline electrolyte, which has obvious advantages in the lower cost of materials which can be employed for the electrodes, current collectors and other cell parts.

Thirdly, the use of pure gases means that an unvented system is possible, and this eliminates the additional problems which have to be faced when an inert diluent, such as CO_2 in a reformed hydrocarbon fuel, have to be vented from the system at the correct rate under all load conditions; this would seem to present quite an intricate control problem, if undue waste of fuel is to be avoided. Moreover, groups of cells would presumably have to be fed in series with the fuel gases, each group having its own control valve; it would clearly be too complicated to have a monitoring device on each cell to regulate the gas flow individually. Some of these arguments would also apply if air is used instead of pure oxygen; and in addition, control of the rate of water removal from the vented system may be difficult under conditions of varying air temperature and humidity. This is in contrast to the hydrogen-oxygen system, in which the only reaction product is steam which can easily be separated from the hydrogen in a simple air-cooled condenser, provided that the operating temperature of the cells is somewhat above ambient; parallel flow of hydrogen through all the cells in a battery can be used without difficulty, and small inequalities of flow through individual cells are of little consequence. Besides this, the higher partial pressures of the reacting gases, using pure hydrogen and oxygen, lead to a higher cell performance and a higher limiting current.

It must be admitted that even with very pure gases, occasional venting of the system to atmosphere is usually necessary, owing to the gradual build-up of inert diluents; but this, in our experience at Cambridge, need only be done very occasionally, especially if electrolytic gases are used, and can easily be done by hand.

Fourthly, there is the possibility of operating the battery at considerably elevated pressures. This has the advantage of reducing activation polarization of the electrodes and so yielding possible savings in weight, bulk and electrode cost. The use of elevated pressures also makes it possible to operate with an increased partial pressure of water vapour and hence a higher electrolyte conductivity and a more compact condenser. It is relatively simple to supply pure hydrogen and oxygen at elevated pressure, but, with a hydrocarbon-air cell, there would be complications and a heavy parasitic load due to the compressors.

Fifthly, there is the important fact that hydrogen cells can be made self-starting from cold; this was not a feature of the cells developed at Cambridge, where the decision had been taken to operate at the highest practicable temperature so as to minimize the problems associated with electrode activity. However, other workers have demonstrated hydrogen-oxygen cells with lower temperatures of operation, which will start from cold though relatively cheap catalysts are used; alternatively, very small amounts of precious metal catalysts may be employed with good results in this respect; it is assumed that one of the many new types of electrode, which depend on a degree of semi-wetness in the active layers, would be used.

It should be added that efforts were made, quite early in the work to think in terms of a complete working system rather than in terms of single cells, or even a battery of cells; and before the work was closed down at Cambridge, a complete working system was evolved, including gas admission, and control of temperature, electrolyte concentration and pressure difference across electrodes, under both steady and rapidly varying loads, with a unit of 40 cells which would develop up to 6 kw of power. (1)

Personnel

As it was only possible to employ very small teams, for financial reasons, it was essential to break as little fresh ground as possible, and the practical experience of both battery and electrolyser manufacturers was freely drawn upon; up till 1941, the author worked alone, the work being supported by Merz and McLellan, the well-known consulting engineers. From 1946-51, additional help was given by one part-time consultant, the work being done in the Departments of Colloid Science, and Metallurgy, Cambridge University. After this a small team was gradually built up in the Department of Chemical Engineering, Cambridge, the team consisting of two chemists, one metallurgist, one engineer (author) and three assistants, besides two part-time consultants, one being a physicist and the other an electrochemist. This team was unfortunately completely disbanded in 1956 owing to lack of support. From 1946-56 the work was financed by the Electrical Research Association, with additional help from the Ministry of Fuel and Power, and the Admiralty. In 1957, another team was built up with the help of the National Research Development Corporation, at Marshall of Cambridge Ltd., the total numbers of the team reaching a maximum of fourteen, including one chemist, one metallurgist and three engineers, besides five part-time consultants, one being a chemist, one a metallurgist, one a control engineer and two chemical engineers. Once again the team was completely

disbanded in 1961 owing to lack of industrial support in England. It should be added that the help given by the consultants was invaluable; all were men of wide theoretical knowledge and much practical experience, and without their help some serious mistakes would undoubtedly have been made.

Further Developments in Hydrogen-Oxygen Cells

The author has not carried out any experimental work since 1961, but it has been most interesting to watch the work of others during this time, particularly the wonderful developments which have taken place in the United States.

The stage has now been reached where completely automatic and reliable batteries, using hydrogen and oxygen, have been produced, these batteries being completely equipped with controls which will deal with all load conditions including rapidly varying loads; in addition to this, many are self-starting from cold. The first cost is still high, but this is systematically being reduced. Is it possible that some commercial application could now be found for this type of cell, apart from space and military uses?

Storage of Gases

The principal technical difficulty preventing the use of hydrogen-oxygen batteries for say traction purposes is, in the author's view, associated with the storage of the gases, in particular the storage of hydrogen; it seems inconceivable that liquid hydrogen could ever become a commercial fuel. It is, therefore, very important to watch for any new developments in science and engineering which could have a bearing on this difficult problem of hydrogen storage. As recently as 1959, the best ratio which could be quoted for weight of hydrogen carried to weight of container was 1 to 100; this was for nickel-chrome-molybdenum forged steel cylinders, with a working pressure of 3,000 p.s.i. (2). Since that time, considerable development has taken place in the design of gas vessels and a ratio of 1 to 43 can be quoted for weight of hydrogen to weight of steel with a gas pressure of 3,600 p.s.i.; a low carbon chrome-molybdenum steel is used at present, and welded construction; these figures refer to spheres, and assume that all the gas can be used, which is not strictly accurate but which does not introduce a serious error. Taking an average voltage of 0.8V per cell, and assuming the above weight ratio of 1 to 43 for hydrogen, and assuming also that oxygen is carried as well, the weight of gas vessels + hydrogen + oxygen comes out at about 8.1 lb/kwh. generated; with hydrogen alone, the weight would be 4.7 lb/kwh generated.

These gas vessels are not only used in missiles and military aircraft, but also in civil aircraft where very high standards of safety are of course required. Partly as a result of the American space programme, even further improvements in design appear to be under way; but it seems impossible to prophesy when, or even whether, resin fibre glass containers will become a practical proposition for the storage of hydrogen under ordinary commercial conditions. The whole question of ultra high strength materials is being intensively studied in many parts of the world (3), and it seems possible that, in the future, further reductions in the weight of gas vessels will be achieved.

Other factors which must be taken into account are volume, cost, safety and convenience, but it is not possible to go into these closely in this short paper. In the past, it has always been the weight which has made gas storage relatively unattractive.

Possible Applications for Hydrogen-Oxygen Cells

It has always seemed to the author that road and rail traction are the most promising applications for fuel cells; this applies particularly in the case of short range transport in cities, using public service vehicles. In the United Kingdom quite large numbers of battery driven delivery vehicles are used — the numbers have now risen to over 40,000 — and these are able to compete on level terms with engine driven vans, in spite of the weight and high first cost of the lead/acid batteries; this is basically because of the lower cost per mile of electricity compared with taxed gasoline, and also because of the lower maintenance costs of battery driven vehicles, under the rather special stop-start conditions under which delivery vans have to operate; and this is in spite of a much higher capital cost, part of which is due to the cost of the battery itself, and part to the fact that mass production methods cannot be used for the small numbers of vehicles produced. It is hoped that the fuel cell will eventually extend the field of battery traction into areas where the weight of lead batteries precludes the possibility of electric traction, owing to the fact that a rather higher speed and longer range are required.

The effective capacity of a typical lead-acid traction battery, at 80 amp discharge, has been given as 12.8 kwh.; this was for a 20 cwt pay load delivery vehicle with a speed of 15-18 m.p.h. and a range of 25-30 miles (4). This capacity would require a weight of hydrogen + oxygen + gas vessels of 12.8 x 8.1 = 104 lb. Assuming that the weight of modern low temperature low pressure hydrogen-oxygen batteries on normal load is about 40 lb./kw., and also assuming that a power of 5.3 kw. is required on normal load (4), the weight of the battery alone would be 212 lb.; complete with gas vessels, the total weight would be 316 lb. Taking an up-to-date figure of 10.5 wh/lb for a lead traction battery, on a 2-3 hour discharge basis, a conventional battery would weigh 1,220 lb. If these figures can indeed be substantiated, it would appear that hydrogen-oxygen batteries cannot be ruled out for short range road traction, on a weight basis; in fact, they appear to be more or less substantiated by William T. Reid (5) in an estimate dealing with a passenger road vehicle with a range of 150 miles at 40 m.p.h. It is admittedly extremely difficult to compete on level terms with internal combustion engines, especially if a long range is required between re-fuellings; but a silent fume-free propulsion system would have many attractions for public service vehicles in cities, where they could easily return each night to a central refuelling station, thus avoiding the high cost normally associated with the distribution of hydrogen in cylinders. Reid (5) concludes that running costs, using electrolysers for gas production, would compare favourably with gasoline-powered engines, even in the United States, and the comparison should be even better in the United Kingdom, though the analysis admittedly ignores the tax problem. So far, battery driven vehicles have been exempt from any form of fuel tax in the U.K. As regards the engineering problems

associated with the storage and transfer of compressed gases, much experience was obtained in England, before and during the Second World War, in the use of compressed coal gas as a fuel for propelling buses, and no special difficulties were encountered (2).

Conclusion

It has for many years been realized that there are two alternative applications for fuel cells; one is the task of producing batteries which will consume a hydrocarbon fuel and air; the other concerns the possibility of storing electrical energy; the author has always been drawn towards the latter application. It is true that the overall efficiency of the double process is not likely at present to exceed 50 per cent (6) and might indeed initially be somewhat below this figure (7); but it is hoped that, before long, some of the knowledge acquired by fuel cell workers will be applied to the process of electrolysis; this would entail extensive tests for endurance, in view of the present trouble-free life of at least ten years, which is now expected with existing designs. Further, it is likely that, in the foreseeable future, very cheap off-peak power will become available in the United Kingdom; in an article on "Large Scale Storage of Energy" A. B. Hart (8) states that with nuclear stations off-peak power may be available for storage at a generating cost of 0.25 penny (or 2.9 mils) per kwh, though this does not mean that it could be sold to a consumer at this very low price.

If practical power plants for short range road transport can be achieved, it would not be a very big step to design a larger plant suitable for propelling railcars, where the problems of weight and space are much less severe than with road transport; many battery driven railcars are now in use in Germany, where conditions are favourable for this application.

Lastly, it is hoped that the suggestions contained in this paper, which may be regarded as very reactionary, will not be taken as detracting in any way from the magnificent work which is being done in many parts of the world on hydrocarbon-air cells; but the latter project still seems some way from complete fulfilment, and it would, in the author's opinion, be of immense benefit to the whole fuel cell scene if some substantial commercial application could be found quite soon, even in a limited sphere such as the one suggested.

Acknowledgements

The author wishes to thank the Board of Energy Conversion Ltd. for permission to publish this paper. He would also like to thank his colleagues, particularly Mr. T. M. Fry, for much help and advice during the preparation of the paper.

References

1. Bacon, F. T. (et al.) "Fuel Cells," a C.E.P. technical manual Amer. Inst. Chem. Eng., 1963, p. 66 ff.

2. Clarke, J. S. Proc. Inst. Automobile Eng., XXXIV, 1939-40, p. 43 ff.

3. Cottrell, A. H. et al. Proc. Roy. Soc., Series A, No. 1388, Oct. 1964. Vol. 282. "A Discussion on New Materials."

4. Sheers, W. D. and Heyman, H. W. Proc. Inst. Elec. Eng., 99, Part II, No. 71, Oct. 1952, p. 457 ff.

5. Reid, William T. Battelle Technical Review, 1965, 14 (4), pp. 9-15.

6. Bacon, F. T. U.N. Conf. on New Sources of Energy, Rome, Aug. 1961. Preprint 35/Gen/9.

7. Euler, J. World Power Conference, Lausanne, Sept. 1964, Paper 110, 11E. "The Storage of Electrical energy by means of galvanic fuel cells." (in German)

8. Hart, A. B. Science Journal, May 1965, pp. 70-75. "Large scale storage of energy".

HYDROCARBON-AIR FUEL CELL SYSTEMS

Dr. Galen R. Frysinger

Energy Conversion Laboratory
U. S. Army Engineer Research and Development Laboratories
Fort Belvoir, Virginia 22060

INTRODUCTION

In reviewing the state-of-the-art I wish to include all hydrocarbon-air system configurations. This is defined broadly to include all fuel cell systems which utilize a hydrocarbon fuel and an air oxidant. The four variations which have been under investigation at this laboratory are shown schematically in Figure 1.

EXTERNAL REFORMER INDIRECT SYSTEM

The external reformer indirect systems are based on the use of separate hydrocarbon reformers to liberate the bound hydrogen energy of a liquid hydrocarbon fuel. Hydrogen produced from hydrocarbons by the conventional steam reforming process has been of commercial importance for some time. Only recently, however, has emphasis been placed on simplification and miniaturization of these process plants to become compact hydrogen generators for fuel cell systems. The first hydrogen generators for fuel cell systems which were constructed over the last few years using natural gas, methanol, or JP-4 as the fuel were quite bulky and heavy because they utilized largely state-of-the-art, off-the-shelf type process components. These hydrogen generators, themselves, weighed between 100 and 200 lbs/KW equivalent of hydrogen produced. In one instance, with the Engelhard reformer fabricated under contract to USAERDL, a special fuel and water pump and air blowers were developed to greatly reduce the weight and the electrical power consumed by these auxiliaries. Only recently has emphasis been placed on the design of very lightweight systems. Based on hydrogen reformer systems which are still at the design (Contract DA-44-009-AMC-967(T) with Pratt and Whitney Aircraft) or very early development stage, it is estimated that about 40-45 lbs/KW must be assigned to this major component.

A second major component of an indirect system is the hydrogen-air fuel cell stack or module. Based on electrode performances of greater than 200 amps per square foot at 0.8 volts per single cell, this component should have a weight of 15-20 lbs per KW for a 28 volt stack in the 2-10 KW size range.

A third major component for an a.c. fuel cell powerplant is the combination voltage regulator and inverter. Recent experience with hardware procured by USAERDL indicates that inverter weights are within the range of 10-15 lbs/KW of net a.c. output. By adding together the weights of these major components it is evident that only about 20 to 30 lbs/KW are allowable for the auxiliaries if a

power density of 100-110 lbs/KW is to be obtained for a total a.c. output, fuel cell powerplant. A power density of 100 lbs/KW is roughly that obtained with conventional engine generators.

Therefore, for a fuel cell powerplant to be weight competitive, a major emphasis must be placed on process simplification. Major weight reduction is best achieved by elimination of unneeded components. To cite one example, in an Army fuel cell powerplant for operation in the field, adequate moisture must be reclaimed for use in the steam reformer to avoid the need for makeup water. In the present Allis Chalmers 5 KW system (USAERDL Contract DA-44-009-AMC-240(T)), Figure 2, part of this moisture is reclaimed from the air exhaust, but the major portion comes from the evaporation and condensation in an air stream of water removed from a circulating KOH stream. This requires that a water removal plate be included next to each hydrogen electrode in each single cell to allow the excess moisture to come in contact with and dilute the circulating KOH. In this system part of the water is reclaimed also from the reformer combustion exhaust.

In a much simplified system now being studied (Contract DA-44-009-AMC-967(T) with Pratt and Whitney Aircraft) all of the moisture from the cell is removed in the air exhaust which is used as the combustion air for the reformer burner. A single condensor is therefore all that would be required to condense the required water from the burner exhaust. This simplification would eliminate two condensors, blowers, valves and piping as well as simplifying the cell stack construction.

Future wide application of indirect systems will be dependent on research to achieve greatly improved current densities and to protect the reformer catalyst from the sulfur impurities found in presently available liquid hydrocarbon fuels. Research now in progress indicates that current densities several times the 200 ASF at 0.8 V, which is now state-of-the-art, may be achieved in hydrogen-air cells with very low or no platinum metal content of the electrodes. Likewise, research studies indicate that the "guard catalyst", renewable cartridge, technique may be applicable to protect the compact hydrogen generator catalyst from excessive degradation due to sulfur impurities.

INDIRECT ACID ELECTROLYTE SYSTEMS

The description and weight predictions already given are based on a pure hydrogen alkaline electrolyte system which involves a major weight penalty due to the inclusion of a scrubber to remove the small amounts of carbon dioxide present in the incoming air and for a hydrogen diffusion membrane purification system. For an indirect system based on an acid electrolyte hydrogen-air fuel cell module, the carbon dioxide scrubber would not be required and also the possibility exists that an impure hydrogen contaminated with small or moderate amounts of carbon monoxide, may be utilized directly. The attractiveness of the acid electrolyte system, however, depends largely on the power density which can be achieved in the hydrogen-air cell stack and the efficiency with which hydrogen and air can be electrochemically converted in the acid electrolyte system. Because of the

significant system simplifications, research emphasis is being placed on electrode structures and electrocatalysts for the anodic oxidation of hydrogen-carbon monoxide mixtures with air. Under Contract DA-44-009-AMC-479(T) with General Electric a tungsten oxide-platinum black electrocatalyst system has shown high activity for this mixture. Using very thin electrodes and lightweight plastic cell components and a circulating electrolyte coolant, a module of comparable power density to that of an alkaline system may be achieved even with the lower voltages of the acid electrolyte single cell.

INTERNAL REFORMER INDIRECT SYSTEM

The principal disadvantages of an external reformer are the need to operate the reformer at temperatures of about 1400°F to produce significant quantities of hydrogen, and the need to control the hydrogen production rate to match exactly the fuel requirements of the cell at all times. The internal reforming cell developed by Pratt and Whitney (Contract DA-44-009-AMC-756(T) for operation with hydrocarbons and air may overcome some of these problems. In this cell, the hydrocarbon-steam reaction occurs in a catalyst bed which is in direct contact with the fuel cell anode. With a concentrated potassium hydroxide electrolyte the cell can be operated at 500°F, at which the equilibrium for hydrocarbon-steam reactions is such that only a small percentage of hydrogen is produced. However, as the fuel cell anode consumes the hydrogen by diffusion through the silver-palladium anode, the equilibrium is shifted so that it is possible to convert a high proportion of the fuel to hydrogen and to utilize this hydrogen in the anode reaction. This type of cell can be more efficient since the endothermic reform reaction takes its heat requirement directly from the waste heat of the cell. Such a system is largely self-controlling since hydrogen is produced only as fast as it is required by the anode.

The status of this system and its ability to utilize hydrocarbon fuels will be discussed in detail in another paper in this symposium.

The principal research problem is to find the optimum reforming catalyst. The catalyst should have very high activity (fast kinetics for the hydrocarbon to hydrogen reaction) at 500°F and be stable for long term operation. The commercially available reforming catalysts designed for higher temperature (1500°F) operation are not necessarily the best for this lower temperature reforming. Serious catalyst activity decay problems have been encountered. The relative attractiveness of the internal reforming hydrocarbon-air system will depend largely on what improvements are possible in the long term stability of the reformer catalysts.

PARTIAL OXIDATION OF LIQUID FUELS
AND MOLTEN CARBONATE FUEL CELLS

The air partial oxidation of liquid hydrocarbon fuels is insensitive to the fuel type or the amounts of sulfur found in military fuels. Under Contract DA-44-009-AMC-54(T) (Texas Instruments), marine white gasoline, JP-4, kerosene, Number 2 diesel fuel, and CITE engine fuel, ranging in sulfur content from 30 ppm to 3,200 ppm, were successfully converted to electrical power in a partial

oxidation molten carbonate fuel cell system. The unpurified product of partial oxidation is utilized directly in the molten carbonate fuel cell. The sulfur is carried into the anode as hydrogen sulfide but does not adversely affect performance. The molten carbonate electrolyte system, Figure 3, due to its higher temperature of operation tends to be more rugged and heavier than competing systems. The auxiliaries are simplified; no liquid water must be condensed and the stacks can probably be air cooled. The cell stack in this case represents about 50% of the total weight. This means that the current densities which can be achieved are a very important factor in determining the total weight of the system. Today 30 watts/sq ft is routinely achievable and 40-60 watts/sq ft can most likely be achieved by minor engineering improvements. Power densities of greater than 100 watts/sq ft are required, however, if the molten carbonate system is to be competitive in the 3-10 KW power range. Significantly more research emphasis must be placed on understanding the electrode limitations with this mixed fuel and air and the design and testing of more active electrode structures.

DIRECT OXIDATION

The status of direct oxidation hydrocarbon fuel cell research and preliminary engineering is being ably discussed by others in this symposium. I wish to add to this only by stressing two major points.

Tremendous progress has been made over the last several years in anodically oxidizing hydrocarbon fuels at an electrode. Whereas, three years ago the ability to oxidize saturated hydrocarbons at lower temperature (150-200°C) and atmospheric pressure was questioned, today 10-15 watts/sq ft with n-octane can be routinely obtained with electrodes with useful lives of over 1000 hours. Twenty watts/sq ft is a legitimate goal for this year. The current density at a cell voltage of 0.5 to 0.6 volts, however, must be greatly increased for a direct oxidation system to become attractive. A several fold increase in current density must be achieved while at the same time greatly reducing the platinum content of the electrodes. The progress has been very encouraging but a tremendous amount of research must still be devoted to understanding the complex nature of hydrocarbon anodic oxidation.

Most of the work to date has been done on pure single component hydrocarbon fuels. Work now in progress is determining the tolerance of electrodes to olefinic, napthalinic and aromatic components. The future "fuel cell fuel" may not be what we burn in our automobiles today, but economics dictate that it will be a multi-component fuel which can be produced from a petroleum refinery. Greater research emphasis must be placed on the direct oxidation of raffinates and other complex fuel mixtures.

CONCLUSIONS

Indirect hydrocarbon fuel cell systems are closest to the hardware stage but require additional research to simplify auxiliary systems, to increase current densities with less costly electrodes, and to protect reformers

from the effect of sulfur impurities present in liquid hydrocarbon fuels. An internal reformer system can achieve major efficiency and control advantages if present research aimed at long life low temperature reformer catalysts is successful. Major current density gains are required for the molten carbonate system to be competitive for portable power plants. Tremendous progress has been made with direct oxidation but much higher current densities must be achieved with multi-component fuels for a practical system.

ACKNOWLEDGEMENT

Portions of the analyses and research results presented here were done under contract to the U. S. Army Engineer Research and Development Laboratories by Allis Chalmers, Engelhard Industries, General Electric, Pratt and Whitney Aircraft, Texas Instruments and Varo, Incorporated.

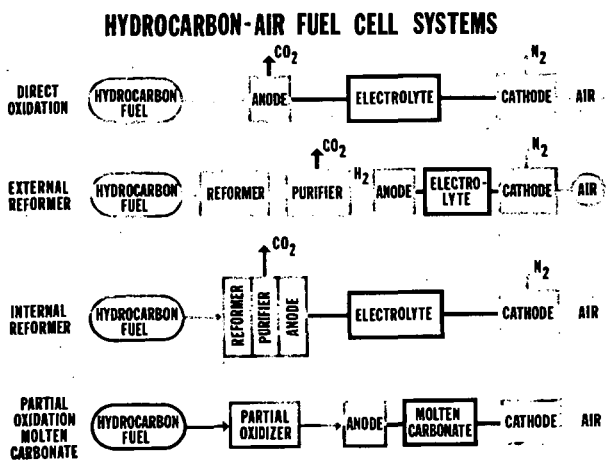

Fig. 1.-ALTERNATIVE HYDROCARBON-AIR FUEL CELL SYSTEMS

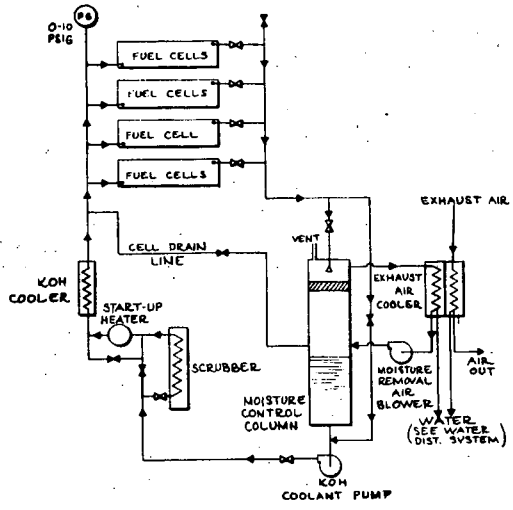

Fig. 2.-MOISTURE SUBSYSTEM

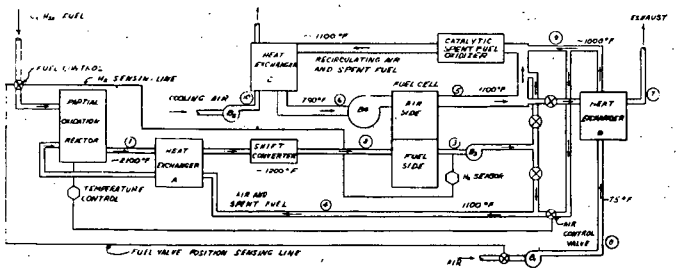

Fig. 3.-PARTIAL OXIDATION-MOLTEN CARBONATE SYSTEM

CARBON-AIR ELECTRODES FOR LOW TEMPERATURE FUEL CELLS

by K. V. Kordesch
Union Carbide Corporation, Development Department
Parma Technical Center, Parma, Ohio

I. INTRODUCTION

The economy of a terrestrial, low temperature fuel cell system depends strongly on the feasibility of using air at atmospheric pressure. High current densities are required to keep battery weight and size down; simple operation, preferably at atmospheric pressure, is desired to avoid costly and energy-consuming accessories. Last, but not least, the use of noble metal catalysts and expensive structural materials must be restricted to a minimum.

At the present time, low temperature, acidic-electrolyte, fuel cell systems have not reached the development stage which would indicate their practical utilization in the near future. For this reason, the discussion will be limited to alkaline electrolytes only. With hydrophobic carbon electrodes, it is a matter of technical choice whether liquid or immobilized electrolytes are used; therefore, no differentiation will be made.

II. DISCUSSION

1. The Performance of Carbon-Air Electrodes.

a) Comparison of Polarization Curves. - The potential of an electrode at a given load is dependent on the activity of the catalytic system used. Carbon-oxygen (air) electrodes function as hydrogen peroxide-producing, gas-diffusion electrodes, and for this reason show a strong dependence on the peroxide-decomposing capability of the electrode surface. (1)

Figure 1 shows the polarization curves of three differently catalyzed carbon electrodes. Characteristic is the high voltage level of the Pt-catalyzed cathodes—Pt is deposited in a quantity of 1 milligram per cm^2 of geometric surface. A very remarkable performance is shown

by the third electrode, containing no specially added metals--only the peroxide-decomposing catalytic activity of the basic $CoOAl_2O_3$ spinel-containing carbon is demonstrated. (2) While the initial performance level is lower, the current-carrying ability is greater at very high current densities.

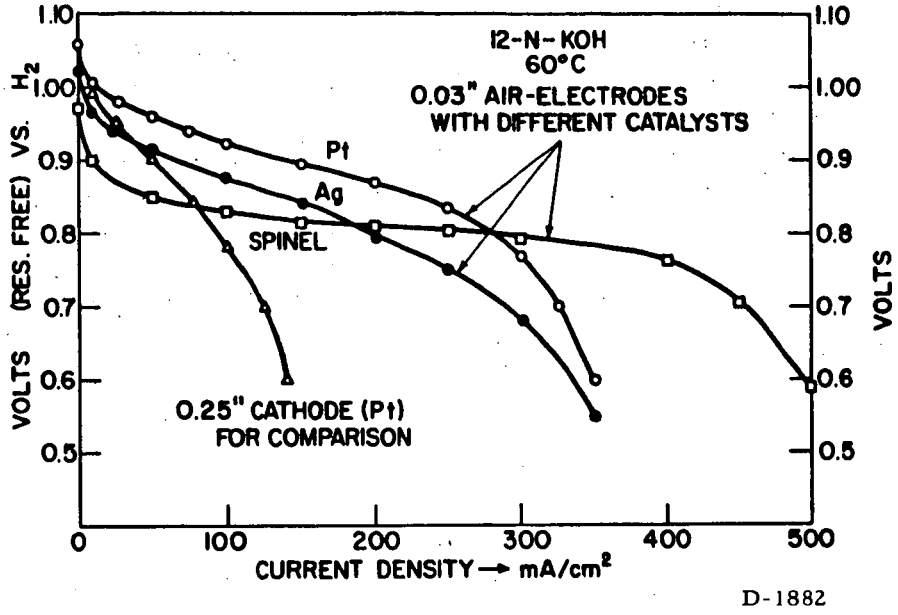

Fig. 1 Electrode Polarization Curves Employing Different Catalysts (Linear Diagram).

The upper-three curves of Fig. 1 were obtained with so-called "fixed-zone", 0.03-inch thick composite electrodes consisting of a repellent porous nickel plaque (0.008-inch thick) coated with layers of catalyzed carbon. (3) The fourth curve in Fig. 1 was obtained with a platinum-catalyzed, 0.25-inch thick carbon electrode (1 mg Pt/cm^2). While pure oxygen performance (not shown) of 0.25-inch and 0.03-inch electrodes is essentially equal, the performance with air is very different. The thicker electrode is clearly diffusion-limited.

The same voltage-current curves of Fig. 1 (linear diagram) are replotted in Fig. 2 using a logarithmic abscissa. The similarity in elec-

trochemical behavior of the four electrodes becomes more apparent in the second figure. The Tafel slopes are identical (40 to 50 mv per decade at low current densities), but the voltage levels are different in accordance with the chosen catalyst. Also different is the extent of the "mass-transport limitation" (as expected, considering the difference in electrode thicknesses). The cross-over of the "spinel-catalyzed" thin electrode is not accidental—this characteristic is consistently observed.

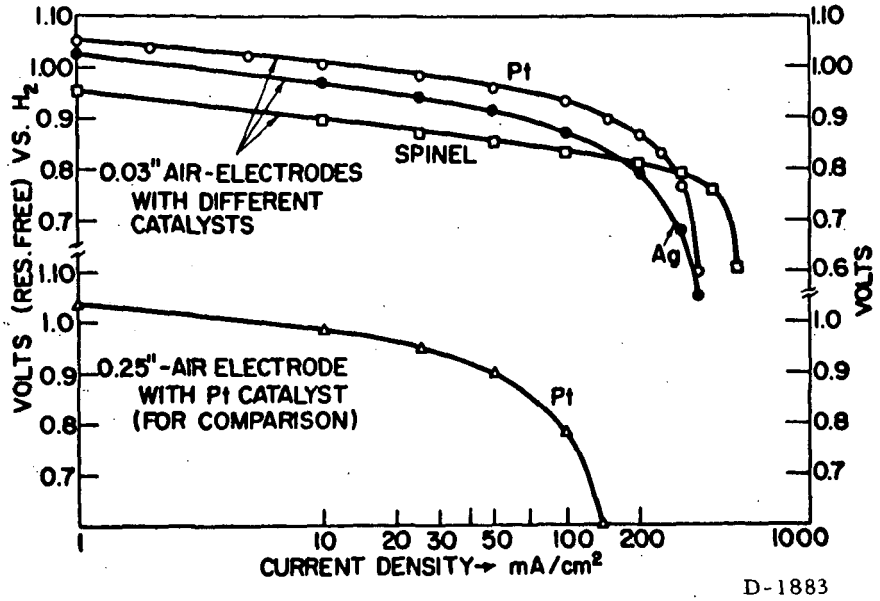

Fig. 2 Electrode Polarization Curves Employing Different Catalysts (Logarithmic Diagram).

b) Operational Life of Air Electrodes. - Life of the electrodes depends, first of all, upon the current density. Current density determines the operational voltage (as Figs. 1 and 2 demonstrate). The "polarization level" (terminal voltage minus the voltage drop in the resistive components of the cell) is a more decisive parameter than the "terminal voltage". This "resistance-free" voltage can be determined by means of current interrupter devices (4), or suitably placed reference electrodes.

The relationship between current density and operational life seems to be an exponential function. Doubling the current density usually decreases life to one-fourth the time, or vice versa; cutting the current density in half prolongs the electrode life fourfold. This should be considered only as a "rule-of-thumb" fitting our present experience.

Figure 3 shows the performance life of 1965 Union Carbide thin electrodes operating on a continuous load corresponding to 100 A/SF (105 ma/cm^2). It should be noted that CO_2-free (scrubbed) air has been used.

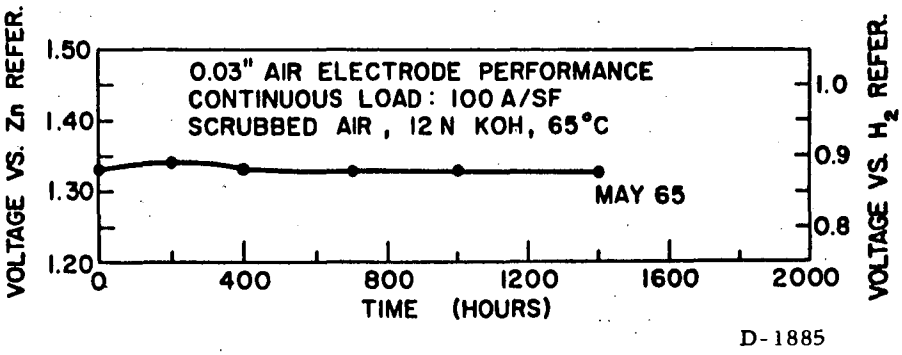

Fig. 3 Operational Life of Union Carbide Fixed-Zone, Air Electrodes(1965).

2. The Effect of Carbon Dioxide from the Air.

The approximate 0.03% CO_2 contained in air is known to be detrimental to alkaline cell performance. Consequently, most tests are performed with CO_2-free air; and less data are available about the nature and extent of carbon dioxide's damaging effects.

However, for economical operation of larger fuel cell batteries, the cost of air scrubbing is important. In addition, size and weight problems are introduced by air-scrubbing accessories. Therefore, an attempt has been made to answer a few principal questions concerning this matter:

a) The effect of carbonate in the electrolyte;

b) The rate of CO_2-pickup through the operating electrode;

c) The effect of CO_2 on electrode life (catalysts, variation in electrolytes, etc.), and

d) Possible explanation of the effects.

a) The Effect of Carbonate in the Electrolyte. - For comparison, two identical cells were operated in 6 molar KOH containing 0.4 mol potassium carbonate, and 6 molar KOH containing 1.0 mol potassium carbonate. The air supplied to the cell was cleaned in a gas wash tower containing KOH; no additional CO_2 was absorbed during operation. No noticeable difference in performance was observed.

b) Rate of CO_2-Contamination through the Operating Electrode. - The speed of CO_2-pickup from the air through the wall of cathodes was first tested with 0.25-inch carbon cathodes continuously exposed to room air in a concentric, triangular, 7-cell battery (5). Table I gives the data which show that the CO_2-takeup from the air (for 6 M KOH) was rapid during the first few days, then slowed down considerably.

TABLE I

RATE OF CO_2-CONTAMINATION OF 6 M KOH IN AIR-EXPOSED CELLS (15 ma/cm^2 LOAD)

Time Elapsed Since Exposure of Cathodes (6 M KOH) to Air	Titrated M CO_3^{--}
72 Hours = 3 Days	0.4 M
720 Hours = 4 Weeks	1.0 M
2160 Hours = 3 Months	2.5 M

Adding KOH pellets to the partially neutralized caustic solution until the OH^- ion concentration corresponded to 6 M KOH restored the original performance.

c) The Effect of CO_2 on Electrode Life. - The 0.25-inch carbon electrodes used in the concentric (triangular) cells, mentioned above, carried no special metal catalyst. Most of the test cells survived 4000 hours at a current density of 15 ma/cm^2; some operated for 7000 hours. Cell life was only about 800 hours under the same conditions of operation and air exposure when 0.25-inch, platinum-catalyzed (1 mg/cm^2) cathodes were employed.

Figure 4 illustrates the average results of these tests. The voltage level of the noble metal-catalyzed cathodes was higher, but life was far shorter.

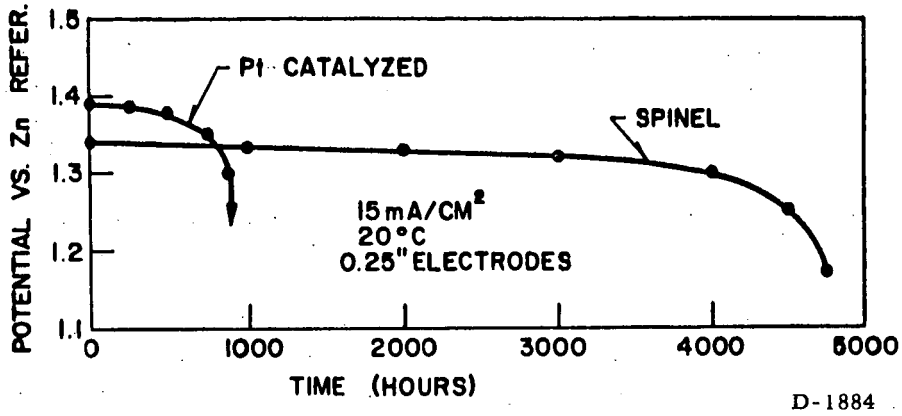

Fig. 4 Performance with CO_2-Containing Air, Comparing Noble Metal-Catalyzed vs. Spinel-Catalyzed Cathodes.

In another series, platinum-catalyzed, thin electrodes (1963) were operated with CO_2-containing air, using 6 N KOH for one set of cells, and 6 N NaOH for the other. Figure 5 shows the results—the cathodes in NaOH outlived the cathodes in KOH by a wide margin, again at the cost of the voltage level, however.

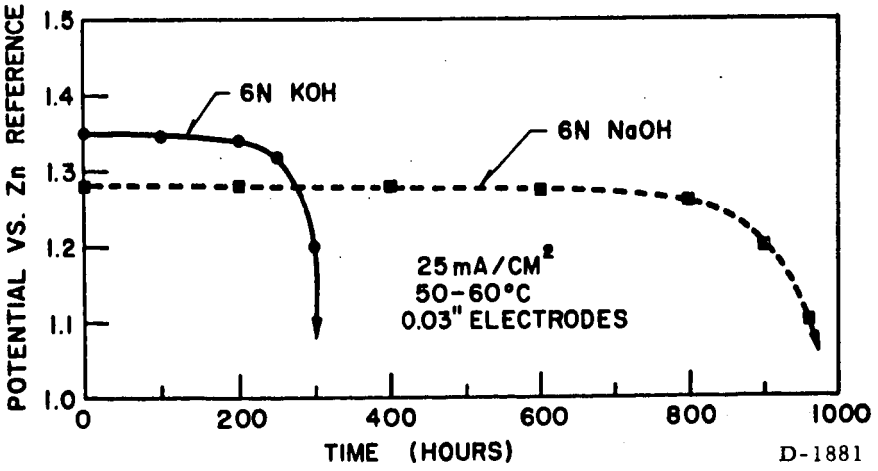

Fig. 5 Performance with CO_2-Containing Air, Comparing Platinum-Catalyzed Cathodes—6 N KOH vs. 6 N NaOH.

A third combination (uncatalyzed electrodes in NaOH electrolyte) did not look promising from the cell-performance standpoint at that time. This combination will be tried in the future using newer, more active electrodes.

d) Possible Explanation of Effects - Physical examination of the CO_2-damaged electrodes always revealed a mechanical blockage. It seems that the degree of repellency of an electrode determines the degree of resistance against CO_2 damage. NaOH is less wetting than KOH, and platinum-catalyzed electrodes are less repellent than electrodes without platinum catalyzation. CO_2-damage is also current-density dependent; a heavily polarized air electrode has a shorter life in the same electrolyte than does one showing a lesser degree of polarization.

Experiments with porous metal electrodes indicate that "wet"-operated electrodes (gas pressure balance) have an extremely low tolerance for CO_2. The pores of such electrodes plug within a few hours, and physical damage (possibly by expanding carbonate) is irreversible. Carbonate-plugged, 0.25-inch carbon electrodes were usually permanently damaged, and could not be revived. However, the newer thin composite electrodes have frequently been washed and reused.

III. CONCLUSIONS

Carbon-containing cathodes seem to be the most desirable electrodes for high-power density, economical, air-fuel cells. The fuel source for such low temperature cells may be hydrogen from hydrocarbon reformer units, or hydrogen from alcohol or ammonia converters.

At present, CO_2 removal is necessary during air operation in order to attain long life at high current densities. However, recognition of the nature of carbon dioxide effects on today's electrodes is the first step towards possible future remedy.

In the author's opinion, of all the available cathodes, the carbon electrode is the least sensitive to carbon dioxide damage.

REFERENCES

(1) K. V. Kordesch in "Fuel Cells," (G. J. Young, ed.), p. 14, Reinhold Publishing Corp., New York, 1960.

(2) K. V. Kordesch in "Fuel Cells," (W. Mitchell, ed.), p. 346, Academic Press, New York, 1963.

(3) M. B. Clark, W. G. Darland, and K. V. Kordesch, "Composite Carbon-Metal Electrodes for Fuel Cells," paper presented at the 1964 Washington Meeting of Electrochem. Soc. To be published in Electrochem. Tech.

(4) K. Kordesch and A. Marko, J. Electrochem. Soc. 107, 480(1960).

(5) L. M. Litz and K. V. Kordesch in "Fuel Cell Systems," (G. J. Young and H. R. Linden, eds.), p. 166, Am. Chem. Soc., Washington, 1965. (Advances in Chemistry Series No. 47.)

PERFORMANCE OF A REFORMED NATURAL GAS-ACID FUEL CELL SYSTEM

Part I. Hydrogen Generator Design

by

John Meek
B. S. Baker
A. C. Allen

Institute of Gas Technology
Chicago, Illinois

INTRODUCTION

Natural gas can be used in low-temperature fuel cell systems in several ways. Although the direct methane cell has proven feasible,[1,2] present and forseeable technology of such systems will be very costly because of the quantity and type of catalyst required for direct anodic oxidation. The indirect cell, which requires the reforming of methane followed by the utilization of hydrogen, seems more attractive at the present time. With alkaline electrolyte systems it is necessary to use high-purity hydrogen as the fuel. This may be obtained by steam reforming in an external reformer and purifying the gas with a palladium-silver diffuser, or by reforming the gas in situ in a fuel cell that employs a palladium-silver-hydrogen diffusion anode. For application in the gas industry, it is essential that both first costs and operating costs remain low. Accordingly, the program at IGT has focused its attention on development of a hydrogen generator-fuel cell system in which the feed from the reformer is rich in hydrogen but unpurified, the enrichment being achieved by conventional chemical processing techniques. It is realized that this implies the use of a fuel cell of the acid electrolyte type which is presently more expensive than the alkaline electrolyte fuel cell. Nevertheless we believe that the cost of the acid electrolyte cell can be greatly reduced especially where the fuel is hydrogen. The other factors affecting the decision to pursue this system have been outlined in an earlier publication in this series.[3] Design of a natural gas-fueled hydrogen generator is described here in which the product is suitable for use in any acid electrolyte fuel cell.

HYDROGEN-GENERATION PROCESS

The hydrogen generation process used in the IGT system has been described in detail.[3] It consists of three stages: First, natural gas is steam-reformed at 800°C to produce a hydrogen-carbon

monoxide-carbon dioxide mixture. The effluent from this first reactor is then cooled and fed to a carbon monoxide shift reactor operating at about 270°C, wherein the carbon monoxide content of the gas is reduced from a typical 15% (dry basis) to about 2000 parts per million. For certain acid fuel cells operating above 100°C this gas might prove to be an acceptable feed, but, for lower temperature cells it is desirable to further reduce the carbon monoxide content of the feed gas. This is achieved in the last stage by passing the effluent from the carbon monoxide shift reactor through a low-temperature (190°C), selective methanation reactor in which the carbon monoxide content of the gas is reduced to approximately 20 parts per million by reaction with hydrogen to produce methane. Typical gas compositions along with the free energy for these reactions are summarized in Tables 1 and 2. It can be seen that the reforming and carbon monoxide shift reactions proceed, for practical consideration, to equilibrium. The reaction based on the methanation of carbon monoxide alone is a long way from equilibrium and improvement might be expected. The large deviation from equilibrium is probably due to reaction of carbon dioxide with hydrogen to produce carbon monoxide.

HYDROGEN GENERATOR DESIGN

For the hydrogen generation process to be attractive it is necessary that an integrated three-stage, gas-fired hydrogen generator that is self-controlling be designed and constructed. Limited data is available on the design of complete hydrogen generation systems with small capacity.[4,5]

In the IGT system an annular reactor design was chosen because it represented a readily packageable easily fabricated unit with low pressure drop.

The first problem encountered in the design was the development of a gas-fired burner that could operate on low-pressure gas (6 in. wc), bring the relatively compact reformer reactor to operating temperature, and maintain the desired heat input to sustain the endothermic steam-reforming reaction. It was found that reactors of the present design, or of almost any design, did not have sufficient heat transfer area to permit heating by a convective process. To obtain a higher effective heat transfer coefficient, both sides of the annular reactor were encased in annular sections filled with the refractory material of high surface area. The sections could be brought to the desired temperature by convection and would in turn heat the reformer by radiation from the refractory. A typical burner design for this system is shown in Fig. 1. The reforming stage of the hydrogen generator, which is capable of reforming 25 cu ft of methane per hour, is shown in Fig. 2.

The second problem encountered in the present system was to find a means for reducing the temperature of the hot flue gases to maintain the second- and third-stage reactors at their proper operating temperatures. The solution was to cool both the flue gas from the natural gas burner and the product gas from the reformer reactor by generating and superheating process steam. The flue gas and the product gases are effectively cooled by this procedure but the achievable temperature control was not accurate

enough for the shift and methanation stages. Obtainment of temperature control in these two reactors within the desired limits, was made possible by jacketing the reactors with constant boiling fluids. Dow-Therm A and Dow-Therm E have been chosen for this purpose. The jacketed shift and methanation units are shown in Figs. 3 and 4. Temperature control of these reactors is achieved by dependence of pressure on temperature of the Dow-Therm liquid-vapor systems. The Dow-Therm vapor pressurizes a Sylphon bellows which transmits a pressure signal to actuate damper valves which control the direction of flow of hot flue gases. Water flow valves which, in turn, control the flow of cooling water to the Dow-Therm vapor condensers also activated by this means.

This mode of control is especially suited to a hydrogen generator that supplies a constant amount of product gas. The Sylphon bellows (Fig. 1) has the further advantage of not requiring any parasitic power from the fuel cell system; it is also relatively inexpensive. The only auxiliary power on the present reformer is that needed for a small air blower which provides combustion air. This blower draws about 40 watts at maximum air demand. The complete system is shown schematically in Fig. 5. The actual unit with a 100 cu ft/hr capacity is shown in Fig. 6.

PERFORMANCE CHARACTERISTICS

Hydrogen generators very similar in design to the one described in the present paper have been successfully operated at IGT, producing the gas given in Table 1. The best overall efficiency achieved with this type reformer in 150 hours of intermittent operation has been 41%. This figure was obtained with a unit that has an output of 50 cu ft of hydrogen per hour. The system presently under test has an output capacity of 100 cu ft of hydrogen per hour; overall efficiency figures of about 50% are anticipated.

Gas of the type produced by this hydrogen generator has been extensively tested in low-temperature acid fuel cells. Use of these gases is the subject of Part II of this paper.

ACKNOWLEDGMENT

The authors wish to thank Southern California Gas Company, Southern Counties Gas Company of California and Con-Gas Service Corp., who are sponsoring this investigation, for permission to publish these results.

REFERENCES

1. Binder, H., Köhling, A., Krupp, H., Richter K. and Sandstede, G., "Anodic Oxidation of Derivatives of Methane, Ethane and Propane in Aqueous Electrolytes" in Fuel Cell Systems, 283-291, Advances in Chemistry Series 47. ACS, Washington D.C., 1965.

2. Grubb, W. T. and Michalske, Carol J., "Hydrocarbon Fuel Cells," in Proceedings: 18th Annual Power Sources Conference 17-19, PSC Publication Committee. Red Bank N.J., 1964.

3. Meek, J. and Baker B.S., "Hydrogen from Natural Gas from Fuel Cells," in Fuel Cell Systems, 221-231, Advances in Chemistry Series 47 ACS Washington, D.C., 1965.

4. Geissler, H. H., "Compact H_2 Generators for Fuel Cells," in Proceedings: 17th Annual Power Sources Conference, 75-77, PSC Publication Committee, Red Bank, N.J., 1963.

5. Geissler, H. H., and Goodman, L.E., "Hydrogen Generators," in Proceedings: 18th Annual Power Sources Conference, 28-31, PSC Publication Committee, Red Bank, N.J., 1964.

Table I

Reactor	Composition, Mole percent							
	H_2	CO_2	CH_4	CO	H_2O	N_2	T°C	$\frac{\Delta F}{RT}$
Reformer In	0	0.107	*	0	87.268	0.046	800	$-\infty$
Reformer Out	34.644	3.773	0.045	6.847	54.654	0.036	800	-7.287
Shifter In	34.644	3.773	0.045	6.847	54.654	0.036	270	-5.18211
Shifter Out	41.346	10.475	0.045	0.146	47.952	0.036	270	-2.30975
Methan. In	41.346	10.475	0.045	0.146	47.952	0.036	190	-26.50958
Methan. Out	41.030	10.505	0.190	0.001	48.236	0.036	190	-20.05782

*See Table II

Table II

Fuel	CH_4	C_2H_6	C_3H_8	C_4H_{10}	C_5H_{12}	C_6H_{14}	C_7H_{16}	N_2	CO_2
Comp, mole %	12.027	0.394	0.097	0.033	0.009	0.010	0.009	0.046	0.107

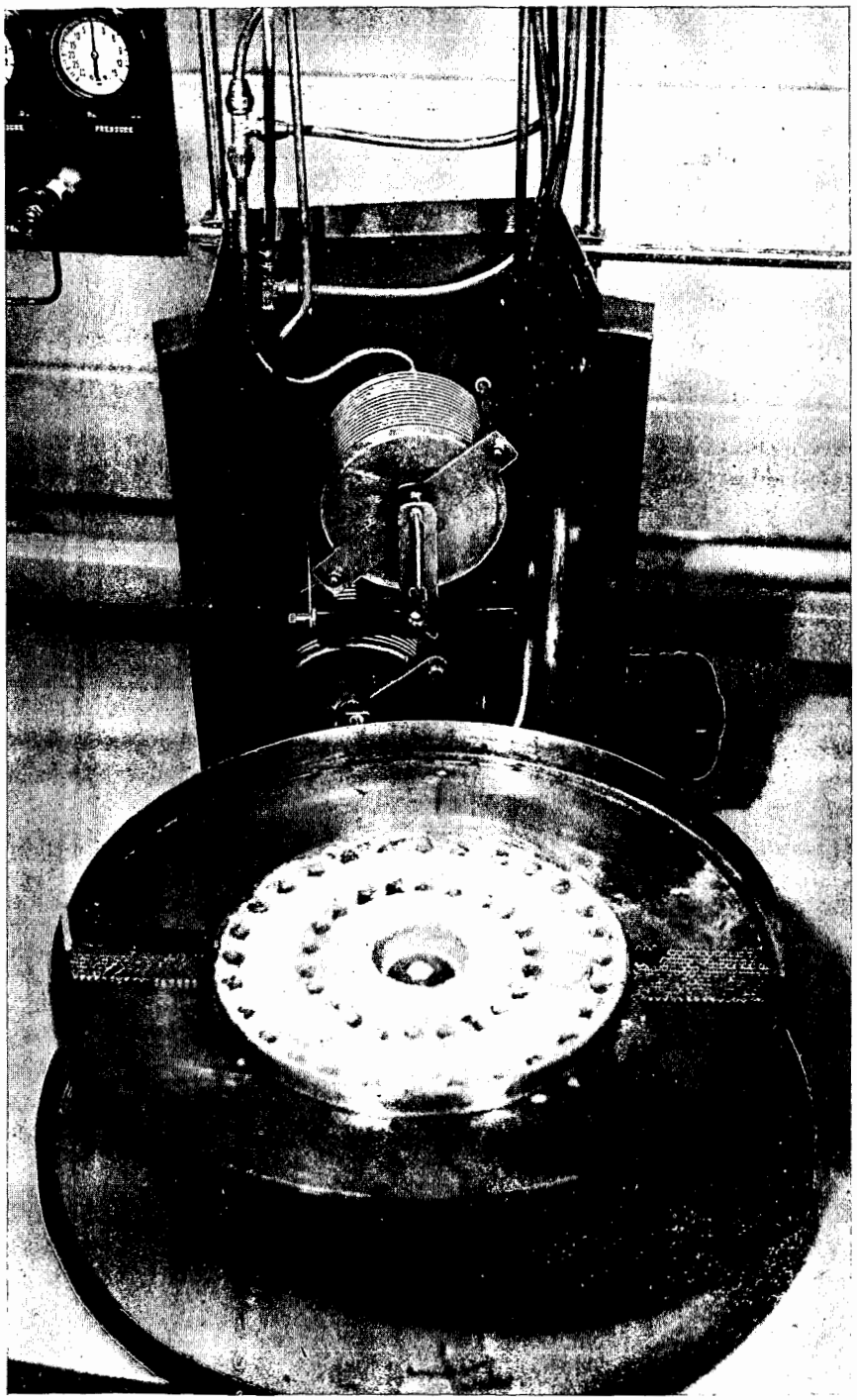

Fig. 1.-NATURAL GAS BURNER USED AS PRIMARY HEAT SOURCE FOR HYDROGEN GENERATOR.

Fig. 2.-REFORMER AND CONTROL SECTION OF THE HYDROGEN GENERATOR

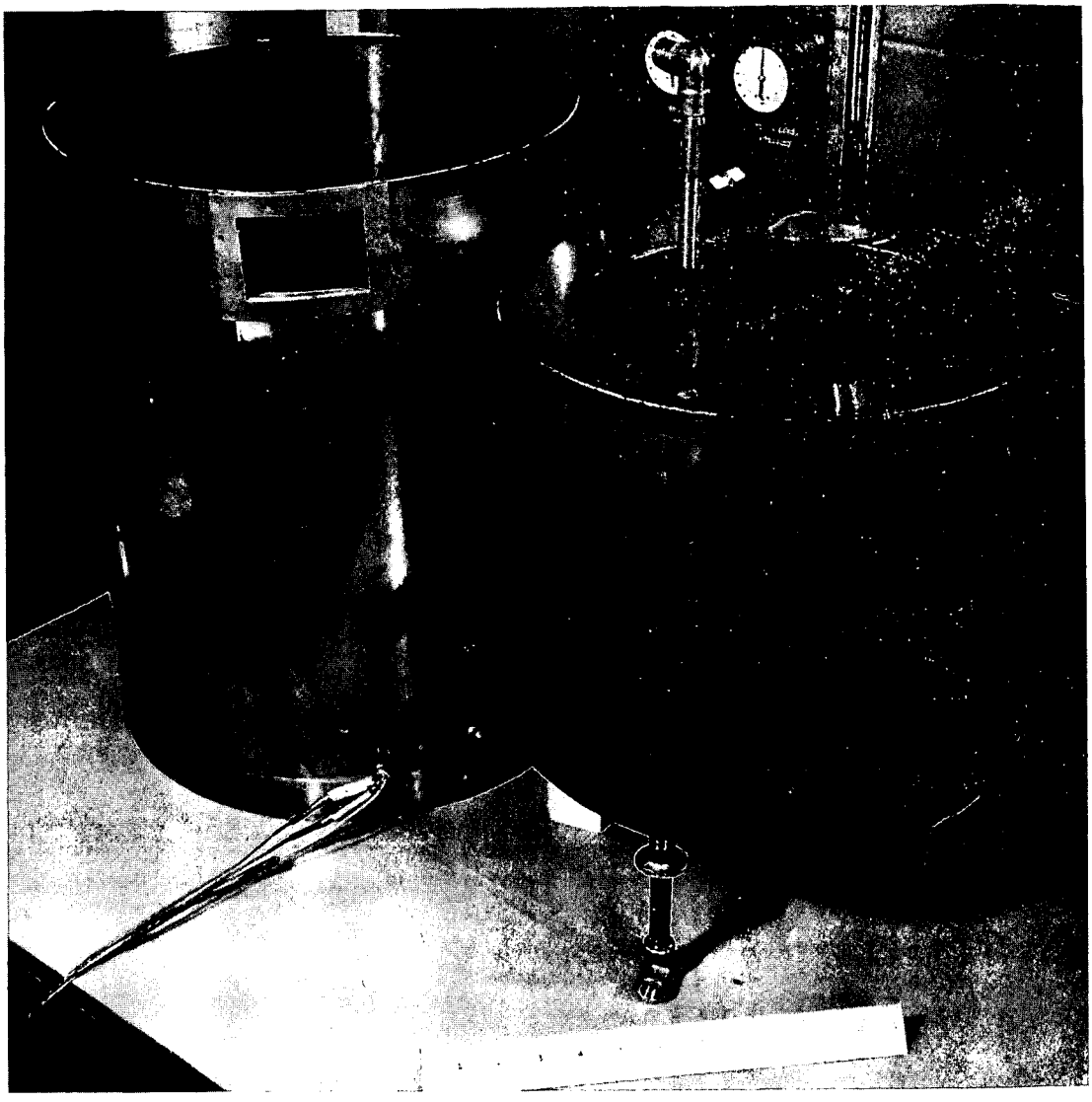

Fig. 3.-JACKETED CARBON MONOXIDE SHIFT REACTOR

Fig. 4.-JACKETED METHANATION REACTOR

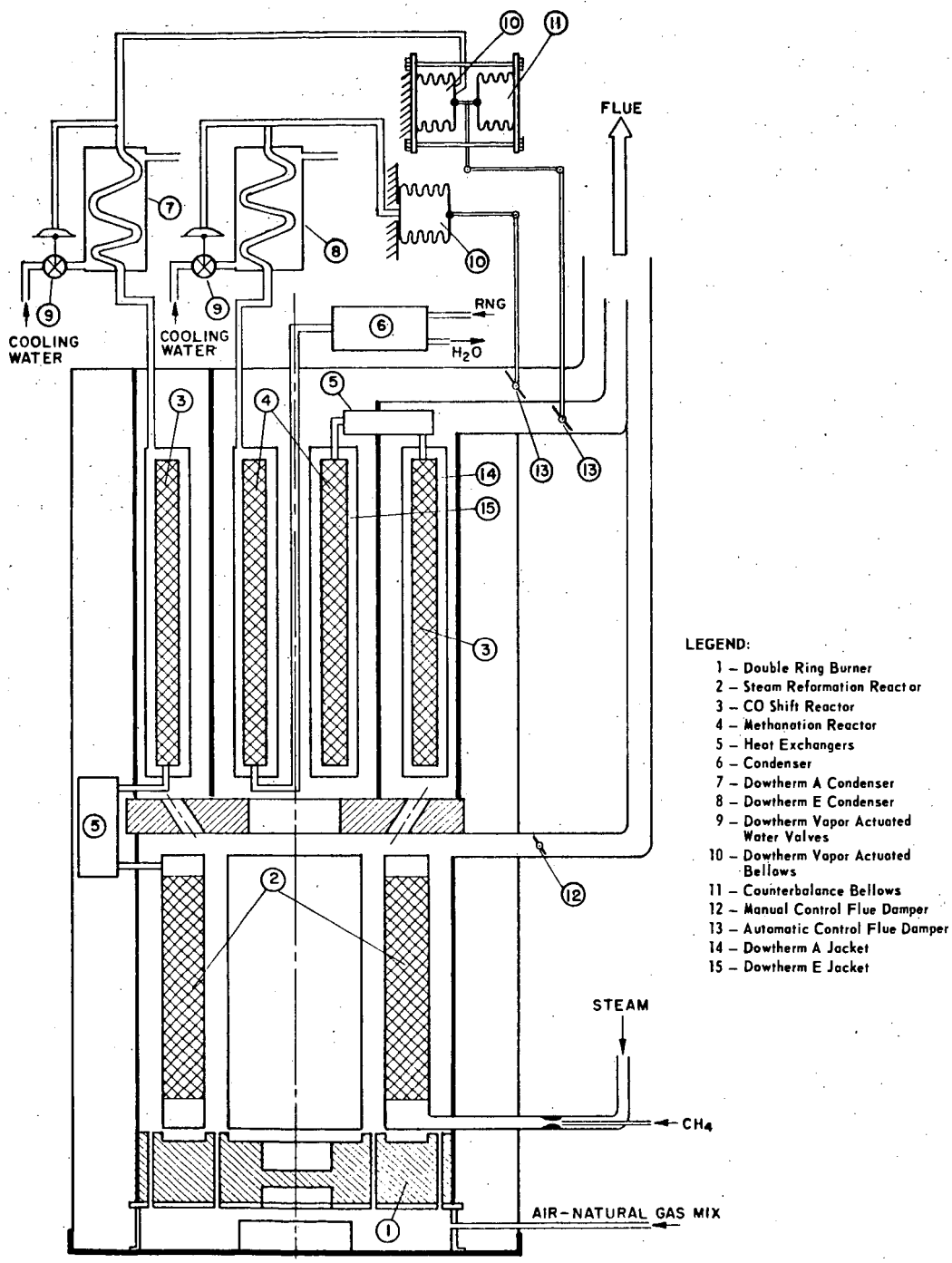

Fig. 5.-SCHEMATIC REPRESENTATION OF IGT HYDROGEN GENERATOR SHOWING REACTORS AND CONTROL LOOPS

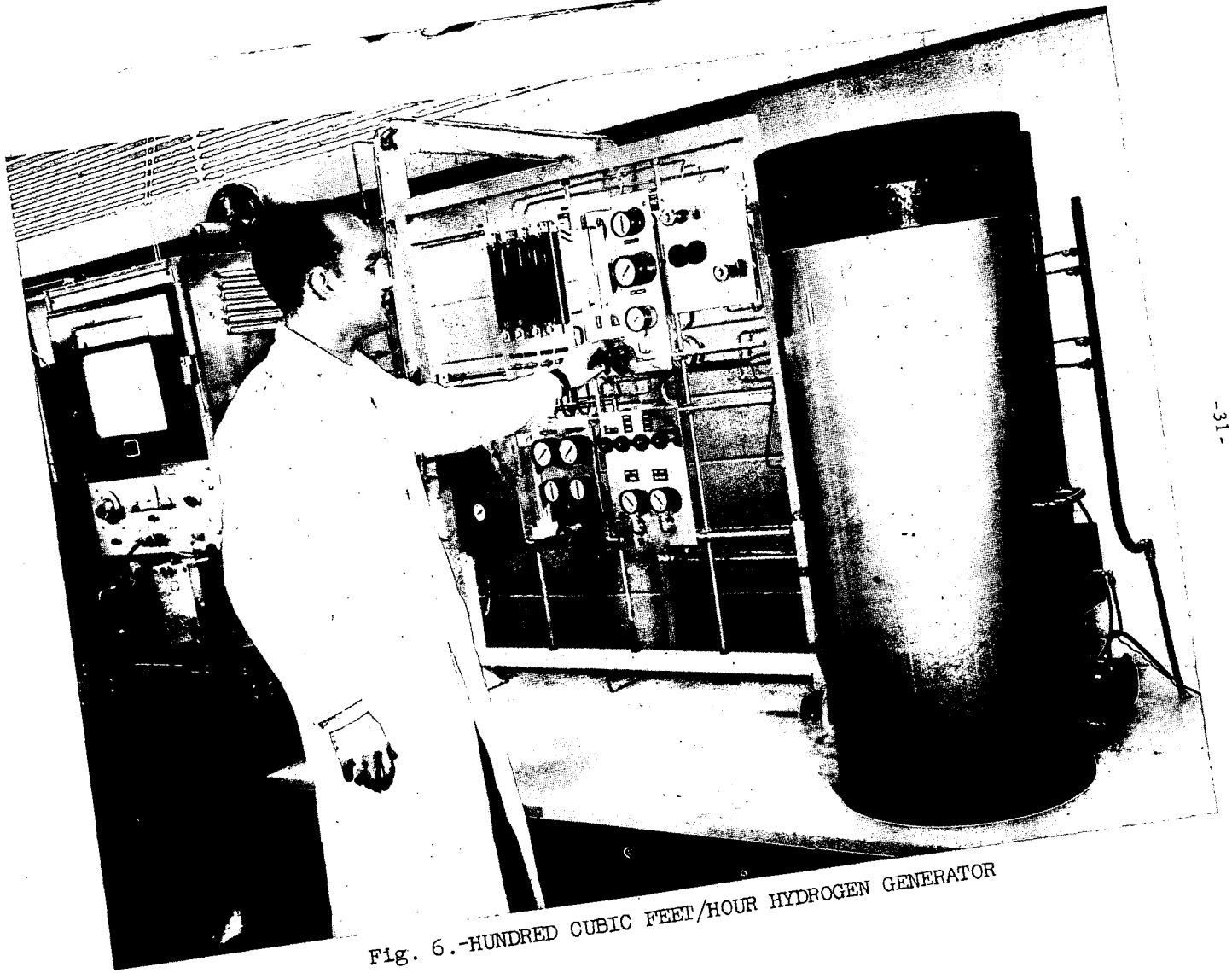

Fig. 6.-HUNDRED CUBIC FEET/HOUR HYDROGEN GENERATOR

PERFORMANCE OF A REFORMED NATURAL GAS-ACID FUEL CELL SYSTEM

Part II. Fuel Cell Battery

F. B. Leitz and W. Glass
Ionics, Inc., Cambridge, Mass.

D. K. Fleming
Institute of Gas Technology, Chicago, Ill.

INTRODUCTION

This is a report on a joint effort of Ionics, Inc. and The Institute of Gas Technology to develop an air-breathing fuel cell system powered by natural gas. The long range objective of the project is the development of an economical power source using this readily available fuel, and which has a high degree of reliability and safety for relatively long periods of unattended operation. The system selected for this program was a low temperature, hydrogen-oxygen fuel cell with an acid electrolyte.

The hydrogen-oxygen system is well advanced. It provides relatively high efficiency with fuels and oxidants that are easy to obtain. The fuel can be generated from natural gas or other hydrocarbons and the oxidant is available from the air. The process to generate hydrogen for this fuel cell has been presented in an earlier publication in this series.[1] The description of a 100-CFH reformer unit has been discussed in another paper during this session.[2]

A low temperature system was selected for the investigation because of its long life, reduced corrosion problems, and low pressure operation. These advantages are counterbalanced in part by the present high cost of the catalyst.

An acid electrolyte system was dictated by the need for compatibility with the carbon dioxide which is formed during the reforming of natural gas and which is also present in room air. With the acid system, expensive steps to purify the hydrogen are not required. Also, the air does not have to be scrubbed to remove carbon dioxide.

A dual ion-exchange membrane battery was chosen for its inherent safety and reliability. With the acid electrolyte contained between two membranes, and the gases on the outside of these membranes, the chances of gas intermixing are minimized. A pinhole in one membrane does not bring two reactant species together in the presence of an active catalyst which would cause failure. The safety of operation is consistant with the goals of the project.

BATTERY CONSTRUCTION AND OPERATION

General Description

The battery is an internally manifolded stack of cells wired in series and with parallel flows of gas and electrolyte. An individual cell is diagramed in Figure 1. The acid compartment, in the center of this diagram, is filled with a polyethylene-

polypropylene woven cloth (70% void) to maintain the electrolyte spacing. On either side of the acid compartment are cationic ion-exchange membranes with woven glass backing. Each of these membranes is intimately contacted by an electrode, either anode or cathode. These, in turn, are held in place by ribbed plates. The plates are embossed niobium sheets, 5 mils thick. They electrically connect one cathode to the adjacent anode and simultaneously distribute the flow of gas to the electrodes. The gas and electrolyte compartment frames are made of 65 durometer butyl rubber. This is sufficiently firm to retain dimensional stability but still has enough flexibility for sealing. The electrodes are platinum-black bonded to a tantalum screen as manufactured by the American Cyanamid Company.[3] The catalyst loading in the present battery is 9 grams per square foot. The total thickness for a single cell is 140 mils or about 1/7 inch.

The internal manifolding technique is shown in Figure 1. The manifolds for the movement of fresh and spent material are holes punched in the margins of the components. Channels connect the appropriate compartments and manifolds. In the present geometry, 70 percent of the total area is active. The active area of a cell is 1/4 square foot.

In operation, the reactant gases are fed to the top of their respective compartments. Spent gas is removed from the bottom of the battery to sweep out the liquid formed by the reaction or which has passed through the membrane by osmosis. The 25 percent sulfuric acid electrolyte flows from the bottom of the compartment to the top. This removes gas which may be in the compartments during start-up. The current is taken from the battery from the terminal collector plates. These are heavier than the interior sheets to reduce the battery's electrical resistance.

Heat and Mass Balance

A detailed analysis of the heat and mass balance problems within the cathode compartment of the cell was performed on a digital computer using finite difference techniques. This study indicated that the air required for a thermal balance is greater than that for a water balance by a factor of approximately 30. Therefore, the heat of reaction must be removed by other means.

Figure 2 shows the heat and mass balances during steady-state operation on reformed natural gas. The operating conditions are typical of those realized in the laboratory. All of the heat generated in the battery, plus that which is equivalent to the water condensed, is removed by the rise in the acid's temperature. If the humidity of the inlet air were lower during operation, water would be removed from the battery and the acid concentration would rise. The exit air is a few degrees higher than the acid temperature because most of the irreversibility of the reaction is at the cathode. The inlet air temperature and humidity are maintained at the conditions of the exit air. The fuel, on the other hand, need not be excessively heated or humidified for stable operation.

Pressure Drop

The pressure drop of the gas streams within the battery is important in the design of the entire system. Air must be supplied at enough pressure to overcome the losses in the humidification process and within the battery. Of greater importance, the reformer must be designed to supply gas at enough pressure to overcome the losses on the anode side of the battery from a line pressure of six inches.

The pressure drop in the present battery design is shown in Figure 3. From this graph, it can be observed that the flow in the cathode chamber is laminar; the pressure drop varies directly with the flow rate. With the same design, the pressure drop for an 80 percent hydrogen-20 percent carbon dioxide fuel mixture, similar to the generator product, should be significantly less than that of the air. The pressure drop with this fuel mixture is so low that uneven distribution within the battery results. To correct the distributional problem, the resistance in the inlet to the fuel compartment from the fuel manifold is increased. In the present design, the restriction is 1/2 inch of 19 mil. I.D. tantalum tubing. With this restriction, the pressure drop to fuel flow is about the same as the pressure drop to air flow. The flow within the anode compartment, according to the slope of the line in Figure 3, is not laminar but is in the transition region.

The pressure drop at expected operating conditions is three to five inches wc. From the earlier paper on the reformer construction, it will be noted that this fuel pressure is readily obtainable from the hydrogen generating system. Enough energy is available in the reformer flue gas to generate steam for ejecting the air required. As the air must be heated and humidified, according to Figure 2, an ejector is a convenient technique for air movement.

If extrapolated, the pressure drops, at increased power levels, would be quite high. This problem can be avoided by embossing the bipolar plates more deeply and shortening the length of the restrictive tubing in the anode compartment.

The plates are now pressed manually and are not identical. This non-uniformity presents a problem with uneven flow distribution within the battery. Relatively high pressure drops must be used in the experimental units for uniform gas distribution.

BATTERY PERFORMANCE

The initial investigations of this program were performed on cells having an area of four square inches. Performance of the batteries is better than that of the small cells. This is due to improved control facilities. Four of these batteries have been constructed and tested. Each has 13 cells with 1/4 square foot of active area. The power is nominally rated at 100 watts each when operated on reformed natural gas and air.

Hydrogen-Oxygen Performance

Polarization curves for a 13 cell battery operating on various fuel and oxidant gases are shown in Figure 4. The data for Figure 4 were taken with 500 hours total operation on the electrodes, and just after a 100 hour run, to minimize the effects of fresh catalyst. The hydrogen-oxygen performance of the battery at 60°C is the standard of comparison for the operating conditions. When these data are plotted IR-free, with each electrode against a reference, it is found that the anode reaction is essentially reversible over the range of current density. By contrast, the oxygen electrode shows substantial polarization, even when the circuit is open. The irreversibility of oxygen electrodes is well-known. It is an area for further catalyst investigation.

Internal Resistance

Preliminary measurements of the internal resistance of the battery show 0.002 ohms-square foot for each cell. This value was determined by interrupting the load on the battery and instantaneously measuring the voltage rise on an oscilloscope. This resistance figure is probably high. More accurate determinations will be possible when faster battery switching techniques have been perfected. Figure 4 shows a curve for the hydrogen-oxygen performance on an IR-free basis.

Conductivity measurements of the membranes and electrolyte indicate that a negligibly small fraction of the internal resistance is in the metallic components of the battery. The liquid electrolyte area resistance is 0.00046 ohm-square foot and the membranes, which act very much like porous media containing 25 percent electrolyte, are responsible for the balance.

Hydrogen-Air Performance

The goals of the project require a system that operates with air at the cathode. The prime disadvantage in the use of air is the loss of cathode potential because of dilution. This potential loss ranges from 40 to 80 millivolts per cell if sufficient air is used. The voltage loss increases as current is increased. The loss at 60 amps per square foot (ASF) is approximately 70 millivolts per cell or .91 volts for the battery. A polarization curve for hydrogen-air operation is included in Figure 4.

The loss of cathode potential, as stated above, depends upon the use of sufficient air. This is designated as a maximum effective feed rate – that is, the point at which any further increase in air flow does not measureably increase the electrode potential. A determination for this air flow rate is presented in Figure 5. For a single cell, the air flow rate at which a potential drop occurs is only slightly more than the stoichiometric equivalent. This is less than 20 percent excess air for 300 millivolt drop from a linear extrapolation of the polarization curve, and less than 25 percent excess air for

100 millivolt drop. At twice stoichiometric flow (100 percent excess air), no deviation from the straight line curve can be observed.

If the oxidant gas supply is interrupted briefly while current can flow through the battery, a noticeable improvement occurs in the battery's performance. This may amount to .65 volts at 60 ASF with a decay time of up to 6 hours depending upon the past history of the battery. Since this lack of reactant shifts the cathode potential almost to the anode potential, a strongly reducing condition is produced at the cathode which apparently cleans the electrode.

Dilute Fuel Performance

The product of the hydrogen generator is primarily 80 percent hydrogen and 20 percent carbon dioxide, with trace amounts of methane and carbon monoxide. The methane and carbon dioxide dilute the anode feed whereas carbon monoxide has a polarization effect which will be discussed later.

The investigation of reactant dilution is straightforward since only hydrogen and carbon dioxide need be considered. The concentration effects due to the dilution of the hydrogen are shown in Figures 6 and 7. Polarization data is included on Figure 4. In treating the data, it is convenient to define a unit gas flow rate as a stoichiometric equivalent (or stoich). This is a gas flow equal to the rate at which the reactant gas is consumed under specified conditions. For example, with a 13-cell battery operating at 15 amperes current, 1 stoich equals 1460 milliliters per minute of hydrogen. Figure 6 shows the stoichiometric relationships. Lines of constant fresh feed (j), and recycle ratio (R), are shown for an 80-20 percent mixture of hydrogen and carbon dioxide.

Experimentally, the indicated feed and recycle rates were simulated by feeding a mixture of the corresponding values of the pure gases. The average potential loss at 60 ASF was then calculated for each condition. This voltage, expressed as millivolts per cell, appears on Figure 6 near the intersection of the corresponding lines. The average potential loss is strongly influenced by excess feed and only slightly affected by the recycle ratio.

The arithmetic mean of battery inlet and outlet conditions was used for average reactant concentration. A graph of potential loss against the average concentration is presented in Figure 7. The correlation is good. The three poorest points occurred at low total flow rates. With this condition, poor distribution between cells was the most likely cause, that is, one or two cells behaved differently from the rest. According to Figure 7, there is a wide range of conditions under which the potential loss can be held to approximately 20 millivolts at 60 ASF.

Figure 7 is plotted on semilog paper for convenient presentation of the data. Also included on this graph is the line for the Nernst Equation which expresses the theoretical open

circuit potential loss. At low average feed concentrations, there appears to be a significant diffusion problem at 60 ASF current. In the range of probable operation, without recycle, the concentration effect is not large.

Figure 4 includes a curve for the polarization of the 13-cell battery on 80 percent hydrogen-20 percent carbon dioxide fuel mixture vs. air. Approximately 200 percent excess fuel was used in the collection of these data.

To check for carbon monoxide production in the anode chamber, the carbon monoxide concentrations of the battery inlet and outlet gases were measured with a sensitive infra-red analyzer. With an inlet concentration from a bottled mixture of 80 percent hydrogen-20 percent carbon dioxide containing 3 ppm of carbon monoxide, the battery outlet concentration was 4 to 5 ppm of carbon monoxide without load. The thermodynamic equilibrium of the reverse water gas shift reaction at 60°C is 20 ppm. Under the flow conditions in the battery, the reaction does not proceed rapidly over the platinum catalyst.

Performance with Reformed Natural Gas Fuel

The purpose of this project is to achieve satisfactory battery operation on a fuel derived from natural gas. The product gas of the hydrogen generator contains 3000 ppm of methane and 20 ppm of carbon monoxide in addition to the hydrogen and carbon dioxide. The methane exerts a negligible dilution effect only, but the carbon monoxide, even in small amounts, significantly affects the battery's operation. It is believed that the carbon monoxide is adsorbed at the reaction site and results in a poisoning effect.

Figure 4 includes a line for the polarization of the 13-cell battery at 60°C when operating on reformed natural gas (RNG) fuel and air. These data were taken after 300 total hours on RNG fuel and immediately after a 100 hour run at 40 ASF. The polarization at 60 ASF is 1.2 volts for the 13 cells, or less than 100 millivolts per cell, when compared with pure hydrogen feed. As expected from the previous section, the concentration polarization due to the presence of carbon dioxide is less than 20 millivolts per cell. The remainder is due to the effect of the carbon monoxide. The maximum power of the battery is 112 watts at 80 ASF.

The poisoning effect just mentioned has occurred for 60°C operation. From tests on small cells, the effect at room temperature is approximately 300 millivolts per cell. The operating temperature of 60°C was selected to minimize the poisoning effect without reaching the temperature at which the fuel reduces the sulfuric acid to hydrogen sulfide.

The long term effects of carbon monoxide in the feed stream are now being investigated. At present, the total operating time on reformed natural gas is 800 hours.

Apparently, the anode can be rejuvenated by two techniques. If the battery load is removed for about an hour, the output

voltage of an 80-20 fuel mixture is produced when the load is restored. Another technique to remove the anode poisoning is to short circuit the battery without fuel. In this case, the carbon monoxide apparently is oxidized. It is not known if either of these rejuvenation techniques can be repeated indefinitely. There is evidence of increasing potential falloff rate with repeated anode treatment.

FUTURE IMPROVEMENTS

When this program was started two years ago, the approximate material cost was $50,000 per kilowatt of power on hydrogen-oxygen feeds. The present cost is $3,000 per kilowatt with an RNG-air feed. The cost must still be reduced significantly for this fuel cell battery to be an economical power source. There are several points of potential improvement in the battery.

The electrical resistance of the electrolyte accounts for a substantial loss of cell potential. A majority of the resistance is in the ion-exchange membranes. Research at Ionics has produced a membrane which could reduce the resistance by more than half, doubling the power output. It is likely that additional effort will result in further improvements in membrane technology.

Experimental electrodes with a greater tolerance for carbon monoxide are now being studied. These electrodes may reduce the load on the methanation system of the hydrogen generator and permit lower temperature operation. Improvement of the carbon monoxide polarization may be possible with increased unit power output.

Electrode costs are a significant fraction of the total battery material costs. Although the electrodes have a high scrap value, the platinum is a high cost investment. While it is unlikely that platinum will be replaced as a catalyst, at least on the oxygen side, the possibility of a more effective use of the catalyst is significant. Experiments with electrodes using different amounts of platinum indicate that the effectiveness of the platinum (at constant potential) increases significantly as the platinum loading decreases. Some success may be expected from attempts to place small amounts of catalyst on the electrode surface most favorable to the reaction. The anode polarization curve indicates that reduction in catalyst loading may be possible now without penalty to performance.

ACKNOWLEDGEMENT

The authors wish to thank Southern California Gas Company, Southern Counties Gas Company of California, and Con-Gas Service Corp., who are sponsoring this investigation, for permission to publish these results.

REFERENCES

1. Meek, J., and Baker, B. S., "Hydrogen from Natural Gas for Fuel Cells," Fuel Cell Systems, pp. 221-231, American Chemical Society, Washington, D. C., 1965.

2. Meek, J., Baker, B. S., and Allen, A., "Performance of a Reformed Natural Gas-Acid Fuel Cell System, Part I, Hydrogen Generator Design," presented at Fuel Chemistry Division of the American Chemical Society, 150th Annual Meeting, Atlantic City, N. J., Sept. 12-17, 1965.

3. Haldeman, R G., Colman, W. P., Langer, S. H., and Barber, W. A., "Thin Fuel Cell Electrodes," Fuel Cell Systems, pp. 106-115, American Chemical Society, Washington, D. C., 1965.

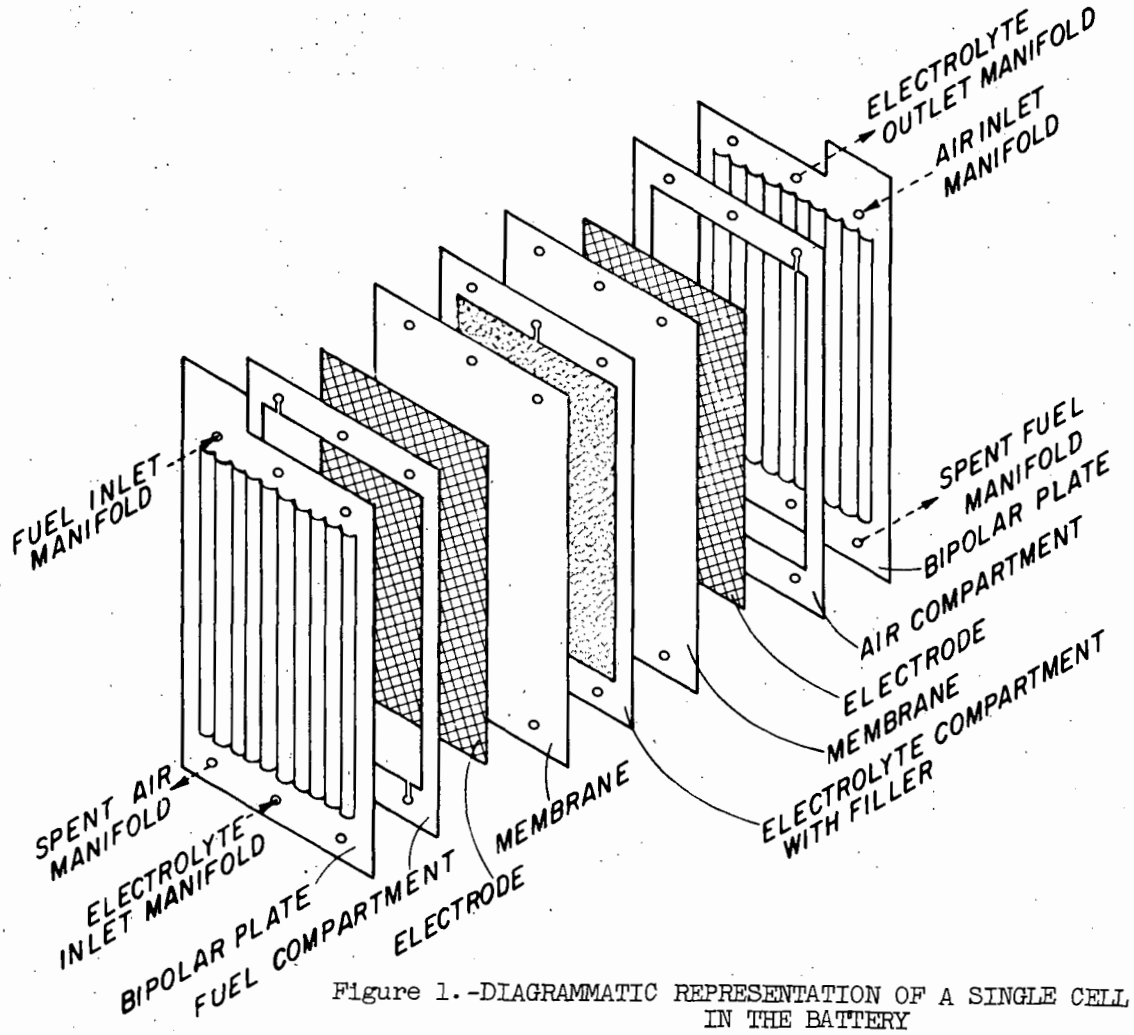

Figure 1.-DIAGRAMMATIC REPRESENTATION OF A SINGLE CELL IN THE BATTERY

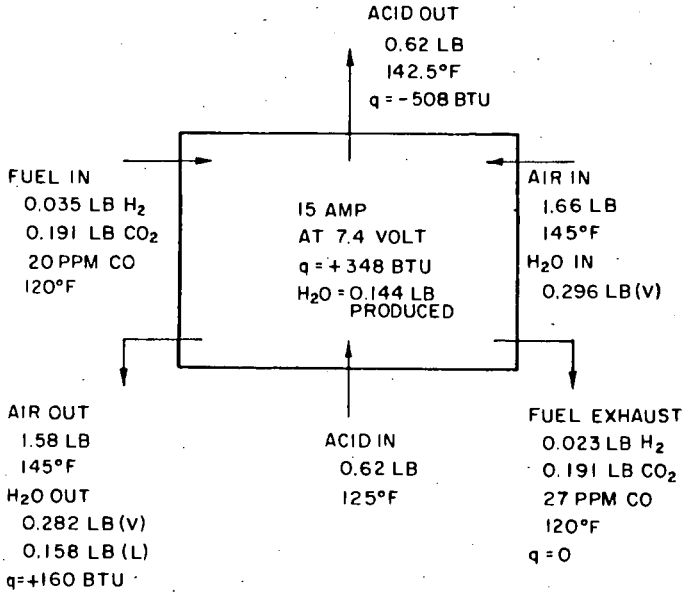

Figure 2.-HEAT AND MASS BALANCES AROUND THE OPERATING BATTERY (13 CELLS, 1/4 SQ FT EACH, 1 HR OPERATION, STEADY STATE)

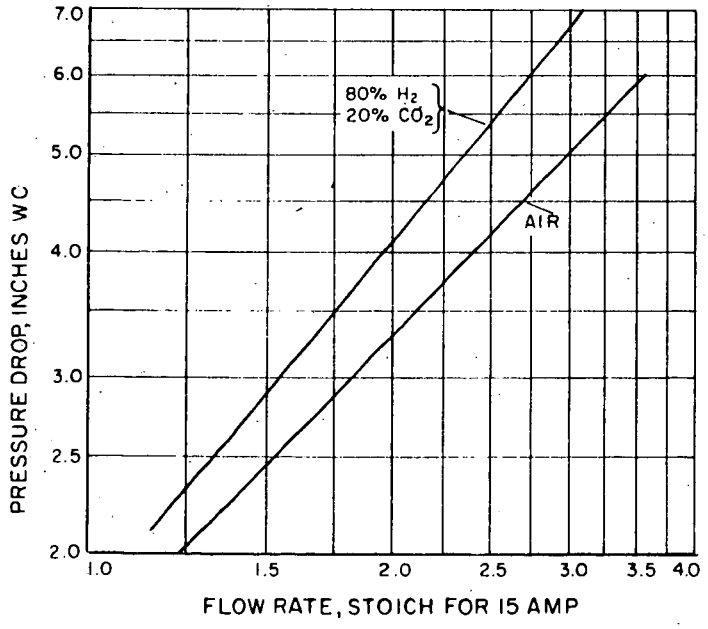

Figure 3.-PRESSURE DROPS IN THE BATTERY GAS STREAMS

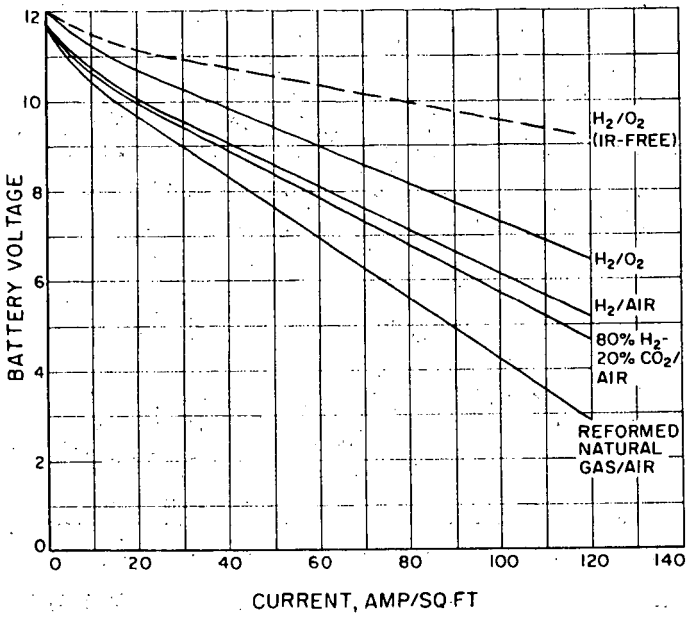

Figure 4.-OPERATING PERFORMANCE OF A 13-CELL BATTERY AT 60°C

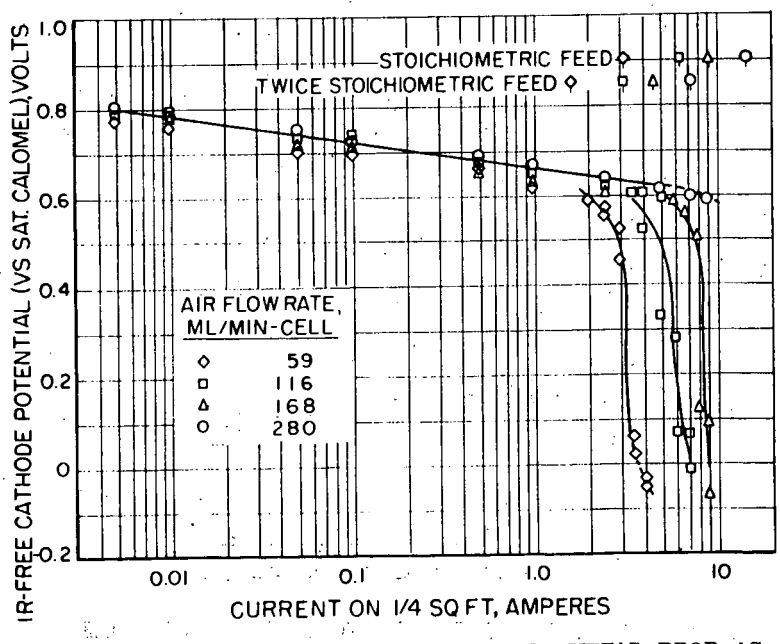

Figure 5.-POLARIZATION CURVE SHOWING POTENTIAL DROP AS CURRENT APPROACHES STOICHIOMETRIC EQUIVALENT OF AIR FEED

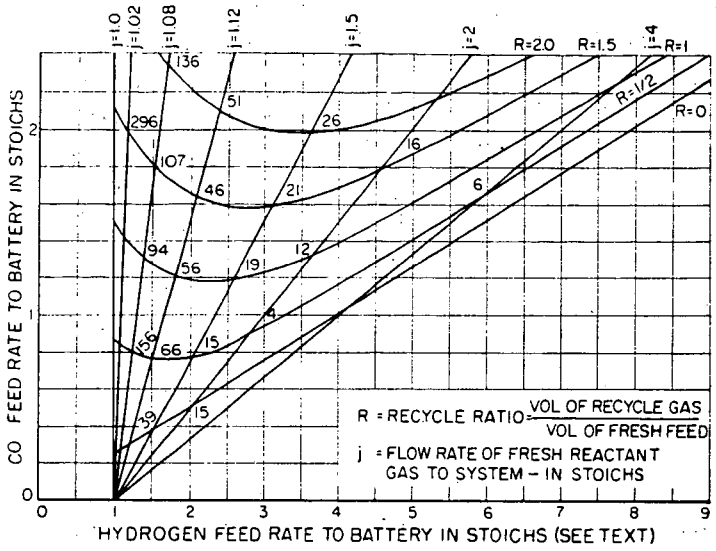

Figure 6.-VOLTAGE DIFFERENCE BETWEEN PURE HYDROGEN AND DILUTE ANODE FEEDS. NUMBERS ARE MILLIVOLTS LOSS PER CELL

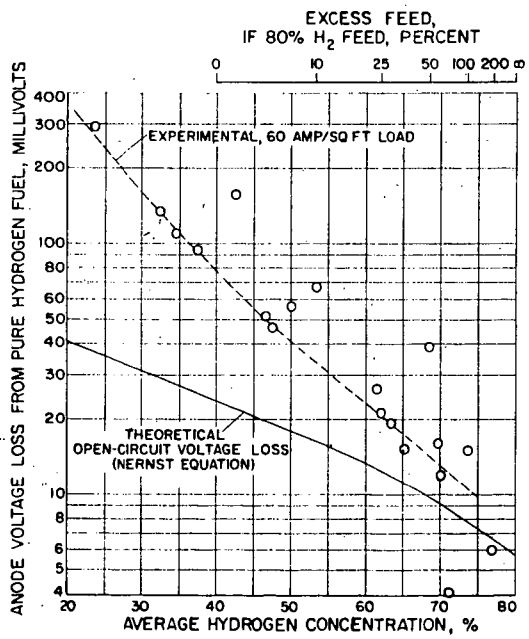

Figure 7.-VOLTAGE LOSS DUE TO DILUTE ANODE FEED.

THE PERFORMANCE OF SOLID-ELECTROLYTE CELLS AND BATTERIES ON CO-H_2 MIXTURES; A 100-WATT SOLID-ELECTROLYTE POWER SUPPLY*

D. H. Archer, L. Elikan, and R. L. Zahradnik

Westinghouse Research Laboratories
Beulah Road, Churchill Borough
Pittsburgh 35, Pennsylvania

INTRODUCTION

Fuel cells employing a ZrO_2-based electrolyte are customarily operated at temperatures around 1000°C in order to promote high oxygen ion conductivity in this solid, ceramic material. At such high temperatures commercial fuels – coal and hydrocarbons – are thermodynamically unstable; they tend to crack forming solid carbon and hydrogen gas. The deposition of carbon in solid-electrolyte batteries can be prevented by mixing with the incoming fuel a portion of the CO_2 and H_2O products emerging from the battery. These gases reform the fuel producing CO and H_2 which are then oxidized in the solid-electrolyte cells to produce power. Essentially, therefore, in utilizing commercial fuels solid-electrolyte cells operate on CO-H_2 mixtures.

Experiments have been performed to characterize the performance of solid-electrolyte cells on fuel gas mixtures containing CO, H_2, CO_2, and H_2O in various proportions. Open circuit voltages have been determined in single cells at various temperatures; the measured values of voltage agree with those computed from thermodynamic data within 3%. The dependence of the operating voltage of solid-electrolyte cells on the current drain (or current density) has also been studied at various temperatures for different fuel mixtures. In general, cells operating on CO-CO_2 mixtures develop less output voltage than those operating on H_2-H_2O because of increased polarization voltage losses. The addition of H_2-H_2O to CO-CO_2 mixtures, however, greatly reduces these losses. And the insertion of a catalyst into the cell which promotes the shift reaction

$$CO + H_2O \rightarrow CO_2 + H_2$$

causes further reduction in the observed polarizations to the extent that cell performance on CO-H_2 fuel duplicates that on pure H_2.

Tubular, solid-electrolyte batteries containing 20 bell-and-spigot cells of 7/16 in. diameter and 7/16 in. length have been produced. They are leak-tight. Their resistance has been

---

*The work recorded in this paper has been carried out under the sponsorship of the Office of Coal Research, U.S. Department of the Interior, and Westinghouse Research Laboratories. Mr. George Fumich, Jr., is head of O.C.R.; Neal P. Cochran, Director of Utilization, and Paul Towson have monitored the work for O.C.R.

of oxygen to gm-atoms of carbon in the fuel gas mixture – and n'_H, a similar ratio for hydrogen and carbon. Experimental values of open-circuit voltage are plotted together with theoretical curves in Figures 2 and 3. Except at $n'_O = 1.0$ (usually corresponding to pure CO) and $n'_O = 2.0$, $n'_H = 0.0$ (pure CO_2) where E_t changes very rapidly with n'_O, E_t values are within ± 3% of the predicted values. This agreement is considered to be within the limits of accuracy of the measurements of composition, temperature, and voltage involved.

VOLTAGE-CURRENT RELATIONS

The single solid-electrolyte cell shown in Figure 1 was also used to determine voltage-current curves for various mixtures of CO, H_2, CO_2, and H_2O at different temperatures. Some of the experimental results are shown in Figures 4-7.

When a current is drawn from the terminals, the voltage of the cell drops below the open-circuit voltage because of resistance losses in the electrolyte and electrodes and because of polarization voltage losses associated with irreversible electrode process.

$$V = E_t - IR - V_p \qquad (2)$$

where V = the terminal voltage of the cell, volts

E_t = the open circuit voltage of the cell (which can be determined from Figures 2 or 3), volts

I = the load current passing through the cell, amperes

R = the electrical resistance of electrodes and electrolyte, ohms

V_p = the polarization voltage loss, volts.

An approximate value for the resistance of the cell shown in Figure 1 can be computed from

$$R = \rho_b \delta_b / A_b + (\rho_e / \delta_e)(L_e / P_e) \qquad (3)$$

where ρ_b = electrolyte resistivity, about 70 ohm-cm at 1000°C

δ_b = electrolyte thickness, 0.09 cm

A_b = active cell area, 27.6 cm^2

ρ_e / δ_e = resistivity-thickness quotient for the cell electrodes, estimated to be 0.8 ohms

L_e = mean distance traveled by the electronic current in the electrodes passing from the plus to the minum terminal of the cell, estimated to be 4 cm

P_e = mean width of the electrode perpendicular to the direction of electronic current flow, calculated as 3.4 cm

$$R = [(70)(0.09)/27.6] + [(0.8)(4/3.4)]$$

$$= 0.23 \text{ ohms} + 0.94 \text{ ohms}$$

$$= 1.2 \text{ ohms.}$$

The cell resistance has also been determined by measuring the voltage loss over the cell while passing a current with air at both inner and outer electrodes. The constant slope of this curve at higher current densities is termed the air-air resistance. Generally, this resistance value checks the resistance as computed above. Immediately after its construction the air-air resistance of the cell of Figure 1 checked the calculated resistance. Before the data for Figures 4-7 were obtained – three months later, the electrolyte component of cell resistance had gradually doubled. Presumably, the active cell area had decreased to about one-half the superficial electrode area.

Values of the polarization voltage V_p have been computed by Equation 2 from data of the type presented in Figures 4-7. For these computations the air-air resistance values were used, and E_t values were corrected by the use of Figures 2 and 3 where the cell current produced any appreciable change in $n\delta$, the oxygen content of the fuel stream passing through the cell. Table 1 presents the V_p values and also gives derived values of αn and i_o in the simplified Tafel equation[3]

$$V_p = \frac{RT}{\alpha n} [\ln(i/i_o)] \qquad (4)$$

where α is an empirically determined fraction of the electrical work output by which the free energy of activation is increased. An α value of about 0.5 is usually assumed in cases where specific knowledge is lacking.

n is the number of electrons transferred for each occurrence of the irreversible event causing the polarization voltage loss; n is assumed to be 2 in the electrochemical oxidation of CO.

i is the current density I/A_b, amperes/cm^2.

i_o is the exchange current density, the equal but opposite rates at which the polarization-causing process and its reverse occur at open circuit (assuming a reversible electrode at this condition).

The following general observations can be made based on the data for pure, dry CO-CO_2 fuel mixtures presented in Figures 4-6 and Table 1:

1) Polarization losses in solid-electrolyte cells with conventional electrodes are much greater than those observed with H_2-H_2O fuel.

2) Polarizations with CO-CO_2 tend to decrease with increasing temperature.

determined by passing a current through the battery with air at both electrodes, and their fuel cell performance has been measured with pure H_2 and with H_2-CO mixtures as fuel, and with air as the oxidant. Over twenty-four of these batteries have been tested. Their average internal resistance is 8.2 ± 1.8 ohms; and their power output, 6.7 ± 0.8 watts. Twenty of these batteries have been assembled into a system which produces over 100 watts with H_2 or H_2-CO fuel and air.

OPEN-CIRCUIT VOLTAGES

A single solid-electrolyte cell has been employed to measure the open circuit voltages developed by mixtures containing CO, H_2, CO_2, and H_2O in various amounts. This cell was fabricated by applying conventional, sintered-platinum electrodes outside and inside of the central portion of a tube of $(ZrO_2)_{0.85}(CaO)_{0.15}$ electrolyte material as shown in Figure 1. A platinum screen was placed in the tube to serve as a current collector. A cell lead wire was attached directly to this screen. Platinum wires were wound around the electrode on the outside of the tube and could be used either as current leads or as voltage probes.

Fuel mixtures obtained by mixing varying amounts of pure hydrogen with premixed CO-CO_2 mixtures flowed inside the tubular cell, which was maintained at the desired temperature in an electrically-heated furnace. An air atmosphere surrounded the tube.

The thermodynamically predicted open-circuit voltage of the cell can be calculated by

$$E_t(4F) = RT \ln (P_{O_2,a}/P_{O_2,f}) \qquad (1)$$

where 4F = 4(the Faraday number) = quantity of charge transferred per mole of O_2 passing through the electrolyte 386,000 coulombs/mole

R = universal gas constant, 8.134 watt-sec./°K mole

T = absolute temperature of cell, °K

$P_{O_2,a}$ = the partial pressure of oxygen in the air surrounding the cell, 0.21 atm.

$P_{O_2,f}$ = the partial pressure of oxygen in the fuel gas atmosphere within the cell.

The value of $P_{O_2,f}$ can be calculated from the composition of the fuel by standard thermodynamic methods.[1,2] If the water gas equilibrium,

$$CO + H_2O \rightleftharpoons CO_2 + H_2 \quad ,$$

is achieved in the cell, then the fuel composition, $P_{O_2,f}$, and hence E_t can be determined from two parameters n_O — the ratio of gm-atoms

3) The CO-CO_2 polarizations decrease with decreasing velocity of fuel flow.

4) Polarizations tend to increase more rapidly with current at fuel compositions where the $E_t - n\delta$ curve is sharply dropping; conversely the polarization voltage loss tends to remain more nearly constant with varying i at CO-CO_2 fuel compositions where the $E_t - n\delta$ curve is horizontal.

5) The αn values in the Tafel equation average about 1.0 as might be expected from simple theory which assigns α the value 0.5 and n the value 2. For the particular cell employed in this investigation the exchange current densities, i_o, averaged about 0.7 milliampere/cm^2. Insufficient data are available to draw any firm conclusions about trends of αn and i_o with operating conditions in the cell.

The data presented in Figures 6 and 7 demonstrate that small quantities of hydrogen added to CO-CO_2 greatly reduce polarization voltage losses. With a hydrogen-carbon ratio $n'_H = 0.5$ the performance of the cell is essentially the same as with pure H_2. A hydrogen content of 5 mol % in a CO-H_2 mixture flowing at 1.0 cc/sec will alone support a current of 400 milliamperes; at this current the observed value of V_D from Figure 7 is about 0.15 volts if the effect of current on $n\delta$ and hence on E_t is considered. At a total current of over 1000 milliamperes (equivalent to about 40 milliamperes/cm^2) the cell polarization voltage loss has risen only slightly to 0.20 volts. If the current in excess of 400 milliamperes were supported by the oxidation of CO, the data of Table 1 indicate that polarizations losses in excess of 0.30 volts could be expected at 1000 milliamperes. Apparently, the water gas shift process,

$$CO + H_2O \rightarrow CO_2 + H_2 \ ,$$

has provided sufficient hydrogen to maintain cell polarization losses low.

To investigate further the effect of hydrogen additions on the polarization losses associated with CO-CO_2 fuel mixtures – a three-cell battery, illustrated in Figures 8 and 9, was utilized. In operating on hydrogen and air this battery had higher resistance than is usually encountered in solid-electrolyte batteries of this type[4,5] but polarization losses were negligible as shown in Figure 11. In operating on CO-CO_2 and air, however, polarizations were observed as shown in Figure 11 and in Table 2. The Tafel constants derived from the data are in good agreement with those obtained with the single cell. The difference between E_t for the CO-CO_2 fuel mixture and the observed open circuit voltage per cell in the battery is about 0.23 volts; the Tafel equation indicates that such a polarization corresponds to a current density of 6.2 milliamperes/cm^2

(or 12 milliamperes/total current) passing through the cells at open circuit. This current is attributable to shunt paths in the seal regions.[5]

In a successful effort to reduce polarization losses, the $CO-CO_2$ fuel stream was humidified by passing it through a water bath at room temperature. At most 3 mol % H_2O was added to fuel stream. A catalyst material, Cr_2O_3, was sintered on the outside of the fuel feed tube and placed in the battery as shown in Figures 10 and 8. The performance of the battery is shown in Figure 11. (Catalyst Tubes 1 and 2 differ slightly in the quantity of Cr_2O_3 applied to the tube and the conditions of sintering.) Essentially the performance curves for the $CO-CO_2$ fuel mixture differ from the H_2 fuel curve only by an amount equal to three – for three cells – times the difference in E_t for the different fuels; $CO-CO_2$ mixtures can be utilized in solid-electrolyte cells with low polarization losses if some H_2 or H_2O is present and if a suitable shift catalyst is employed.

Additional experience on the performance of $CO-H_2$ fuel mixtures at higher current densities has been gained by a series of tests on a 20-cell solid-electrolyte battery whose construction and H_2-air performance have been previously described.[5] The two H_2 performance curves of Figure 12 check with predictions based on the calculated cell resistance and on the variation of the open circuit voltage E_t with the composition of the fuel as it is gradually oxidized along the length of the battery. Polarization voltage losses are apparently neglible. The $CO-H_2$ performance curve was obtained without any shift catalyst present in the battery. The voltage with the $CO-H_2$ mixture at a current density of 450 milliamperes/cm^2, 0.9 ampere, is 0.1 of a volt per cell less than with pure hydrogen at the same net flow of H_2, 3 cc/sec. It can be expected that the addition of catalyst will bring about appreciable improvement of this 20-cell battery.

TWENTY-CELL BATTERIES

Twenty-five batteries identical in construction to the one whose performance is presented in Figure 12 have been fabricated and tested. All except one proved leak-tight. At the operating temperature of 1000°C battery air-air resistance – the voltage loss divided by the current value of 1.0 ampere – ranges from 6.4 to 9.4 ohms; the average and root mean-square deviation values are 7.8 ± 1.0 ohm. This average battery resistance is about 30% greater than the value calculated from the electrolyte resistivity and electrode resistance/thickness values. The open circuit voltage developed by these batteries on H_2 or H_2-CO fuel and air ranges between 19 and 20 volts; losses in the generated voltage of the solid-electrolyte bell-and-spigot cells due to shunt currents in the seal region[5] are thus less than 7% of the reversible voltage. The maximum power output of the batteries is 6.7 ± 0.8 watts with complete combustion of H_2 fuel at about 0.87 amperes or 435 milliamperes/cm^2.

The resistance, open circuit voltage, and power output of these batteries are in reasonable agreement with theoretical calculations.[5] And the methods used in fabricating the batteries yield a reasonably uniform product.

100-WATT SOLID-ELECTROLYTE FUEL-CELL POWER SUPPLY

Twenty of the 20-cell batteries described above have been used to construct a 100-watt solid-electrolyte fuel-cell power supply shown in Figure 13. The batteries are mounted on a 4.5 in. diameter metal base plate (see Figure 14) which provides support and manifolding for up to twenty-four batteries. The flow to each battery from the fuel plenum is regulated by a fine needle valve — one of which is shown on Figure 14. The valve position push rods are adjusted to equalize the flows to the batteries. The fuel flows up the feed tube to the top of the battery; it then flows downward inside the tube of cells reacting with the oxygen which passes through the electrolyte as current is drawn from the battery. The combustion products are carried down into the upper plenum of the base plate and then into the exhaust pipe.

Air surrounds the batteries inside the 3-zone furnace (see Figure 13) which is used to maintain the cells at the desired operating temperature. Plugs of insulation 5 in. in diameter and 4-1/2 in. thick are used to reduce heat losses from the top and bottom of the cylindrical heated region of the furnace. The temperature distribution throughout the batteries is indicated in Figure 15; the small circles represent individual batteries in a plan view of their arrangement in the furnace. At the top are the temperatures of the uppermost cell in three batteries indicated by Pt-Pt-10% Rh thermocouples. The middle temperatures are those on the tenth cell from the top; at the bottom are shown temperatures of the lowest cells in the batteries. With the exception of one low temperature reading on a battery opposite the "crack" of the split-tube furnace the temperatures are within ±30°C of the average value. Even better uniformity can be achieved by a more careful adjustment of the heat input to the various sections of the furnace.

The twenty batteries are divided into two groups of ten; in each group the batteries are electrically connected in series. The two groups, each containing 200 series-connected cells, are used in parallel to supply power to the load. The electrical performance of this power supply is shown in Figure 16. The open-circuit voltage is 200 volts; the maximum power is 102 watts at 1.2 amperes with H_2 flow at a rate corresponding to 2.1 amperes. This power output is about 20% lower than that which might be expected from the measurements of the power output of single batteries. A reduction in temperature of batteries caused by heat losses through the "split" in the furnace and a non-uniform distribution of air flow through the batteries have been shown to cause in part this reduction in power. With excess H_2 flow, the performance of the battery is improved as shown in Figure 17 and a maximum power of 110 watts is achieved.

The 100-watt power supply demonstrates the feasibility of generating fuel-cell power by means of banks of solid-electrolyte batteries. This, plus the demonstrated ability of the batteries to produce

power efficiently from carbon monoxide – carbon dioxide – water – hydrogen mixtures with the employment of a chrome oxide catalyst, demonstrates the technical feasibility of generating this power from coal.

REFERENCES

1. D. H. Archer and E. F. Sverdrup, "Solid-Electrolyte Fuel Cells" in Proceedings of the 16th Power Sources Conference, 34 (1962).

2. D. H. Archer, E. F. Sverdrup, and R. L. Zahradnik, "Coal Burning Fuel Cell Systems" Chemical Engineering Progress, 60,6, 64 (1964.

3. L. G. Austin, "Electrode Kinetics and Fuel Cells" Proceedings of the IEEE, 51, 820 (1963).

4. D. H. Archer, J. J. Alles, W. A. English, L. Elikan, E. F. Sverdrup, and R. L. Zahradnik, "Westinghouse Solid-Electrolyte Fuel Cell" in Advances in Chemistry Series (R. F. Gould, ed.), 47, 332 (1965).

5. D. H. Archer, R. L. Zahradnik, E. F. Sverdrup, W. A. English, L. Elikan, and J. J. Alles, "Solid-Electrolyte Batteries" in Proceedings of the 18th Power Sources Conference, 36 (1964).

Table 1

Polarization Voltage Losses, V_p, and Tafel Equation Constants at Various Fuel Flow Rates, Compositions and Temperatures

Cell Operating Conditions			Polarization Voltage Losses at Various Current Densities, volts				Tafel Constants	
% CO in CO + CO_2 100 (n_o' - 1.0)	Temperature T, °K	Fuel Flow Q, cc/sec	i = 2 ma/cm^2	i = 4 ma/cm^2	i = 6 ma/cm^2	i = 12 ma/cm^2	αn	i_o, ma/cm^2
100	1215	0.7	0.19	0.27	0.30	0.39	1.1	0.33
100	1215	0.17	0.12	0.17	0.21	0.27	0.8	0.47
100	1050	0.7	0.32	0.32	0.32			
100	1050	0.17	0.19	0.20	0.21			
90	1330	0.7	0.13	0.23	0.31		1.4	0.94
25	1215	0.7	0.11	0.175	0.22		0.9	0.64
25	1215	0.17	0.065	0.14	0.195		1.1	1.20
25	1050	0.7	0.29	0.375				
25	1050	0.17	0.28	0.34				
10	1215	0.7	0.09	0.16	0.19	0.24	0.8	0.80
10	1215	0.17	0.09	0.11				
10	1050	0.7	0.275	0.34				
10	1050	0.17	0.235	0.255				

Table 2

Polarization Voltage Losses with CO-CO_2 in a Three-Cell Solid-Electrolyte Battery

Fuel: 90 mol % CO, 10 mol % CO_2
$n' = 1.1$
5.7 cc/sec
Oxidant: air
Temperature: $1000^{\circ}C$
Cell area (active): 2.0 cm^2

Current density, $I/A_p = i$, milliamperes/cm^2:	25	50	100	150
Polarization voltage loss, V_p, volts:	0.37	0.44	0.51	0.55

Derived Tafel constants: $\alpha n = 0.92$
$i_o = 0.6$ milliamperes/cm^2

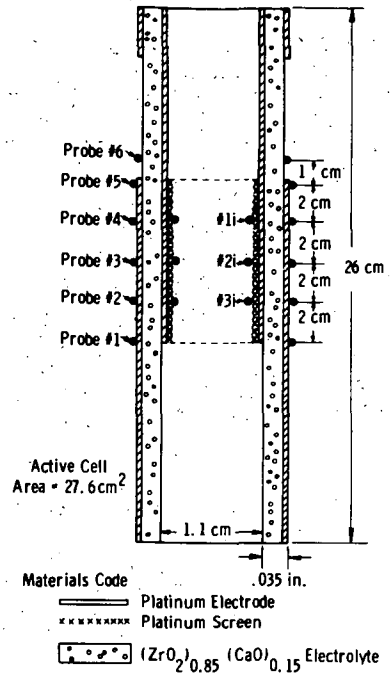

Fig. 1—Schematic cross section of fuel cell TC#8

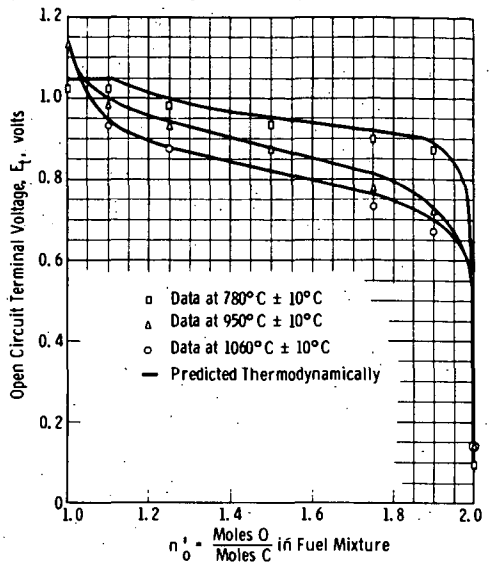

Fig. 2—Generated voltage of a fuel cell using a C-O fuel mixture as a function of fuel mixture composition

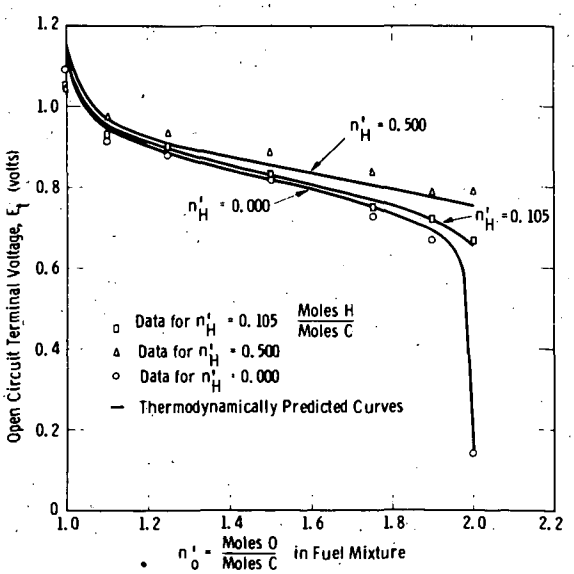

Fig. 3—Generated voltage of a fuel cell using a C-H-O fuel mixture at 1060°C as a function of fuel mixture composition

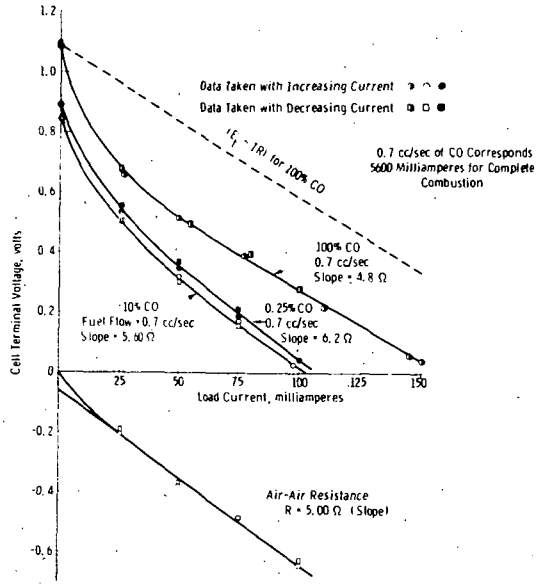

Fig. 4 —Load curves for fuel cell TC #8 using CO-CO_2 fuel mixtures at 780°C

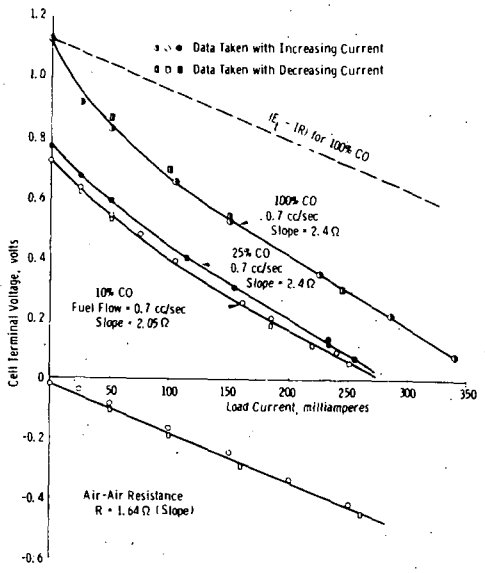

Fig. 5 —Load curves for fuel cell TC #8 using CO-CO_2 fuel mixtures at 940°C

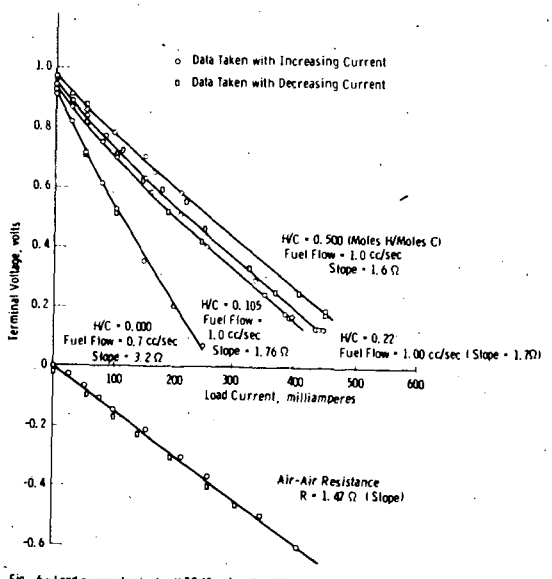

Fig. 6 —Load curves for fuel cell TC #8 using C-H-O fuel mixtures at 1060°C with n_o^c = 1.10 (Moles O/Moles Cl in fuel chamber

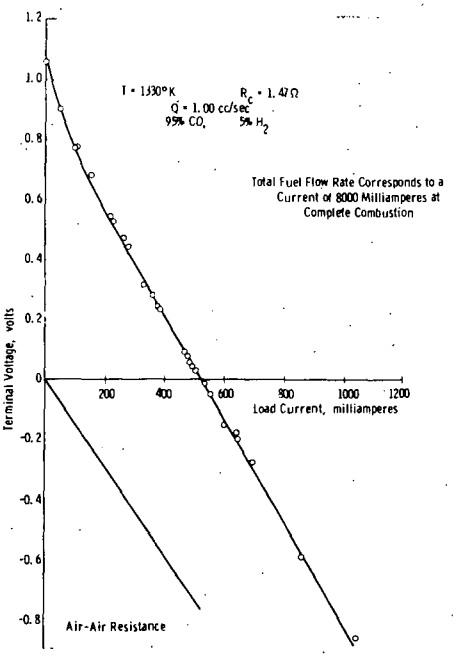

Fig. 7 —Load curve demonstrating effectiveness of water-gas reaction in improving fuel cell performance in TC #8

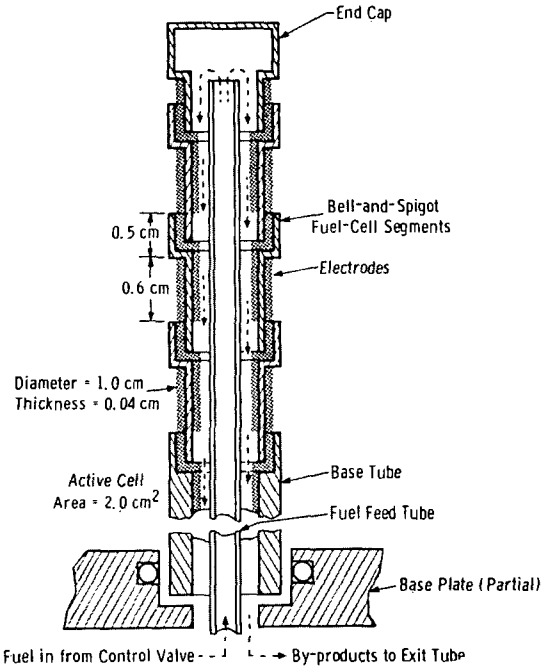

Fig. 8—Schematic axial cross-section of a three-cell solid electrolyte battery showing feed-tube

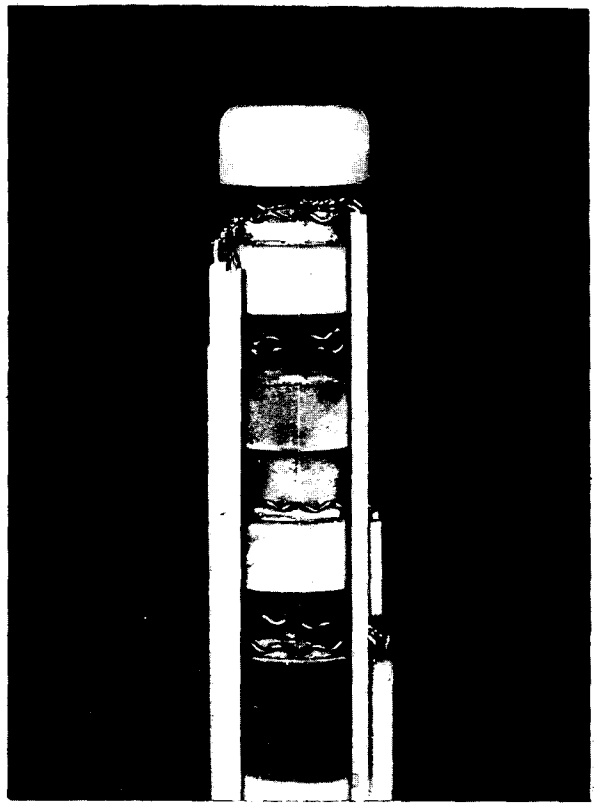

Fig. 9—Three-cell solid-electrolyte battery with current leads, voltage taps, and thermocouple probes

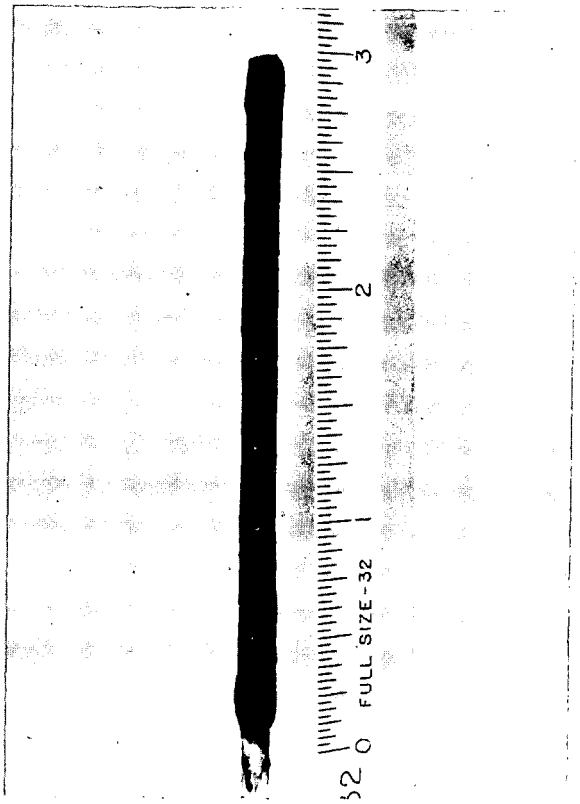

Fig. 10—Fuel feed tube for three-cell battery with Cr_2O_3 catalyst coating

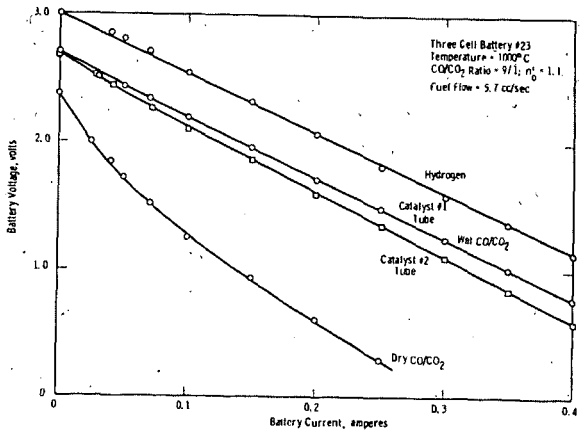

Fig.11—Performance of three cell battery using chrome-oxide catalyst sintered to fuel feed tube

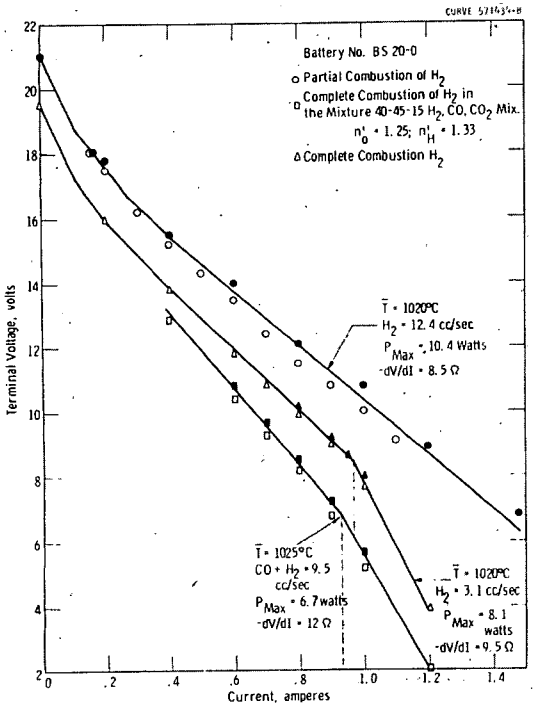

Fig. 12—Twenty-cell solid-electrolyte battery performance

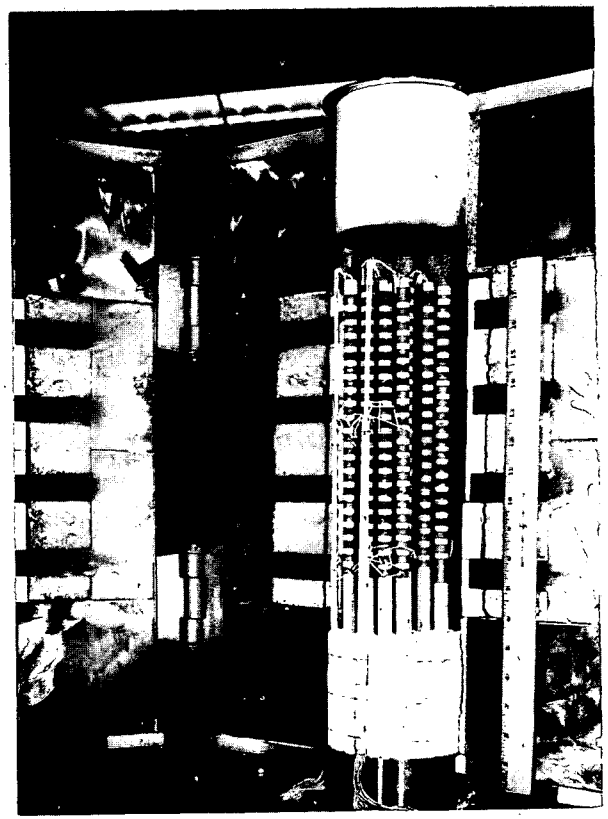

Fig. 13—100-watt solid-electrolyte fuel-cell power generator with furnace door open

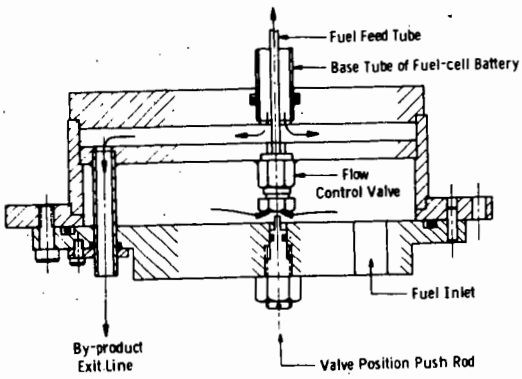

Fig. 14–Section view of base plate

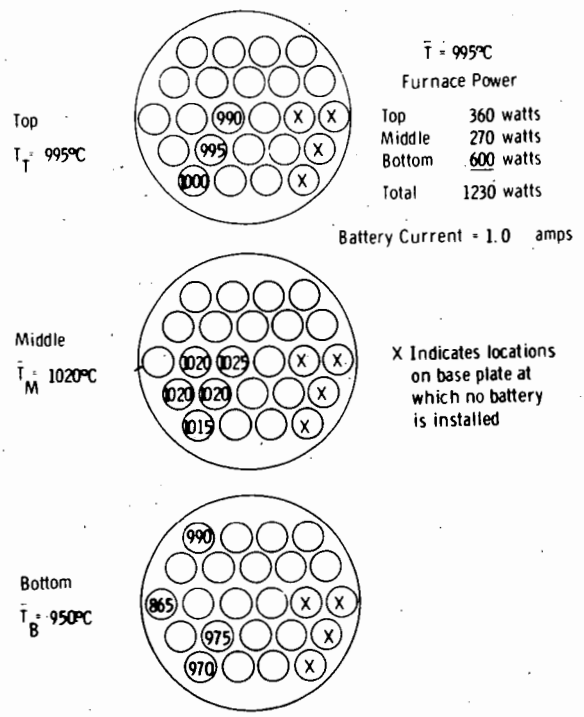

Fig. 15–Battery temperature distribution as a function of axial position --at operating temperature

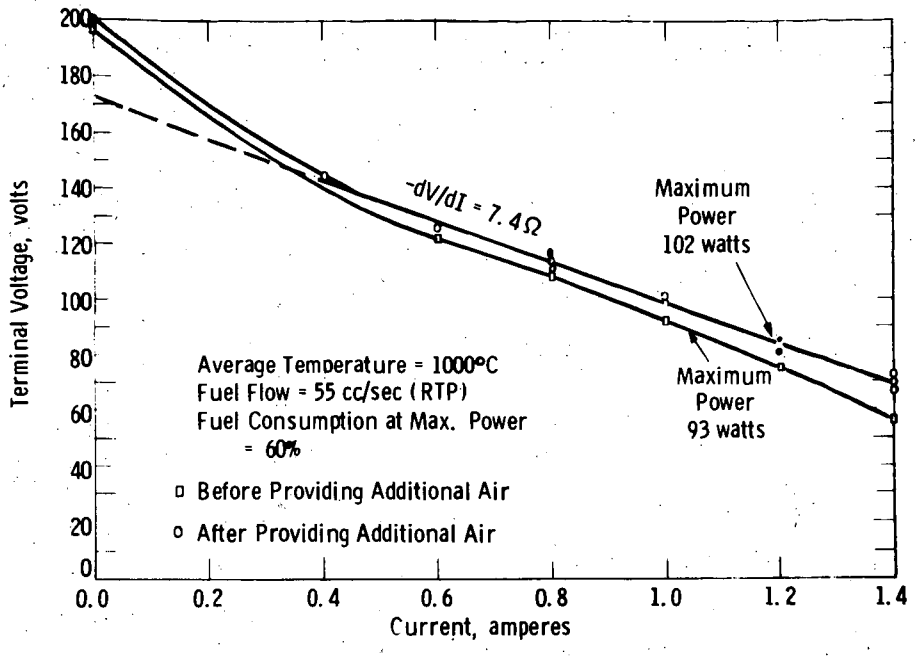

Fig. 16—100-watt battery performance before and after increasing air flow

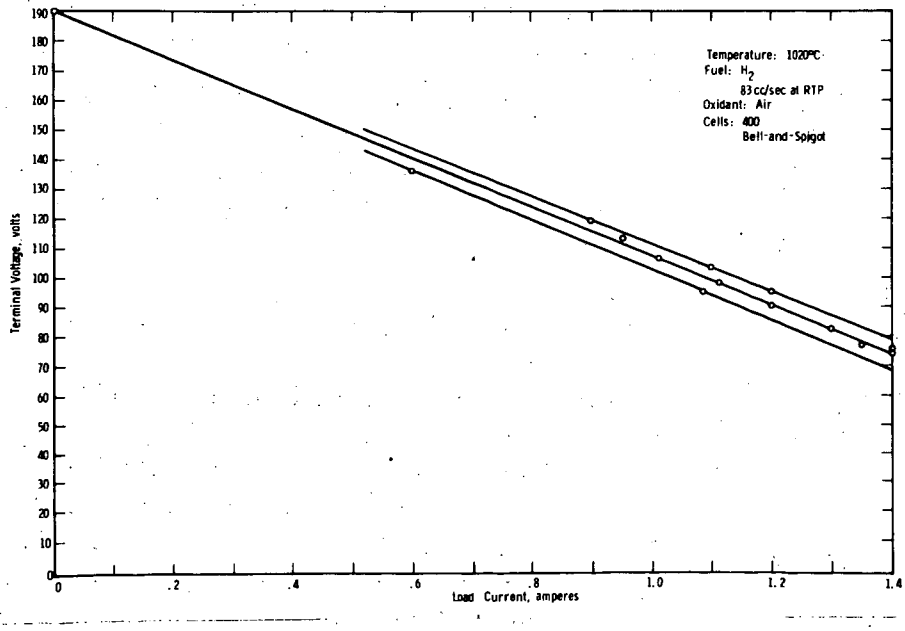

Fig. 17—Performance of 100-watt solid-electrolyte fuel-cell power system

ALCOHOL AIR FUEL CELLS - DEVELOPMENT AND APPLICATION

W. Vielstich

Institut für Physikalische Chemie der Universität Bonn

INTRODUCTION

Taitelbaum (1) in 1910 was the first to convert the chemical energy of liquid fuels (e.g. petroleum, stearic acid and starch) in a galvanic cell into electricity. But the use of fuels like alcohols or aldehydes was proposed many years later by Kordesch and Marko (2) and by Justi et al (3).

Kordesch and Marko studied the system formaldehyde/air. The cell with the alkaline or acid electrolyte contains an oxygen diffusion electrode and a porous fuel electrode. The fuel or fuel/electrolyte mixture penetrates the fuel electrode from the back. In this manner an enlargement of the two phase boundary is obtained. Moreover, under proper operating conditions the fuel concentration is relatively small in the vicinity of the oxygen electrode, even if no diaphragm is used. This is particularly important if the oxygen electrode contains a metal which catalyses the fuel reaction.

In an other method of construction the alcohol is dissolved in the electrolyte and both electrodes dip into the fuel-electrolyte mixture (3,4).

The use of liquid fuels in general obviates the need for a three-phase boundary, and thus facilitates the construction of the fuel electrode. An additional advantage is that the fuel can be brought to the catalytic electrode in high concentration. Thus, if the reaction is fast enough, high current densities can be obtained (up to 1 A/cm^2 at room temperature). Such battery systems can be used conveniently for maintenance-free, continuous operation if air at ambient temperature and pressure is supplied to the oxygen electrode. Some examples of this type of fuel cell are discussed in the following.

METHANOL AIR CELL FOR OPERATION AT LOW CURRENT DENSITIES

General Remarks

In recent experiments (5,6) it has been shown, that the anodic oxidation of methanol proceeds via formaldehyde, and formate or formic acid respectivly. On open circuit at platinum metal electrodes one observes a hydrogenation/dehydrogenation-equilibrium (7), while under load also methanol is not electrochemically active itself. At potentials $\varphi <$ + 400 mV versus the H_2 potential in the same solution a preliminary dehydrogenation takes place. At more positive potentials the fuel reacts with the oxygen which has been chemically adsorbed by the electrode surface (8,9). Therefore, a suitable combination of catalyst, electrolyte and temperature has to be arranged to obtain the required current density in the desired potential range over the total oxidation up to CO_2 or CO_3^{--} respectively. In this connection two problems have to be solved when using an alkaline solution, which is the most suitable electrolyte for practical cells.

(i) An appreciable enrichment of formate has to be avoided: the use of mixed platinum and palladium catalysts is one possible solution (10).

(ii) The electrode polarization increases with the concentration of CO_3^{--}-ions at current densities $j > 5 - 10$ mA/cm^2 at 20 - 50°C (11). To obtain a flat voltage/time curve over the total capacity of 6 electrons per molecule (i.e. $CH_3OH + 8\ OH^- \longrightarrow CO_3^{--} + 6\ H_2O + 6\ e^-$), the critical current density should not therefore be exceeded.

Experimental Results with Laboratory Cells

For the investigation in the laboratory glass vessels containing 1 liter of electrolyte/fuel mixture (10 N KOH and 4.5 M methanol) were used. KOH is used because cells with NaOH have higher polarizations, particularly on the oxygen side. The KOH concentration is chosen in such a manner that even after complete reaction of the fuel the OH^--concentration will be 1 - 2 molar.

Platinum on a porous carrier was found to be a better catalyst than Raney-nickel. Up to now 2 - 5 mg Pt/cm^2 have been used. At this fuel electrode the oxidation potentials for methanol and formate up to current densities of 5 mA/cm^2 are about the same. So the formate content of the electrolyte when using methanol as fuel is very low. This results in a flat voltage-time curve (see Fig. 1).

Since, for the intended application (see below), only a few mA/cm^2 are needed, porous carbon without metallic additions is used on the oxygen side. Plate-like or cylindrical electrochemically active carbon electrodes (surface area: 250 cm^2) are made hydrophobic with polyethylene dissolved in benzene to such a degree that the methanol/electrolyte mixture will not penetrate through the electrode even after 10.000 hours (the thickness of the electrode plates is 5 - 10 mm).

The EMF of this methanol/air cell is about 0.9 volt; at a current drain of 0.5 amp the terminal voltage is 0.75 - 0.6 volt. For short periods of time 2 amps can be withdrawn at 0.6 - 0.5 volt. The long term experiments are performed taking into consideration that the end use will be periodic loads (2 seconds at 0.5 amp and 4 seconds O.C.). The periodic current interruption not only makes the diffusion of air easier but it also increases the life time and preserves the activity of the fuel electrode.

Typical discharge curves are shown in Fig. 1. The difference between theoretical and experimental current yields can be explained on the basis of analysis of the electrolyte by evaporation of methanol through the porous carbon. The analysis also shows that the diffusion of CO_2 from the air through the carbon can be neglected.

The influence of temperature on the oxidation rate at constant electrode potential is very pronounced. Current density-potential plots obtained after operation for one day at 10 mA/cm^2 are given in Fig. 2.

Discussion

The special feature of a methanol/air cell as described above is a high Ah-capacity per unit volume or per unit weight: 5.000 Ah/litre methanol, up to 1.000 Ah/l fuel-electrolyte mixture, or about 3 kg/kWh for an operating time 6.000 hours.

The experimental results reveal, however, the following disadvantages:

(i) The current densities at the fuel electrode at ambient temperatures are relatively low, if small amounts of noble metal catalysts are used.

(ii) The vapour pressure is unfavourable for moderate temperature applications.

(iii) With decreasing temperature the power output of the cell drops considerably.

FORMIC ACID AND FORMATE AS FUEL

Anodic oxidation of formic acid, nature of the intermediate product

In acid electrolytes methanol and formaldehyde are less reactive than formic acid (9,12,13). The oxidation rate at potentials $\varphi <$ 0.6 volt (vs. SHE) is determined by the poisoning effect of an intermediate product. The particles adsorbed at a Pt-electrode are probably formate radicals and certainly not carbon monoxide or oxalic acid (14). A potentiostatic potential scan is especially suited to give a qualitative view of the reaction mechanism. Fig. 3 shows three current peaks during the anodic scan. The first maximum is due to the reaction step (14)

$$HCOOH_{ad} \longrightarrow HCOO_{ad} + H^+ + e^- \quad \text{or}$$

$$HCOOH_{ad} \longrightarrow COOH_{ad} + H^+ + e^-$$

In the region of the second and third peaks the fuel reacts with chemisorbed oxygen as described above for the methanol oxidation. The adsorbed intermediate too is oxidized in this potential range. Fig. 4 clearly demonstrates the poisoning

effect of the adsorbed product on a smooth platinum electrode at 0.5 volt.

Application of a mixed Pt/Ru-catalyst

Recently Frumkin (15) has discovered that the use of a mixed platinum ruthenium catalyst diminishes the poisoning effect. This has been confirmed by the following experiment. An active carbon electrode (geom. surf. 24 cm^2, 12 mg Pt-metal/cm^2) was prepared (a) with 3 % Pt (b) with 3 % Pt/Ru (9:1) ratio by weight. The current densities observed at the two electrodes at 0.5 volt were for electrode (a) 2 mA/cm^2 and for electrode (b) 10 mA/cm^2. In a long duration experiment with an HCOOH/air cell (50cm^2 electrodes, 20°C) the ratio of power outputs using the two types of electrode was about 3. The current yield which is about the same for the two cells is surprisingly low, less than 20 % on a 2 electron/molecule basis.

Formate ion-oxidation on mixed noble metal catalysts

In early investigations of the anodic oxidation of methanol in alkaline solution with Raney-nickel (9) or platinum (6,10) electrodes formate ion was usually found as the primary oxidation product. The further oxidation of the formate ions occured at a less favourable potential. Grimes and Spengler (10), however, have observed that the use of mixed platinum and palladium catalysts allows the complete oxidation of methanol to carbonate. A formate ion/oxygen fuel cell with a nickel substrate as anode (9 mg Pd/Pt (5:1)/cm^2) produced twice the power output of a similar methanol cell at the same temperature.

These results demonstrate that the oxidation rate of formate ions is very sensitive to the composition and the structure of the metal catalyst. Moreover, the electrocatalytic effects are different for formate ion and methanol.

Our studies have shown that the formate oxidation rate on platinum and palladium alloys varies over more than two orders of magnitude. The formate oxidation has been investigated on a series of smooth metal electrodes by use of the potentiostatic scanning method. An example of the current voltage dia-

grams obtained in 6 N KOH + 4 M HCOOH is given in Fig. 5. The height of the high anodic current peak (during the anodic scan) is taken as measure of the catalytic activity of the metal. The activity of the metal surface is controlled by the potential range covered and the scanning speed (100 mV/sec). Fig. 6 shows the strong influence of the electrode material on the peak current density for 20 and 40°C.

The relationship between electrode material and current density obtained offers of course only a first insight into the selection of the most suitable catalyst. In battery practice one has to deal with porous electrodes and continuous discharge. Therefore factors other than metal composition are also important.

In preliminary tests of formate ion/air cells about 10 times the power output compared with methanol as fuel has been observed. Continuous discharge at 20 mA/cm^2 at 20°C is readily obtained.

Discussion

By use of mixed Pt/Ru-anode catalysts the power output of a HCOOH/air cell at ambient operating conditions is of the same order as that of an alkaline methanol/air cell. The reaction product of the formic acid cell is CO_2 and therefore electrolyte renewal is not required. On the other hand one needs for both electrodes noble metal catalysts. Another disadvantage is the high rate of the current-less decomposition. The influence of the current density on the reaction yield has not yet been investigated.

Due to the moderate current densities at ambient temperature and pressure the formate ion/air cell with mixed Pt-metal catalysts at the fuel electrode offers a new field of applications. In contrast to methanol the vapour pressure is low, so that operating temperatures up to 100°C can be used. Compared to methanol, however only 2 electrons per molecule are obtainable.

EXPERIMENTS WITH GLYCOL AS FUEL

In acid electrolytes the anodic oxidation of glycol leads to CO_2 as end product. The working potential is, however, less favourable than with formic acid as fuel (9). The oxidation at alkaline pH results in the formation of oxalate. But at moderate temperatures (60 - 90°C) a strong dehydrogenation takes place

$$CH_2OH\text{-}CH_2OH + 2\ OH^- \longrightarrow C_2O_4^{--} + 8\ H_{ad}$$
$$8\ H_{ad} + 8\ OH^- \longrightarrow 8\ H_2O + 8\ e^-$$

and current densities up to 600 mA/cm^2 can be obtained (9,16).

Grüneberg et al (9,16,17) have developed a glycol/air cell operating at ambient temperature and pressure.

The air electrode was pressed from activated carbon and polyethylene powder (500 kg/cm^2, 160°C) and built up in two layers. The layer on the electrolyte side was made only weakly hydrophobic and contained Ag_2O as catalyst. The electrode had such good mechanical stability that it could be used as an end plate in the cell. Between the air electrodes there is a fuel electrode of the same size: coarse grained Ni-DSK (3) is held in place by nickel screens.

The open circuit potential of such a cell (6 N KOH + 2 M glycol) is about 1.1 volt. At a load of 3 mA/cm^2 such a cell will have a potential of 0.8 volt at room temperature. For short periods of time current densities up to 30 mA/cm^2 can be withdrawn.

For the investigation of high current density glycol/air cells we have used as fuel electrodes, flame-sprayed Raney-nickel on a nickel substrate. Electrodes up to a geometric area of 20 x 30 cm^2 have been studied. As already stated by Boies and Dravnieks (18) the activity of the electrode is critically dependent on the grain size, and the substrate must be carefully prepared to obtain good and stable contact to the catalytic layer. The increase of the dehydrogenation rate with temperature has a strong influence on the shape of the current/voltage-curve (Fig. 7).

The featuresof the glycol cell operating at moderate temperatures are:

noble metal catalysts are not required, high current densities can be obtained in direct oxidation from an easily handled liquid fuel, and strong gas evolution does not take place. The price of the fuel and the necessary renewal of the electrolyte are the main disadvantages.

APPLICATIONS OF ALCOHOL AIR/CELLS

General Remarks

Ambient air cells with methanol or formate ion as fuel are particularly suited for a maintenance-free, continuous operation at low or moderate current densities. Therefore they could be used to supply signal devices, stationary or mobile communication systems, isolated weatherstations etc. Such alcohol/air cells can start to compete with dry batteries and wet batteries of the system zinc/NaOH/air.

The high power glycol cell should be applicable e.g. as an emergency unit. In contrast to such a fuel cell the presently used Diesel engine has several disadvantages:
it requires maintenance, unreliability of the rotating parts, uncertain starting in an emergency.

Beside battery construction cost, fuel cost and availability, the amount of noble metal used for the electrodes is a peculiar problem in commercial fuel cell application. In the alkaline methanol and formate cells developed so far 2 - 5 mg/cm^2 platinum and palladium are needed. To what extend this amount has to be decreased to make such cells economic depends very much on the special application.

Test of a 60 Watt methanol/air battery for sea buoys

On the basis of our laboratory investigations described above Brown, Boveri a. Cie. have built a 6 volt 10 amp battery for a flashing buoy. The module contains 10 cylindrical cells (Fig. 8). In each cell 18 pairs of electrodes are connected in parallel in order to equalize the different performance of the individual cells and to prevent the failure of single electrodes. From the 400 litre fuel/electrolyte-mixture 180 kWh

can be obtained. By using an electronic device the power output of the battery is stabilised (30 Watt in signal operation between 5 and 30°C) against changes of temperature and changes in fuel concentration which occur over a two years period of operation (intermittend 2 sec load, 4 sec O.C.).

The battery is presently in field test for serveral months. It is felt that the operation cost (methanol and caustic) will be cheaper than the present propane-consuming buoys.

Literature

1. I. Taitelbaum, Z. Elektrochem. Ber. Bunsenges. physik. Chemie 16, 295 (1910)
2. K. Kordesch and A. Marko, Oesterr. Chemiker Zeitung 52, 125 (1961)
3. E. Justi and A. Winsel, "Fuel Cells - Kalte Verbrennung", Steiner, Wiesbaden, 1962
4. M. Janes, Trans. Electrochem. Soc. 77, 411 (1940)
5. M.J. Schlatter, Symposium Amer. Chem. Soc. Chicago 1961, B 149
6. O. Bloch, P. Degobert, M. Prigent and J.C. Balaceanu, 6th WPC Frankfurt 1963, Section VI-paper 3 - Pd 10
7. A.N. Frumkin and B.I. Podlovchenko, Ber. Akad. Wiss. UdSSR 150, 349 (1963)
   V.S. Bagotzky and Y.B. Vasiljev, Electrochim. Acta (London) 8, 869 (1964)
8. W. Vielstich, Chem. Ing. Techn. 35, 362 (1963)
   A. Kutschker and W. Vielstich, Electrochim. Acta (London) 8, 985 (1963);
   J. Giner, Electrochim. Acta 9, 63 (1964)
9. W. Vielstich, "Brennstoffelemente - Moderne Verfahren zur elektrochemischen Energiegewinnung", Verlag Chemie, Weinheim, 1965
10. P.G. Grimes and H.M. Spengler, ECS-Meeting, Washington 1964, Battery Div. Ext. Abstr. No. 27
11. J.N. Murray and P.G. Grimes, "Methanol Fuel Cell", Res. Div. Allis Chalmers, Milwaukee, 1963
12. W. Vielstich, Chem. Ing. Techn. 35, 362 (1963)
13. R. Jasinski, J. Huff, S. Tomter and L. Swette, Ber. Bunsenges. physik. Chemie 68, 400 (1964)

14. W. Vielstich and U. Vogel, Ber. Bunsenges. physik. Chemie 68, 688 (1964)

15. A.N. Frumkin, paper presented at the 4th Intern. Symp. on Batteries, Brighton, 1964

16. H. Spengler and G. Grüneberg, Dechema Monogr. 38, 579 (1960)

17. G. Grüneberg and M. Jung, BPA 592 862

18. D.B. Boies and A. Dravnieks, Elektrochem. Techn. 2, 351 (1964)

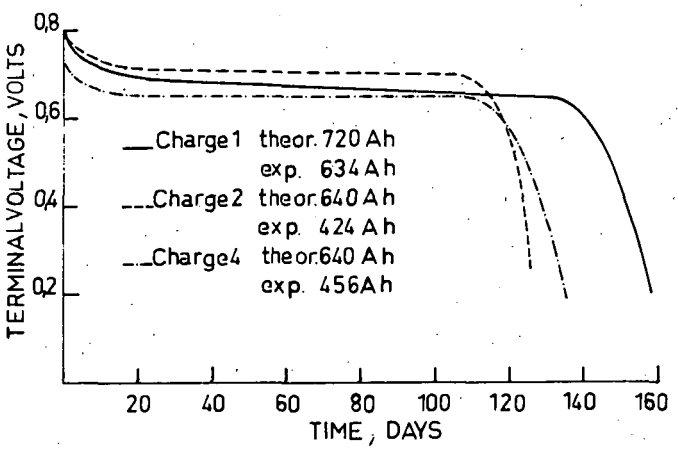

Fig. 1 Terminal voltage at periodic loads (2 sec load and 4 sec O.C.) of a methanol/air cell, operating time $\tau >$ 12.000 hours with 4 electrolyte charges, temperature 10 - 20°C

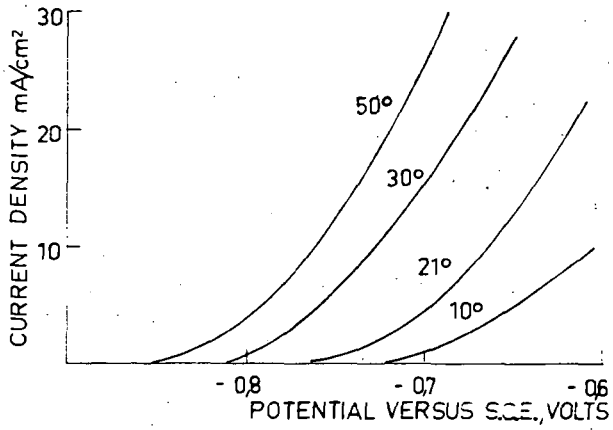

Fig. 2 Effect of temperature on the performance of a platinum activated carbon electrode in 6 N KOH + 2 M CH_3OH solution, F = 12 cm^2, 4.8 mg Pt/cm^2; curves taken after 1 day operation at 10 mA/cm^2

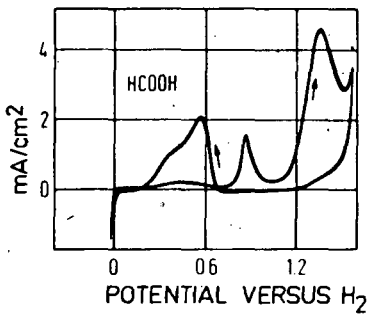

Fig. 3 Triangular potential scan on smooth Pt in 1 N H_2SO_4 + 1 M HCOOH, 50 mV/sec, 20°C

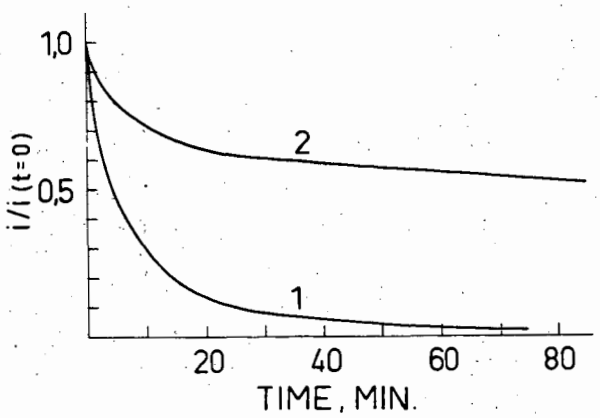

Fig. 4 Decrease of current with time on smooth Pt in 1 N H_2SO_4 + 1 M HCOOH at constant potential
(1) at 0.5 volt (first current peak in Fig. 3)
(2) at 0.9 volt (second peak in the anodic scan of Fig. 3)

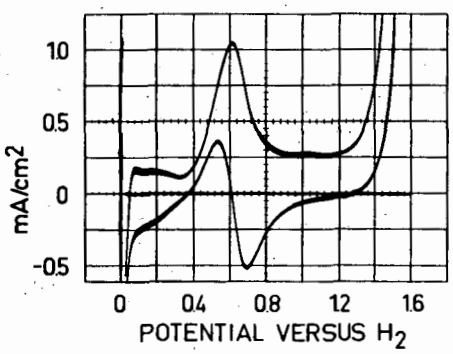

Fig. 5 Triangular potential scan on smooth Pt/Ir (75:25)-alloy in 6 N KOH + 4 M HCOOK, 100 mV/sec, 40°C

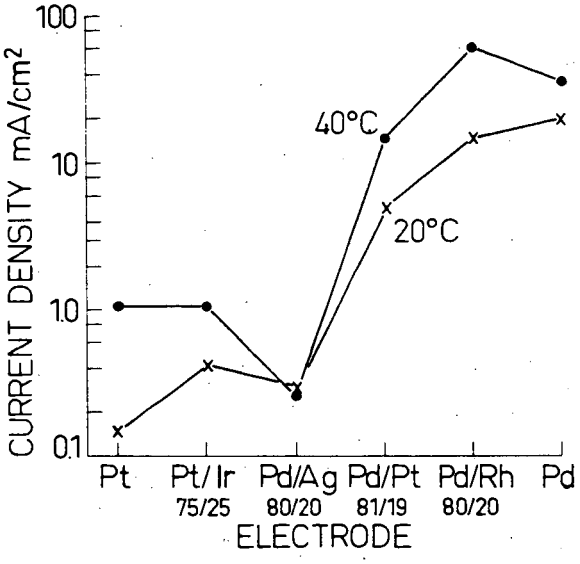

Fig. 6 Peak current density of a triangular potential scan according to Fig. 5 on different smooth metal electrodes in 6 N KOH + 4 M HCOOK

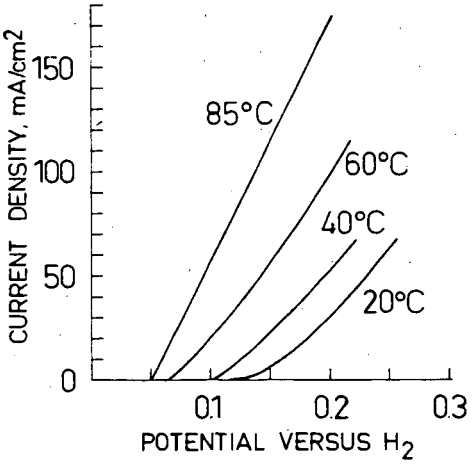

Fig. 7 Current density-potential curves on flame sprayed Raney-nickel (grain size 200 μ) in 6 N KOH + 2 M Glycol, plots taken after 2 day operation at 50 mA/cm^2

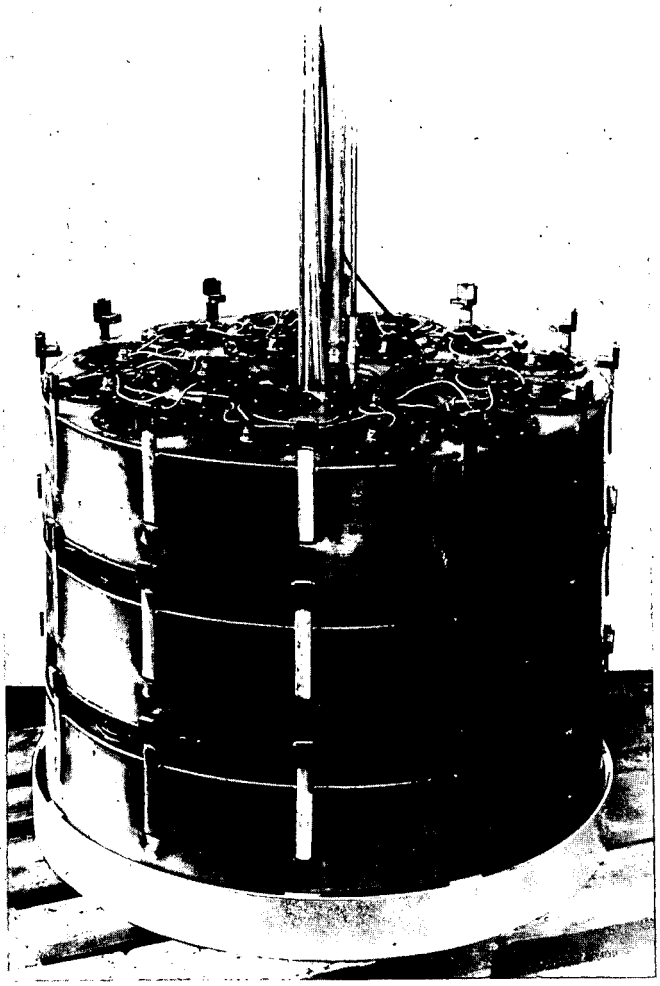

Fig. 8 Three cells of a 10 cell 60 Watt-methanol/air battery with cylindrical air diffusion electrodes for a flashing sea buoy
(by courtesy of Brown, Boveri and Cie., Baden/Schweiz)

The Anodic Oxidation of Methanol on Raney-Type Catalysts of Platinum Metals

A. Binder, A. Köhling, G. Sandstede

Battelle-Institut e.V., Frankfurt/Main, Germany

1. INTRODUCTION

For a couple of years methanol has played an important part in fuel cell research and development. It has proved to be the only alcohol that can be completely oxidized to carbon dioxide and water in a fuel cell operating with an aqueous alkaline electrolyte at temperatures below 100°C and a platinum catalyst (1). The disadvantage of a fuel cell system of this type is the consumption of the alkaline electrolyte due to formation of the carbonate. Therefore, acid electrolytes would be more desirable; however, on platinum the oxidation of methanol requires a much higher overvoltage in acids than in alkaline solution.

It has been the objective of these investigations to develop a suitable catalyst which does not require the large overvoltage during the anodic oxidation of methanol. From our previous investigations (2) it was concluded that there might be a more active catalyst among the group of platinum metals and their alloys and that the Raney method might be suitable for preparation of alloy catalysts at low temperatures.

2. EXPERIMENTAL CONDITIONS

In our comparative appraisal of the catalysts we used electrodes of the type described in an earlier communication (3). Accordingly, it contained the Raney catalyst in a gold skeleton to which sodium chloride was added for formation of macropores. The proportion of catalyst was kept constant with all electrodes. The catalysts were prepared in situ from Raney alloys of type $PtAl_4$ or $A_{0.5}B_{0.5}Al_4$ by treatment with potassium hydroxide solution in the preformed electrode disk. In separate experiments following the periodic potential sweep method the electrochemically active surface area of the catalyst of such a test electrode was determined to be about 35 sq.m. per g. in the case of platinum. X-ray diffraction measurements for the example of the ruthenium-platinum catalyst showed a solid solution of ruthenium in platinum which is not quite homogeneous but still contains proportions of free ruthenium.

The electrolyte was 5 N potassium hydroxide solution and 4.5 N sulfuric acid (reagent grade: "pro analysi", E. Merck, Darmstadt). In all experiments the methanol was used in a

concentration of c = 2 mole/liter (reagent grade of methanol: "pro analysi", E. Merck, Darmstadt).

The electrochemical measurements were made in the half-cell arrangement likewise described previously (3) according to the galvanostatic method. The current densities reported in this paper refer to the projected surface area and the potential relates to a hydrogen electrode in the same solution. The ohmic drop between Luggin capillary and electrode was not accounted for.

The plots were taken first at decreasing and then at increasing current densities. This implies that a certain proportion of the reaction products was present in the electrolyte.

3. RESULTS

3.1 Measurements in 6.5 N KOH Solution

Figures 1 and 2 show the differences in the catalytic behavior of platinum metals in the oxidation of methanol in 5 N potassium hydroxide at 25°C and 80°C, respectively. Measurements on electrodes with Raney gold serve for reference.

It is noted that two platinum metals at a time show a similar activity. The three groups thus obtained conspicuously correspond to the dyads

Ru	Rh	Pd
Os	Ir	Pt

of the platinum metals in the Periodic Table. Osmium and ruthenium, and also gold are found to be unsuitable as fuel cell catalysts, since there will not be a constant potential at high polarization. At 80°C, however, polarization with respect to the potential at a current density of 50 mA/cm^2 which is reasonable in fuel cell operation, does not exceed that measured on iridium and rhodium.

3.2 Measurements in 4.5 N Sulfuric Acid

3.2.1 Pure Platinum Metals

In sulfuric acid polarization with all platinum metals is much larger than in potassium hydroxide solution. Particularly striking is the increased polarization in the case of palladium at 25°C (Fig. 3), which even at comparatively small current densities reaches a potential range where corrosion occurs.

Even at 80°C (Fig. 4) palladium shows only slightly lower polarization so that this metal is the least active catalyst in the conversion of methanol in sulfuric acid, whereas osmium,

featuring only low conversion at 25°C, is the most active catalyst among the platinum metals. If the potential at a current density of 50 mA/cm^2 is taken as a measure for the "activity" of the electrode and thus of the catalyst, the order at 80°C is as follows: Os > Ir = Ru > Pt > Rh > Pd.

In sulfuric acid the platinum metals do not form three groups as has been observed in the conversion of methanol in potassium hydroxide solution.

3.2.2 Alloys of Platinum Metals

The experimental results on pure platinum metals suggest that catalysts of the lowest activity are found among the palladium alloys. Figures 5 and 6 depict the potential/current density curves of alloys of palladium with the addition of one of the other platinum metals (50 atomic per cent).

A distinct increase in the activity is observed by the addition of the second component. Worth noting is the effect of ruthenium which at a current density of 50 mA/cm^2 and 80°C (Fig. 5) results in a decrease in polarization by 280 mV and 25°C even causes a decrease by 300 mV(Fig. 6). It should be borne in mind that pure ruthenium proved almost inactive at 25°C.

It now turns out that the most active catalysts are found especially among alloys containing ruthenium (Figs. 7 and 8). A combination of pronounced activity is obtained by a ruthenium-platinum alloy. At a current density of 50 mA/cm^2 and at 80°C (Fig. 7) such a Raney ruthenium-platinum electrode shows a potential of 230 mV. Even at 25°C (Fig. 8) the corresponding potential does not exceed 400 mV. These values for the polarization are only about 50 mV higher than the corresponding values for the most active catalyst in potassium hydroxide solution, viz. platinum.

This Raney ruthenium-platinum catalyst is the most active of all platinum metal alloys evaluated. This is illustrated by Table 1 which summarizes the potentials of all alloy catalysts of the composition A50B (atomic per cent) and confronts them with those of the pure metals, as observed at a current density of 50 mA/cm^2 and temperatures of 25°C (lower values) and 80°C (upper values).

Next in the activity scale ranges the osmium-platinum alloy. A very low activity at 80°C is registered not only for palladium-gold but also for palladium-rhodium.

Our test electrode consisting of Raney ruthenium-platinum on a gold skeleton enabled current densities of at least

5000 mA/cm^2 to be reached (Fig. 9), the potential remaining constant for extended periods of time. At a current density of 2000 mA/cm^2 the potential did not increase by more than 20 mV within 600 h (Fig. 10), provided that the concentration of methanol was kept approximately constant.

Ruthenium-platinum electrodes can also be used in the oxidation of methanol in a potassium bicarbonate electrolyte from which the resultant carbon dioxide gas escapes. Also in this case polarization is much lower than in the case of platinum as catalyst (Fig. 11).

Figure 12 shows the potential of electrodes with Raney platinum metal catalysts at 80°C and a current density of 50 mA/cm^2 as a function of the composition of the catalyst. It is worth noting that in most cases the potential reaches a minimum only with catalysts where the two components are present in about equal proportions, whereas in gas-phase reactions a synergistic effect is often caused even by minute additions. Attention is also called to the fact that an addition of rhodium to palladium hardly affects the potential within a comparatively wide range.

Discussion

The order of the activity of platinum metals in the oxidation of methanol in potassium hydroxide solution determined by our measurements is Pt $\succ$ Pd $\succ$ Ru = Rh $\succ$ Ir $\succ$ Os $\succ$ Au and thus varies from the order Pd $\succ$ Rh $\succ$ Au $\succ$ Pt reported in an earlier publication (4). Particularly striking is the extreme discrepancy in the case of platinum, which may possibly be explained by the fact that Tanaka (4) - in contrast to us - used the smooth metals. In addition, it has to be borne in mind that catalysts prepared by the Raney method contain aluminum in varying proportions (order of magnitude from 0.1 to 1 %), which may have a bearing on the activity.

In acid solutions, too, the order of the activity of platinum metals Os $\succ$ Ru = Ir $\succ$ Pt $\succ$ Rh $\succ$ Pd as determined by us varies from that reported by earlier authors (5). However, Breiter's values (5) are non-stationary values, since they were derived by the periodic potential sweep method. These measurements do not involve enrichment of intermediates in the electrolyte to such an extent as would always be encountered in fuel cell operation (6), (7).

Since the consecutive products of the oxidation of methanol continue to react at different rates in the presence of the different platinum metals, the enrichment varies from one metal to the other. Formic acid, for example, in contact with Raney platinum in alkaline electrolytes is oxidized more slowly than methanol, but more rapidly in the acid medium. In

contact with Raney palladium, on the other hand, formic acid reacts at a higher rate than methanol even in the alkaline electrolyte (3). Owing to this enrichment of the consecutive products all methanol electrodes act as multiple electrodes so that the measured potentials are mixed potentials.

Because of these difficulties there is still some doubt about the oxidation mechanism of methanol, and this applies even to platinum, a material often examined thoroughly in extensive investigations. The differences in the activity of platinum metals in sulfuric acid as found by our measurements encourage us to make the following speculations:

As the activity drops in the order Os > Ru = Ir > Pt > Rh > Pd, the paramagnetic susceptibility of the metals qualitatively rises in almost the same order (cf. Table II); palladium with the largest susceptibility value is the least active catalyst.

Table II: Paramagnetic Susceptibility of Platinum Metals (10^{-6} cgs)

Ru	Rh	Pd
43.2	111	567
Os	Ir	Pt
9.9	25.6	202

Since the paramagnetism of platinum metals results from unpaired d-electrons - the very high value for palladium is connected with quasi-ferromagnetic regions (8), (9) - it is not unreasonable to assume a relationship between paramagnetic susceptibility and catalytic activity.

Even for the activity of alloys of platinum metals such a tendency can be qualitatively deduced: the addition of rhodium to palladium improves the activity but slightly up to an amount of 50 at. %, whereas the addition of ruthenium has a favorable effect (Fig. 12). With respect to susceptibility (Fig. 13), the addition of small quantities of rhodium results in a minor increase, and only additions of larger quantities effect a decrease (10). Addition of ruthenium, even in low concentrations, reduces the susceptibility significantly (11).

The synergistic effect on the anodic oxidation of methanol observed with ruthenium-platinum alloys might be ascribed to an optimum value of susceptibility leading to optimum sorption of all reactants. Since quantitative values for the paramagnetic susceptibility of our alloys are not yet available, the speculative nature of this statement is emphasized once more. Evidence for relatively weak sorption is provided by

the fact that intermediates of the anodic oxidation of higher or multivalent alcohols are desorbed by ruthenium-platinum to such an extent that they condense to form brown-black products (12).

Hence, ruthenium-platinum alloys are almost specific for the conversion of methanol and its consecutive products, but these catalysts have also been found superior to platinum in other reactions (13), (14). Even in the oxidation of methanol the consecutive product - formaldehyde - is desorbed more easily than in conversions on platinum so that in coulometric measurements according to those described in (1) complete conversion to carbon dioxide and water is not obtained at a temperature of 80°C unless formaldehyde is not allowed to escape (12).

In the meantime further references on the excellent properties of platinum-ruthenium catalysts in the anodic oxidation of methanol have been mentioned (15). The catalyst described in these publications has been prepared according to Brown's method (16) by reduction of suitable salts with sodium borohydride.

The experimental results available now show characteristic differences among the binary alloys of the platinum metals as concerns the activity in the anodic oxidation of methanol in acid medium. Some reveal a synergistic effect whereas others not even show an addition of the activity as a function of composition. This dissimilar behavior might be due to the differences in the galvano-magnetic properties of the alloys. Further data are necessary for a quantitative explanation of the phenomena observed.

Acknowledgment

This work was conducted under a contract and in co-operation with the Robert Bosch GmbH, Stuttgart, Germany. Its permission to publish these results is gratefully acknowledged. We greatly appreciate the interest and the valuable suggestions by Drs. Herrmann, Ilge, Jahnke, Neumann and Simon, members of the sponsoring company. Furthermore we wish to acknowledge the valuable assistance of Miss K. Spurk and Mr. K. Richter, members of Battelle-Institut, Frankfurt (Main), Germany.

Literature Cited

(1) H. Binder, A.Köhling and G.Sandstede, paper presented at ACS meeting, New York, 1963; Advances in Chemistry Series 47,283(1965)

(2) H.Krupp, H.Rabenhorst, G.Sandstede, G.Walter and R.McJones, J.electrochem.Soc. 109,553(1962)

(3) H.Binder, A.Köhling, H.Krupp, K.Richter and G.Sandstede, paper presented at ACS meeting, New York, 1963; Advances in Chemistry Series 47,269(1965).
(4) S.Tanaka, Z.Elektrochem. 35,38(1929)
(5) M.W.Breiter, Electrochim.Acta 8,973(1963)
(6) M.Prigent, O.Bloch and J.-C.Balaceanu, Bull.Soc.Chim. France, 1963, p.368
(7) M.J.Schlatter, in "Fuel Cells" (G.J.Young,ed.), p.190, Reinhold, New York, 1963
(8) N.F.Mott, Proc.physic.Soc. 47,571(1935)
(9) E.C.Stoner, Proc.Roy.Soc.London (A)154,656(1936)
(10) D.W.Budworth, F.E.Hoare and J.Preston, ibid. 257,250 (1960)
(11) W.Köster and D.Hagmann, Z.Metallkunde 52,721(1961)
(12) H.Binder, A.Köhling and G.Sandstede, publication in progress
(13) A.Amano and G.Parravano, Advan.Catalysis 9,716(1957)
(14) D.W.McKee and F.J.Norton, J.Phys.Chem. 68,481(1964)
(15) C.E.Heath, Proc. 18th Ann.Power Sources Conf., May 1964, p.33
(16) H.C.Brown and C.A.Brown, J.Am.Chem.Soc. 84,1493(1962)

2M CH_3OH
4.5N H_2SO_4; 80°C
50 ma/cm²

	Ru						
Ru	350 / >900	Rh					
Rh	300 / 500	420 / 540	Pd				
Pd	290 / 490	520 / 580	570 / 800	Os			
Os	290 / >900	320 / 540	340 / 720	320 / 880	Jr		
Jr	300 / 440	380 / 520	400 / 580	350 / 500	350 / 560	Pt	
Pt	230 / 400	330 / 510	480 / 610	250 / 440	290 / 490	370 / 540	Au
Au	310 / >900	460 / 580	650 / 780	400 / >900	300 / 540	380 / 580	>900 / >900

Table I Potentials at alloy catalysts (50 atomic %) with methanol in 4.5 N H_2SO_4 at 25°C (lower figures) and 80°C (upper figures); current density: 50 ma/sq.cm.

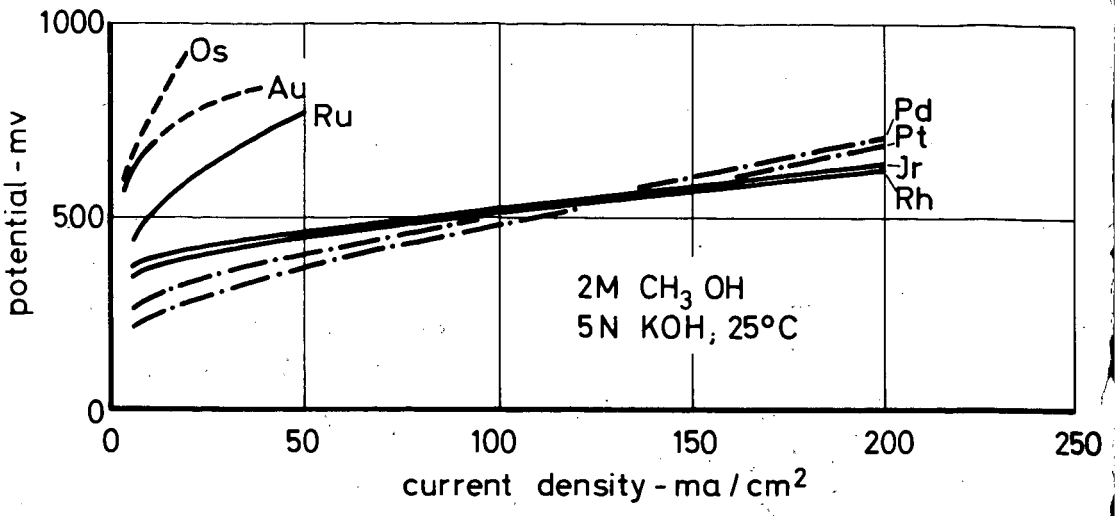

Fig. 1 Potential/current density plots of electrodes containing Raney platinum metals with methanol in 5 N KOH at 25°C

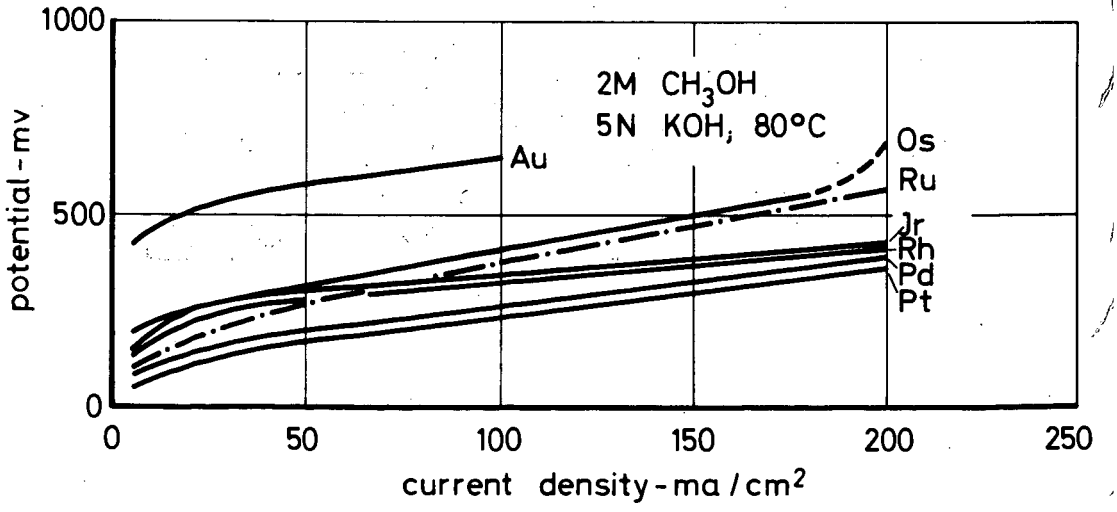

Fig. 2 Potential/current density plots of electrodes containing Raney platinum metals with methanol in 5 N KOH at 80°C

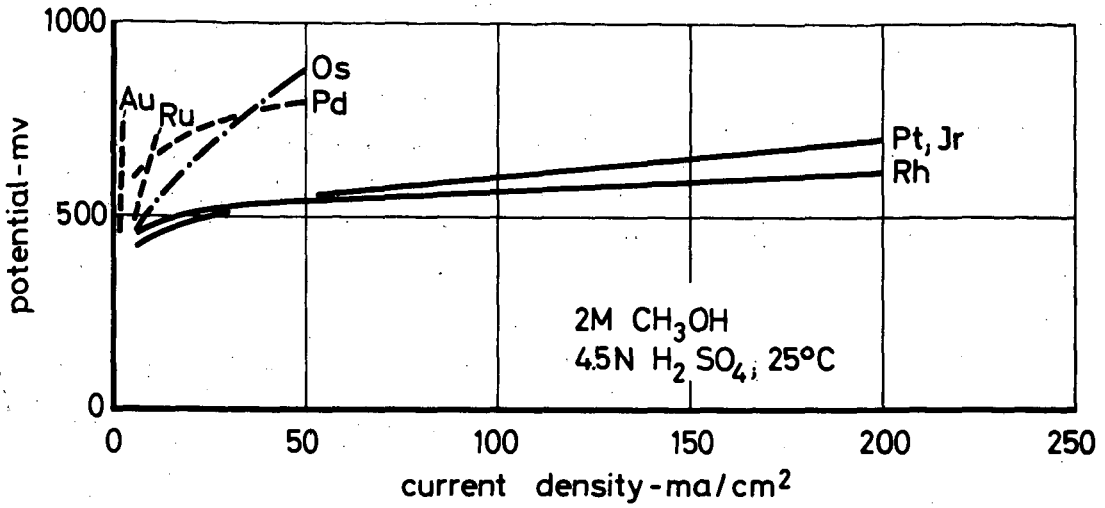

Fig. 3 Potential/current density plots of electrodes containing Raney platinum metals with methanol in 4.5 N H_2SO_4 at 25°C

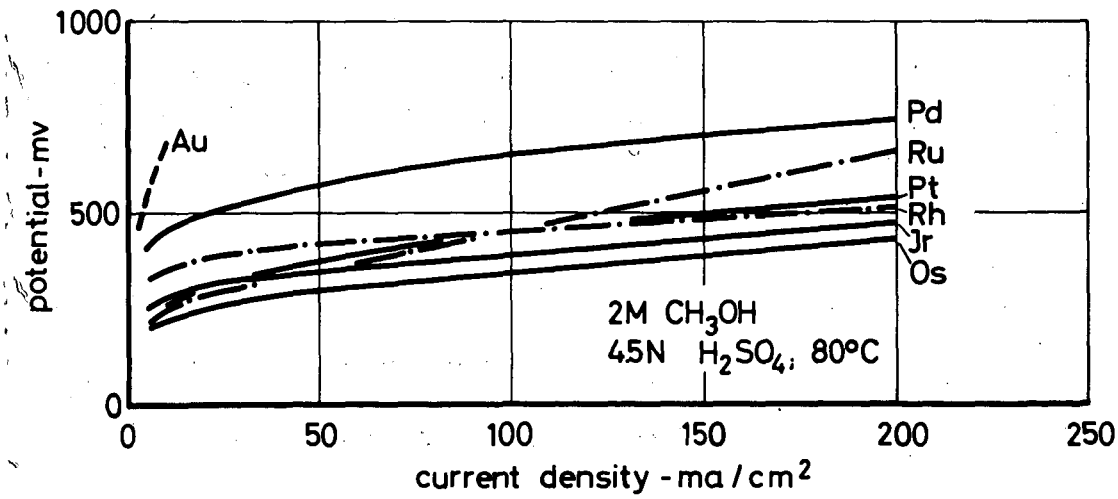

Fig. 4 Potential/current density plots of electrodes containing Raney platinum metals with methanol in 4.5 N H_2SO_4 at 80°C

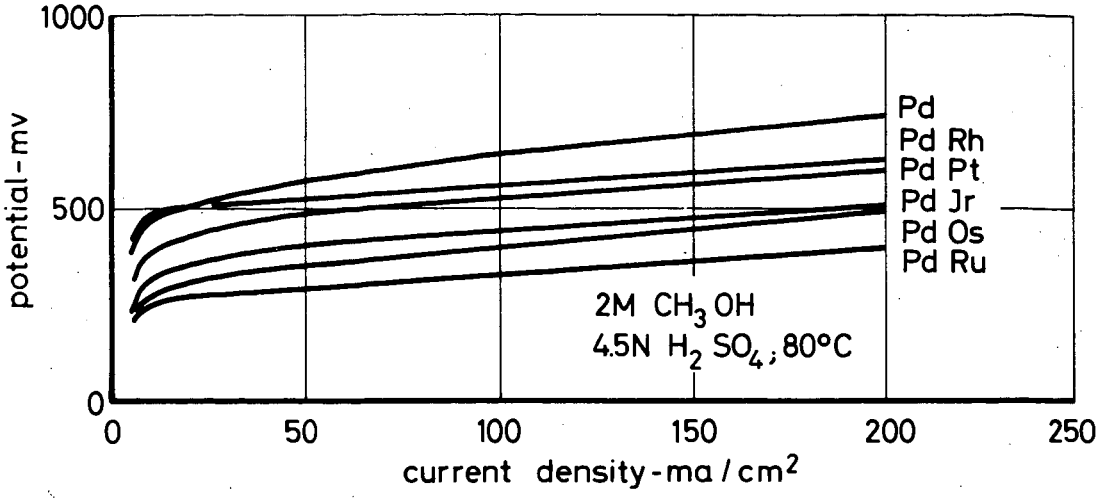

Fig. 5 Potential/current density plots of electrodes containing Raney palladium alloys with methanol in 4.5 N H_2SO_4 at 80°C

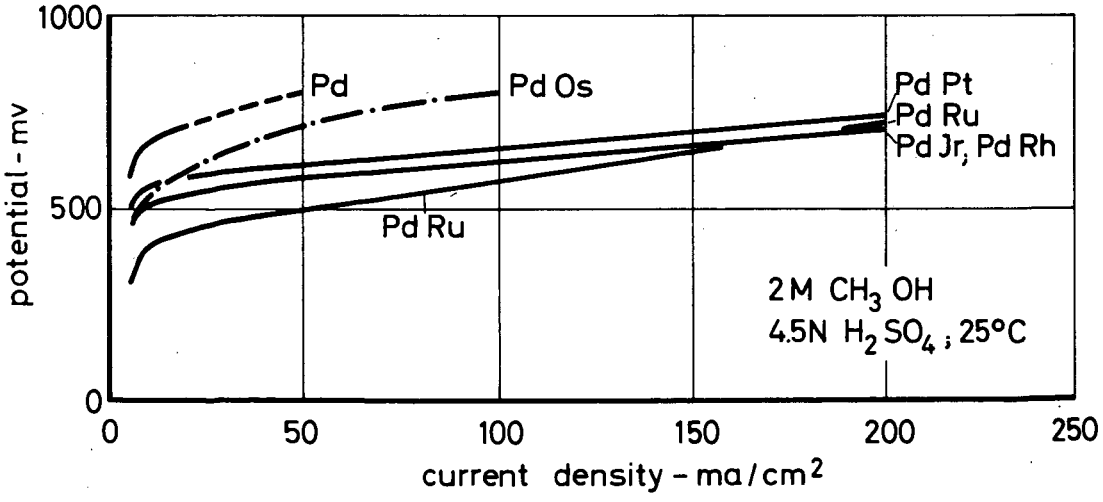

Fig. 6 Potential/current density plots of electrodes containing Raney palladium alloys with methanol in 4.5 N H_2SO_4 at 25°C

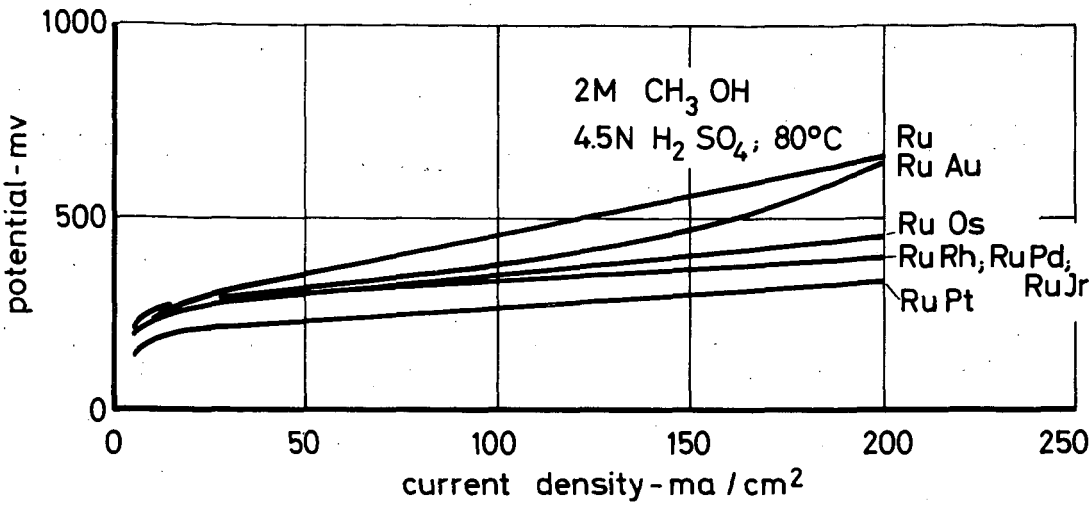

Fig. 7 Potential/current density plots of electrodes containing Raney ruthenium alloys with methanol in 4.5 N H_2SO_4 at 80°C

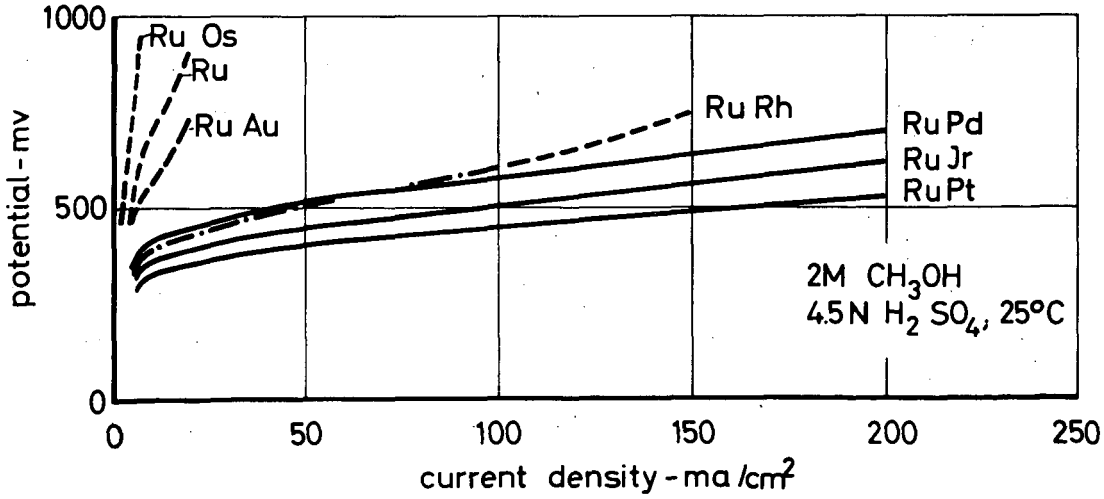

Fig. 8 Potential/current density plots of electrodes containing Raney ruthenium alloys with methanol in 4.5 N H_2SO_4 at 25°C

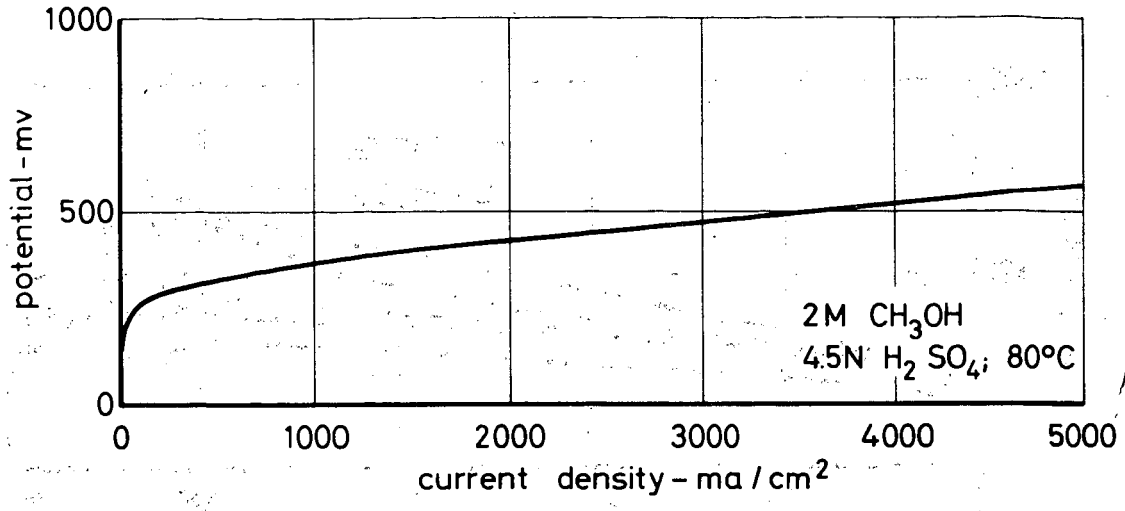

Fig. 9 Potential/current density plot of a Raney ruthenium-platinum electrode with methanol in 4.5 N H_2SO_4 at 80°C

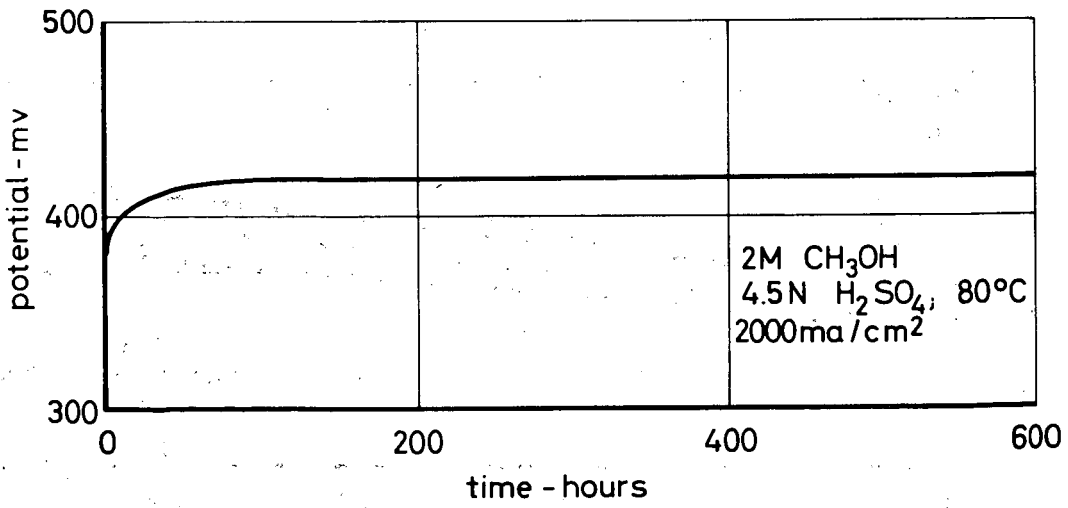

Fig. 10 Change of potential with time on a Raney ruthenium-platinum electrode with methanol in 4.5 N H_2SO_4 at 80°C and a load of 2000 ma/sq.cm.

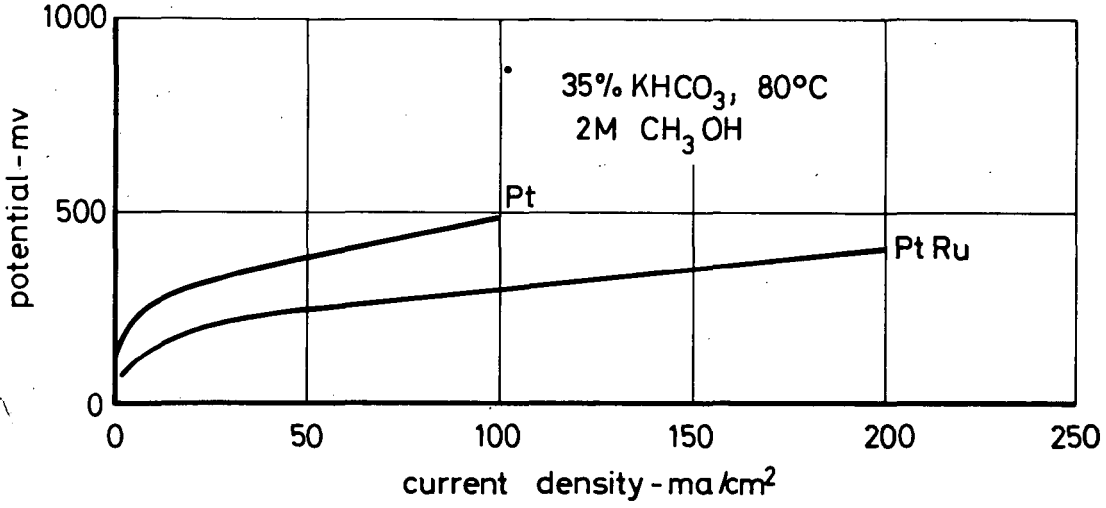

Fig. 11 Potential/current density plots of Raney platinum and Raney ruthenium-platinum with methanol in 35 % (by weight) $KHCO_3$ at 80°C

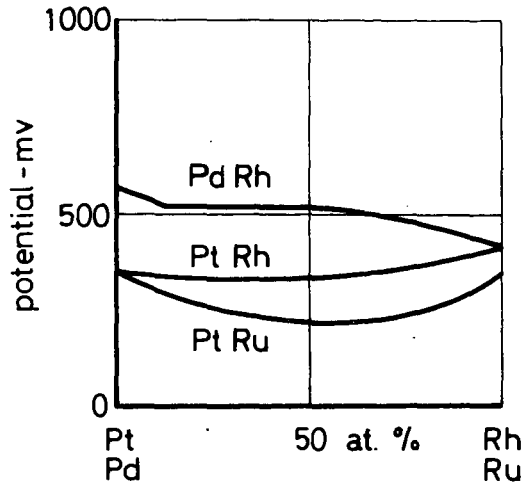

Fig. 12 Potential plots of platinum alloys with methanol in 4.5 N H_2SO_4 at 80°C as a function of composition

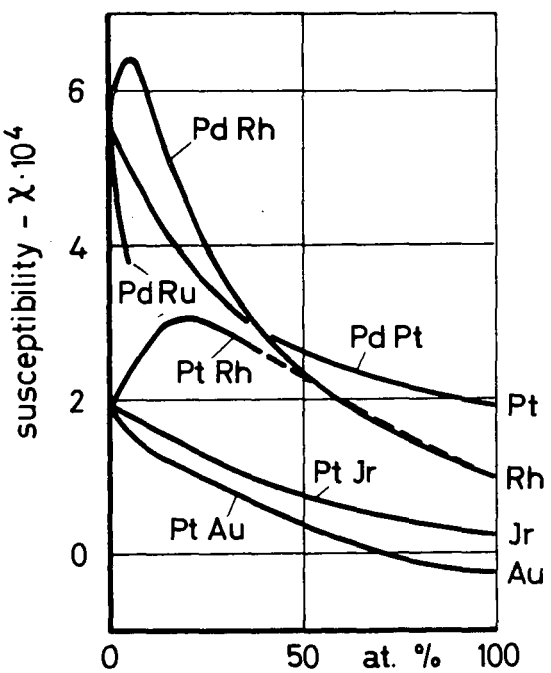

Fig. 13 Magnetic susceptibility of alloys of platinum metals as a function of composition (data from the literature)

THE ANODIC OXIDATION OF METHANOL ON PLATINUM IN ALKALINE SOLUTION

D. Pouli and J.R. Huff*
Research Division, Allis-Chalmers Manufacturing Co.
Milwaukee, Wisconsin

ABSTRACT

The electrochemical oxidation of methanol on platinum was studied as a function of temperature, composition of electrolyte and pretreatment of the electrode. The majority of the data were obtained with the linearly varying potential technique. Results indicate that the oxidation of methanol in alkaline solution proceeds at a potential some 200-300 mV. less positive than in acid, (potentials versus the hydrogen electrode in the same solution). Peak currents for a bright platinum electrode are independent of stirring and increase with increasing voltage sweep rates. From the effect of temperature on the reaction rate, it is evident that the formation of platinum oxide is not the rate determining step. Current transients at low potentials indicate that the initial step involves the abstraction of a hydrogen atom; and that the oxidation of the remaining methanol fragment determines the reaction rate.

INTRODUCTION

In recent years, the anodic oxidation of methanol on platinum in both acidic and basic media, has been studied in considerable detail. The impetus for these investigations is derived from a search for suitable fuels to replace hydrogen in the fuel cell. Breiter et. al. (1,2) have studied the oxidation processes in acid solution; and found the current to be proportional to the amount of methanol adsorbed on the surface of the electrode. These authors propose that the initial step in the reaction is the direct oxidation of the methanol molecule (adsorbed) to a methanol radical and a hydrogen ion.

The anodic oxidation in alkaline solution has been studied by Vielstich (3) and Buck and Griffith (4). Vielstich (3) concludes that rather than the direct electrochemical oxidation of the methanol, the platinum reacts to form a platinum hydroxide which in turn oxidizes the methanol chemically. The formation of the platinum hydroxide must then be rate determining. Vielstich supports his hypothesis by the fact that the current peak in the current-voltage characteristic is normally independent of the oxidizable substance. The fact that methanol in 6-8 Molar alkali is oxidized spontaneously at temperatures exceeding 80°C is explained by assuming a base catalyzed dehydrogenation mechanism.

Buck and Griffith (4) studied the anodic oxidation processes in both acid and alkali media. For the basic system, these authors

---

* Present Address: Globe-Union, Milwaukee, Wisconsin

calculated a Tafel slope of 0.21 - 0.28V.; and they concluded that the rate determining step in alkaline solution involves the reaction of a methylate and two hydroxide ions with the transfer of two electrons.

Some further work was done recently by Liang and Franklin (5), who studied the anodic oxidation of formic acid and formaldehyde in addition to that of methanol. Oxley, et. al. (6) investigated the anodic processes in acid by studying the potential decay curves. The effect of the reductive adsorption of CO_2 was studied by Giner (7).

Although a good deal of work has been done in this field, the factors which govern the shape of the current - voltage curve obtained by the linearly varying potential technique (L.V.P.) are, in general, still unknown. In this paper, we describe some work carried out in order to ascertain which variables dictate the general shape of the i-V curve determined by the technique cited above. Furthermore, we will examine the theories outlined above concerning the oxidation of methanol in the light of some current transient measurements, and the effect of temperature.

EXPERIMENTAL

The electronic equipment used in these experiments is based on the use of operational amplifiers to control the potential of the working electrode. The basic circuitry is due to De Ford (8). A modification permitting compensation of the IR voltage drop between reference and working electrodes has been described elsewhere (9). A block diagram indicating the essential components of the instrument is shown in Fig. I. The integrator shown in Fig. I may be used to generate a single sweep or a triangular wave. In normal experimentation, a triangular wave was applied to the working electrode.

The electrolysis cell was of the conventional H-type with a sintered glass disc between anode and cathode compartments. A working electrode of bright platinum foil ($1cm^2$) was spot-welded to a platinum wire sealed in soft glass. The counter electrode consisted of a platinized platinum foil, of $1cm^2$ geometric area.

The electrode assembly and cell were washed initially with aqua regia followed by a dilute solution of hydrofluoric acid. Further washing with copious quantities of distilled water was carried out before the cell was assembled for use. The hydrofluoric acid solution did not appear to have any deleterious effects on the platinum-soft glass seal.

The electrochemical cell was thermostatted in a water bath to $\pm 0.2°C$. Nitrogen was normally bubbled through the cell at all times. The nitrogen was pre-conditioned by passing it through a solution identical to that in the cell.

A mercury-mercuric oxide reference electrode was used in all experiments. Since adequate IR (reference to working electrode) compensation was achieved electronically, no great care was taken to place the tip of the reference electrode very near the working electrode surface. All potentials in this paper will be cited with respect to the potential of the hydrogen electrode in the same

solution. Rather than calculate the potential of the Hg/HgO electrode versus that of this hydrogen electrode for each set of conditions, its value was determined experimentally. Before the potential of the Hg/HgO reference electrode was measured, it was established that the potential of the hydrogen electrode is not significantly affected by the presence of methanol at temperatures below 60°C.

Harleco carbon dioxide free sodium hydroxide and ACS analytical reagent grade methanol were used in all experiments. The appropriate concentrations of reactant and electrolyte were prepared by dilution of the concentrated material with doubly distilled water.

Since it is normally difficult to obtain reproducible results when the history of the electrode is not clearly defined, a pre-treatment was devised to promote reproducibility. Initially, oxygen was evolved from the electrode at $5mA/cm^2$ for 5 seconds. The electrode potential was then reduced to the initial value for the subsequent linearly varying potential sweep. After maintaining the potential at this value for 2 minutes, a repetitive triangular wave was applied to the working electrode. Nitrogen was bubbled through the electrolyte to remove oxygen produced during the pre-treatment as effectively as possible. This type of pre-treatment normally gave results reproducible to $\pm 5\%$.

RESULTS AND DISCUSSION

The major portion of this work consisted of an investigation of the system, bright platinum/2M methanol, 4.5 M sodium hydroxide. Unless stated otherwise in the text, it will be assumed understood that this is the experimental system. The advantage of the high concentration of methanol is that normally the background current caused by charging of the double layer and adsorption of oxide or hydroxide species is negligibly small over an appreciable potential range, as compared to the oxidation current of the methanol. The last statement is not necessarily true at temperatures near 0°C.

The system cited above was chosen to study the effects of voltage sweep rate, temperature, and voltage sweep range on the current-voltage characteristic. In addition, a study was made of the effects of electrolyte and methanol concentration on the general features of the current-voltage curve, and on the current at constant potential.

The normal voltage sweep range was within the limits of +300 to +1400 mV. It is felt that the adsorption and possible evolution of hydrogen at lower potentials and the evolution of oxygen at higher potentials only complicates the interpretation of the data. Of course, in basic solution even at +300 mV. a small amount of hydrogen is adsorbed.

LINEARLY VARYING POTENTIAL EXPERIMENTS

General Current-Voltage Curve and the Effect of Temperature

In Fig. 2 we show the least complex of the i-V curves obtained in this study. The curve is for the 2M CH_3OH/4.5M NaOH system at 60°C and a voltage sweep rate of 100 mV./sec. Both the

i-V curves for the initial sweep and a "steady state" curve are shown. By steady state, we refer to the condition when subsequent voltage scans do not alter the curve significantly.

From Fig. 2, we note that the current at low potentials for the initial sweep lies below that for the steady state curve. At higher potentials, the i-V curves cross and the current for the initial sweep exceeds that of the steady state scan. This sequence of events is a function of the experimental conditions. The i-V curve for increasing potentials in Fig. 2 (later referred to as the forward sweep) has a single maximum and no plateaus or inflections. This feature is rather different from the curve obtained by Breiter (2) for the oxidation of a molar methanol in molar perchloric acid solution. Fig. 2 also shows the i-V curve for the decreasing potential sweep (later referred to as the reverse sweep). The current maximum for the reverse sweep does not lie outside the forward i-V curve as has been observed for some methanol-acid systems (1). The actual potential of the current peak for the reverse sweep depends markedly on the experimental conditions; and will be considered in some detail later on in this paper.

As shown in Fig. 2 the currents in the low potential region, i.e. at potentials below that of the current maximum are greater for the reverse than the forward sweep. This "hysteresis loop" is less pronounced in the alkaline than in the acid system (c.f. Breiter (4)). Although the effect decreases with increasing temperature, it is still present at 60°C.

Fig. 3 depicts the i-V characteristic for the same system at 0°C. The actual currents at the same potentials are obviously much lower than at 60°C. Decreasing the temperature has altered the general shape of the i-V curve quite considerably. The current for the initial forward sweep lies below that of the steady state curve at all potentials; and the loop formed as a result of the difference between currents for forward and reverse sweeps is appreciably larger than at 60°C. Furthermore, at the lower temperatures the i-V curve for the reverse sweep is much less symmetrical about the potential of the current maximum, and the curve shows an inflection. The "back" side (negative resistance portion) of the forward curve, i.e. at potentials exceeding that of the current maximum, shows a shoulder at 0°C which is absent at 60°C.

Having discussed the general properties of the i-V curves in some detail, we shall now consider possible explanations for the "hysteresis loop" for forward and reverse sweep currents, and the effect of temperature on the shoulder and inflection on the i-V characteristic shown in Fig. 3.

A number of suggestions have been made to account for the hysteresis loop referred to above. Giner (7) has suggested that a reduced form of CO_2 is adsorbed on the electrode surface while the electrode is maintained at its initial potential; say below 250 mV. in molar acid. The reduced CO_2 may be formed from either CO_2 or carbonate in solution or from methanol. This reduced CO_2 then acts as a poison to the oxidation reaction. It has also been suggested that the effects might result from a lower concentration of adsorbed methanol during the reverse sweep, and that oxidation proceeds more readily on a bare surface.

Although it cannot be denied that both explanations, in view of experimental results for the acid system, appear reasonable; the results for the basic system do not support this explanation. Let us consider the reduced CO_2 hypothesis. We have found that the hysteresis loop is not significantly dependent on the initial potential and on the time that the potential was maintained at its initial value. In our work, the initial potential was always maintained above the potential of the hydrogen electrode in the same solution. Giner (7) reports that in the acid system the reduced CO_2 species is produced below 250 mV.; but in the basic system the corresponding potential should be several hundred millivolts less positive. According to this author, the reduced species is oxidized at potentials exceeding 400 mV. Hence, it does not seem likely that the reduced CO_2 hypothesis is applicable to the basic system. Furthermore, one should observe an effect of the holding time (time that the potential is maintained at its initial value) at the initial potential. This is not observed. A possible explanation is that the adsorption of the reduced species is so rapid that when the holding time exceeds one second, no further effect will be observed.

To account for the hysteresis loop by assuming that the reaction occurs more rapidly on a bare surface would seem contradictory to the fact that the current at relatively high surface coverages, 0.3 - 0.8, appears to be proportional to the surface coverage.

A possibility that the hysteresis loop is due to removal of a poisonous intermediate at potentials when the surface oxide is present does not seem applicable since the loop is present even when the most positive potential is less than that where oxide adsorption is possible. It could be thought that the increased currents on the reverse sweep are due to activation of the electrode by adsorption. and reduction of the surface oxide resulting in a different reaction product. Although this possibility cannot be discounted for the alkali system, it does not seem valid in the acid system where the difference in current for reverse and forward sweeps is much too large. The reason for postulating a different reaction product for a more active electrode is that the reaction product is known to depend on the electrode catalyst material (11).

A possible explanation for this phenomenon, which to the best of our knowledge has not been explored previously, is that a reaction consisting of an adsorbed methanol species and a methanol molecule involving a bare surface site is responsible. It is proposed that this reaction occurs in conjunction with the normal reaction of the adsorbed methanol. In this manner, the lower surface coverage in the reverse sweep should yield a somewhat higher reaction rate and at coverages between 0.3 and 0.8 the reaction rate could be proportional to the adsorbed material. It must be emphasized, however, that this explanation is speculative and more data regarding the various steps in the reaction mechanism are necessary.

The fact that the hysteresis loop in alkali is somewhat smaller than that in acid may be due to a closer concurrence of the adsorption isotherm for the forward and reverse sweeps. To our knowledge, no data regarding these isotherms are available for the basic system.

The inflection on the i-V curve for the reverse sweep may be due to an appreciable oxide reduction current. Such an explanation is not satisfactory, however, since the inflection changes to a minumum when this cathodic current is made negligibly small. It is possible that this inflection results from the same process as that which causes the shoulder on the forward curve at 0°C. The shoulder is presumeably caused by interaction of the surface oxide, a methanol species and a bare site. It seems improbable that the current can be ascribed to removal of adsorbed methanol, or a different reaction occurring on the oxide surface. At these potentials the surface concentration of methanol must be very small, and if a different reaction on the surface oxide causes the shoulder, then one would not expect the current to decrease with increasing potential. The oxide concentration (surface coverage) at the potential of the inflection in the i-V curve for the reverse sweep should be very similar to that at the potential of the shoulder on the forward curve. It is, therefore, not inconceivable that a relation exists.

The lack of an inflection at higher temperatures (60°C) is probably due to the fact that the surface oxide is reduced at a higher potential and hence the peak current for the main reaction for the reverse sweep is much higher, thereby making the "surface phenomena" less significant.

The shift of the potential of the current maximum on the reverse sweep to lower values as the temperature is lowered is also thought to be a result of a shift in the potential at which the surface oxides are reduced. It is known that the reduction of the surface oxides occurs at less positive potentials as the temperature is lowered (12). Hence, the current peak should also be shifted to less positive potentials.

The Dependence of the Tafel Slope on Temperature

A few log i-potential curves for the anodic oxidation of methanol at 60°C are depicted in Fig. 4. The Tafel slopes for the initial, and steady state forward and reverse sweeps are 125± 15 mV. and 170± 20 mV., respectively. These values were found to be essentially independent of temperature for the initial and steady state reverse sweeps.

The Tafel slope for the steady state forward sweep for this range of potentials is markedly dependent on the temperature. Decreasing the temperature from 60° to 0°C caused its value to rise from 170±20 mV. to 240±25 mV. The latter value is in reasonable accord with that reported by Buck and Griffith (4) for the oxidation of methanol on a platinized platinum ball at 25°C, at a voltage sweep rate of 8 mV./sec. and methanol concentration below 0.025M. Hence, as the temperature is raised, the Tafel slopes for steady state reverse and forward sweep converge.

A value of 125±15 mV. is readily, although possibly naively, interpreted in terms of a one electron transfer mechanism having a symmetrical energy barrier. However, since the surface concentration of methanol changes with potential during the scan it cannot be assumed that this slope is characteristic of the electron transfer reaction. Breiter (1), assuming Langmuir kinetics, and correcting the observed currents for the effect of the surface coverage, calculated a value of 0.67 for αn. If we consider that the effect of

decreased surface coverage results in an apparently increased Tafel slope, it would appear that our value of 125mV. is similar to that observed by Breiter (1), indicating that the rate determining steps are the same in acid and base.

The Effect of Voltage Sweep Range

In general, the Tafel slopes are not significantly affected by the voltage sweep range provided the maximum and minimum potentials are not within the range of oxygen or hydrogen evolution.

The current maxima normally decrease with decreasing most positive potentials attained during the sweep and the number of cycles required to attain a steady state i-V curve increases. Fig. 5 depicts the effect of decreasing the maximum potential attained during a potential scan. Reference has already been made to the inflection on the i-V curve for the reverse sweep (see Fig. 3). This inflection changes to a marked minimum as the most positive potential during the sweep is decreased from 1400 to 900mV. The nature of the hysteresis loop is not significantly affected by the maximum potential provided it exceeds the potential of the current maximum during the forward sweep.

The Effect of Voltage Sweep Rate

As found by other investigators, the current maximum rises with increasing voltage sweep rate. The fact that stirring does not effect the current-voltage characteristic shows that increased currents at higher sweep rates cannot be accounted for by a diffusion process in the bulk of the solution. In addition, the increased currents can neither be accounted for by higher double layer charging currents, since these are negligible at the higher methanol concentrations. It would appear that this phenomenon is a result of a higher concentration of adsorbed materials at the peak potential as the sweep rate is increased. It has been shown indirectly that the concentration of methanol on the surface at constant potential increases with increasing sweep rates (1). Furthermore, the inhibiting effect of the surface oxide should decrease as the sweep rate is raised since the oxide adsorption reaction is rather irreversible.

Earlier reference has been made to the shoulder on the i-V curve at potentials exceeding that for the current maximum (see Fig. 3). The data on Fig. 2 would seem to indicate that this feature disappears as the temperature is raised. However, even at 60°C, the shoulder may be made to reappear when the voltage sweep rate is increased to 500 mV/sec. Such behavior is characteristic of a surface reaction; and it was interpreted in this manner earlier. The greater prominence of the shoulder at the lower temperatures may be ascribed to the fact that the current for the main reaction is relatively more temperature dependent.

Raising the voltage sweep rate causes the potential of the current maximum for the reverse sweep to decrease. This is not too surprising since it was assumed that the decrease in current beyond the maximum on the forward sweep is caused by surface oxides; and the peak current for the oxide reduction shifts to lower potentials

as the sweep rate is increased. At increased sweep rate, the inflection on the i-V curve for the reverse sweep becomes more prominent. This feature appears only at the lower temperature.

The Effect of Solution Composition

As the methanol concentration is raised, the current at constant potential increases. However, at concentrations exceeding 10 Molar, the current begins to decrease. For the concentration range 0.1 -2M, the slope of the log i vs. log c plot at constant potential is unity, indicating that the reaction is directly proportional to the methanol concentration. The shape of the current voltage curves over the range of concentrations where the log i vs. log c plot is linear is not significantly affected unless the surface reaction i.e. oxide adsorption, becomes appreciable. This occurs at the higher sweep rates.

Fig. 6 depicts the curve obtained for a solution 0.1M in methanol. During the reverse sweep, cathodic currents are observed and the normal reverse sweep peak current is absent. Furthermore, a current minimum and a plateau are observed on the forward sweep. Similar features have been observed for the anodic oxidation of methanol in acid. The phenomena are different in nature, however, in that for the basic system the minimum and plateau are due to the oxide adsorption currents which cannot be the explanation for the acid system since the observed currents are too high.

The effect of the concentration of sodium hydroxide between 0.01 and 4.5M is small. The general shape of the current-voltage curve does not seem to be affected significantly as the concentration is varied between the limits cited.

Current Transients

In these experiments, the potential was raised to a value between 1200 and 1400 mV., and maintained at this point for about 10 minutes. The potential was then decreased instantaneously to a value between 200 and 400 mV.; and the current recorded. Fig. 7 depicts the current transient for the conditions cited. The initial portion when the current is negative has been omitted and the current to the left of the graph is a combination of the reduction of surface oxide and the oxidation of methanol. The peak current at 400 mV. is about 2.5mA/cm^2, some 20-50 times greater than that observed after one second. The area under the curve corresponds to the charge required to oxidize a monolayer of hydrogen. The reason for the experiment was to gain some insight into the relative rates of adsorption and oxidation at lower potentials. It must not be concluded that the peak current represents the maximum rate of methanol adsorption at this potential. Obviously the rate of adsorption is considerably faster, since the peak value includes a cathodic oxide reduction current.

Furthermore, it would appear that the initial reaction involves the abstraction of one or more hydrogen atoms which are oxidized instantaneously at a potential of 400 mV. The sluggish reaction is then ascribed to the oxidation of the remaining methanol radical.

CONCLUSIONS

We have already cited the reaction mechanism proposed by Vielstich (3), who assumes that the anodic oxidation of platinum to a platinum hydroxide is the rate determining step. The methanol subsequently reacts chemically with the metal hydroxide. The author supports his hypothesis by the fact that normally the potential of the peak current is independent of the oxidizable substance. This phenomenon is equally well explained by the assumption that a surface oxide or hydroxide inhibits the oxidation reaction. For, the formation of this inhibitor is essentially independent of fuel. Furthermore, it has been shown by Vielstich that at higher temperatures the potential required to oxidize methanol decreases. Although the author explains this phenomenon by assuming a base catalyzed dehydrogenation mechanism, we have found no evidence for his hypothesis since the i-V curves and Tafel slopes for the initial sweeps are not significantly dependent upon temperature between 0° and 60°C.

Furthermore, examination of the i-V curves for acid and base systems shows that the potentials at which appreciable currents are obtained shift about the same amount for both systems (about 300 mV.) as the temperature is raised from 25° to 85°C. It should also be stated that the equilibrium potential for the basic system is some 250 mV. more negative than that for the acid system; and if the reaction mechanism, Tafel slope and exchange current are the same for both systems, the oxidation of methanol in the basic system at 80°C should be quite appreciable near the potential of the hydrogen electrode in the same solution. It would then be reasonable to assume that if the dehydrogenation is base catalyzed it is also acid catalyzed.

In the basic system complete dehydrogenation of methanol would result in the formation of a carbon monoxide species on the electrode surface. It has been shown that the final product of the oxidation of methanol is either formate or carbonate (3). This implies that carbon monoxide fragments on the surface are further oxidized. Since the carbon monoxide normally inhibits anodic processes (7) it may be assumed that the substance is strongly adsorbed; and should, therefore, decrease the rate of dehydrogenation since the electrode surface is no longer available for catalysis. It appears to us, therefore, that a base catalyzed dehydrogenation mechanism is not responsible for the increased currents in the base system.

It is our hypothesis, in view of the current transient measurements, that even at the lower temperature the radicals are most difficult to oxidize and enhanced dehydrogenation should not influence the rate appreciably, at least not at the lower potentials. It seems to us that the initial reaction sequence can best be described by the following mechanism

$$CH_3OH \xrightarrow{fast} CH_3O_{ads} + H_{ads}$$

$$H_{ads} \xrightarrow{fast} H^+ + 1e$$

The CH_3O_{ads} is then further oxidized, and at potentials below 600 mV. this oxidation process is the rate determining step in the reaction. The actual intermediate formed from the adsorbed CH_3O will probably depend on the final product, whether this be

the carbonate or the formate ion. In general, it would be reasonable to assume that the intermediate lies between CH_3O and formaldehyde (or adsorbed formaldehyde) since the latter is much more readily oxidized than methanol (3).

ACKNOWLEDGMENT

Our thanks are due to Mr. J.C. Pearson for faithfully carrying out the experiments, and to Mr. J. Seibold for many helpful discussions during the writing of this paper.

REFERENCES

1. S. Gilman and M.W. Breiter, J. Electrochem. Soc., 109, 1099 (1962)
2. M.W. Breiter and S. Gilman, ibid, 109, 622 (1962).
3. W. Vielstich, Chemie-Ing-Techn., 35, 362 (1963).
4. R.P. Buck and L.R. Griffith, J. Electrochem. Soc. 109, 1005 (1962).
5. C. Liang and T.C. Franklin, Electrochimica Acta, 9, 517 (1964).
6. J.E. Oxley et. al., ibid., 9, 897 (1964).
7. J. Giner, ibid, 9, 63 (1964).
8. D.D. de Ford, Division of Analytical Chemistry, 133rd National Meeting, A.C.S., San Francisco, Calif., April 1958.
9. Dirk Pouli et.al., Anal. Chem., in course of publication.
10. W. Böld and M.W. Breiter, Electrochimica Acta, 7, 25 (1962).
11. P.G. Grimes, Private communication.
12. J.R. Huff and Dirk Pouli, unpublished data.

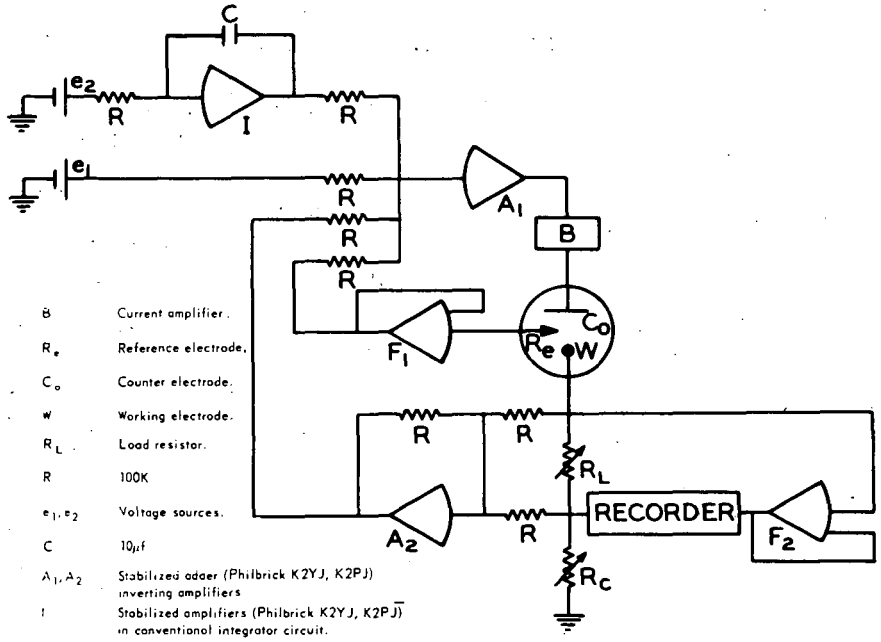

B	Current amplifier.
R_e	Reference electrode.
C_o	Counter electrode.
W	Working electrode.
R_L	Load resistor.
R	100K
e_1, e_2	Voltage sources.
C	10μf
A_1, A_2	Stabilized adder (Philbrick K2YJ, K2PJ) inverting amplifiers
I	Stabilized amplifiers (Philbrick K2YJ, K2PJ) in conventional integrator circuit.
F_1, F_2	Stabilized follower (Philbrick K2YJ, K2PJ).
R_c	Compensating resistor, continuously variable to 10 ohms.

FIGURE 1

Voltammetric Circuit for Continuous Ohmic Voltage Compensation

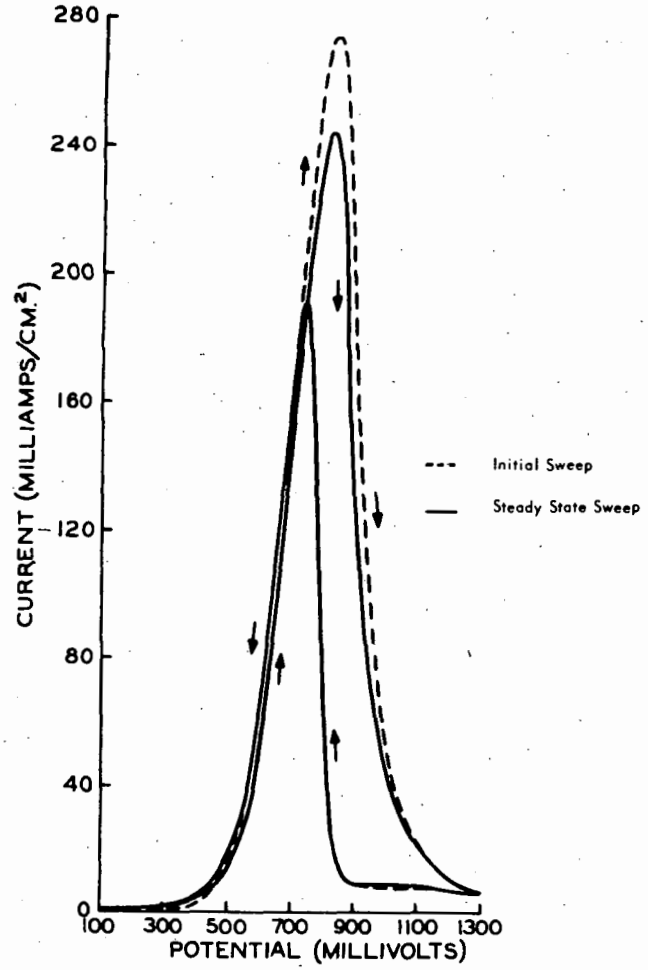

FIGURE 2

Current – Potential Curve for the System, Bright Pt/2M CH_3OH/4.5M NaOH at 60°C and a Voltage Sweep Rate of 100 mv/sec.

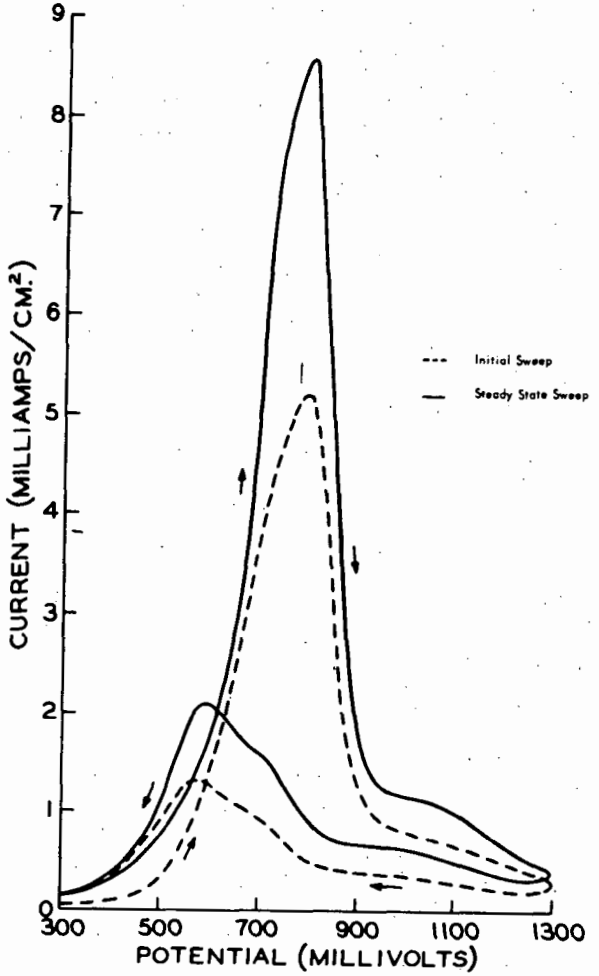

FIGURE 3

Current – Potential Curve for the System, Bright Pt/2M CH_3OH/4.5M NaOH at 0°C and a Voltage Sweep Rate of 100 mv/sec.

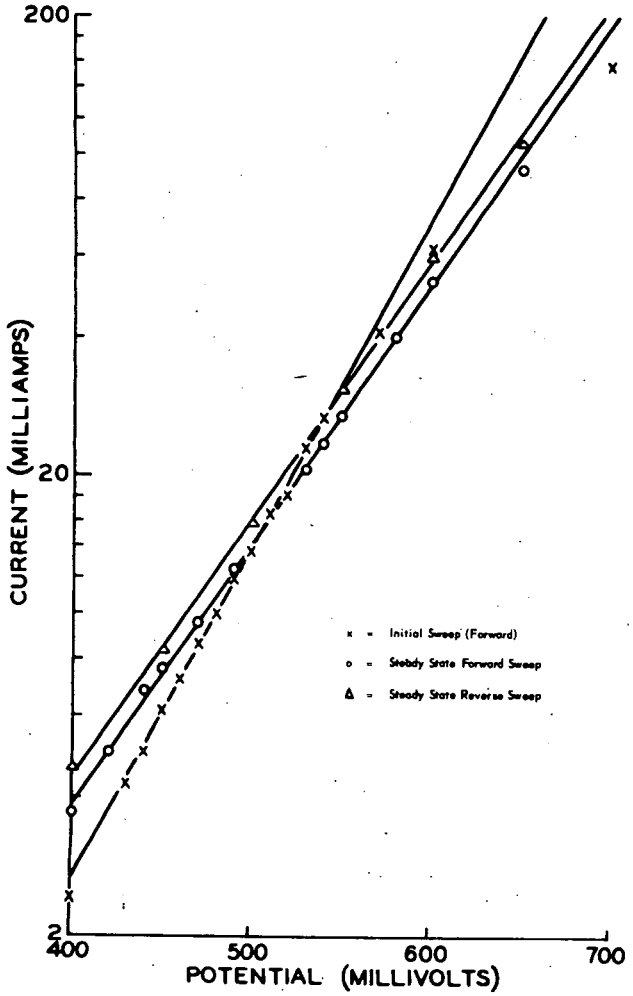

FIGURE 4

Log i Vs Potential for the System, Bright Pt/2M CH_3OH/4.5M NaOH at 60°C and a Voltage Sweep Rate of 100 mv/sec.

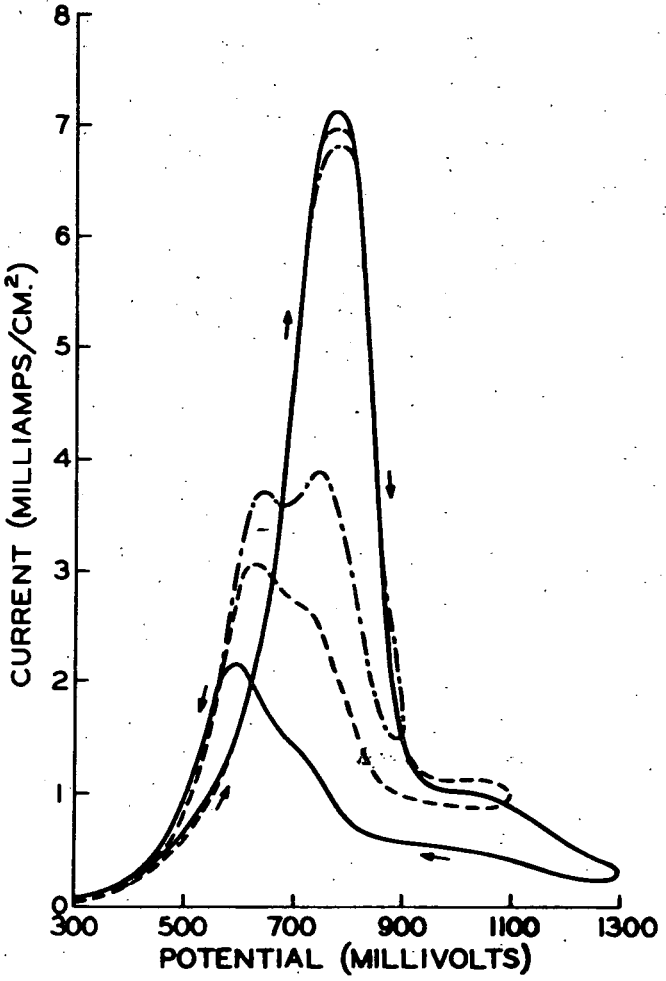

FIGURE 5

The Effect of the Final Potential on the Shape of the Current – Potential Curve at 0°C, Sweep Rate 100 mv/sec.

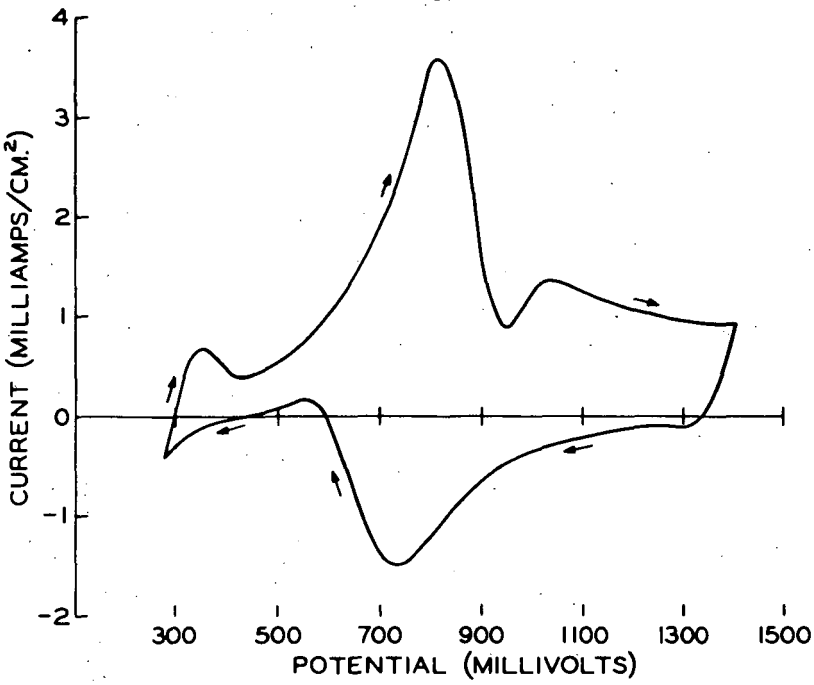

FIGURE 6

Current – Potential Curve of the System, Bright Pt/0.1M CH_3OH · 4.5M NaOH at 30°C and 500 mv/sec.

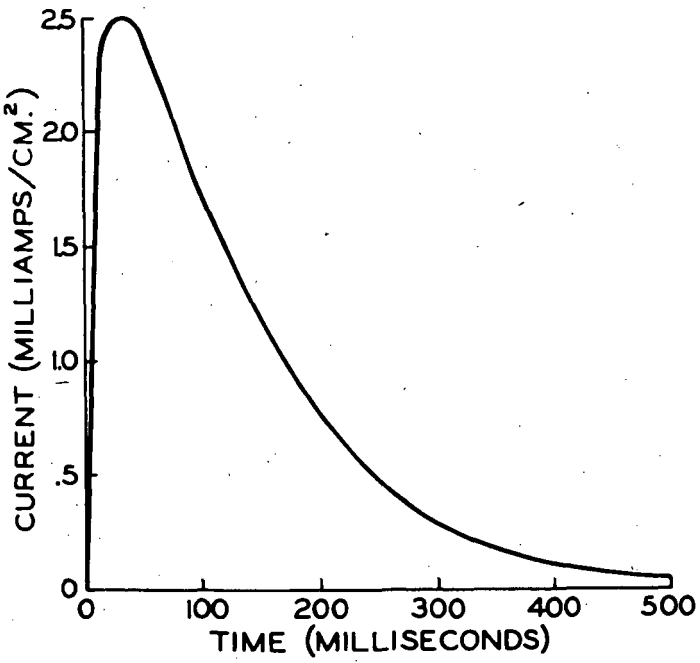

FIGURE 7

Current Transient at 400 mv for the System Bright Pt/ 1M CH_3OH/ 1M NaOH at 30°C.

FORMATE ION - OXYGEN FUEL CELLS

P. G. Grimes and H. H. Spengler
Research Division, Allis-Chalmers Mfg. Co.
Milwaukee, Wisconsin

Introduction

Formate ion is one of the more readily oxidizable carbonaceous fuels in basic electrolyte. In the range 80-100° C, formate ion-oxygen fuel cells, using a platinum-palladium catalyst, have a performance approaching that of hydrogen or hydrazine fuel cells. Formate ion-oxygen fuel cells with a platinum-palladium catalyst have been shown to have about twice the output of methanol fuel cells at ambient temperature (1).

Formate salts are easily handled as solids or in solution, are stable, have low toxicity and are potentially low in cost. Formic acid may also be used as the fuel. It also is stable, and potentially low priced. However, its corrosive properties demand that it be handled with some care. Formate solutions in base are stable at 100° C. At this temperature, the fuel is not volatile in contrast to methanol.

The investigations of the formate fuel cells were extended to study the effects of temperature on the cell output. Further studies involved variation of catalyst and electrolyte composition and fuel concentration.

Experimental

A sandwich type fuel cell was used in these studies. Grooved and manifolded stainless steel end plates held the electrodes and allowed uniform flow of electrolyte-fuel and oxygen over the electrode surfaces. An asbestos sheet (0.060 inch thick) served as the separator-spacer between the electrodes (2).

The electrolyte-fuel mixture, heated in an external chamber, was pumped through the cell anode compartment and then back to the external heater chamber. Oxygen was supplied to the cell at or slightly above atmospheric pressure. Appropriate cell temperature was maintained within $\pm$ 1° C with an auxiliary heating pad. The external heating and pumping system was constructed of Teflon, glass and stainless steel materials. The reference saturated calomel electrode (SCE) was connected to the electrolyte system by means of an external Luggin capillary tube.

Porous nickel plaques (0.028 inch thick) were used as catalyst support material. Electrode plating solutions were prepared by mixing appropriate amounts (in accordance with the required catalyst ratio) of the noble metal chloride solutions containing 2 mg. of

metal per ml. and then adjusting the pH level to 1 with hydrochloric acid. A vacuum filtration technique was used to draw the plating solution through the porous nickel plaque at a slow flow rate. The ratio of the Pd/Pt chemideposited on the plaques was the same as that in the mixed plating solutions (3). Plated plaques were then washed with distilled water and stored in a dry atmosphere. A waterproofing coating of Teflon was applied over the catalyzed surface of those platinum-palladium electrodes which were to be used as cathodes to prevent electrode "flooding." All electrodes were plated with a total of 60 mg/in^2 of noble metal catalysts. The geometric area of the electrodes was 6.25 in^2; and the current data presented are expressed in terms of amperes per square foot (ASF).

Fuel cell electrodes were evaluated with a sine wave (4) and a square wave commutator. The square wave current was generated by a mercury switch function generator. Operating power was supplied by a 12 volt storage battery; a second 12 volt battery supplied the power to operate the auxiliaries of the square wave generator. Voltage readings were taken with a Tektronix 564 Storage Oscilloscope and a R.C.A. Senior vacuum tube voltmeter when using the square wave or sine wave commutators, respectively.

For the half cell studies a current equivalent to 60 ASF was supplied to the cell for a pre-polarization period of five minutes. Experimental data at 60 ASF were then taken, i.e. anodic and cathodic half cell voltages, total cell voltage (ohmic free), and the ohmic voltage (IR drop) of the cell.

The cells were normally kept at the appropriate current density for a three minute polarization period before the potentials were measured. For the lower temperature (30° C) tests, the cell was operated at alternately high and low current densities to maintain a nearly constant temperature in the cell, however, it was not necessary to follow this procedure at 100° C.

Results and Discussion

Anode and Cathode Studies

Formate solutions in basic electrolyte are stable at elevated temperatures, allowing operation of cells near the boiling point of the electrolyte at atmospheric pressure. Studies at ambient and elevated temperatures were conducted to determine the polarization curves for anodes and cathodes using different noble metal catalyst mixtures with formate and oxygen. The standard potential for the anode reaction is 1.02 volts.

$$HCOO^-(aq) + OH^-(aq) \longrightarrow CO_3^=(aq) + H_2O\ (l) + 2e$$

Previous studies have shown that formate ion is readily oxidized on an anode catalyzed with a platinum-palladium mixture or with palladium (1, 3). Platinum catalyzed anodes are severely polarized under applied load. Increasing the palladium content of the catalyst improves the activity of the anodes at 30° C (Figure 1). All electrodes had a total noble metal catalyst loading of 60 mg/in^2. The palladium anode was the least polarized on initial tests. Upon

extended testing for over a thousand hours at ambient temperature, a ratio of five parts palladium to one part platinum by weight proved to be the superior catalyst (1).

Formate ion fuel cells were shown in these studies to have about twice the performance of methanol fuel cells under the same conditions at ambient temperature. Performance of the methanol anode is not greatly changed (Figure 2) when the cell temperature is raised to 60° C (limited by the vapor pressure of methanol). However, anode performance of the formate cell is markedly improved by the temperature increase.

Anode polarization curves obtained for cells operating at 90° C with 4M potassium formate and 4M potassium hydroxide electrolyte are shown in Figure 3. The porous nickel electrodes were catalyzed with a total of 60 mg/in^2 of catalyst. The performance of all the anodes improves with temperature (compare with Figure 1). Obviously, the data show that on initial tests, the palladium anode gave the highest potential for currents between 1 and 200 ASF at 90° C. The same trend, noted at the lower temperature, of decreasing anode activity with increasing platinum content was observed, except that the platinum anode was comparable in performance to the palladium and 50 Pd/10 Pt/in^2 anodes.

The effect at 30° and 90° of increasing platinum content of anodes is depected schematically in Figure 4. The markedly improved activity of a platinum anode at 90° C was unexpected and is inexplicable at this time.

Previous cathode studies with hydrogen-oxygen cells at ambient temperature have shown that platinum-palladium mixtures are more active than either platinum or palladium (4). In the 4M potassium formate - 4M potassium hydroxide system, the oxygen cathode performance improves with increasing platinum content. The best cathode at 30° has a content of 40 mg Pd/20 mg Pt/in^2 catalyst. The platinum cathode was highly polarized at 30° C.

The oxygen cathode polarization curves at 90° C for 60 mg/in^2 of platinum and/or palladium are shown in Figure 5. At the higher temperatures, the activity of the cathode catalyst increases with increasing platinum content. However, again the platinum cathode is least active at the higher currents. The best cathode catalyst had equal amounts of platinum and palladium. The trend of cathodic activity of platinum-palladium mixtures is opposite that of anodic activity of these same mixtures.

The effect of formate ion concentration on the potential of the oxygen electrode at 90° C is shown in Figure 6. A waterproofed porous nickel electrode with equal amounts of platinum and palladium was used as the cathode. Potassium formate concentration in the 4M potassium hydroxide electrolyte ranged between 0.5M to 4M.

It may be seen from Figure 6 that the formate fuel exerts a considerable polarizing effect on the behavior of the cathode; and that the effect is greater with increasing concentration of potassium formate. Furthermore, the polarization of the anode decreases slightly with increasing concentration of fuel. Similar results have been observed for the methanol-oxygen fuel cell (5). Explanations for an increased polarization of the cathode as the concentration of the dissolved fuels are raised have not been considered in

detail. It is for this reason that we should like to present possible hypotheses for this phenomenon. The decrease in anode polarization as the fuel concentration is raised (Figure 6) may be due to either a decrease in diffusion limitation or increase in concentration of fuel in the pre-electrode layer. Since the i-V curves do not exhibit a diffusion limiting current for any of the concentrations studied, it would appear, therefore, that the effect of fuel concentration may be explained approximately by the concentration term in the rate equation.

Although the net reaction at the oxygen electrode is cathodic, this electrode may still function as an anode for formate ion, provided an adequate supply of fuel is present at the electrode surface. If this occurs, the net cathodic current is less, and increased polarization will be observed.

It has been assumed that the anodic and cathodic reactions are totally independent of one another over the voltage range studied. Since formate ion is probably adsorbed on the cathode, it would be reasonable to assume that the surface covered with formate is not available for catalysis of the cathodic reaction. However, the predominating factor controlling the effect of fuel on the cathode polarization in the system discussed in this paper appears to be the formate oxidation current, rather than adsorption of fuel. This explanation is supported by the fact that increased formate concentration results in greater cathode polarization. Furthermore, the performance of the cathode as a function of the catalyst is the opposite of that shown for the anode in Figure 6.

Operating Cells

A cell was constructed using a platinum anode and a 30 mg Pd/30 mg Pt/in^2 cathode. The selection of these electrodes was based on the catalyst spectrum studies. The performance of the cell using a 4M potassium formate - 4M potassium hydroxide electrolyte is shown in Figure 7. An ohmic free cell voltage of 0.82 volts at 200 amps per square foot was obtained at 90° C.

Based on this data, an operating formate ion-oxygen fuel cell system in strong alkali electrolyte could presently be expected to produce 120-170 ASF at 0.8 volts per cell at 90° C. The system construction would be similar to that of a hydrazine fuel cell (2). This performance approaches that of hydrogen-oxygen and hydrazine-oxygen fuel cells at the same temperatures. Further studies of the effects of temperature, formate ion concentration, and cell design to minimize contact of formate with the cathode should lead to marked improvement in the performance of the formate ion-oxygen fuel cell.

The oxidation of formate ion in this system produces carbonate ion and consumes hydroxyl ion. Continued operation of the system would convert the cell electrolyte to carbonate. If the cell is to be operated at high pH, periodic replacement of the electrolyte would be required. However, if a small reduction in performance is not a detriment, the cell can be operated using a carbonate electrolyte. Figure 8 shows the current-voltage curve of the cell with 4M potassium formate - 4M potassium carbonate electrolyte at 90° C. The

ohmic free cell voltages at 200 and 100 ASF are 0.5 and 0.65 volts, respectively.

The polarization of the formate anode is only slightly greater in the carbonate than in the hydroxide electrolytes. However, the performance of the oxygen cathode is markedly poorer in the carbonate electrolyte. The difference in performance of the two cells shown in Figure 8 is due primarily to the cathode polarization.

In spite of the greater polarization of the cathode in carbonate electrolyte such a system may reasonably be expected to produce 100 to 130 ASF at 0.5 volts at 90° C.

Conclusions

The formate ion-oxygen fuel cell will produce 0.82 volts at 200 ASF (ohmic free) at 90° C with hydroxide electrolyte. Operation of the formate ion cell with a carbonate electrolyte reduced the performance of the cathode, lowering the output to 0.5 volts at 200 ASF (ohmic free) at 90° C.

Palladium and platinum are the best anode catalysts at this temperature. A mixed catalyst containing equal amounts of platinum and palladium is the poorest anode catalyst. At 30° C, however, palladium was the best anode catalyst and activity decreased with increase in platinum content. The mixed catalyst, referred to above, however, is the best for the oxygen electrode at both 30° and 90° C in the presence of formate.

The output of formate ion-oxygen fuel cells approaches that of hydrogen and hydrazine-oxygen fuel cells. This allows the formate ion-oxygen cells to be applied in special applications.

Acknowledgements

The authors wish to express their appreciation to Dr. D. Pouli, Mr. T. Reimer and Mr. W. Jenkin of the Research Division for their technical assistance.

References

1. P. G. Grimes, H. H. Spengler, "Formate Ion-Oxygen Fuel Cell," Fall Meeting of The Electrochemical Society, Washington D.C., October, 1964.

2. S. S. Tomter, A. P. Anthony, "The Hydrazine Fuel Cell System," in "Fuel Cells, CEP Technical Manual," American Institute of Chemical Engineers, New York (1963)

3. P. G. Grimes, J. N. Murray, H. H. Spengler, "Studies on the Anodic Character of Mixed Noble Metal Catalysts: Platinum and Palladium," Fall Meeting of The Electrochemical Society, Washington D.C., October, 1964.

4. G. F. Pollnow, R. M. Kay, "A Transistorized 60 cps Sine Wave Commutator for Resistance and Potential Measurements," J. Electrochem. Soc. 109, 648 (1962)

5. J. N. Murray, P. G. Grimes, "Methanol Fuel Cells" in "Fuel Cells CEP Technical Manual," American Institute of Chemical Engineers, New York (1963).

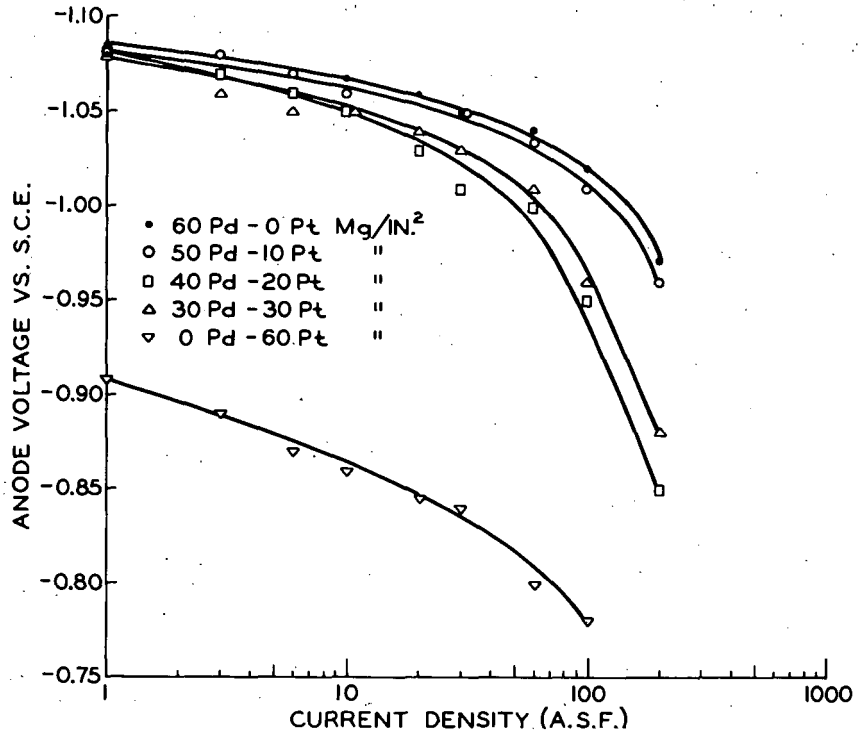

Fig. 1.-EFFECT OF CATALYST ON ANODE POTENTIALS IN 4M POTASSIUM FORMATE AND 4M POTASSIUM HYDROXIDE AT 30°C

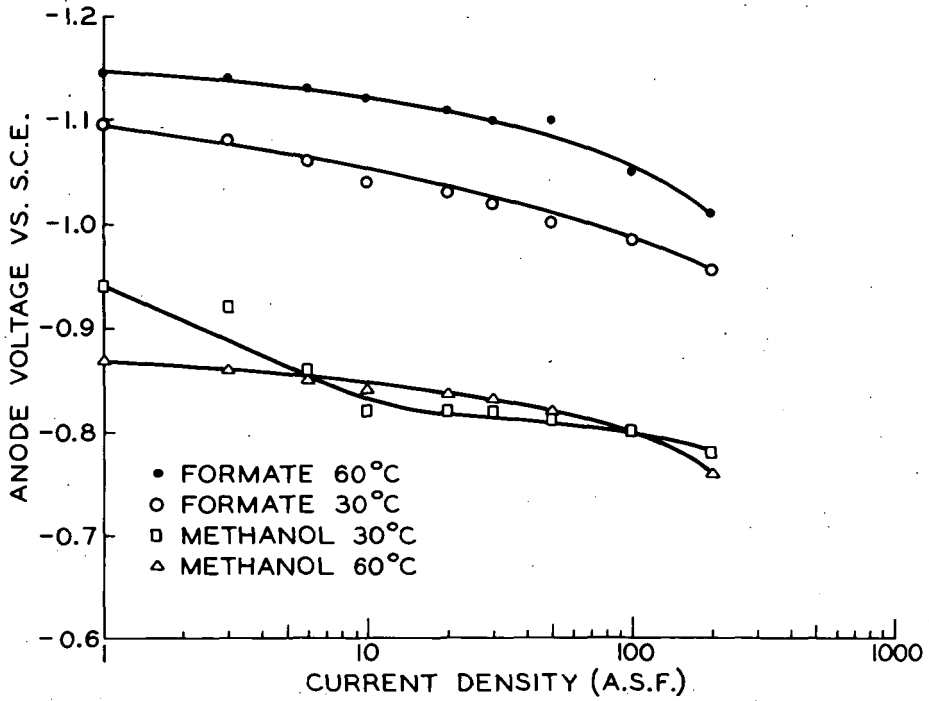

Fig. 2.-ANODE CURRENT-VOLTAGE CURVES FOR THE SYSTEMS 4M METHANOL AND 4M POTASSIUM FORMATE IN 4M POTASSIUM HYDROXIDE AT 30° AND 60°C

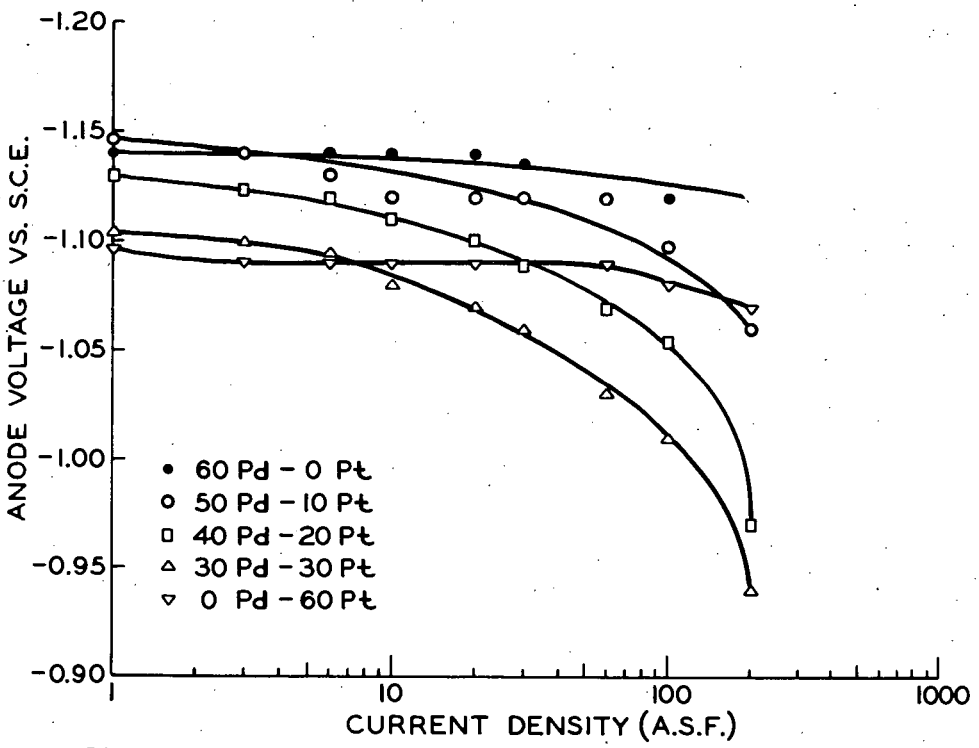

Fig. 3.-EFFECT OF CATALYST ON ANODE POTENTIAL IN 4M POTASSIUM FORMATE AND 4M POTASSIUM HYDROXIDE AT 90°C

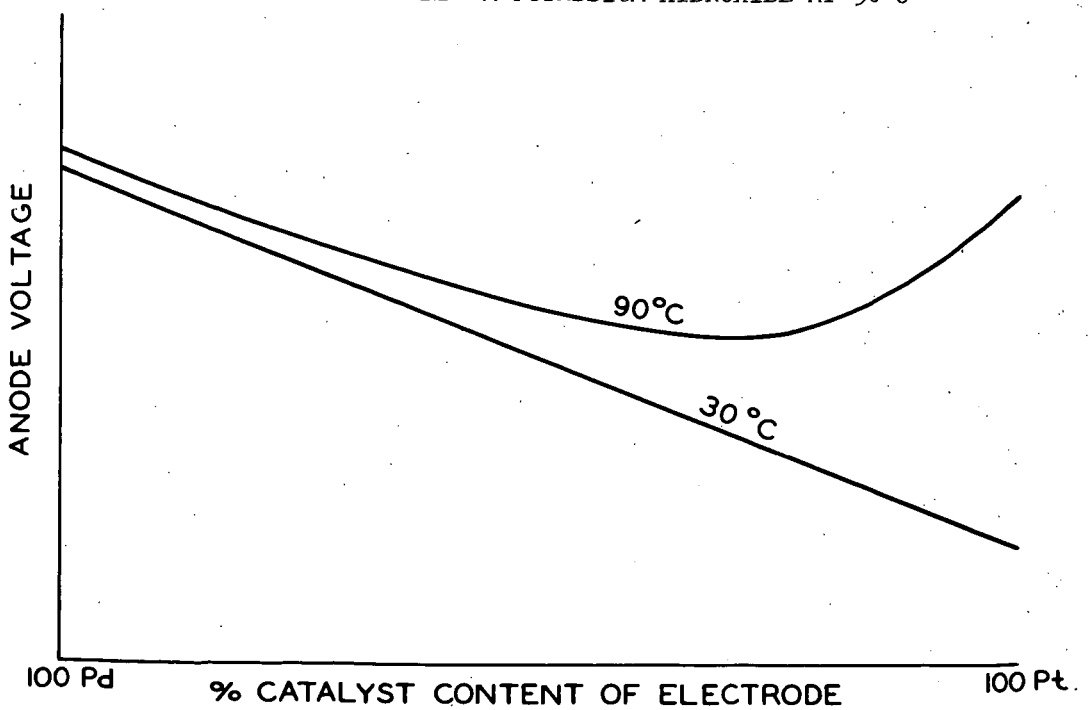

Fig. 4.-SCHEMATIC: ANODE VOLTAGE VS. CATALYST COMPOSITION

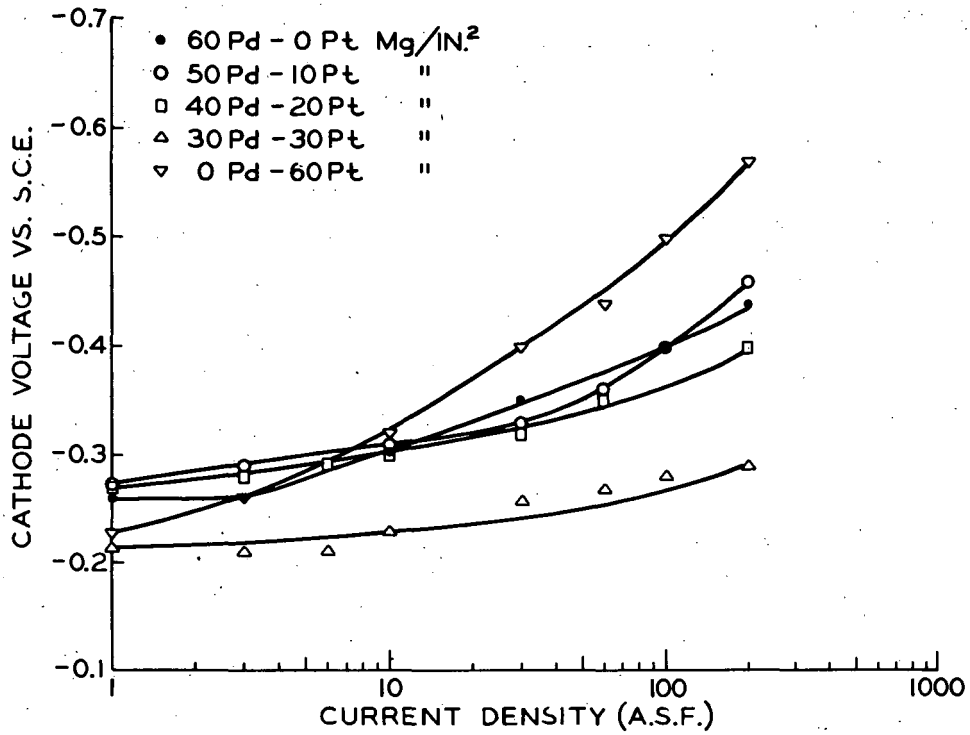

Fig. 5.-EFFECT OF CATALYST ON CATHODE POTENTIALS IN 4M POTASSIUM FORMATE AND 4M POTASSIUM HYDROXIDE AT 90°C

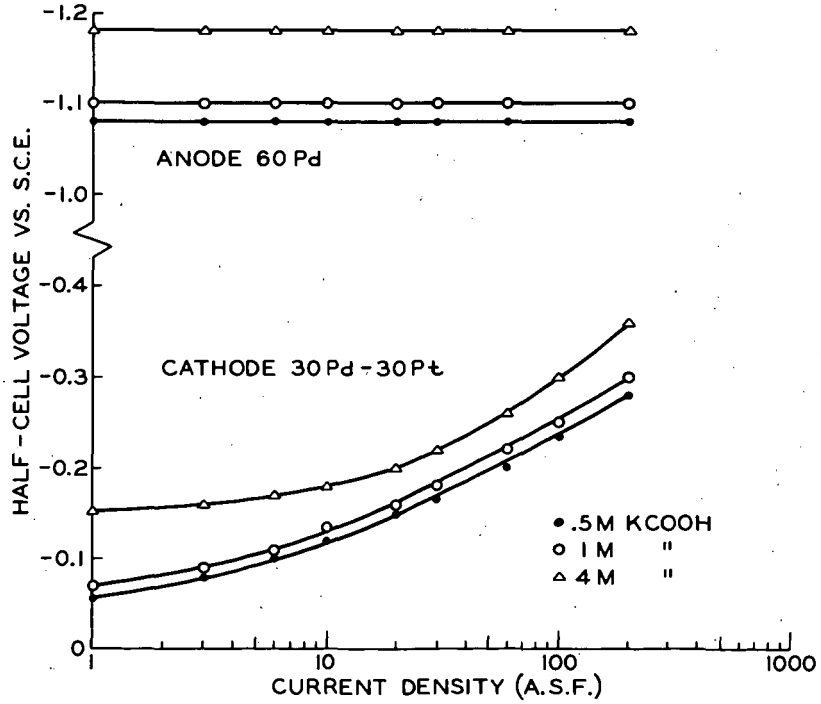

Fig. 6.-EFFECT OF POTASSIUM FORMATE CONCENTRATION ON ANODE AND CATHODE POTENTIALS IN 4M POTASSIUM HYDROXIDE AT 90°C

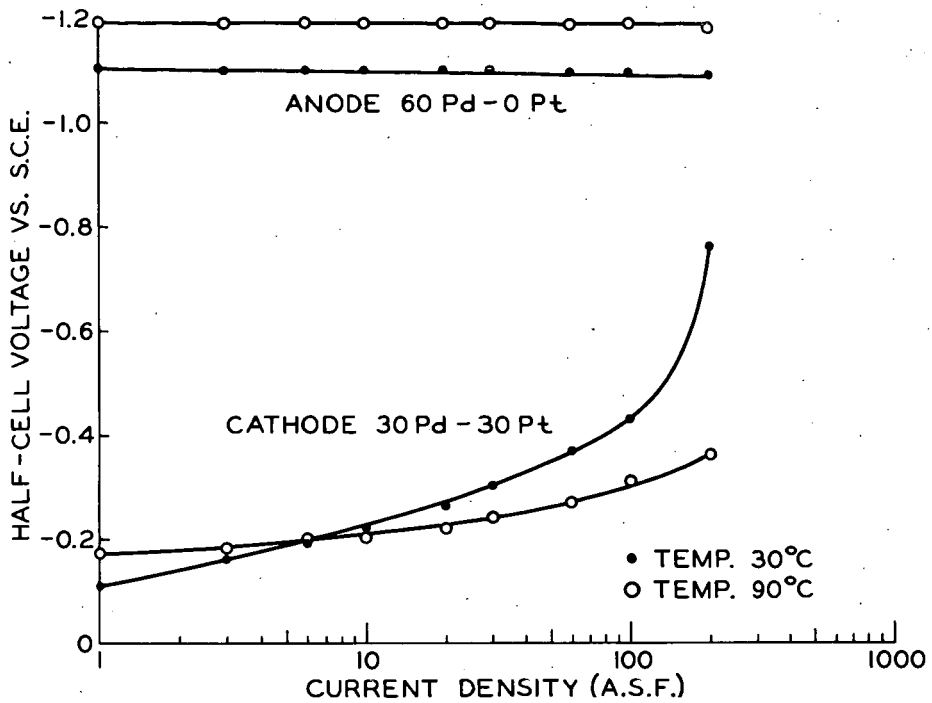

Fig. 7.-HALF-CELL VOLTAGES FOR THE BETTER ANODE AND CATHODE COMBINED IN A SINGLE CELL WITH 4M POTASSIUM FORMATE AND 4M POTASSIUM HYDROXIDE

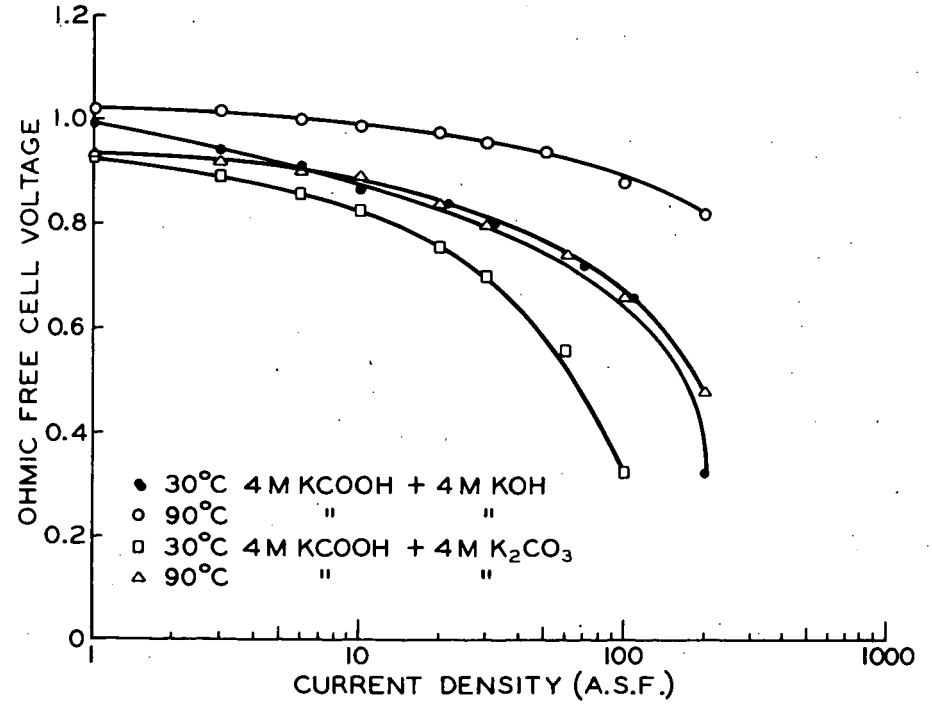

Fig. 8.-CURRENT-VOLTAGE CURVES FOR THE SYSTEMS FORMATE/4M POTASSIUM HYDROXIDE AND POTASSIUM FORMATE/4M POTASSIUM CARBONATE (OHMIC FREE)

AN ALKALINE METHANOL-AIR PRIMARY BATTERY SYSTEM

R. E. Biddick & D. L. Douglas

Research & Development Laboratory - Gould-National Batteries, Inc.

Minneapolis, Minnesota

A primary battery system operating on methanol dissolved in KOH, and air, has been developed to the laboratory hardware stage. Fuel-electrolyte solution flows by gravity through palladium-activated porous nickel electrodes. Teflon waterproofing and semi-permeable separators minimize fuel and electrolyte loss through the cathode. Condensed in a chimney, water is recycled from the emerging air stream. Extensive tests carried out on a battery rated at 30 W (one-third max. power) indicate that in series, 24 cells, individually about one-fourth sq. ft. in area, deliver 12 V. At rated output, utilization of 5 molar CH_3OH/6 molar KOH fuel is ca. 55 Wh/lb. Single cells have been operated one year at room temperatures, and cells in test batteries have maintained 3000 hours of satisfactory output. A preliminary cost analysis indicates that the system can be competitive with existing primary and secondary batteries.

INTRODUCTION

The advantages of a methanol fuel and an alkaline electrolyte are well known in fuel cell lore. The two in combination suffer the disadvantage that alkali is consumed in the fuel cell reaction. Thus, for long term operation either a large reservoir must be provided or the electrolyte must be continuously purified of formate, carbonate and other reaction products.

Three fairly comprehensive studies of alkaline methanol systems have been reported in the literature. Murray and Grimes (1) describe a methanol-oxygen system in which methanol is metered into a circulating electrolyte. Temperature of the battery is controlled by a heat exchanger in the electrolyte loop. No means of reformation of carbonate ion to hydroxide ion was provided, so that the size of the electrolyte reservoir limits the operating time – about five hours in the system described. Electrodes are of a bipolar design. The anode consists of a sintered nickel plaque impregnated with a palladium-platinum catalyst, and the cathodes are fabricated from porous nickel plaques containing silver catalyst and Teflon wetproofing. Considerable methanol is lost through evaporation, but that which is oxidized goes to carbonate.

Vielstich (2) describes a methanol-air fuel battery and its application in a signaling device. In this case, the electrodes are immersed in a container of

fuel-electrolyte solution, the spent solution being replaced as required. Platinum catalyst on an unspecified porous carrier serves as the anode, and the cathodes consist of wetproofed porous carbon activated with silver. Natural convection and diffusion serve to provide an adequate supply of air to open-topped cathodes. A 28-cell battery of this design, fabricated by Brown, Boveri, Ltd. (Baden, Switzerland), was tested as a power source for a river navigation buoy over a six month period. About a 10% loss in methanol (presumably by evaporation) was experienced. Oxidation of fuel consumed is to carbonate ion.

An alkaline methanol system in which dissolved sodium chlorite is used as the oxidizer has been reported by Boies and Dravnieks (3). The development was not carried past the single cell stage. A fuel solution approximately 5M in methanol and 5M in KOH is circulated past an anode which consists of a platinized substrate of flame-sprayed Raney nickel. The oxidant solution (4M in sodium chlorite and 5M in KOH) similarly flows through a cathode chamber. The cathode is flame-sprayed Raney nickel-silver and fuel and oxidant chambers are separated by a dialysis membrane. External heating of the reactant solutions is used to maintain a cell operating temperature of 55°C. An output of 144 mA/cm^2 at 0.6 V is reported. Methanol is not oxidized past the formate stage, and a considerable parasitic loss due to chemical oxidation of methanol by chlorite occurs.

This paper describes a study of a continuous flow alkaline-methanol fuel battery system which has been carried through the laboratory model stage. The work was carried on as part of a joint research and development program of the Pure Oil Company and Gould-National Batteries, Inc. A primary design objective was a reliable system capable of unattended operation over periods of several months. Only slightly less important were first cost and operating cost. A minimum of power-operated controls and auxiliaries are used. Natural forces, i.e., gravity and surface tension, serve to effect and control the flow and distribution of reactants.

CELL DESIGN

Cell design is shown schematically in Figure 1. A nickel sheet forms one side of the anode compartment, and a diaphragm forms the other side. The anode is a standard sintered-nickel battery plaque in which palladium catalyst has been deposited. The cathode contains silver catalyst bonded to nickel screen by Teflon particles in the sub-micron size range. In single-cell tests, electrode size has been two or four inches square, while in batteries the electrodes have been as large as one-fourth square foot in area.

The diaphragm separating the electrodes may be either a semi-permeable membrane or a more porous separator such as asbestos. In most of the cells constructed to date, we have used Permion 300 or 320 type membranes such as have been used in experimental silver-zinc batteries.

Electrical connection between cells is provided by a corrugated nickel screen which serves also to maintain sufficient separation between cells to permit air convection.

Electrolyte containing dissolved fuel is admitted to the cell at the top of the anode, flowing down under the influence of gravity through the anode compartment and dripping out of the cell into a collecting trough.

SYSTEM DESIGN

Cells are stacked three per inch and are held in place by compression between end plates connected by tie bolts. Fuel-electrolyte solution is distributed to the cells in parallel flow by means of a system of wicks and manifold which is operable over a wide range of flow rates.

The battery and fuel distributor are enclosed in a cabinet as shown in Figure 2 of a 24-cell system. Natural draft over the height of the battery cabinet is sufficient to provide adequate air convection past the cells. Controls and design features are provided to maintain flow rates and temperatures within the limits of satisfactory operation over a range of environmental conditions.

Air enters the cabinet through a thermostatically controlled opening near the bottom. Air leaves the cabinet through an opening near the top, entering a chimney of narrow rectangular cross section. Some water is condensed on the walls of the chimney and returned to the battery through the fuel distributor. To provide auxiliary cooling at high ambient temperature, metallic fins extend from each cell through the back wall of the cabinet into a secondary air chamber through which natural air flow is thermostatically controlled. To prevent excessive heat loss in a cold environment, the cabinet and secondary air chambers are covered with a layer of polyurethane foam insulation.

The feed rate of fuel-electrolyte solution is controlled automatically in response to battery output by means of a controller developed by Honeywell. Several types of valves and positioners have been tried. One type which resulted in good control characteristics consisted of a needle valve having a stem with a one-degree taper which was turned by a small reversible DC motor.

OPERATING CHARACTERISTICS

A polarization curve for a typical natural-flow cell at room temperature is shown in Figure 3. In order to permit comparison with other types of cells in which electrolyte concentration changes are negligible, the data in Figure 3 were obtained at a high feed rate. Maximum power output at these conditions was about 10 W/ft^2.

Ordinarily, if this natural-flow system is to be operated with once-through flow of electrolyte, feed rate will be very slow in order to provide good utilization

of reactants. The effect of feed rate on output voltage is shown in Figure 4. These data were obtained with a six-cell uninsulated battery with natural convection of air. Voltage dependence shows two markedly different regions. At feed rates between about 170-300% of the theoretical methanol rate (100-180% of theoretical potassium hydroxide rate), voltage is roughly proportional to feed rate. At higher feed rates voltage increases only slightly with feed rate, and at very high rates voltage would decrease because of the cooling effect of the feed.

The explanation for this operating characteristic lies in the influence of reactant and product concentrations on reaction rate. At low fuel rates concentration changes in the electrolyte are extensive, and a voltage gradient is observed through the cell along the path of the electrolyte. The potentials of anode and cathode vs. a reference electrode both become more positive as the reference electrode is moved from the electrolyte inlet to the electrolyte outlet. Single-cell data illustrating this effect are shown in Table I. At a feed rate of 275% of theoretical methanol, the change in potential between inlet and outlet amounted to 0.14 V.

TABLE I. EFFECT OF FEED RATE ON ELECTRODE POTENTIALS

Feed: 5M CH_3OH - 6M KOH
Current Density: 10 mA/cm^2
Cell Temperature: 30°C

Feed Rate, % of Theoretical Methanol	Electrode Potentials vs. SCE in: Feed E_{Anode}	Feed $E_{Cath.}$	Effluent E_{Anode}	Effluent $E_{Cath.}$	Measured Cell Voltage
750	-.83	-.34	-.83	-.33	.51
470	-.80	-.32	-.80	-.32	.49
345	-.81	-.35	-.79	-.32	.46
295	-.80	-.36	-.74	-.29	.44
275	-.78	-.39	-.65	-.24	.40

Utilization of fuel, in terms of specific power output of the fuel solution in Wh/lb, can be derived from the voltage dependence and is plotted in Figure 4. If output voltage were strictly proportional to fuel rate in the low rate region, then fuel utilization would be independent of fuel rate in this region. However, Figure 4 shows that fuel utilization does increase slightly as fuel rate is decreased.

Maximum fuel utilization with 5M CH_3OH-6M KOH fuel was about 55 Wh/lb. It was limited largely by methanol loss occurring by evaporation through the

diaphragm but also by electro-osmotic flow of electrolyte through the diaphragm and cathode. These losses could be reduced through the use of a more retentive diaphragm. Concentration of formate in the spent electrolyte is less than 0.05 mole/liter, indicating high selectivity to carbonate formation.

Battery temperature is a function of current and of the flow rates of feed solution and air. Table II lists operating temperatures of the 24-cell battery shown in Figure 2 at a fuel rate of about 300% of theoretical based on methanol content of the 5M CH_3OH-6M KOH feed solution used; however, if the fuel rate were calculated on the basis of potassium hydroxide rather than methanol, it would be 180% of the theoretical rate required by the current. In these experiments air was forced through the cabinet at a metered rate rather than being allowed to flow by natural convection.

TABLE II. OPERATING TEMPERATURE OF 24-CELL BATTERY

Ambient Temperature: 25°C

Feed: 5M CH_3OH-6M KOH

Feed Rate: 300% of Theoretical CH_3OH

Current Density mA/cm^2	Air Rate, % of Theoretical	Battery Voltage	Temperature, °C
10	200	10.8	61
10	500	11.2	58
20	200	8.6	79
20	500	12.0	63

At an ambient temperature of 75°F, battery temperature is roughly 60-65°C at current densities of 10-20 mA/cm^2 and at the air rates and feed rates ordinarily used. At a low air rate the boiling point of the fuel can be exceeded, resulting in severe reduction of output voltage. Cell voltages at these currents are ordinarily between 0.4 and 0.5 V.

USE AS A POWER SOURCE WITH INTERMITTENT LOAD

One possible application of this primary fueled-battery system is as a power source for signalling devices, many of which operate intermittently. A load of this type was simulated by means of a timer operating for one second on and nine seconds off in series with a 250 W, 12 V lamp. Since the current surge required to operate this load was greater than could be supplied directly by the fueled battery, a storage battery was connected in parallel with the fueled

battery. The storage battery was a 12 Ah, 10 V assembly of sealed nickel-cadmium cells*. A schematic diagram of the system is shown in Figure 5.

This system operated automatically for a three day test period, during which time the voltage under load remained within the range of 9.0 to 9.7 V. Although the storage battery was operated under severe overcharge conditions for most of the test period, it performed satisfactorily.

LIFE TESTS

Single cells have been tested at room temperature for periods up to one year under a continuous drain of 10 mA/cm^2. Voltage decline has occurred mainly at the anode, amounting to 10 to 30% of the initial voltage output. Cracks in epoxy edge seals have required some increase in feed rate during the progress of the test in order to maintain cell performance at this level.

Cells in test batteries have maintained satisfactory output for 3000 hours of operating time accumulated in successive test batteries. The longest time which a battery has been operated thus far is 2000 hours; the battery was utilized in system tests rather than battery life tests and was subjected to more extreme operating conditions than would be expected in an optimum system design.

In some early batteries containing cells with thin-membrane diaphragms, cell reversals resulted in deposition of palladium and silver in the diaphragms to the extent that electrical shorting occurred. The problem was eliminated by removing the cause of cell reversal, namely, unequal feed rate to individual cells which resulted in excessive fuel depletion in some cells.

OTHER FUELS

Since the major cause of low methanol utilization in this system is the high volatility of methanol, one might expect less volatile fuels to overcome this difficulty. Ethyl alcohol, for example, boils 14°C higher than methyl alcohol. In a single cell test, however, fuel loss was not reduced by the substitution of ethyl alcohol. Ethylene glycol is not an acceptable fuel because it forms an insoluble oxidation product which plugs the cell passages.

COSTS

Based on a specific power output of 50 Wh/lb of fuel solution and a cost of $0.10/lb of methanol and potassium hydroxide, fuel cost would amount to $0.80/kWh.

Catalyst cost is about $3/W, most of which is recoverable. Cost of the complete system would be many times this amount in small scale production.

* Manufactured by Alkaline Battery Division, Gould-National Batteries, Inc.

Even so, with a life of only one year the alkaline methanol-air system might be economically competitive with existing primary and secondary batteries.

CONCLUSIONS

Because a natural-flow fueled-battery system can operate with a minimum of moving parts, it should be inherently reliable. The system can operate automatically and unattended, giving power on demand and maintaining itself in standby condition under no load.

Power capability can be substantially higher than is practical with air-depolarized primary batteries or with secondary batteries. The system is simply recharged for a new period of use by refilling the fuel-electrolyte reservoir with fresh solution. Life tests of single cells indicate a useful life of at least one year and possibly considerably longer.

Costs may be competitive with existing low-energy power sources.

ACKNOWLEDGEMENTS

This work was conducted under a joint fuel cell research program of Gould-National Batteries, Inc. and Pure Oil Company. The assistance of Messrs. E. L. Burkholder, P. S. Chow and W. G. Howard in various phases of battery construction and testing is gratefully acknowledged.

LITERATURE CITED

(1) Murray, J. N. and Grimes, P. G., in "Fuel Cells", CEP Technical Manual, pp. 57-65, Am. Inst. Chem. Engrs., New York, 1963.

(2) Vielstich, W., "Methanol Air Fuel Cell", preprint, Fourth International Symposium on Batteries, Brighton, England, Sept. 29 - Oct. 1, 1964, Pergamon Press.

(3) Boies, D. B. and Dravnieks, A., in "Fuel Cell Systems", pp. 262-268, Amer. Chem. Soc., Washington, 1965.

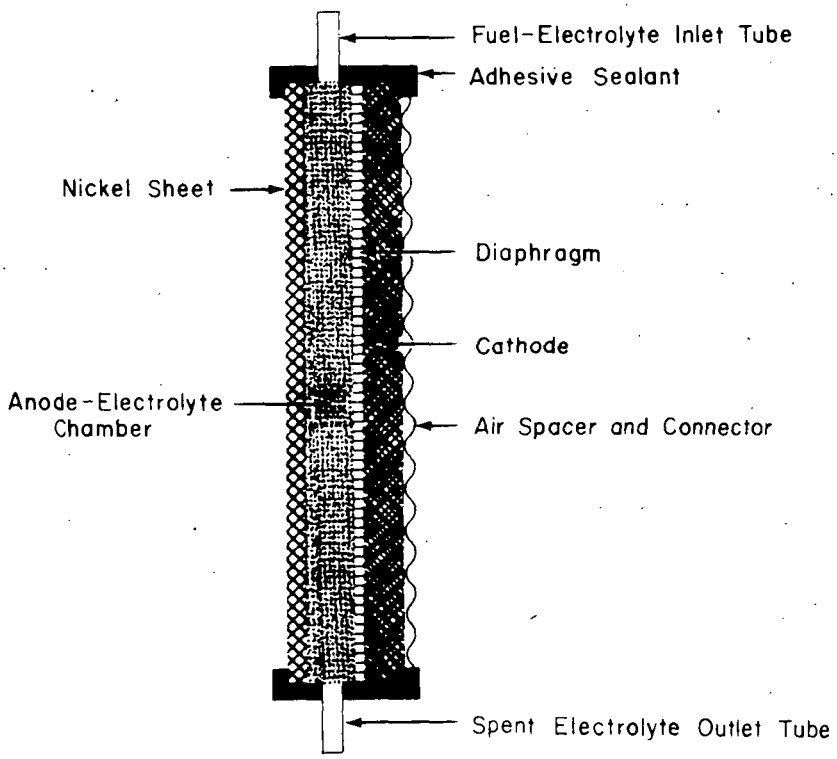

FIGURE 1. CONSTRUCTION OF DISSOLVED-FUEL CELL WITH NATURAL FLOW

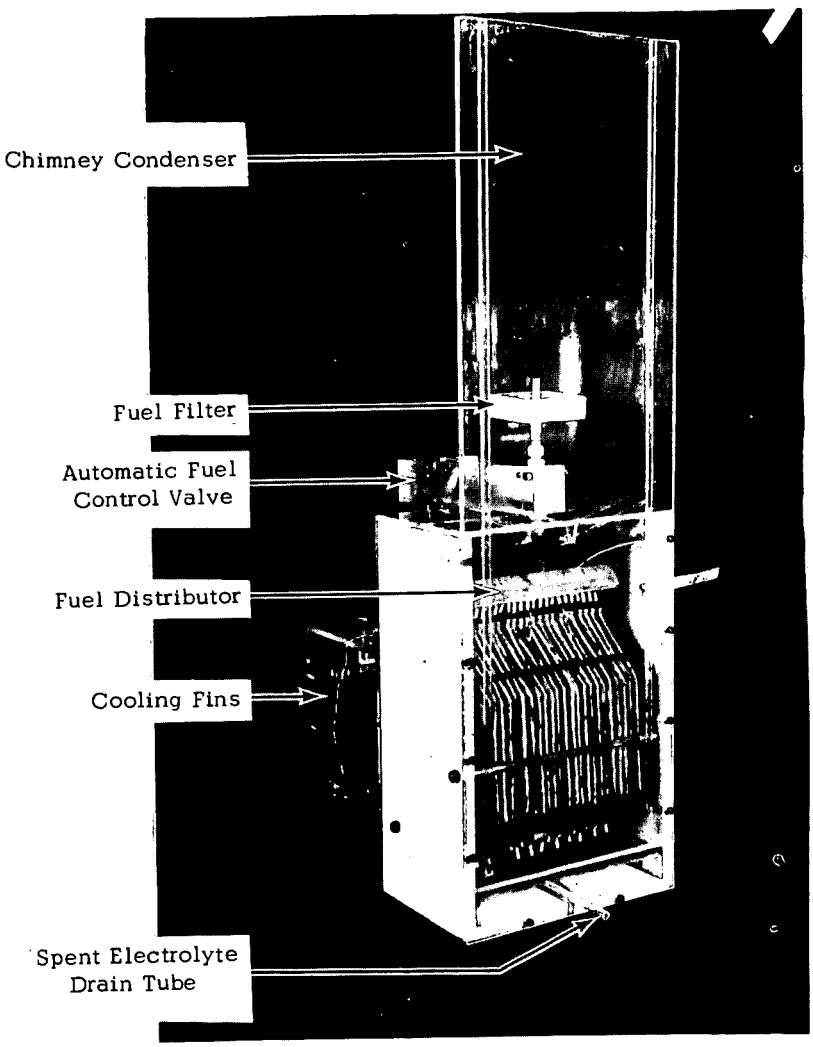

FIGURE 2. NATURAL FLOW ALKALINE METHANOL-AIR SYSTEM

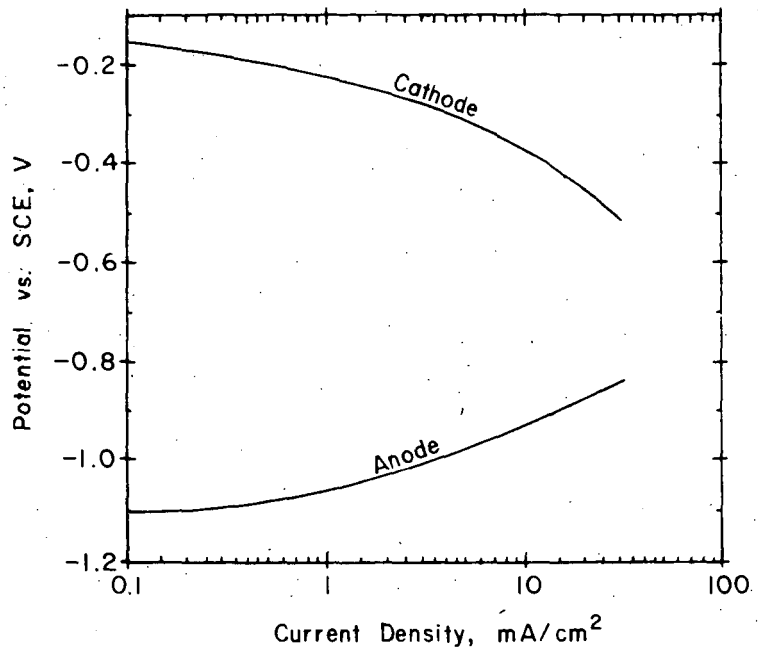

FIGURE 3. POLARIZATION CURVES FOR NATURAL-FLOW CELL

Temperature: 30°C
Fuel Rate: High

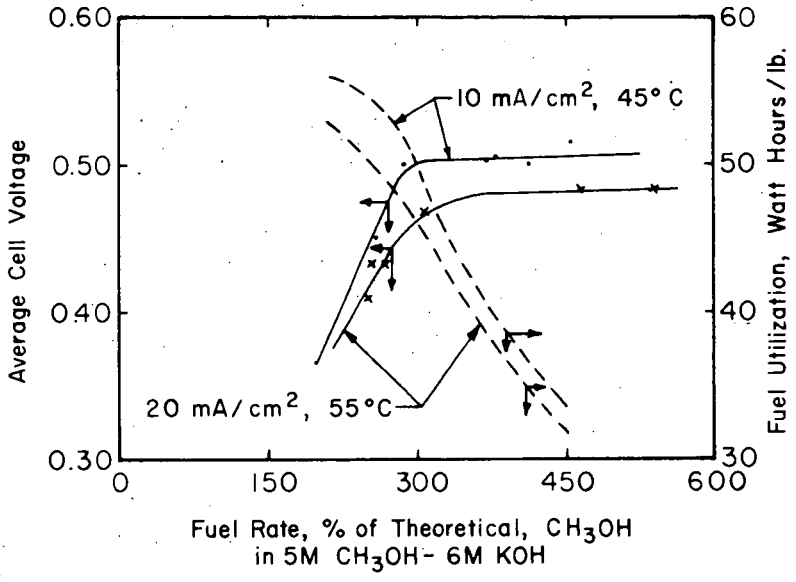

FIGURE 4. EFFECT OF FEED RATE ON AVERAGE CELL VOLTAGE AND ON FUEL UTILIZATION

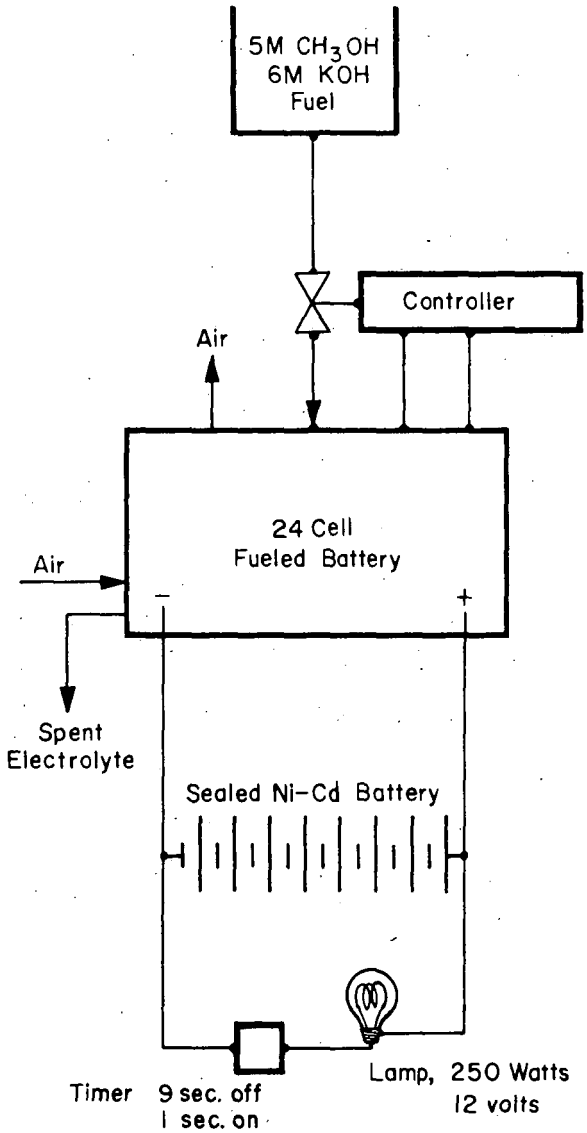

FIGURE 5. SCHEMATIC DIAGRAM OF COMPLETE POWER SYSTEM INCLUDING AN INTERMITTENT LOAD

SOME ASPECTS OF THE DESIGN AND OPERATION OF DISSOLVED METHANOL FUEL CELLS

by

K.R. Williams, M.R. Andrew and F. Jones

"Shell" Research Ltd., Thornton Research Centre, P.O. Box 1, Chester, U.K.

INTRODUCTION

It has long been recognized[1] that a soluble fuel such as methanol may conveniently be used in low temperature fuel cells. However most early attempts to realize this type of fuel cell involved the use of an alkaline electrolyte, which would have been rapidly converted to carbonate. Thus potassium or sodium hydroxide solutions do not meet the requirements of invariance implicit in the definition of a fuel cell. At low temperatures, that is at ambient temperature and slightly above, carbonate electrolytes are unsuitable; not only is the performance of the oxygen electrode poor and the anode subject to concentration polarization, but formation of the bicarbonates, which are of low solubility, makes it difficult to conceive of a reasonably invariant system when such an electrolyte is used. If operation at around 120°C is acceptable, then Cairns and his co-workers[2,3] have shown that caesium and rubidium carbonates can be used as invariant electrolytes for methanol fuel cells. However, the performance of present oxygen electrodes in this electrolyte falls short of that obtained in strong acids and bases. Furthermore, as Williams and Gregory[4] have shown only strong acids and bases can be used as electrolytes for low temperature fuel cells if high current densities are required.

These considerations suggest that a strong acid is likely to be the most satisfactory electrolyte for a direct methanol fuel cell. Of the strong acids, sulphuric seems the best choice if operation at temperatures between ambient temperature and 60 or 70°C is required. This acid has a high specific conductivity, is non-volatile and, although it is

corrosive, the problems attendant upon its use are not insurmountable. In our experience the performance of oxygen electrodes in sulphuric acid is marginally better than in phosphoric acid, the major alternative; also the electrical conductivity of sulphuric acid is higher than that of phosphoric acid at low temperature. Perchloric acid offers no significant advantage over sulphuric acid with our electrodes and as there is a possible fire hazard with perchloric acid and methanol we preferred sulphuric acid.

Another advantage of acid electrolytes is that water removal is easier than with an alkaline electrolyte. This is because, with an acid electrolyte, hydrogen ions discharge on the air electrode to form water which is readily removed. On the other hand in alkaline systems, water has to be transported from the fuel electrode through the electrolyte to the air electrode. This process takes place against the concentration gradient as the concentration of electrolyte is highest, and hence vapour pressure of water lowest, at the region from which water is evaporated.

There are various reasons for accepting an upper limit of operating temperature of 70°C for the dissolved methanol cell. In the first place methanol, even in solution, is sufficiently volatile at temperatures above 60°C as to necessitate stringent precautions against loss by evaporation. Secondly, an upper temperature limit of about 70°C means that a wide range of cheap, commercially available plastics offers sufficient temperature and corrosion resistance to be useful for fuel cell construction. Additionally, corrosion problems, particularly in the vicinity of the air electrode, are aggravated by increased temperatures and offer a further incentive to relatively low temperature operation. Finally, if a cell is designed to run at about 60°C, it will have a reasonable output at room temperature and will start easily from cold.

The ability to operate an invariant acid electrolyte system at a relatively low temperature may be of importance where extreme longevity is required. In our experience the rate of electrode deterioration increases with increasing operating temperatures but even at the present state of the art, lives of the order of years appear possible if temperatures can be kept fairly close to 30°C.

EXPERIMENTAL

For our air electrodes we have developed a structure in which microporous polyvinyl chloride (P.V.C.) is used as the substrate[5]. This substrate is made conducting by being coated with an evaporated metal layer, which may be thickened by electrodeposition of more metal. Finally, a catalyst is applied to the electrode surface. In acid electrolytes we have used gold as the conducting metal layer. Since quite thin layers of gold are acceptable, the intrinsic value of the substrate (microporous polyvinyl chloride together with the gold film) is only about $1.50 per sq.ft.

The performance of oxygen and air electrodes of this type in acid and in acid to which methanol has been added is shown in Figure 1 in which the scale of the ordinate is exaggerated in order to emphasize the differences in electrode performance. It can be seen that the voltage of the air electrode throughout the current range is within 50 mV of that of the electrode using pure oxygen. This is characteristic of electrodes of this type provided that the catalytic activity is high. Whilst the presence of methanol in the electrolyte has a substantial effect on the open circuit voltage of the air electrode, at useful current densities 1M methanol depresses the potential of the air electrode by only 20-50 mV.

We have found that the microporous plastic also makes an ideal substrate for methanol electrodes. This quite naturally led to our using both sides of the material to make a complete cell. One side of the substrate is used for the air electrode and the other side for the methanol electrode, the cell thickness being the thickness of the porous plastic itself. Thus it is now a relatively simple matter to make complete cells with an inter-electrode distance of 0.030 inch and having a very low internal resistance.

The performance of both methanol and air electrodes in a complete cell at 25°C and 60°C is shown in Figure 2. Over this temperature range, the air electrode is relatively unaffected by the temperature of operation whereas the voltage of the methanol electrode at reasonable current densities decreases by about 100 mV as the temperature is raised. The internal resistance of the fuel cells is, of course, varied by electrode separation. A typical voltage loss due to internal resistance at a current density of 100 mA/sq.cm would be 45 mV per cell.

Methanol-air batteries with sulphuric acid electrolyte have been built from cells of this type. The alternative design in which a separate piece of porous plastic is used for each electrode, with a relatively thick electrolyte layer between the electrodes, has also been used in the construction of batteries. Both designs of cell are shown schematically in Figure 3. With both types of battery internal electrical connections from the electrodes to the conducting cell separators were made from gold-plated plastic mesh. Thus series electrical connection is built into the batteries. The mesh chosen allows the free passage of gas past the air electrodes, escape of carbon dioxide bubbles from the electrolyte and current collection from the surface rather than from the periphery of the

electrodes. The construction of this type of cell is described elsewhere[5] and Figure 4 shows a 300 watt methanol-air battery of 40 cells.

During operation of an 8-cell prototype methanol-air fuel cell using 6N sulphuric acid, the fuel-electrolyte mixture developed an ester-like smell. The electrolyte was extracted with ether and the extract analysed by gas-liquid chromatography. In addition to the intermediates normally encountered (formaldehyde and formic acid), traces of acetic, propionic, butyric and isobutyric acids were detected together with some unidentified compounds. These materials were not present in either the methanol used as fuel or in the ether used for the extraction.

These side products are present in small quantities but may be strongly adsorbed on the electrocatalyst thereby causing the observed slow decline in electrical output with time. Experiments in which small quantities of these materials were deliberately introduced into a fresh electrolyte - fuel mixture showed that they had a poisoning effect on the methanol electrode.

We have carried out some preliminary experiments to determine the source of these poisons. The first possibility that occurred to us was that these materials might arise as a result of attack by the acid electrolyte on one or other of the plastics present in the cell (polystyrene, Perspex, P.V.C., or polyethylene). We were able however to detect traces of these organic acids after prolonged anodic oxidation of methanol in 6N sulphuric acid in all-glass apparatus with a platinized-platinum anode.

DISCUSSION

In spite of the difficulties of choosing inexpensive, acid-resistant constructional materials, developing suitable electrocatalysts and minimizing the effects of impurities on the electrodes, we have built a series of satisfactory methanol-air batteries. The first battery - a small 8-cell prototype - was built in September 1963 and is still operational, giving 2.85 watts at 1 amp compared with its initial performance of 3.15 watts at the same current density. This testifies to the longevity of the system, for the only servicing the battery has received is an occasional wash with distilled water.

Since the prototype was built we have been able to build larger batteries using improved electrocatalysts and this work has led to the construction of a 40-cell battery delivering 300 watts at 12 volts at 60°C. With this battery, as with all the other batteries we have constructed, there has always been an ester-like smell and organic acids have been detected frequently. It is interesting to speculate on the origins of these materials.

Whilst radical dimerizations are frequently encountered in electrochemical processes[6], this type of reaction does not seem likely here. If a radical were polymerizing then the expected yields of acids would be butyric $\ll$ propionic $\ll$ acetic. Even though the isolation of the organic acids is only qualitative it seems that they are present in quantities which decrease only slowly as one goes up the homologous series. Thus the likely route appears to be an attack of a radical on a methanol molecule.

The existence of the radical H - $\underset{\underset{M}{\|}}{C}$ - OH has been postulated in the

Fischer-Tropsch synthesis[7] of organic compounds from carbon monoxide and hydrogen. Formaldehyde, which has been detected in solution by several workers[8,9], might have this structure in the adsorbed state and, by progressive condensations with methanol and subsequent rearrangements, would lead to aldehydes which, under the anodic conditions present, would be electrochemically oxidized to the organic acids which have been detected. However, until a more thorough investigation of the spectrum of products is available, the reaction mechanism must remain obscure.

Finally, although these side reactions cause some trouble, the longevity of our prototype battery testifies to the fact that they do not have a disastrous effect on cell life. However, attention will have to be devoted not only to improving the efficiency of electro-catalysts for the methanol oxidation but also to the suppression of side reactions. Probably, if a catalyst is sufficiently good for the overall reaction of methanol to carbon dioxide, the side products will be formed in negligible quantities.

REFERENCES

1. K. Kordesch and A. Marko. Oesterr. Chemiker-Z., 52 (1951) 185.
2. E.J. Cairns and D.I. MacDonald. Electrochem. Technol., 2 (1964) 67.
3. E.J. Cairns and D.C. Bartosik. J. Electrochem. Soc., 111 (1964) 1205.
4. K.R. Williams and D.P. Gregory. J. Electrochem. Soc., 110 (1963) 209.
5. K.R. Williams and J.W. Pearson. Joint Symposium of the Inst. of Chem. Eng. and the Amer. Inst. of Chem. Eng., June 1965, (in press).
6. A.P. Tomilov and M.Ya. Fiochin. Russian Chem. Rev., 32 (1963) 30.
7. G.C. Bond. Catalysis by Metals. Academic Press, London, 1962, p.365.
8. T.O. Pavela, Ann. Acad. Sci. Fernicae, A II 59 (1954) 7.
9. M.J. Schlatter, Fuel Cells, Vol. 2, ed. G.J. Young, Reinhold, New York, 1963, p.190.

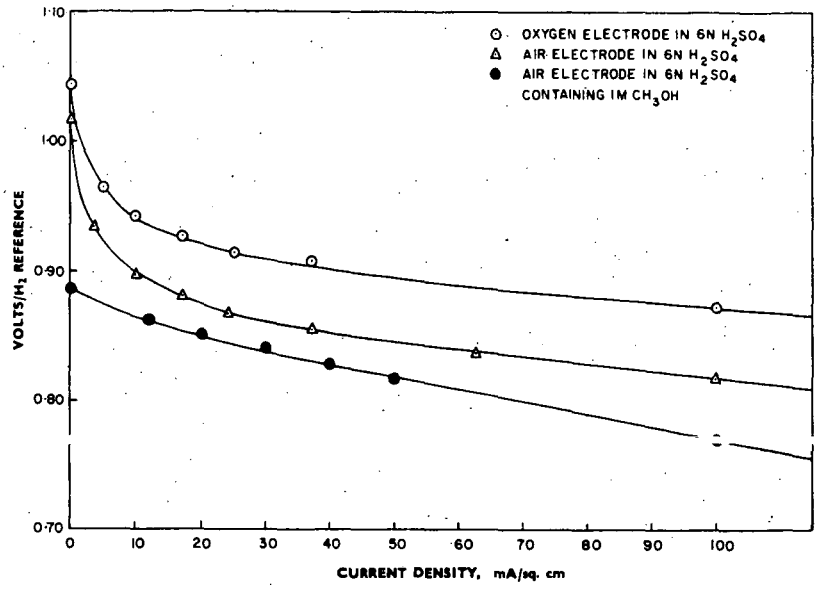

FIG. 1—Polarization curves for oxygen and air electrodes in sulphuric acid solution at 25°C

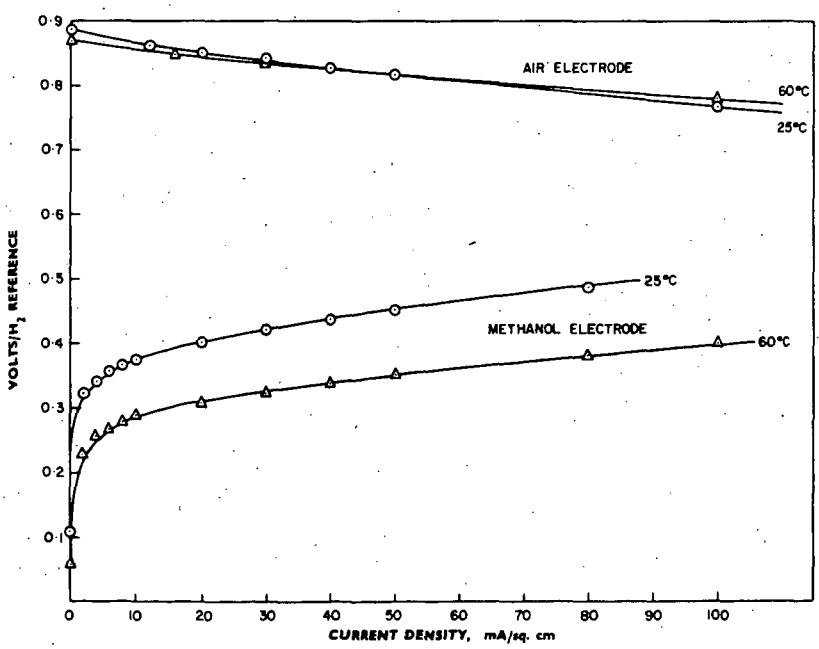

FIG. 2—Polarization curves for air and methanol electrodes in a 1M CH_3OH – 6N H_2SO_4 mixture at 25° and 60°C

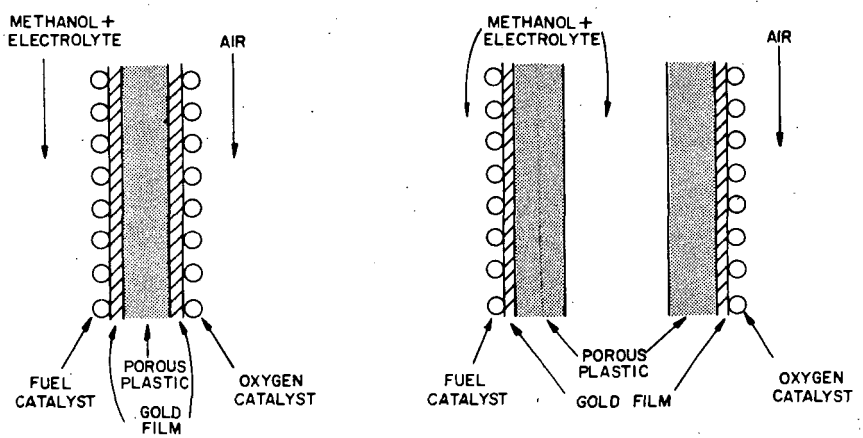

FIG. 3—Schematic drawing of two types of single cell

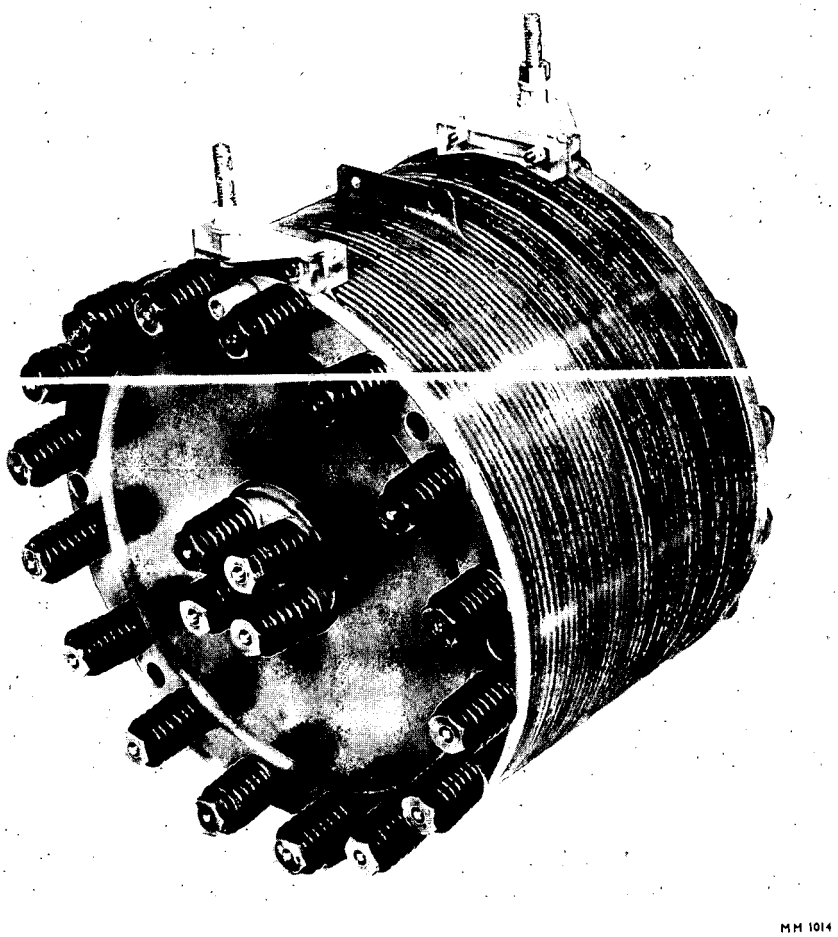

FIG. 4 – 40-cell methanol-air fuel battery

A COMPARISON BETWEEN EXTERNAL AND INTERNAL REFORMING METHANOL FUEL CELL SYSTEMS

Nigel I. Palmer, B. Lieberman and M. A. Vertes

Leesona Moos Laboratories
Division of Leesona Corporation
Great Neck, New York

INTRODUCTION

With the results of several years work in many laboratories now available, it is possible to compare the rather limited number of fuel cell systems capable of operating on carbonaceous fuels. Although many of the approaches are conceptually simple, it must be conceded that none meet the original objectives of ultra-high efficiency and system simplicity. Because of this, it may be misleading to base comparisons only on the characteristics of the central component, i.e., the fuel cell. The object of this paper is to compare designs for two complete 6 kw fuel cell systems operating on methanol and air.

Figure 1 illustrates the basic system options that are available. The direct anodic oxidation approach remains conceptually the most attractive. However, unsolved problems of catalyst cost and stability, corrosion and electrochemical efficiency have so far prevented it entering a development stage. The remaining approaches may all be termed 'indirect' in that the anodic oxidation step involves hydrogen produced from the fuel in a previous stage. System (2), using an acid electrolyte cell retains some of the problems of the direct system; namely, materials and catalyst stability in acid, plus poisoning by trace amounts of carbon monoxide. System (3) which is undoubtedly the most developed, retains the advantages of a basic electrolyte cell by prepurifying the hydrogen -- usually with a palladium/silver diffuser. A variation of this system combining the last two stages by the use of palladium/silver anodes (System 4) has been described by Chodosh and Oswin.[1] More recently, Vertes and Hartner have described an alternative approach[2] originally developed at Leesona Moos Laboratories in which the reforming, purification and anodic oxidation steps are integrated within the anode structure (System 5). This is referred to as an 'integral reforming' or 'internal reforming' fuel cell system.

In principle all the systems shown are capable of operating on any carbonaceous fuel. Methanol, however, offers several advantages for fuel cell use, and the systems compared have been designed for this fuel. Significant factors determining this choice were:

1. The favorable thermodynamics of methanol reforming at relatively low temperature.
2. The favorable kinetics and catalyst stability obtained for the methanol reforming reaction.
3. The complete miscibility of methanol and water with resultant simplification of system design.
4. The availability of relatively cheap, high purity methanol.

INTERNAL REFORMING PRINCIPLES

Before discussing the overall systems, it will be necessary to describe briefly the operating principles of the internal reforming electrodes. Figure 2 illustrates the sequential steps involved. An equimolar mixture of methanol and water is vaporized and passed through a catalyst bed contained in a thin plenum chamber behind the palladium/silver membrane. Here dehydrogenation of the methanol occurs first, followed by shift conversion of the resultant carbon monoxide.

Dehydrogenation	$CH_3OH \longrightarrow CO + 2\,H_2$	(1)
Shift	$CO + H_2O \longrightarrow H_2 + CO_2$	(2)
Overall	$CH_3OH + H_2O \longrightarrow CO_2 + 3\,H_2$	(3)

Hydrogen from this reaction zone diffuses through the palladium-silver membrane to the electrolyte side where it is anodically oxidized. The 75% palladium/25% silver membrane, 1 mil thick, activated with palladium black[3] imposes no restraint on the reaction and limiting currents exceeding 1 amp/cm^2 have been obtained. The electrolyte employed can in principle be either acid or base, but 85% KOH has been preferred because of its lower vapor pressure, lower corrosion, and the higher performance obtained.

The overall reforming reaction is endothermic. In this system the necessary heat can be supplied directly by the waste heat produced in the cell by entropy and polarization losses. Various side reactions such as the methanation reaction can be suppressed by proper selection of the catalyst. Best results have been obtained using a mixed oxide type catalyst. It may be observed here that because of the physical separation of catalyst from electrolyte, optimization of the catalyst is substantially easier than for a direct oxidation anode. Thermodynamically, conversion to hydrogen is 99% complete at 160°C. The lower temperature limit for operation is established at about this point by kinetic considerations. A higher operating limit of 300°C is established by electrolyte and materials limitations within the cell itself. Selection of the optimum operating temperature requires an analysis of several other interrelated factors and is discussed in a later section on system design.

SYSTEM EFFICIENCIES

The primary reason for using a fuel cell is the high efficiency of energy conversion, although account must be taken of other factors such as weight, volume, capital cost, etc. The priority of these will be determined by the requirements of a particular application.

The net thermal efficiencies of both fuel cell systems can be expressed as functions of the same set of component efficiencies; however, the interrelations and limits of these component efficiencies are quite different for the two cases. Figure 3 shows the location of the points of energy loss - expressed as efficiencies.

The efficiencies considered are:

Net system efficiency $\eta_N = \frac{\text{Net electrical energy delivered}}{\text{Heating value of } CH_3OH \text{ supplied}}$

Conversion efficiency $\eta_C = \frac{H_2 \text{ produced in the reformer}}{H_2 \text{ stoichiometrically available from } CH_3OH/H_2O}$

Heat exchange efficiency $\eta_E = \frac{\text{Heat supplied}}{\text{Heat available}}$

Utilization efficiency $\eta_U = \frac{H_2 \text{ anodically consumed}}{\text{Total } H_2 \text{ produced}}$

Cell thermal efficiency $\eta_T = \frac{\text{Gross electrical energy produced}}{\text{Heating value of } H_2 \text{ consumed}}$

Auxiliaries efficiency $\eta_A = \frac{\text{Net electrical energy delivered}}{\text{Gross electrical energy produced}}$

Evidently, defined in this way the net system efficiency is expressed as a product of the component efficiencies.

$$\eta_N = \frac{3\,\Delta H_{ox}'}{\Delta H_{ox}''} \cdot \eta_C \cdot \eta_U \cdot \eta_T \cdot \eta_A \qquad (4)$$

where: $\Delta H_{ox}'$ = lower heating value of H_2 (at cell temperature)
$\Delta H_{ox}''$ = lower heating value of CH_3OH (at room temperature)

At any steady operation condition, a state of thermal neutrality must be obtained for the system.

Case I. External Reforming System. The requirement of thermal neutrality is achieved in this system by oxidizing the purge gases from the hydrogen extractor and supplying the heat produced to the reformer. Provision must also be made for removing the cell waste heat which in this system is not utilized. Writing a simplified energy balance for the system,

$$\eta_C \Delta H_R + \Delta H_V = \eta_E \left[(1 - \eta_U)\, 3\, \eta_C\, \Delta H_{ox}' + (1 - \eta_C)\, \Delta H_{ox}'' \right] \qquad (5)$$

where: ΔH_R = heat required to reform methanol, Kcals/g. mole
ΔH_V = heat to vaporize and superheat methanol and water, Kcals/g. mole

Considering the components of efficiency: The conversion efficiency η_C will have a theoretical limit established by the thermodynamics of reactions (1) and (2). This exceeds 0.99 at 200°C. In practice however, the primary limitation results from kinetic factors, i.e., need to minimize the reformer volume. With external reforming this restriction is not serious and values for η_C as high as 0.95 may be obtained. The cell efficiency η_T has a theoretical limit imposed by the cell entropy losses (approximately 0.9) and a practical limit determined by a tradeoff between the capital cost and operating cost. Since the cell waste heat is not utilized, thermal balance requirements do not impose an additional limit. The auxiliaries efficiency η_A can theoretically approach 1.0 for a simple system; in practice it will be as low as 0.7 in small systems, rising to higher values as the gross power level increases.

The H_2 utilization efficiency η_U has a theoretical limit in external reforming systems, imposed by the need to supply reformer heat. This limit will be determined by the conversion efficiency and the heat exchange efficiency between the catalytic burner and the reformer. The interrelationship between η_U, η_C and η_E is given in equation (5) and is shown graphically in Figure 4. For a given conversion level and heat exchange efficiency, the value of η_U in this graph represents the maximum utilization possible for thermal balance.

Table 1 shows the effect of component efficiencies on the system net thermal efficiency. Three cases are considered; the first refers to ultimate theoretical limits assuming complete reversibility of each component, the second refers to probable practical limits that may be approached, and the third gives state-of-the-art values employed in the present designs. In the second case a limiting operating voltage of 1.0 V is assumed.

Table 1. External Reforming System - Component Efficiencies

Efficiencies		Theoretical Limit	Practical Limit	Present Design (State of the Art)
Conversion	η_C	1.0	0.95	0.91
Cell	η_T	0.9	0.75	0.62
Auxiliaries	η_A	1.0	0.95	0.83
Heat Exchange	η_E	1.0	0.80	0.70
Utilization	η_U	0.78	0.77	0.76
Net	η_N	0.80	0.51	0.40

Case II. Internal Reforming System. Considering now the internal reforming system, it is evident that the same expression (5) for net efficiencies must hold. However, the expression for thermal neutrality is quite different since heat is now supplied by the cell:

$$\eta_C \Delta H_R + \Delta H_V = 3 \eta_C \eta_U \eta_E' (1 - \eta_T) \Delta H_{ox}' \quad (6)$$

The cell thermal efficiency may be expressed in terms of operating voltage (E):

$$\eta_T = \frac{2 E F}{\Delta H_{ox}'} \quad (7)$$

Substituting this into equation (6), an expression is obtained relating the conditions for thermoneutrality to the cell voltage:

$$\eta_C \Delta H_R + \Delta H_V = 3 \eta_C \eta_U \eta_E' \left[\Delta H_{ox}' - 2F E \right] \quad (8)$$

The heat exchange efficiency term η_E' is defined essentially as before, but has components which themselves must be optimized for thermal balance;

$$\text{i.e., } \eta_E' = \frac{\text{heat produced - losses to air - losses to surroundings}}{\text{heat produced}}$$

As in the previous system, no theoretical limits exist for η_C. Because of cell temperature, size, and heat transfer considerations, however, the practical limit for η_C may be lower for internal reforming systems. This is due, it must be emphasized, to kinetic rather than thermodynamic considerations. It may be mentioned at this point that where thermodynamic limitations do apparently occur, as for example with hydrocarbons, they may in practice be circumvented. This results from hydrogen extraction through the membrane,

distorting the equilibrium until complete conversion has occurred. This is discussed more fully elsewhere.[4] [5] With the catalysts currently used at LML, a limit of about 0.9 is obtained for methanol. η_U has no theoretical limit in this system, but a practical limit of 0.97 is probably realistic. η_A tends to be higher for the internal reforming system because of the fewer auxiliaries and simplified controls. Unlike the previous case, η_T is theoretically limited by the requirement of thermal neutrality. Equation (6) shows how this is related to η_C, η_U, and η_E'. Figure 5 shows this relationship graphically and indicates that adequate heat is available from the cell even at low heat exchange values. The apparent excess of heat, however, is balanced by losses from the cell which may impose a heat deficit. This is shown in Figure 6, which presents the components of heat balance around the internal reforming cell as a function of gross power output. The heat requirements for reforming are given for the theoretical limit of 100% conversion.

Allowing for heat input to the reformer plus losses to the cathode air streams and to the surroundings, a small heat deficit occurs. This can then be balanced by some form of heat exchange. Two possible schemes considered are: (a) inlet air to outlet air exchange to reduce air cooling; (b) outlet air to inlet methanol to reduce the vaporization load. Alternatively, if η_C is below 0.9, catalytic combustion of the residual fuel in the cell exhaust may be used, e.g., for fuel vaporization. This is the scheme employed in the present design study.

Table 2 shows values for component efficiencies equivalent to those presented in Table 1 for the external reforming system. Note that the heat exchange efficiency η_E' is determined by assuming a recovery exchanger efficiency of 75% for the non-utilized cell heat losses. It can be seen that higher overall system efficiencies may be anticipated for the internal reforming system at all levels of development.

Table 2. Internal Reforming System - Component Efficiencies

Efficiencies		*Theoretical* Limit	*Practical* Limit	*Present Design* (State of the Art)
Conversion	η_C	1.0	0.91	0.84
Cell	η_T	0.73	0.69	0.64
Auxiliaries	η_A	1.0	0.95	0.86
Heat Exchange	η_E	1.0	0.90	0.69
H_2 Utilization	η_U	1.0	0.97	0.95
Net	η_N	0.83	0.66	0.50

6 KW DESIGN STUDIES

To permit a realistic comparison of the two approaches to be made, design studies of two complete 6kw systems have been made. The normal operating output of 6kw (net) was selected as being appropriate for probable initial commercial applications. The complete systems described have not yet been built, although extensive testing of the components and major subsystems has been proceeding since 1962. As an example, Figure 7 shows a typical internal reforming bicell composed of two 5" x 5" anodes and a single porous nickel bicathode. Figure 8 shows an experimental 0.5 kw

multicell stack with associated instrumentation.

a. External Reforming: Figure 9 shows a simplified schematic of the external reforming system. Methanol/water is pumped to the reformer where it is first vaporized and then catalytically reformed. The reformer is operated at a temperature of 300°C, a pressure of 75 psig, and a space velocity of 1200 IHSV, ‡ with heat supplied by catalytic oxidation of the extractor purge gases. Product gases, largely H_2 and CO_2 are purified in a palladium/silver diffuser containing 8 ft^2 of 1 mil foil and maintained at 300°C by the hot gases from the burner. The fuel cell employed operates at 75°C with circulated 5N KOH electrolyte. Both anode and cathode are lightweight "Teflon" ‡‡ TFE-fluorocarbon resin bonded electrodes operating at 1 psig differential pressure. In the present system, platinum activation is used but cheaper catalysts are under development. Figure 10 shows the current-voltage characteristic for the cell. Electrolyte-water concentration and temperature are controlled in separate subsystems through which the electrolyte is circulated. The cell module contains a total of 189 cells with a total electrode area of 64 ft^2 providing a gross power of 7 kw at normal operating load. The net thermal efficiency of the system at operating load is 40%. System specific weight and volume are 97 lbs/kw and 1.1 ft^3/kw respectively.

Table 3 summarizes the weights and volumes of the major components.

Table 3. 6 kw External Reforming System - Component Parameters

Component	Weight (lbs)	Volume (ft^3)
Fuel Cell	130	1.7
Reformer	61	0.77
Extractor	65	0.53
Battery	87	0.75
Miscellaneous Auxiliaries	239	3.1
Total System --------	582	6.85

b. Internal Reforming: Figure 11 shows a schematic of the internal reforming system. As discussed previously, thermal balance is achieved in the system by catalytic combustion of the cell exhaust gases to vaporize and superheat the methanol/water feed. The thermodynamic and kinetic factors involved in optimization of the cell operating temperature have already been mentioned. Other factors which must be considered are the requirements of heat transfer to the reaction zone and the need to minimize cell volume. As cell temperature is increased, the catalyst activity increases permitting a higher space velocity and thus a thinner catalyst bed for the same conversion level. This also results in increased heat transfer. Analysis of the present system indicated an optimum operating temperature of 225°C. Temperature control of the system is achieved by circulating oil through jackets around the cells. Water of reaction is removed from the cathodes via the excess air on a self-regulating basis. The air is scrubbed before entering the cells to prevent carbonate formation. Figure 12 shows the voltage-current characteristic for the cells. Operating point at rated load is 210 amps/ft^2 at 0.8 V. 121 cells

---

‡ IHSV is the ideal hydrogen space velocity defined as the volume of hydrogen produced by stoichiometric conversion of the fuel supplied per hour divided by the reactor volume.

‡‡ A DuPont registered trademark.

with a total area of 40 ft^2 provide a gross normal operating power of 7 kw. System net thermal efficiency at this operating point is 50%. Specific weight and volumes are 80 lbs/kw and 0.57 ft^3/kw respectively. Weights and volumes of the major components are summarized in Table 4.

Table 4. 6 kw Internal Reforming System - Component Parameters

Component	Weight (lbs)	Volume (ft^3)
Fuel Cell	284	1.5
Battery	87	0.75
Miscellaneous Auxiliaries	109	1.2
Total System ---	480	3.45

OVERLOAD AND CONTROL

The cell operating point is determined by the maximum overload required in a particular operation. In many applications, particularly electromechanical, the overload may be high but of relatively short duration. Under such conditions, an optimum for capital cost and size may be obtained by a hybrid combination of fuel cell and secondary battery. This battery supplies transient overloads and is automatically recharged by the fuel cell. The fuel cell itself may then be scaled to satisfy the integrated power requirement (i.e., total kwh/time) while operating at near peak power densities. This approach has been incorporated in both of the present system designs. It may be noted that a battery will in any case be required to provide the start-up power necessary for indirect systems. The battery capacity will be determined by either the overload requirements or the start-up demands. In the present design, lead acid batteries have been specified to provide 5:1 overload capability.

It is impossible in the present discussion to analyze the system controls in detail; however, some of the factors affecting response to varying loads should be mentioned. In a simple hydrogen/oxygen cell supplied from high pressure tanks, response is limited only by gas flow and regulator operation and is therefore quite rapid. With an indirect system, however, the change in load must be transmitted to each of the previous stages. Depending on the capacity and response of these stages, serious control lags may develop. To provide a smoother response, a small hydrogen surge tank has been incorporated in the external reforming design.

The control problem is minimized in the internal reforming system because of the closer integration of the reaction stages. In addition, the high hydrogen capacity of the palladium/silver membrane provides an effective surge capacity corresponding to approximately 6 coulombs/cm^2. This is roughly two orders of magnitude higher than for a platinum activated electrode.

CONCLUSIONS

An analysis of the various factors presented indicates that a selection between the external and internal reforming systems will depend largely on the requirements of the particular application. It has been shown that substantially higher system efficiencies are possible with internal reforming. This will be

obtained however at the expense of a higher capital cost resulting from the higher palladium content and more expensive materials of construction used in the system. Because of the fewer auxiliaries, the volume of the internal reforming system is substantially smaller, though system weights are similar. The superior response characteristics of this system may be important in variable load applications.

Considering future development, the efficiency of the external reforming system can be improved mainly by increasing cell operating voltages. On the other hand, to further improve the efficiency of the internal reforming system will require development of more active catalysts. This is particularly necessary if operation is to be extended to the use of hydrocarbon fuels. Capital cost reduction will require the use of thinner palladium membranes and higher operating cell current densities. Work along these lines is in progress.

REFERENCES

(1) H. G. Oswin and S. M. Chodosh, "Fuel Cell Systems," Advances in Chemistry Series 47, p. 61 (1965).
(2) A. J. Hartner and M. A. Vertes, London A. I. Ch. E. - I. Ch. E. Meeting, June 1965.
(3) S. M. Chodosh and H. G. Oswin, Brussels Fuel Cell Symposium, June 1965.
(4) M. A. Vertes and A. J. Hartner, Brussels Fuel Cell Symposium, June 1965.
(5) D. P. Gregory, Present Symposium, ACS, September 1965.

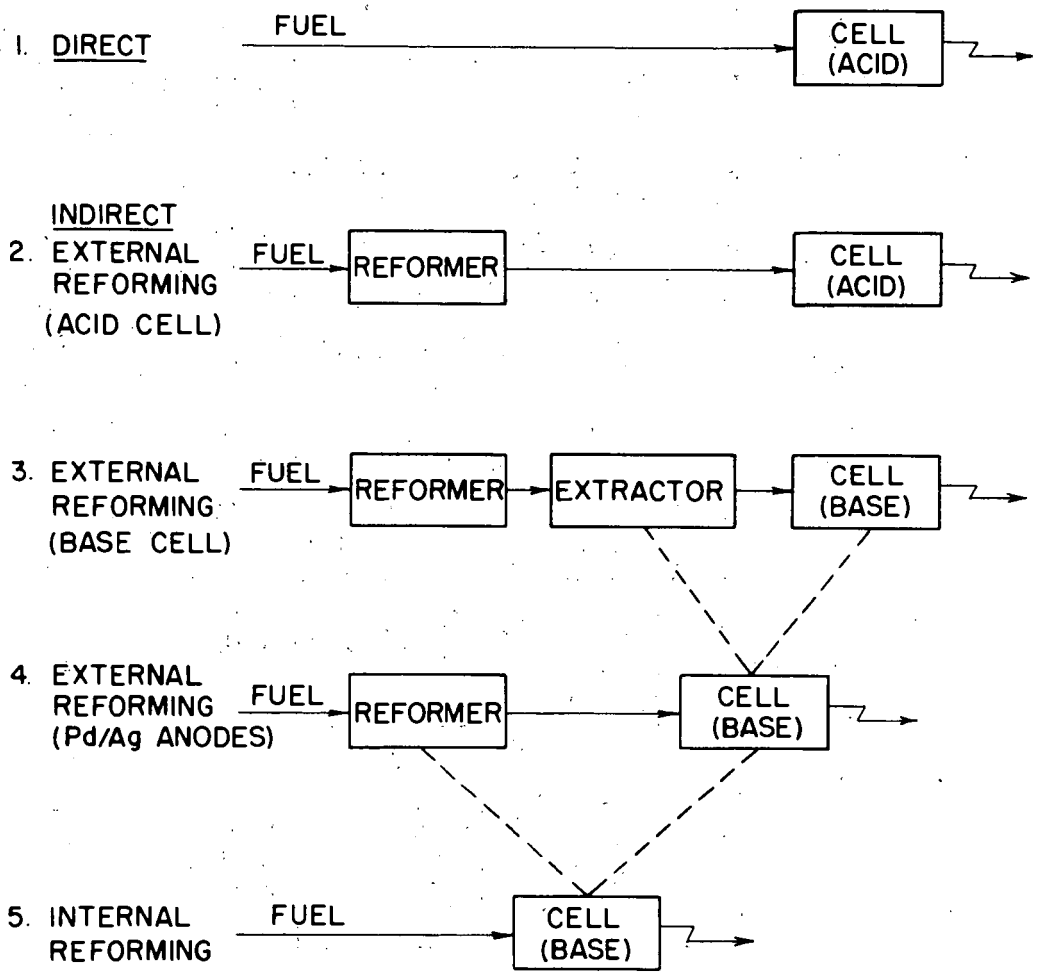

FIG. 1 CARBONACEOUS FUEL CELL SYSTEM OPTIONS

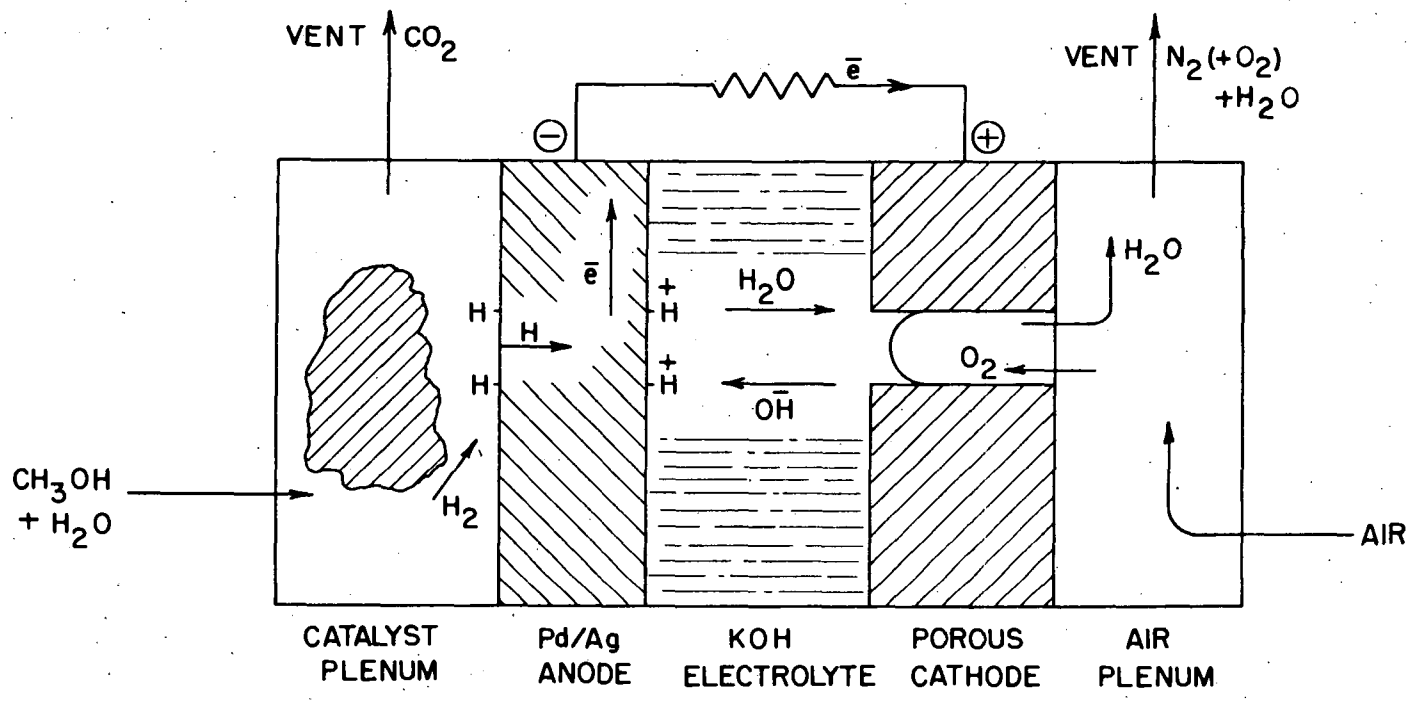

FIG. 2 OPERATING PRINCIPLE OF INTERNAL REFORMING CELL

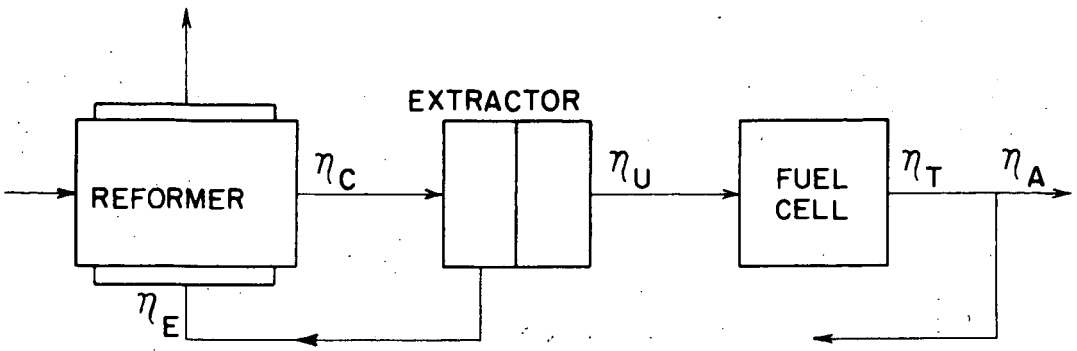

(a) EXTERNAL REFORMING

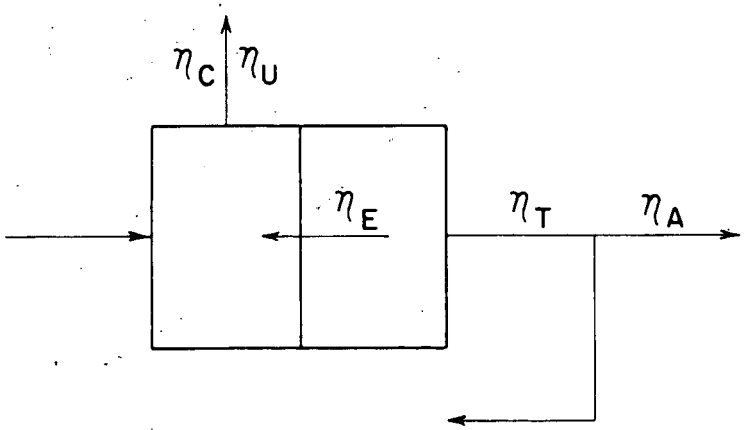

(b) INTERNAL REFORMING

FIG. 3 ANALYSIS OF SYSTEM EFFICIENCIES

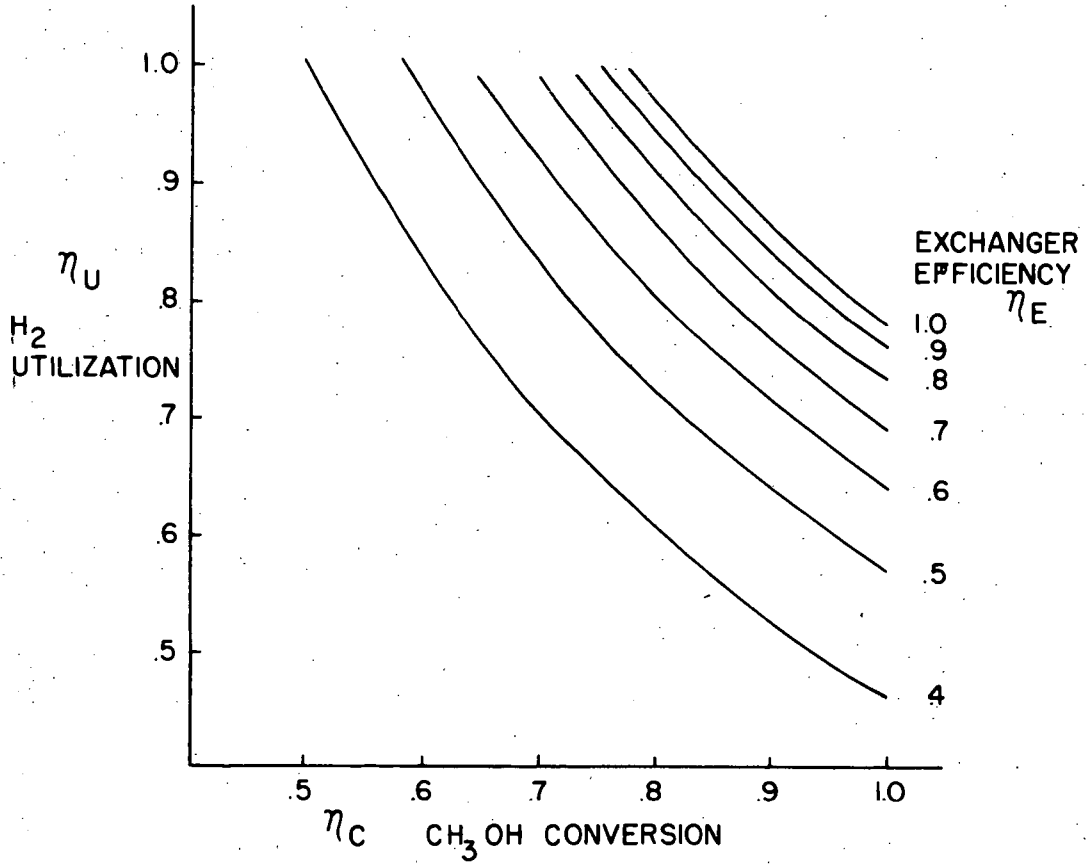

FIG. 4 CONDITIONS FOR THERMAL NEUTRALITY FOR EXTERNAL REFORMING SYSTEM

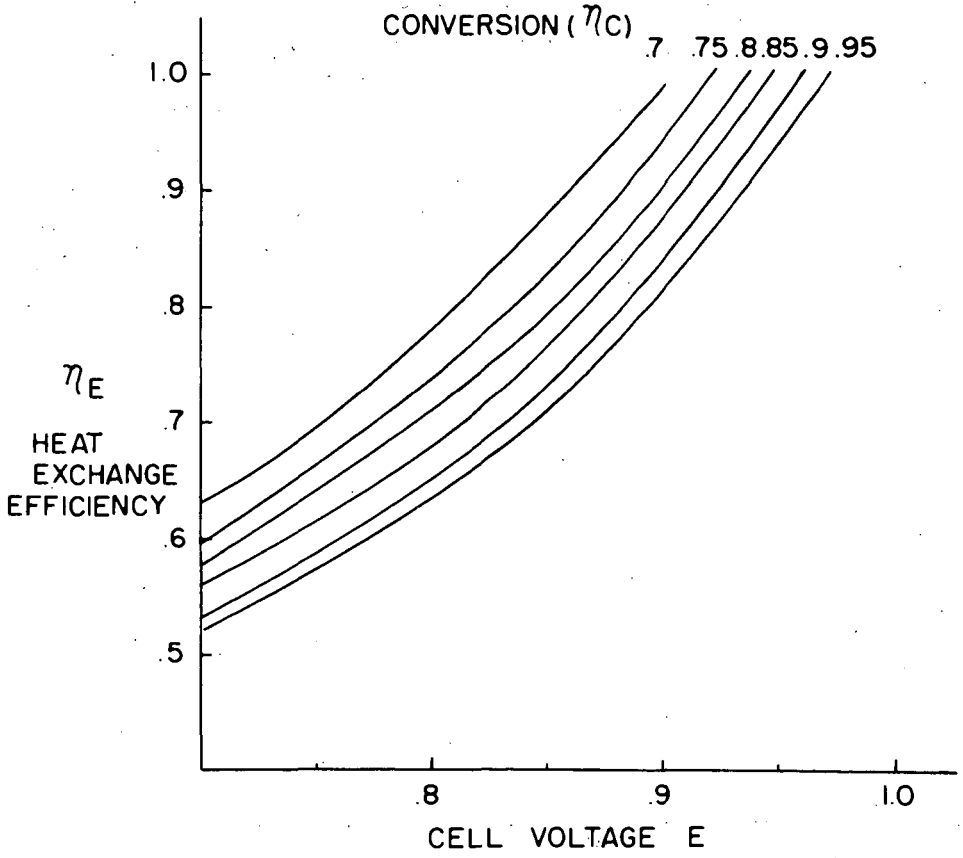

FIG. 5 CONDITIONS FOR THERMAL NEUTRALITY FOR INTERNAL REFORMING SYSTEM

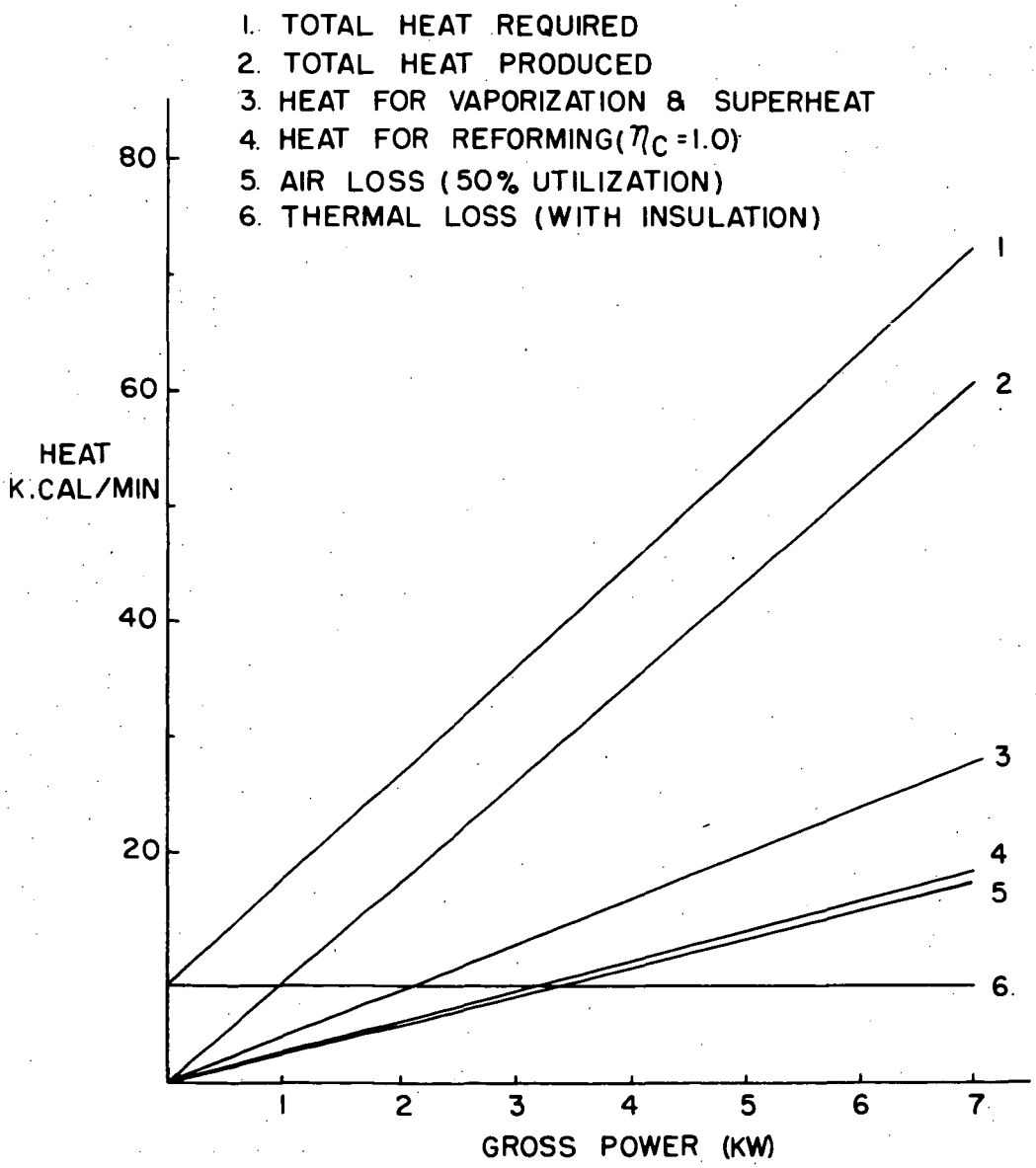

FIG. 6 HEAT BALANCE FOR INTERNAL REFORMING SYSTEM

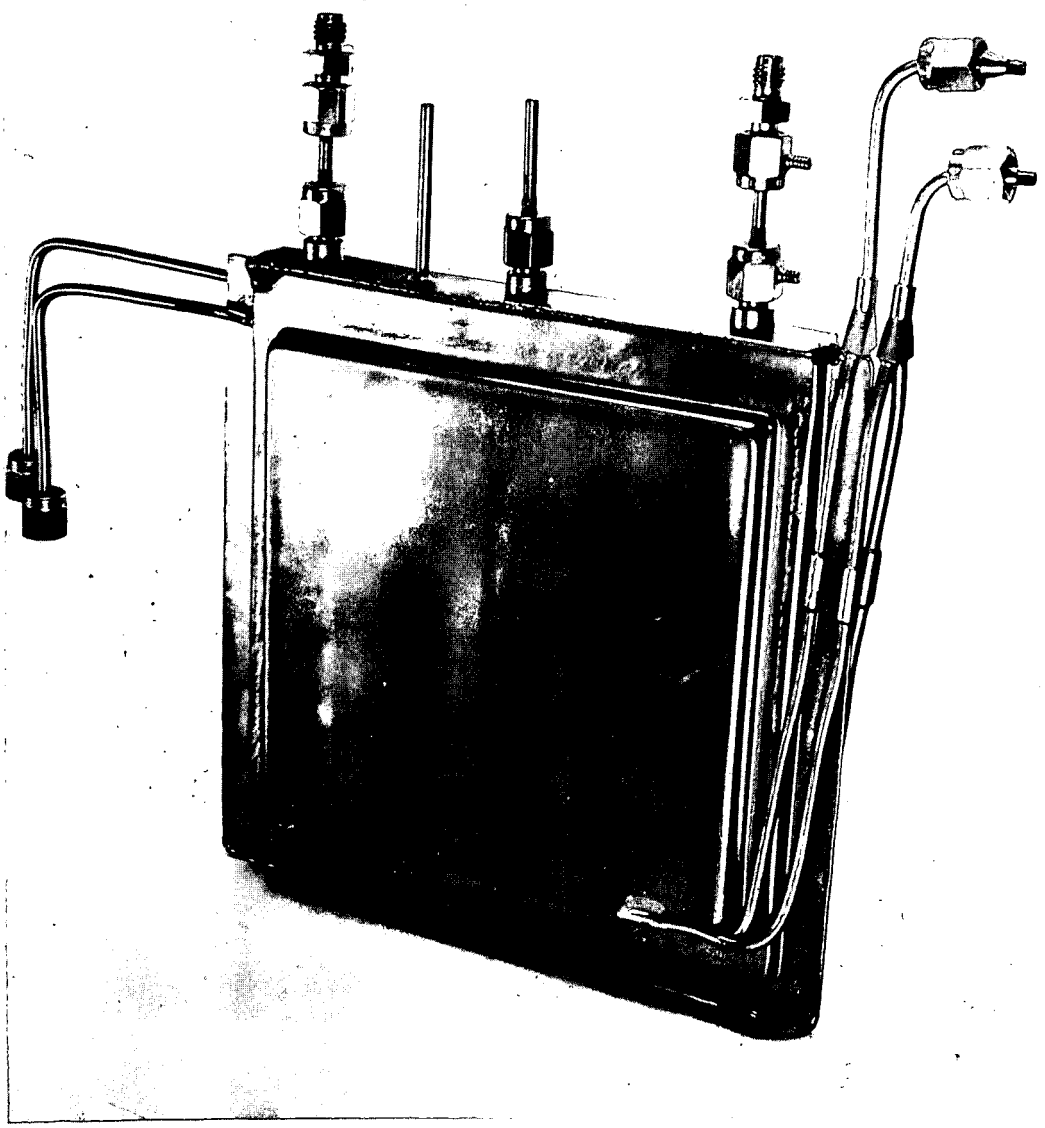

FIG. 7 METHANOL / AIR FUEL CELL

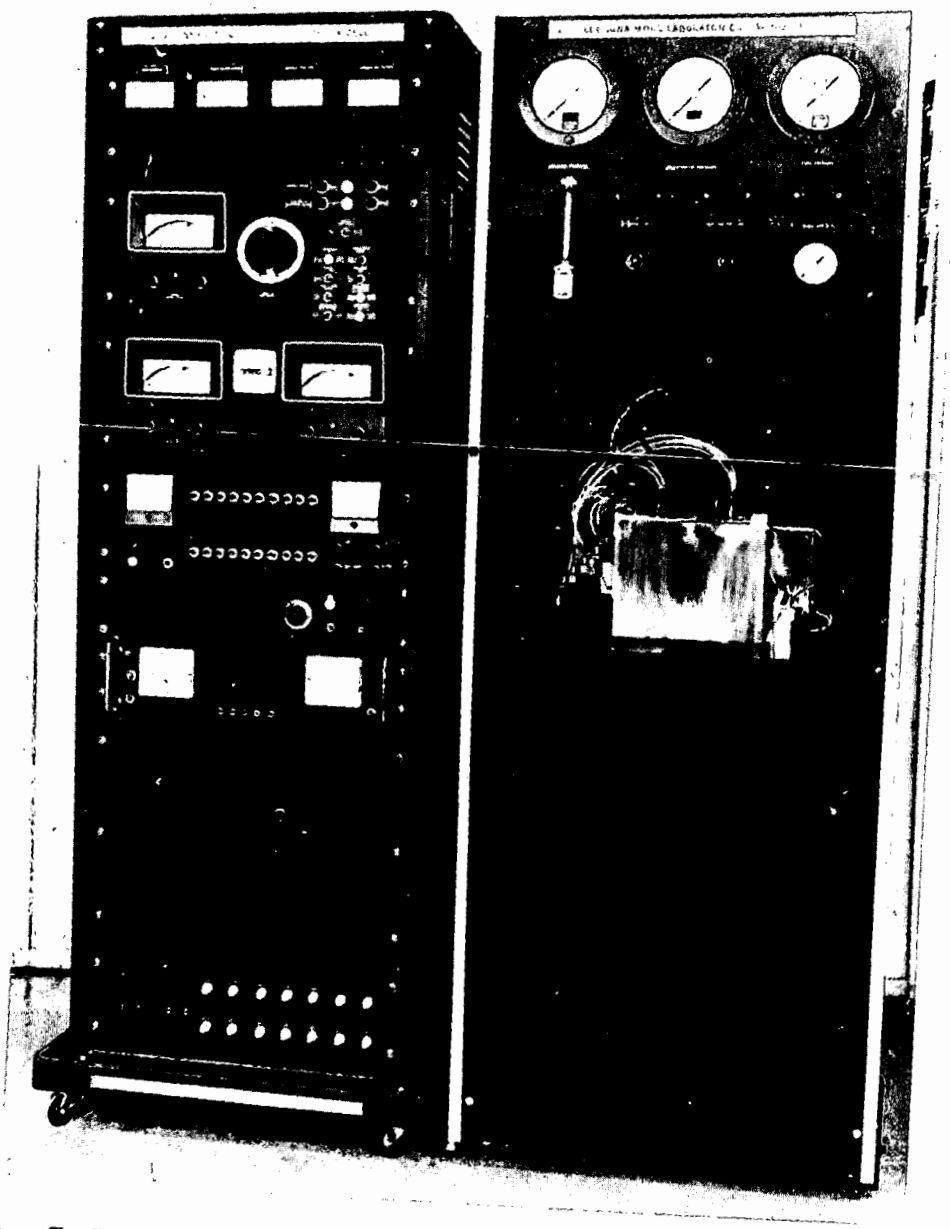

FIG. 8 EXPERIMENTAL 0.5KW INTERNAL REFORMING SYSTEM

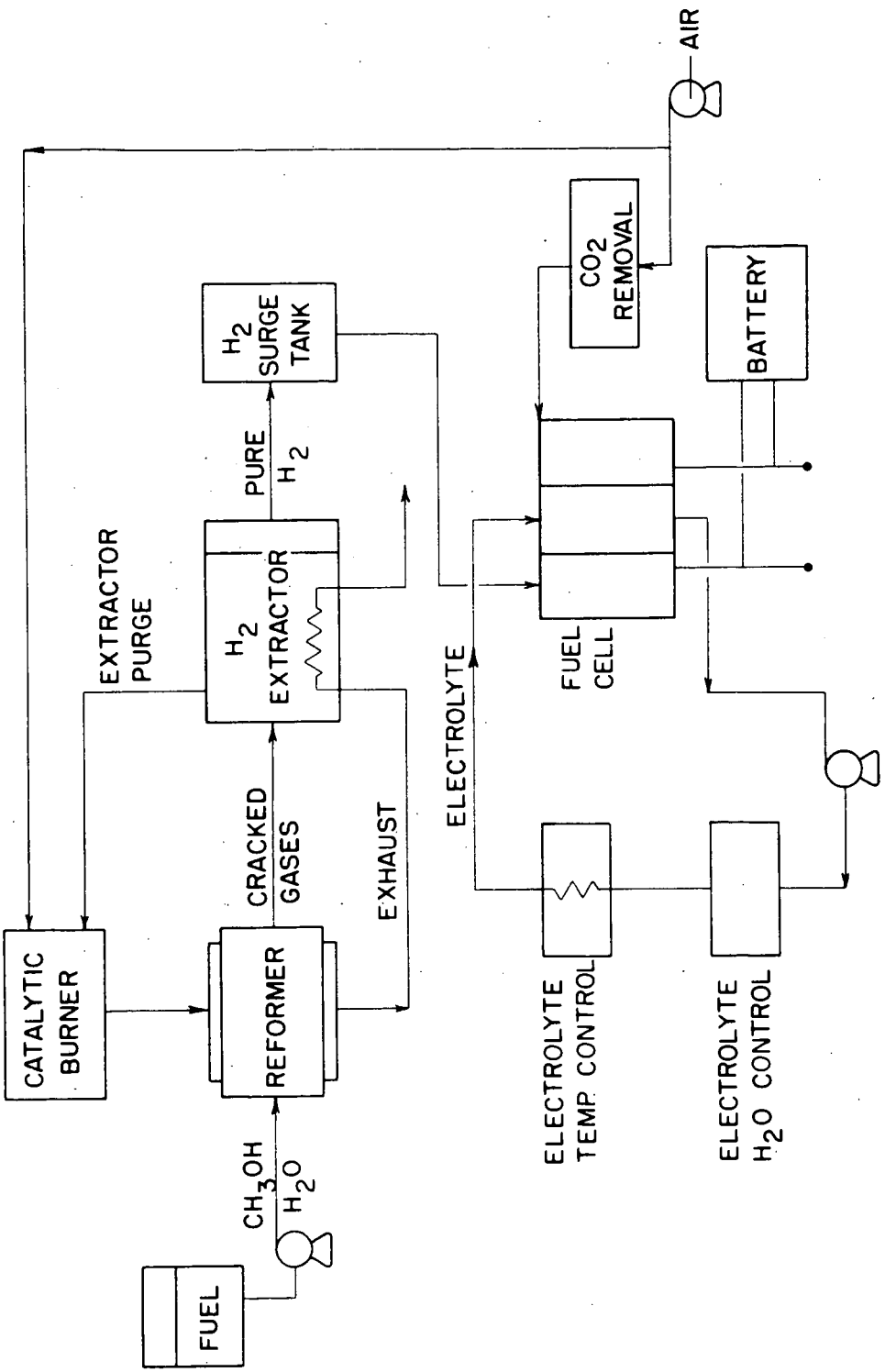

FIG.9 SCHEMATIC OF EXTERNAL REFORMING METHANOL FUEL CELL

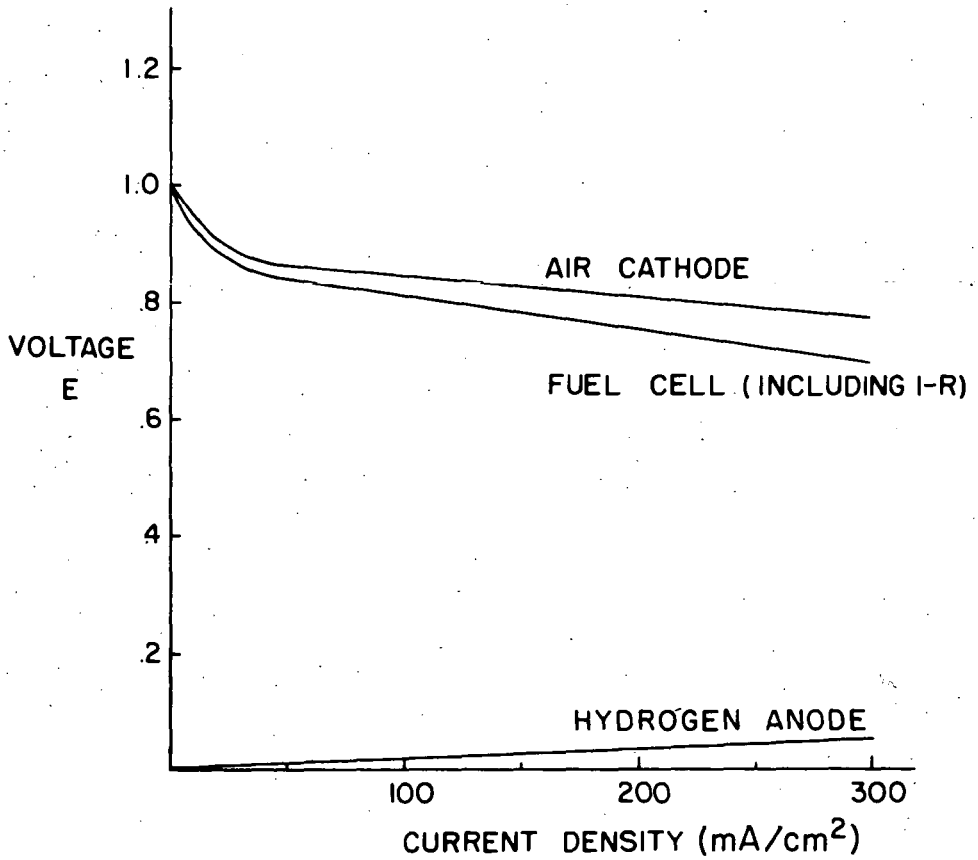

FIG. 10 E/I CHARACTERISTICS – HYDROGEN/AIR CELL

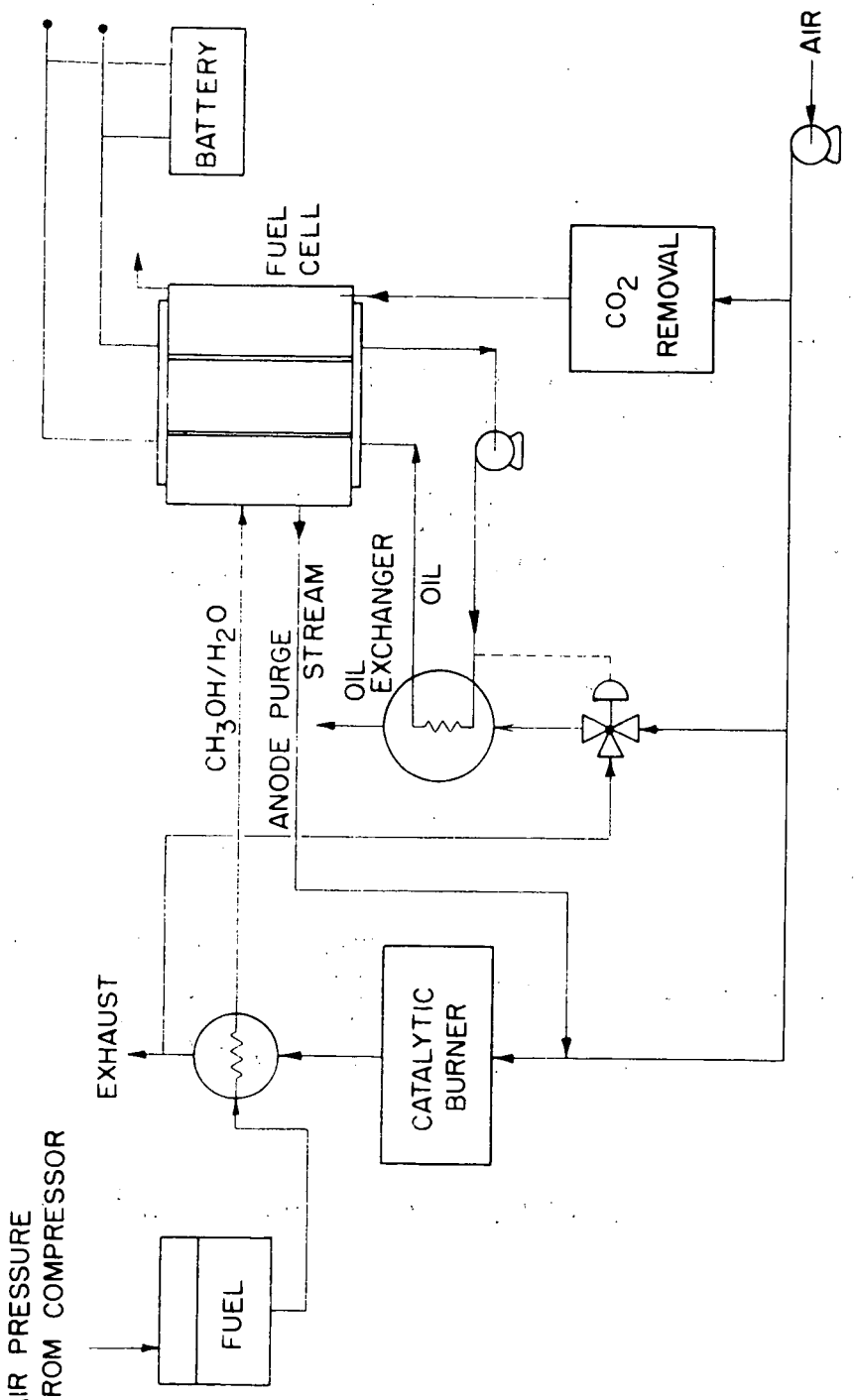

FIG. II SCHEMATIC OF INTERNAL REFORMING METHANOL FUEL CELL

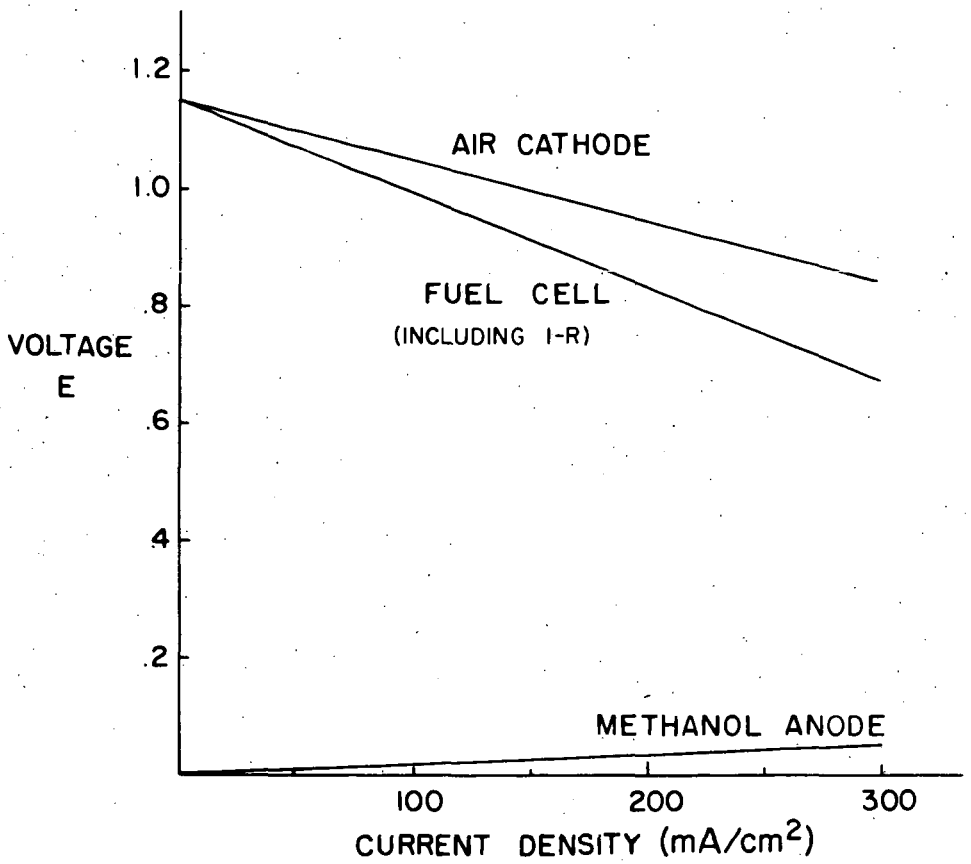

FIG. 12 E/I CHARACTERISTICS - METHANOL/AIR CELL

SOME ASPECTS OF MOLTEN CARBONATE FUEL CELLS

A.D.S. Tantram, A.C.C. Tseung and B. S. Harris

Energy Conversion Limited, Chertsey Road,
Sunbury-on-Thames, England

The ultimate aim of fuel cell development is a system of acceptable capital cost that can operate in an economic manner on low cost fuels. Although much effort has recently been put into investigating the alternative routes, the high temperature cell remains a favoured prospect.

Of the two main classes of high temperature cells (a) solid oxide electrolyte cells and (b) molten carbonate electrolyte cells, the latter has significant advantages in its lower temperature of operation and in the wider available choice of materials.

Work started at Sondes Place Research Institute and continued at Energy Conversion Limited, has investigated a wide range of different concepts of the molten carbonate cell. These may be broadly classified as follows:-

1. Free electrolyte cells.
2. Trapped electrolyte cells.
   - 2.1 Porous magnesia diaphragms.
   - 2.2 "Semi-solid" or "paste" electrolyte diaphragms.
     - Non-eutectic type.
     - Inert filler type.

Various combinations and compromises between these types are also possible.

In this paper we are concerned in particular with our experiences with cells based on the inert filler type of semi-solid electrolyte diaphragm.

Before discussing this work, it is worth summarising very briefly our main findings with the other types.

FREE ELECTROLYTE CELLS

The three-phase interface is established by the use of dual porosity electrodes run with a pressure differential. We had great difficulty in fabricating electrodes of sufficient strength at the operating temperature to withstand the necessary differential pressure. The factors contributing to this were:- the very high surface tension of the carbonate melt (see Table 1), the desirability of a small coarse pore size to obtain a high reaction area and, particularly with the cathode, limited choice of materials. From preliminary experiments with cell designs suitable for battery construction, it

was also clear that the problem of sealing the carbonate melt would be extremely severe.

Table 1. Surface Tension of Carbonate Melts, Dynes/cm.

°C	Li, Na, K 9, 6, 5 mol ratio	Li, Na 1 1
430	219.8	
480	217	
530	214	233
580	211	230.4
630	208.2	228

MAGNESIA DIAPHRAGM CELLS

In the absence of any commercial source, we developed our own porous magnesia diaphragms.

The main problem that we found with these cells was loss of electrolyte due to creep. It became clear that a much smaller pore size was desirable, coupled with very accurate control of the maximum pore size. This would prove very expensive in practice. An additional economic factor was the necessity for a machining operation on the sintered diaphragms. Sealing problems were also difficult.

SEMI-SOLID ELECTROLYTE. NON-EUTECTIC TYPE

This type[1] depends on choosing a carbonate composition that is well away from the eutectic, so that there is a range of temperature where the electrolyte body is semi-solid. An example is Li_2CO_3 78%, Na_2CO_3 12%, MgO 10%. The function of the small amount of magnesia in this context is to act as a nucleating agent to ensure the formation of small interlocking crystals when the electrolyte body solidifies after casting. The example given has a usable range from about 530°C (conductivity limit) to about 630°C (strength limit). It collapses under its own weight at 670°C and is completely molten at 690°C. Above this temperature, it can be cast into any desired shape and this facility is the main advantage of this type. We have successfully used this electrolyte in the form of discs, spun cast tubes and in a cell design involving the casting of the electrolyte around performed porous electrodes. The disadvantages are the narrow working temperature range and the fact that the solid:liquid ratio changes with temperature, making interface control difficult and uncertain.

SEMI-SOLID ELECTROLYTE. INERT FILLER TYPE

In the normal version an extremely intimate mixture of a carbonate eutectic and a substantial percentage of very finely divided inert filler (e.g. MgO) is densified to form an impervious electrolyte diaphragm.

General Properties

The physical properties are dependent, in particular, on the particle size of the inert filler and on the percentage used.

At the operating temperature, the carbonate component is molten and in this state the material is somewhat analagous to a clay-water system over a particular range of composition.

Under compression the material behaves in typical fashion, there being an initial elastic period (with some hysteresis) leading to a final yield point, which is quite high enough to make the material of practical use (e.g. >50 p.s.i. for 63% MgO). Compressive creep is extremely small, being undetectable in normal use. Figure 1 shows the integrity of a diaphragm after a 20-day cell test at 650°C, in which a sealing pressure of 10 p.s.i. was used.

Shear strength is, however, very low and shear stresses must be avoided in any cell or battery construction with this material.

Optimum composition is dependent in part on the filler particle size and represents a compromise between strength which increases with filler content and conductivity which decreases with filler content, e.g. for 50 w% MgO the diaphragm factor is 2.5 and for 63.5 w% MgO it is 4.0.

There are also rather less definable requirements associated with the setting-up of an optimum three-phase interface at the electrodes. Electrolyte retention is only a problem at the lower end of the range of usable filler content.

The forces holding these diaphragms together are almost entirely surface tension forces and depend upon there being, in practice, an extremely high meniscus length (molten carbonate - inert filler) at the surfaces of the diaphragm. This is demonstrated by the fact that a sample fully immersed in molten carbonate loses virtually all its compressive strength.

FABRICATION METHODS

Cold Pressing and Liquid Phase Sintering

It is not possible to produce high density diaphragms by this method, although rather better results are obtained if the sintering is carried out in vacuum. (See Figure 2).

Three steps normally take place in a liquid phase sintering. (a) Particle rearrangement under the influence of surface tension forces. (b) An increase in density by a solution and reprecipitation process. (c) Solid state sintering of the solid component. In the present case, we are liable to start with a continuous magnesia network which will resist (a). The solubility of magnesia in the molten carbonates is too low for (b) to appreciably occur and the temperature is too low for appreciable sintering of the magnesia (c). These factors explain why high density diaphragms cannot be made by cold pressing and liquid phase sintering.

Hot Pressing

(a) Above the carbonate melting point.

We have had little success with straight moulding of diaphragms by this method, due mainly to extrusion of the material between plunger and mould. Some experiments with injection moulding did, however, indicate that this would be feasible with high precision equipment.

(b) Below the carbonate melting point.

We find that just below the carbonate melting point the material exhibits a high degree of plastic flow and this method enables us to mould diaphragms to a high density without any of the problems of extrusion or sticking to the mould. The great advantage of this method is that it enables us to fabricate a wide variety of shapes to a finish as good as that of the moulding equipment. Figure 3 shows some electrolyte diaphragms made in this way. They are shown "as pressed," some of the graphite used as the mould release agent still being present. They are cavited to form the electrode gas space, baffled to give good gas distribution and have silver current collectors and connecting gaskets pressed on in the same operation. We have also found it possible to form gasporting in the same moulding operation. It is also possible to press on electrodes at the same time, thus giving a complete unit cell from one pressing operation. (Figure 4). We find, however, that the conditions normally used result in an excessive reduction in electrode porosity leading to poor performance. Subsequent attachment of the electrodes is therefore preferred.

Pretreatment of the material is important. The magnesia filler and the alkali metal carbonates are intimately mixed by ball milling and prefired at 700°C to 750°C. This prefiring treatment is to ensure intimate mixing, complete reaction of impurities and complete elimination of adsorbed water, (more about this later). It is important that the prefiring temperature be above the maximum ultimate cell operating temperature. This pretreatment is repeated at least once more. The material is then ground to below 20 mesh to provide the feed for the hot pressing operation. Alternatively, it may be further ground, cold pressed and sintered, to form a "biscuit" blank for the hot moulding operation.

The effects of some of the variables are shown in figure 2.

One of our standard compositions is 63.5% MgO, which was based on measuring the porosity of pure MgO hot pressed under the same conditions and computing the amount of molten carbonate necessary to just fill this porosity. We see that in practice (figure 2) much higher MgO contents can, in fact, be used due to the lubricating action of the carbonate component.

Our normal selected pressing conditions are 5 t.s.i. at 490°C when using binary eutectic (Na and Li carbonates) and at 385°C when using ternary eutectic (Na, Li, K carbonates).

Our density figures for the carbonate melts are:-(t in ^{o}C)

For Li, Na

1, 1 mol ratio, $2.030 - 4.30 \times 10^{-4}(t-500)$ g/cc

For Li, Na, K

9, 6, 5 mol ratio, $2.085 - 4.87 \times 10^{-4}(t-400)$ g/cc

Infiltration

An infiltration method has also been used successfully for the fabrication of electrolyte diaphragms. A cold pressed diaphragm of 100% magnesia will break up on infiltration, but the prccess may be successfully carried out if the starting material contains an appreciable percentage of the alkali metal carbonates. An example is as follows:-

> A mixture of magnesia 63.5w% with sodium-lithium carbonates prefired, ground and cold pressed at 10 t.s.i. This diaphragm is sintered at 600^{o}C, cooled and placed on a prepressed disc of 100% sodium-lithium carbonate. The whole is then reheated to 600^{o}C for half an hour. The additional carbonate infiltrates into the diaphragm as it melts. There is some danger that the infiltrating liquid will bypass some of the pores and leave these unfilled, but this can be overcome if the operation is carried out under reduced pressure, a carbon dioxide atmosphere being advisable. Excess electrolyte is ground off the diaphragm after cooling. The product contains 46 w% of the carbonate electrolyte, has a density of greater than 97% of the theoretical and the linear shrinkage is less than 0.5%.

Operating Experience

We will limit ourselves here to points that are specifically relevant to the use of semi-solid electrolyte. We have made and tested some 120 2-1/2" diameter cells (20 cm^{2} active area) and about 60 of 4-1/2" diameter (80 cm^{2} active area). We have also made some experimental stacks of 4-1/2" diameter, giving about 50 watts output. Figure 5 shows one of these stacks complete with heater and insulation.

A variety of electrode materials have been used, but a typical example would be — for the anode, "B" nickel, granulated, presintered and graded to -100 + 120 mesh — for the cathode, cosintered Ag/Cu_2O/ZnO (25/2.5/72.5% by wt.) and graded —100 + 120 mesh. In both cases these materials are made into a slurry with a silver suspension containing a temporary binder (giving 1% added silver) and applied to the faces of the electrolyte diaphragm in this form. The electrcdes are then sintered in situ as the cell is brought up to operating temperature. Typical electrode thickness is 1 mm, porosity 50% on a 3 mm thick electrolyte diaphragm.

As the electrolyte component of the diaphragm melts, it expands to partially wet the electrode and a stable three-phase interface is set up. This process takes rather longer to equilibrate than one might imagine and is illustrated in figure 6, where the internal resistance of a new cell is followed over an initial temperature cycle of 2 hours duration. The extent and location of the three-phase interface will depend on the balance between the surface tension forces in diaphragm and electrodes. It will be affected in particular by the very fine microstructure in the electrode, for instance by the activation treatment mentioned later. These factors are difficult to control and this is one of the disadvantages of this type of cell construction.

Performance and Endurance

We must first of all distinguish between "unactivated" electrodes and those specially activated. The nickel anode may be activated in situ by a controlled partial oxidation, using a small percentage of oxygen in nitrogen such that about 5w% of the nickel is oxidised, followed by reduction with the fuel gas. The effect of such an activation is shown in figure 7.

An electrode activated in this fashion does, however, show a fall in activity with time and after about 60 hours the performance is the same as an unactivated electrode, which would remain unchanged over this period. We have experimented, with some success, with methods of stabilising this activation, but the long term results reported here refer to the lower level of performance. Figure 8 shows the performance obtained with an activated nickel electrode on pre-reacted methane-steam and on hydrogen. Figure 9 shows the effect of the fall in anode activity and the longer term performance deterioration discussed below.

Initial endurance tests with these cells showed that there was a progressive deterioration in performance occurring in the hundreds of hours region. The behaviour was not particularly reproducible and did not show any trend with temperature of operation or with current density and, in fact, similar results were obtained with cells left on open circuit for the bulk of the time. It was suspected that the fall-off was due to deterioration of the electrolyte diaphragms. Physical examination of the diaphragms after the tests, showed the presence of laminar faults. Examples of these are shown in figure 10. It should be noted that we have chosen particularly extreme examples to illustrate the phenomenon, the faults being usually considerably less marked. These faults result in (a) an increased internal resistance and (b) increasing inter-electrode leaks leading to falling performance. Using gas chromatographic techniques we were able to obtain a correlation between falling performance and increasing leaks. The procedure was as follows:-

With the cell on open circuit, hydrogen feed to the anode and air/carbon dioxide to the cathode, the nitrogen content of the anode effluent was analysed. This nitrogen could come by inter-electrode diffusion or by diffusion through a gasket leak from the external air. The cathode feed was then temporarily replaced by methane and the nitrogen estimation in the anode effluent was repeated. In this manner a semi-quantitative measure of both gasket and inter-electrode "leaks" could be obtained. The gasket leak did not normally alter with time and we were, in fact, able to eliminate this, by making the seal directly between the electrolyte diaphragm and the separator i.e. in effect by abolishing gaskets. Figure 11

shows an example of the correlation between falling performance and increasing inter-electrode leak.

Diaphragm deterioration was overcome by ensuring complete elimination of chemisorbed water from the material used for hot pressing. Any still present would be evolved during operation of the cell and initiate the lamination faults. These would tend to get worse with time, due probably to erosion effects arising from chemical combustion of the fuel and oxygen diffusing into the diaphragm. Water is very tenaciously held by magnesium oxide and much longer prefiring times are necessary than might be thought. In addition, the prefired material will quite readily readsorb water and strict precautions have to be taken to ensure that this does not occur. Figure 12 illustrates the stable performance that can be obtained when strict attention has been paid to these factors. The increase in performance seen in the middle of this particular test was not explained. Finally figure 13 shows the absence of faults in an improved diaphragm after a cell test of 450 hours.

Conclusions

Practical cells, based on "semi-solid" electrolyte diaphragms, can be made with promising performance and endurance characteristics. Further improvements are desirable and there are indications that these can be achieved.

Careful battery design should be able to obviate the disadvantages of this type of cell and to exploit its advantages.

The hot pressing fabrication technique should be amenable to mass production methods, since the required conditions are not too far removed from existing plastic moulding practice. This could prove an important factor in achieving low capital cost.

THE ANODE MECHANISM

For the high temperature cell to fulfill its promise considerably higher power densities are required. To be able to take logical steps in this direction a better understanding of the electrode processes and their rate controlling steps is desirable. We are, therefore, taking a fresh look at this problem and the preliminary results are reported here. The anode process was chosen for the initial study, since in practical cells the greater part of the polarisation is normally at this electrode.

Experimental

The test cell used is shown schematically in figure 14. Also included, but not shown, were a reference electrode and a thermocouple pocket. Both the counter electrode and reference electrode were of platinum gauze partially immersed in the electrolyte and both were supplied independently with a 2.5:1 air - carbon dioxide mixture. The electrolyte was an equimolar mixture of sodium and lithium carbonates.

The positioning device enabled the electrolyte crucible to be raised or lowered thus, controlling the degree of electrode immersion. Starting with the electrolyte level below the bottom of the test electrode, the crucible is raised slowly until "first

touch" is registered by an electrical continuity test. The results quoted here are all with a further immersion of 0.1 inches. In addition to this there will be a meniscus about 0.25 inches high.

Initially both nickel and silver-palladium foils were chosen for examination, one point being that the large difference in possible hydrogen diffusion rates through the bulk metal could lead to instructive results. The foil electrodes were 0.005" thick and 1.15 cms wide. The silver-palladium used was the 23% silver alloy. The foils were used as received, with no pretreatment.

The anode compartment was swept with a large excess of hydrogen at 1 atm.

Results and discussion

Figure 15 shows the corrosion curve for the silver-palladium obtained under "white spot" nitrogen, and indicates that only relatively low corrosion currents are possible in the potential range of interest.

Figure 16 compares the current voltage curves for hydrogen oxidation on nickel and silver-palladium at 550°C. The nickel curve was not very reproducible. The reproducibility of the silver-palladium curves is discussed later.

Figure 17 shows plots of E versus log i for hydrogen oxidation on silver-palladium at 550°C and 600°C respectively. It is seen that there is a very well defined linear portion extending over nearly two decades.

At this stage it was noticed that the relationship between E and i was very similar to that between E and x, where x describes the composition of a partially reacted fuel in the manner shown below.

Assume that we start with 1 mol of H_2 and that x mols react with CO_3^{2-},

$$H_2 + CO_3^{2-} = H_2O + CO_2 + 2e$$

and that b mols of H_2 react further with the CO_2,

$$H_2 + CO_2 = H_2O + CO$$

equilibrium being reached.

For 1 atm total pressure, the partial pressures in the resulting mixture are therefore,

$$P_{H_2} = \frac{1 - (x + b)}{1 + x}, \quad P_{H_2O} = \frac{x + b}{1 + x} \quad P_{CO_2} = \frac{x - b}{1 + x}, \quad P_{CO} = \frac{b}{1 + x}$$

and we can write for the water gas equilibrium

$$\frac{(x + b)\, b}{[1 - (x + b)][x - b]} = K \qquad \ldots\ldots\ldots\ldots\ldots\ldots\ldots\ldots (1)$$

At a given temperature this equation can be solved to obtain values of b to correspond with selected values of x. The corresponding partial pressures may then de derived and, from them, the c rresponding values for E using the equation

$$E = \frac{RT}{4F} \log_e K_o P_{O_2}^* P_{CO_2}^* + \frac{RT}{2F} \log_e \frac{P_{H_2}}{P_{H_2O} P_{CO_2}} \quad \ldots\ldots\ldots\ldots (2)$$

$P_{O_2}^*$ and $P_{CO_2}^*$ refer to the partial pressures at the cathode. K_o is the equilibrium constant for $2H_2 + O_2 = 2H_2O$.

At a given temperature and for constant cathode conditions we can write

$$E = \text{Constant} + \frac{RT}{2F} \log_e \frac{[1 - (x + b)]\ (1 + x)}{(x + b)(x - b)} \quad \ldots\ldots\ldots\ldots (3)$$

It is found that the plot of E versus $\log_{10} x$ is linear over a wide range and it is the slope (S_x) of this plot that corresponded closely with the observed slopes (S_i) of the initial experimental $E - \log_{10} i$ plots at 550°C and 600°C. These figures are tabulated in table 2.

Table 2. Values of K, S_x, S_i, and α_x.

°C	K	S_x mV	S_i mV	α_x
550	0.219	197	197	0.414
600	0.295	226	233	0.383
650	0.385	246		0.372
700	0.49	262		0.368
887	1	336		0.343

α_x is the value derived from writing $S_x = \frac{2.3\ RT}{2F\alpha_x}$

These considerations suggested the following picture. In the low current region (i.e. down to about 0.95v) the most important factor is the diffusion rate of reaction products away from the reaction site, on the immersed portion of the electrode, through the meniscus to the bulk gas. Thi rate should be proportional to the concentration difference and so the concentration of products at the reaction site has to build up appreciably before a reasonable diffusion rate is possible. This build up will affect the electrode potential in a similar manner to that defined by equation 3. As the current is further increased the rate of hydrogen diffusion to the reaction site would become the most important factor. Confirmatory evidence for this view is that silver-palladium, which has an additional route for hydrogen diffusion through the bulk metal, supports much higher currents than nickel.

A more precise statement of the hypothesis is as follows:- At a given current the observed polarisation is due to the change in surface concentrations necessary to produce the diffusion rates of both reactants and products to meet the requirements of the processes occurring.

Making the following assumptions:-

The partial pressures of CO_2, H_2O and CO in the bulk gas (H_2 at 1 atm.) are all zero.

The surface concentrations at the reaction site can be described in terms of partial pressures, P_{H_2} etc., in atm.

The diffusion rates are directly proportional to the partial pressure differences.

Rate of discharge of CO_3^{2-} = i $\quad (CO_3^{2-} + H_2 = CO_2 + H_2O + 2e)$ fast.

Rate of formation of CO = y $\quad (H_2 + CO_2 = CO + H_2O)$ fast,

the rates being expressed in units of current, i.e. coulombs/sec. Then we can write,

Rate of H_2 in $= i + y = k_1 (1 - P_{H_2})$ hence $P_{H_2} = \dfrac{k_1 - (i + y)}{k_1}$

Rate of H_2O out $= i + y = k_2 P_{H_2O}$ hence $P_{H_2O} = \dfrac{i + y}{k_2}$

Rate of CO_2 out $= i - y = k_3 P_{CO_2}$ hence $P_{CO_2} = \dfrac{i - y}{k_3}$

Rate of CO out $= y = k_4 P_{CO}$ hence $P_{CO} = \dfrac{y}{k_4}$

The k's involve the diffusion coefficient, Henry's law constant and the geometry of the diffusion path. The units will be coulombs. sec^{-1} $atm.^{-1}$.

For the water gas equilibrium,

$$\frac{(i + y)\, y}{[k_1 - (i + y)][i - y]} = K. \quad \frac{k_2 \cdot k_4}{k_1 \quad k_3} = K^1 \quad \ldots\ldots(4)$$

For the cell e.m.f. at a given temperature

$$E = \text{Const} + \frac{RT}{2F} \log_e \frac{k_2 \cdot k_3}{k_1} + \frac{RT}{2F} \log_e \frac{k_1 - (i + y)}{(i + y)(i - y)} \quad \ldots\ldots(5)$$

We cannot solve these equations without a knowledge of the k values, but a certain amount of information can be obtained using the analogy with the equations in x and b, (1) and (3), which can be solved. We find (a) that S_i will be very little affected by the value of k_1 provided that k_1 is appreciably greater than i + y i.e., provided we are not near the limiting current condition and (b) that S_i will be appreciably affected by the value of K^1. The extent of this variation can be seen by comparing the variation of α_x with K in table (2). To explain the experimental fit noted earlier, $\frac{k_2 k_4}{k_1 k_3}$ would have to be fairly close to 1.

Attempts to obtain confirmatory experimental results, however, met with some difficulty. In all cases a well defined linear range on the E – log i plot was found, the individual curves reproduced well with rising and falling current, and the values of S_i in a given series increased with temperature. On the other hand the values for S_i, obtained in different series, done for example on different days, showed a wide scatter. The following figures show the extremes recorded.

(a) At a given temperature (650°C)

Lowest S_i = 165 mV , (α_i = 0.555)

Highest S_i = 530 mV , (α_i = 0.173)

(b) At any temperature.

Lowest S_i = 147 mV , (α_i = 0.536) at 520°C.

Highest S_i = 800 mV , (α_i = 0.121) at 700°C.

At first sight it was difficult to explain these variations on the diffusion theory, since they implied a very wide variation in the value of $\frac{k_2 k_4}{k_1 k_3}$ and it was hard to see how this could occur.

It was, however, noticed that the value of S_i was dependent on the history of the anode compartment conditions in the following manner. If the anode compartment had been left for a long period under pure hydrogen, low values for S_i were obtained. If, however, it had been left under carbon dioxide before the tests with pure hydrogen, high values were obtained for S_i. This observation suggested the following explanation. In the former case some decomposition of the carbonate electrolyte in the anode compartment will occur, leaving it CO_2 depleted and rich in M_2O. This will mean that there is a chemical sink available for the carbon dioxide, produced when taking a current, and would be expected to result in a very high value for k_3 (CO_2) as compared with diffusion through the liquid to the bulk gas. There would also be a tendency for $k_2(H_2O)$ to increase for the same reason, but since the equilibrium

$$2\ MOH + CO_2 = M_2\ CO_3 + H_2O \quad \ldots\ldots\ldots\ldots\ldots\ldots\ldots\ldots (6)$$

is well over on the carbonate side we might expect the effect on k_2 to be considerably less marked. If this is true then we can see that the value of K^1 will be considerably reduced and this will result in an abnormally low value for S_i. One can also postulate that when the anolyte has been under CO_2, but starved of H_2O, similar considerations will dictate a low value for k_3 (CO_2) and a high value for k_2 (H_2O) due to the reverse of reaction (6) above. In this case therefore we would expect a high value for K^1 and hence S_i. Confirmatory evidence is that, in the CO_2 deficient condition, unnaturally low open circuit voltages were observed on hydrogen. This is to be expected if the concentration of oxygen ions in the anolyte is increased[2].

Finally the limiting current region was explored for various hydrogen-carbon dioxide mixtures on silver-palladium and the results are shown in figure 18. With pure hydrogen the limiting current region was very unstable.

Conclusions

It is possible to explain the experimental results in terms of a diffusion control mechanism, but further, more rigorously controlled experiments are necessary to obtain a valid quantitative correlation. We postulate that at a given current density the observed polarization is due to the change in surface concentrations necessary to produce the diffusion rates of both reactants and products to meet the requirements of the processes occurring. It follows that in the lower current density region the diffusion rates of the products are the dominant factors and that in the higher current density region the rate of hydrogen diffusion will become dominant. In the latter case the rate of diffusion of hydrogen through the bulk metal can be of great significance.

An essential part of the treatment is the assumption that the water gas shift occurs at the electrode surface and reaches equilibrium.

Any explanation in terms of activation control seems unlikely in view of the wide variation in α_i that was found.

Partial decomposition of the anolyte could strongly influence the diffusion rates of CO_2 and H_2O.

The investigation will continue with studies on other metals and other fuels.

ACKNOWLEDGEMENTS

The authors wish to thank their colleagues, past and present, who have contributed to this work and the Board of Energy Conversion Limited for permission to publish.

REFERENCES

(1) H. H. Chambers and A. D. S. Tantram, British Patent 806592.

(2) J. Dubois and R. Buret, Bulletin de la Societe Chemique de France, 1963, p.2552.

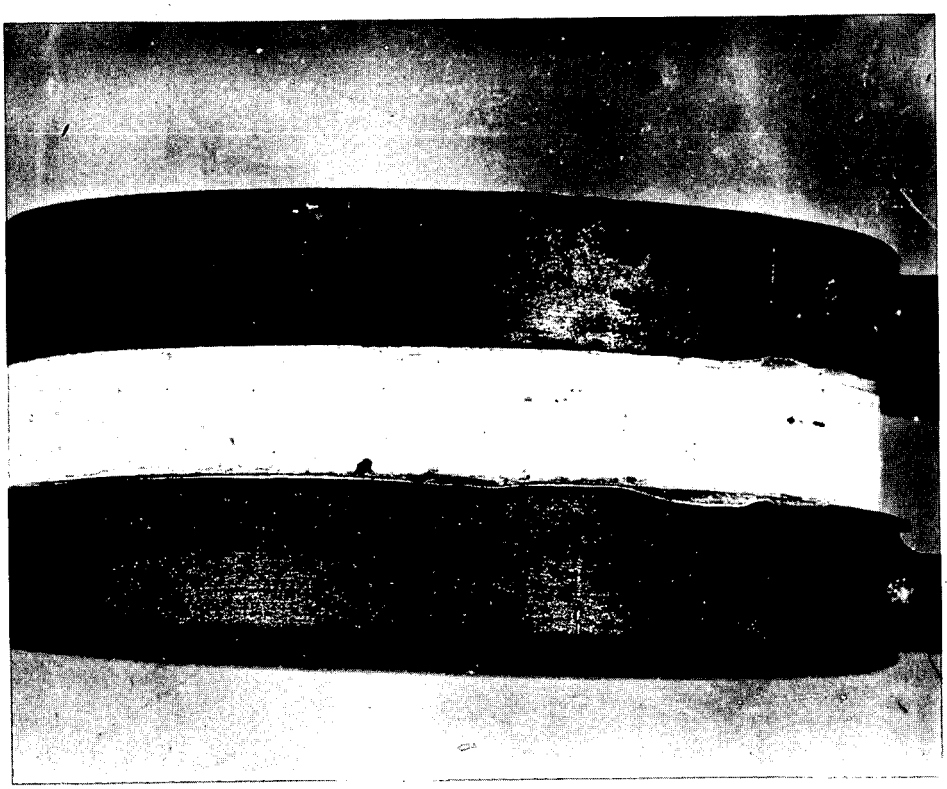

Fig. 1.-CELL AFTER 20 DAYS AT 650°C AND 10 PSI SEALING PRESSURE, SHOWING LACK OF DIAPHRAGM CREEP

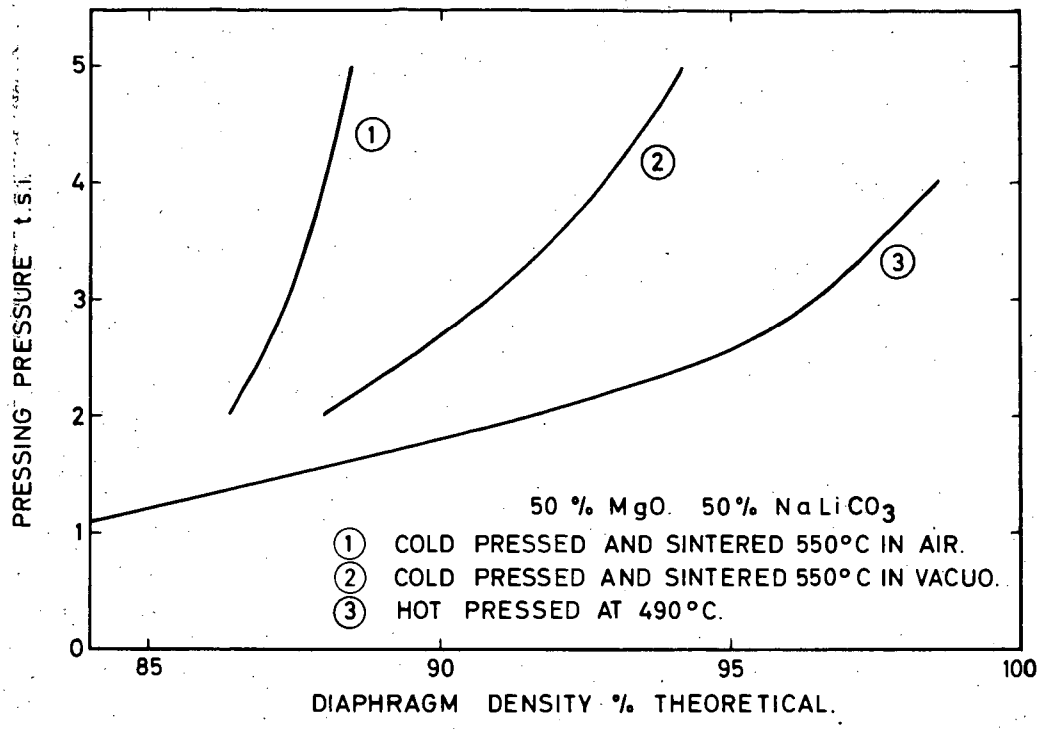

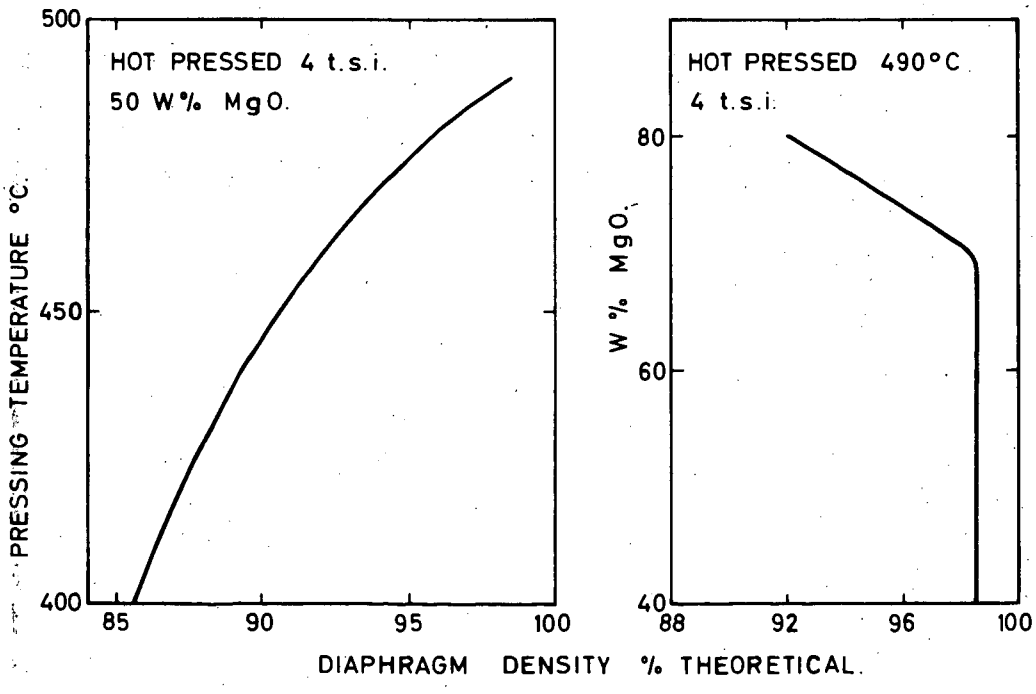

FIG. 2 THE EFFECT OF PRESSING CONDITIONS.

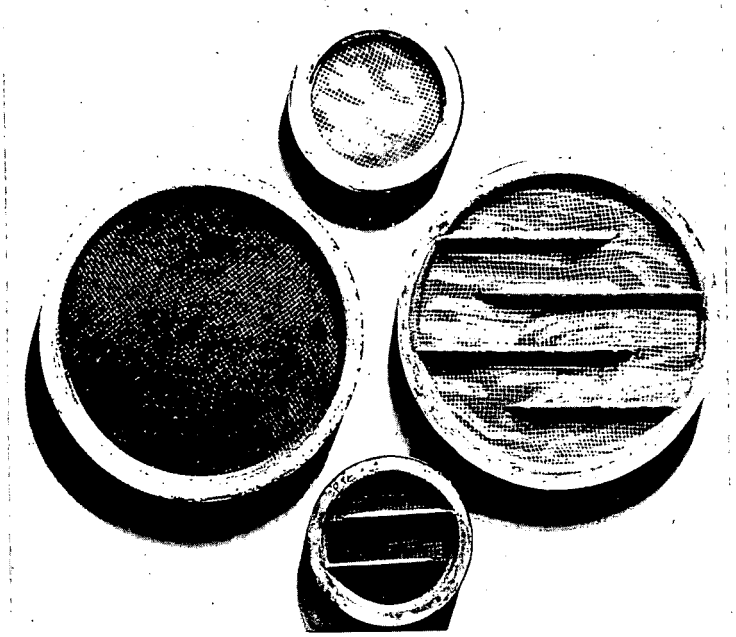

Fig. 3.-HOT-PRESSED ELECTROLYTE DIAPHRAGMS, 2.5" AND 4.6" IN DIAMETER

Fig. 4.-SECTION OF INTEGRAL CELL ELEMENT MADE BY SINGLE HOT-PROCESSING OPERATION

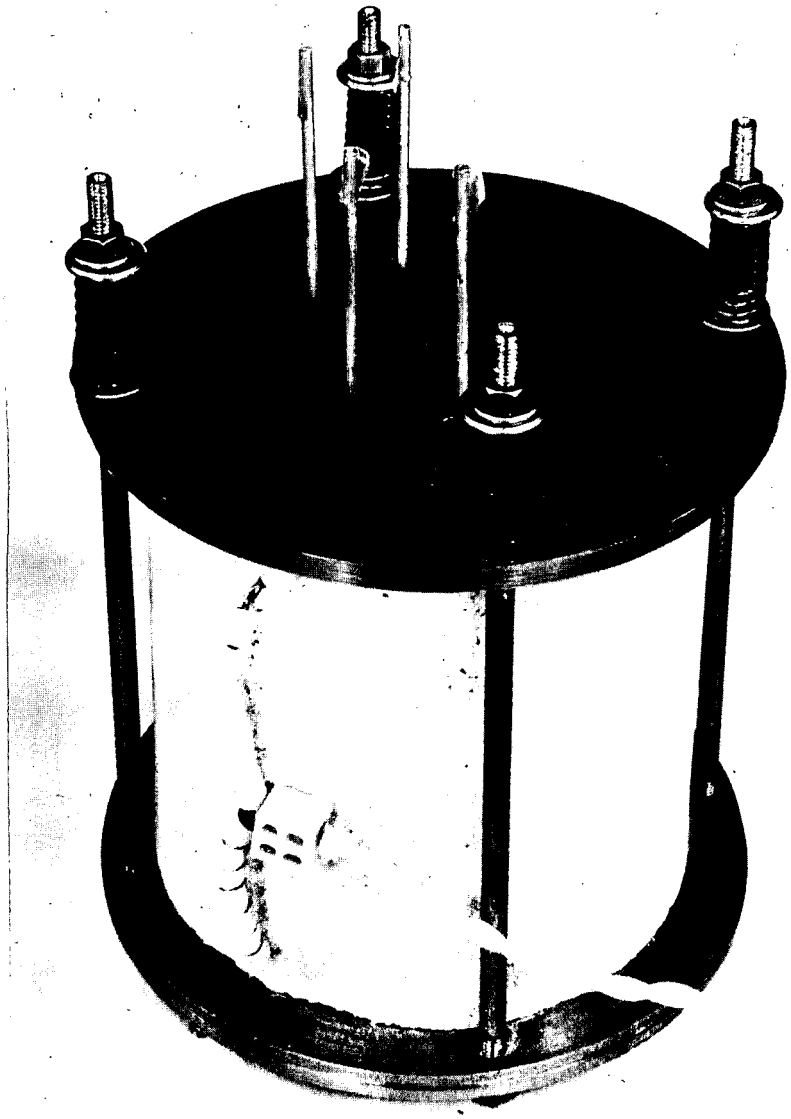

Fig. 5.- FIFTY-WATT BATTERY WITH HEATER AND INSULATION

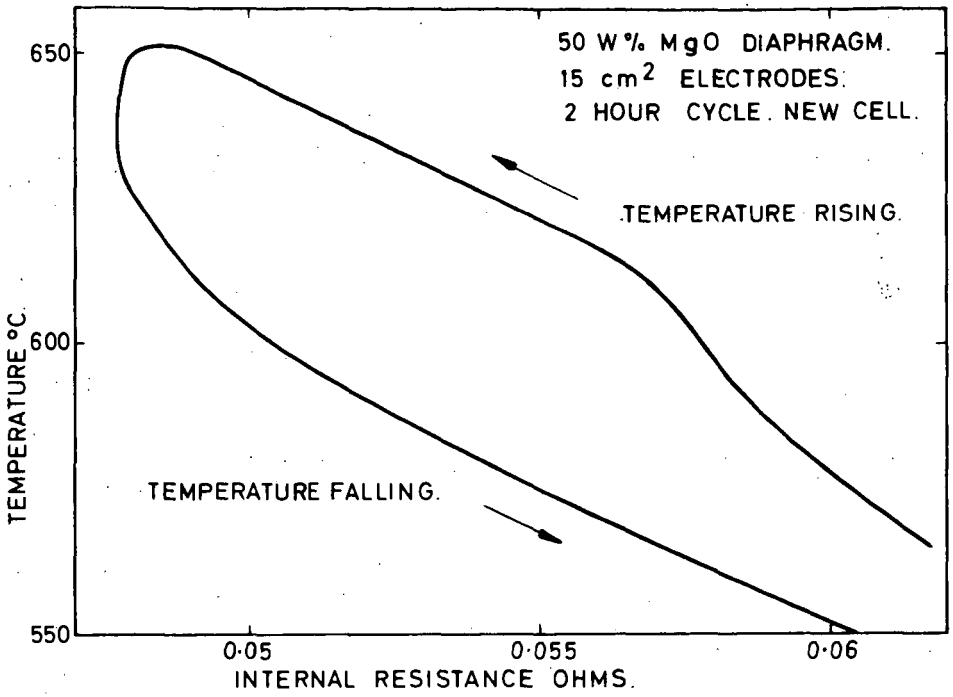

FIG. 6 ESTABLISHMENT OF 3 PHASE INTERFACE.

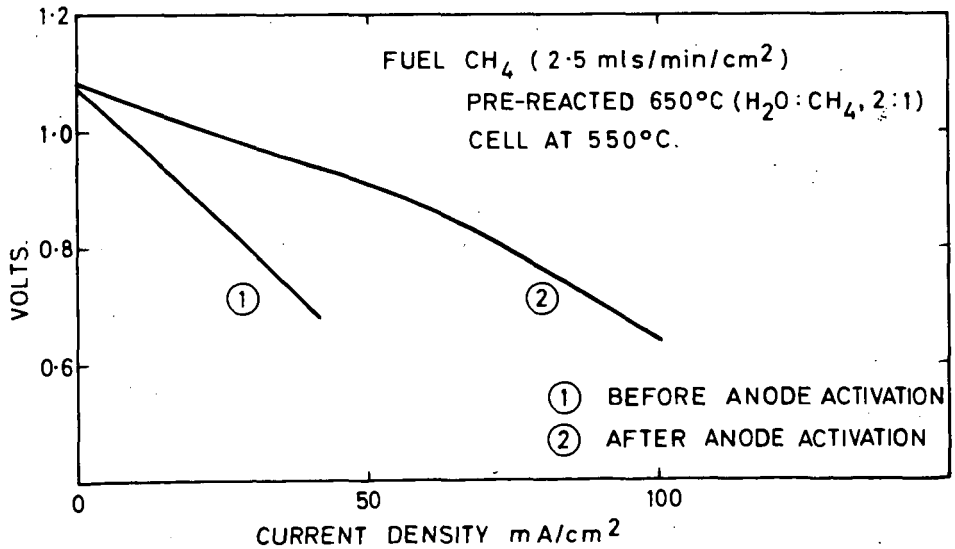

FIG. 7 EFFECT OF ANODE ACTIVATION.

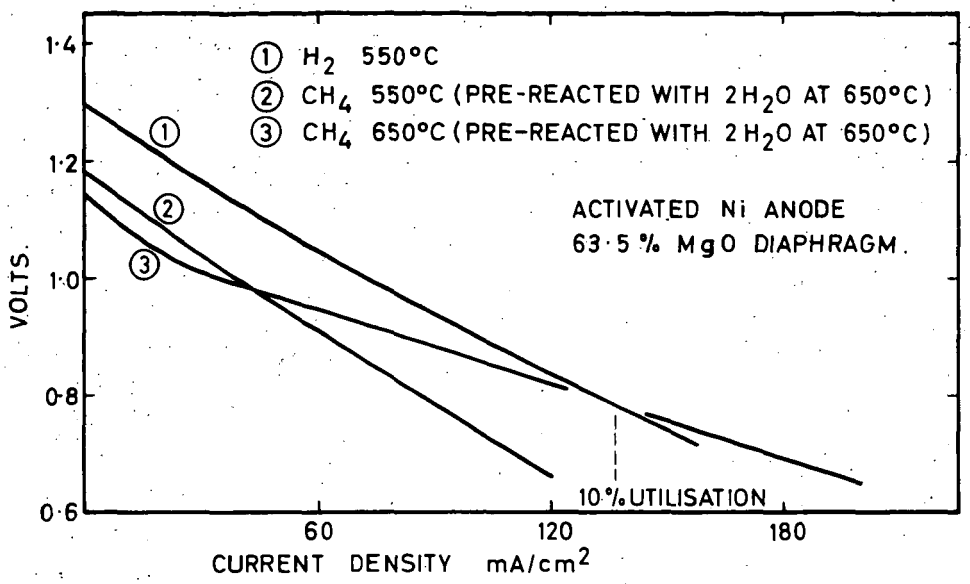

FIG. 8 INITIAL PERFORMANCE CELL H.P 48.

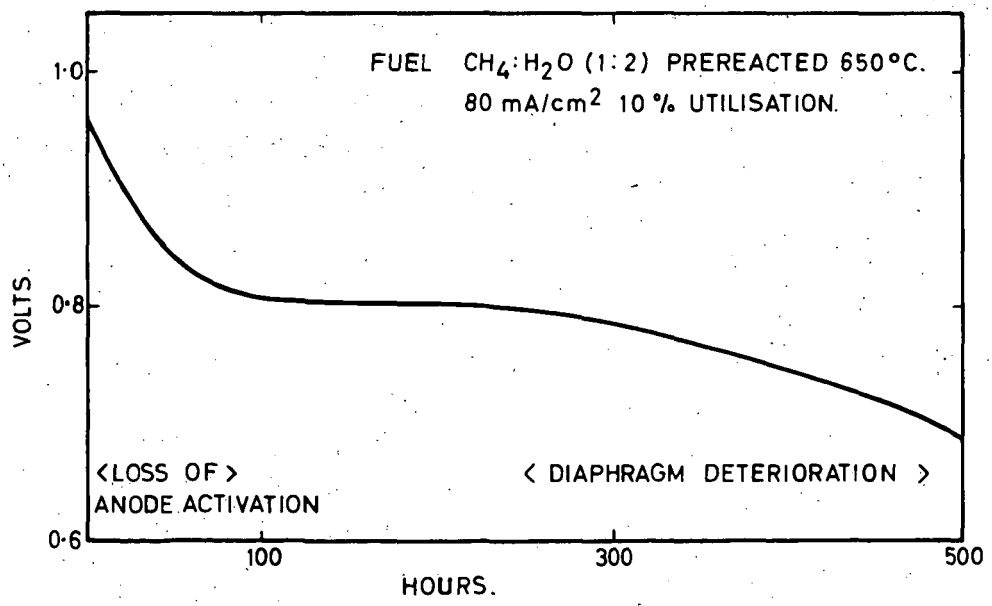

FIG. 9 ENDURANCE OF CELL H.P. 48 AT 650°C.

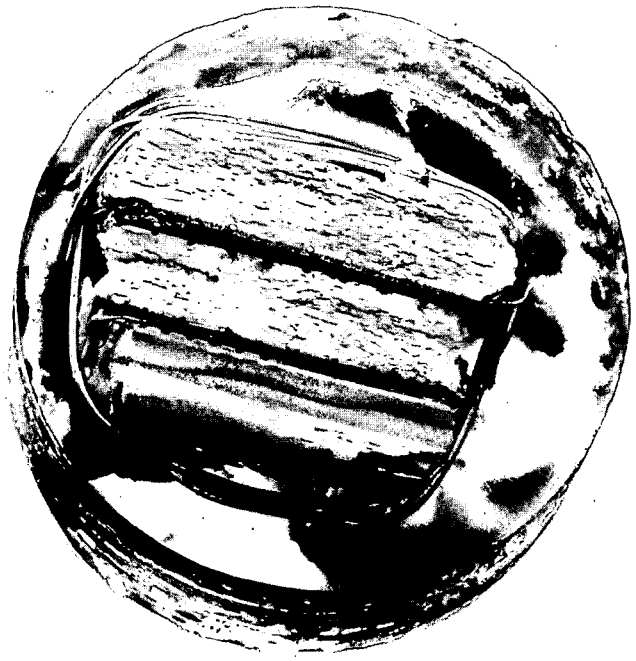

Fig. 10.-SECTIONS OF ELECTROLYTE DIAPHRAGMS AFTER 450 HOURS AT 600°C, SHOWING SEVERE LAMINAR FAULTS

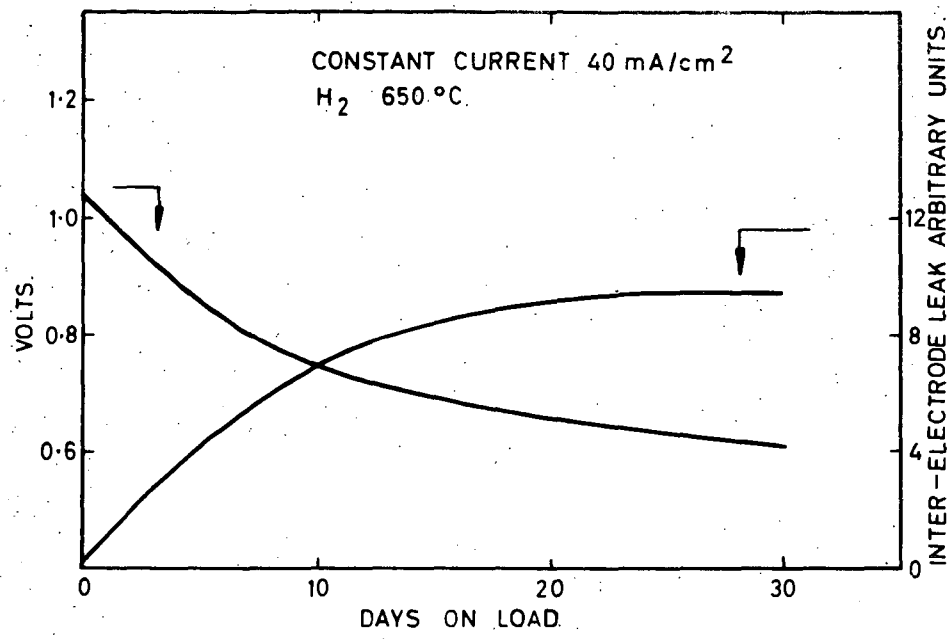

FIG. 11 DETERIORATING DIAPHRAGM. PERFORMANCE — LEAK.

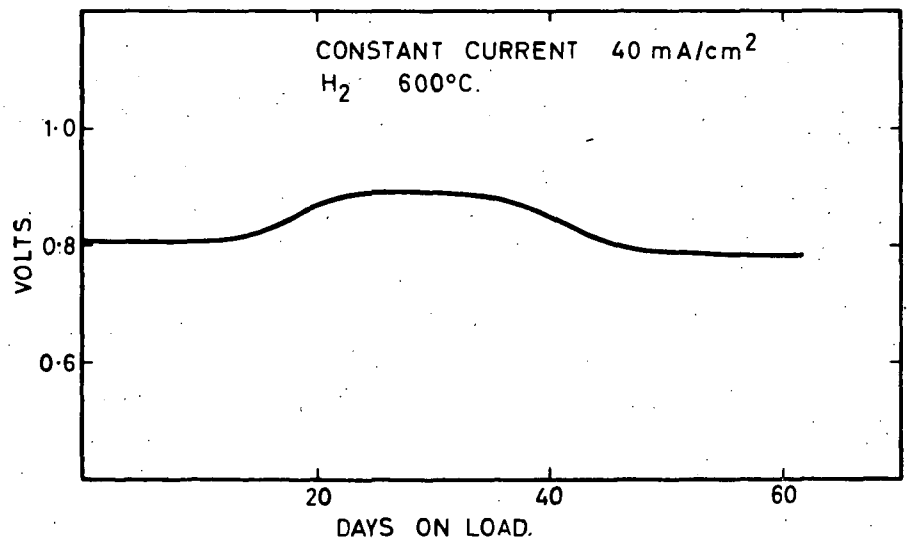

FIG. 12 IMPROVED DIAPHRAGM. ENDURANCE.

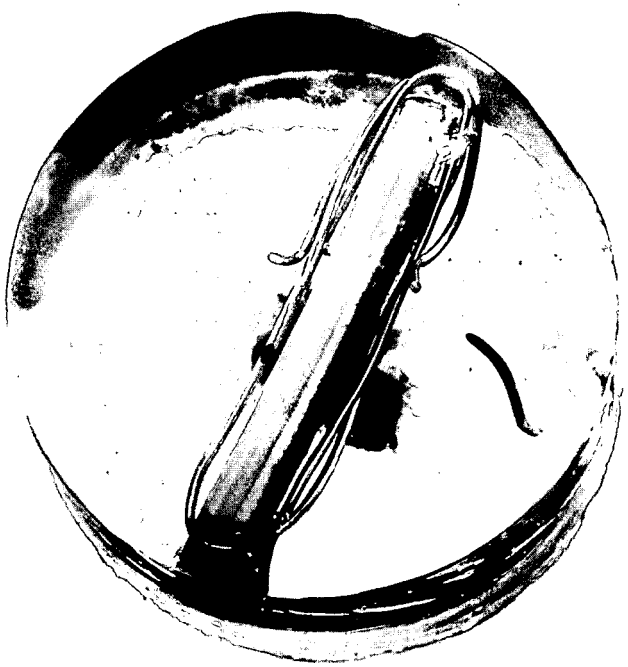

Fig. 13.-SECTION OF IMPROVED DIAPHRAGM AFTER 450 HOURS AT 600°C, SHOWING ABSENCE OF LAMINAR FAULTS (see Fig. 10)

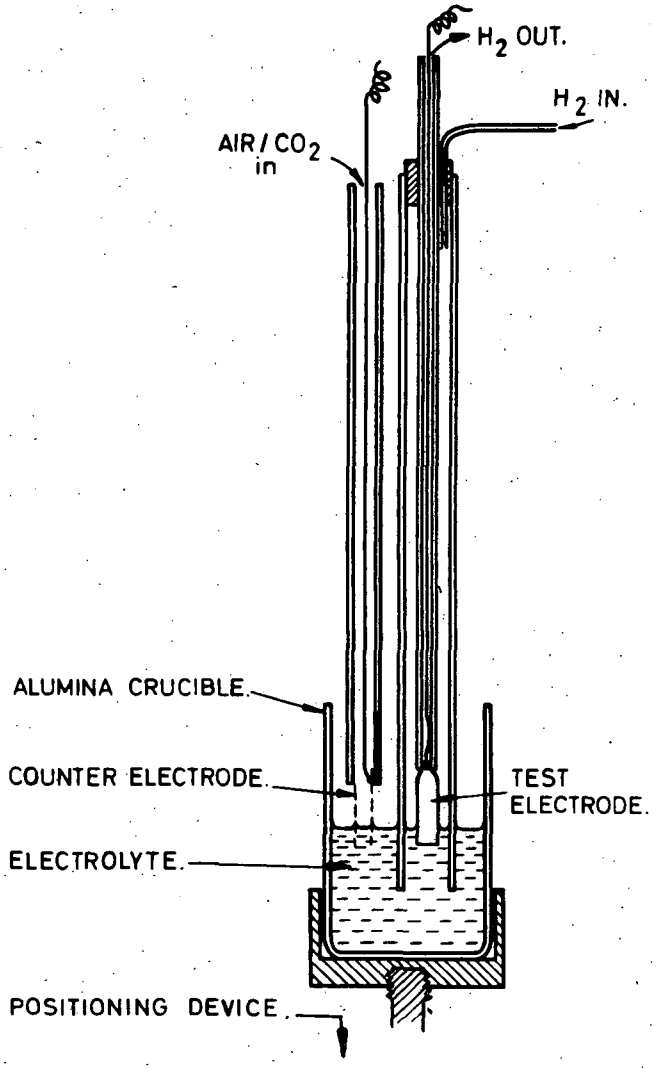

FIG.14 SMOOTH ELECTRODE TEST CELL.

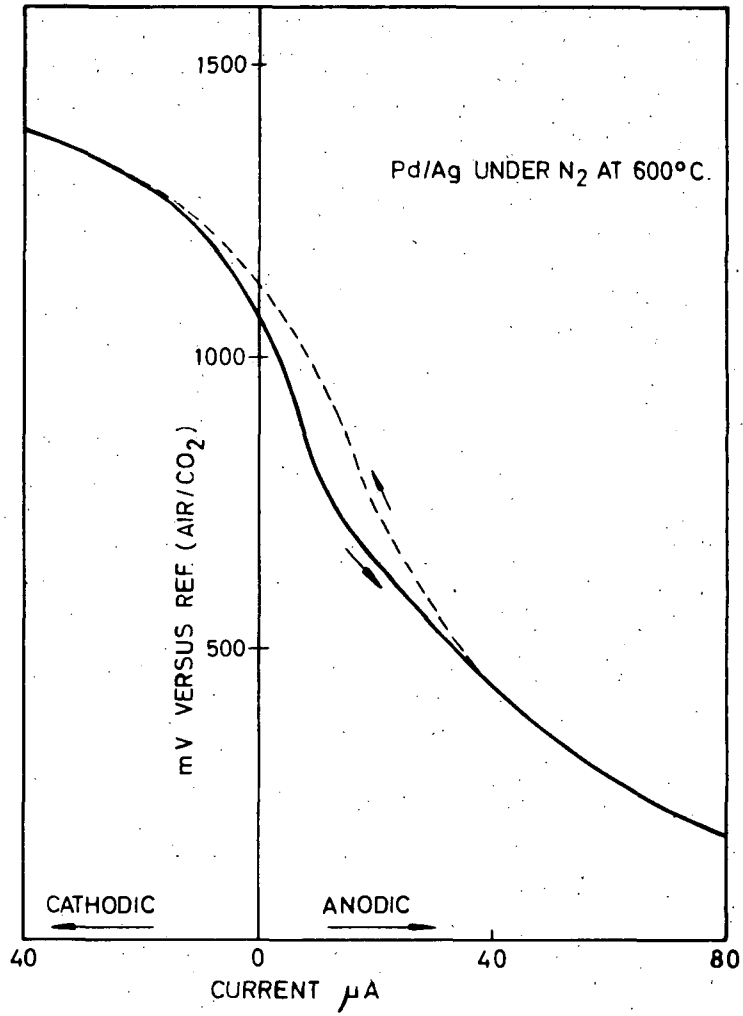

FIG. 15 CORROSION CURVE FOR Pd/Ag.

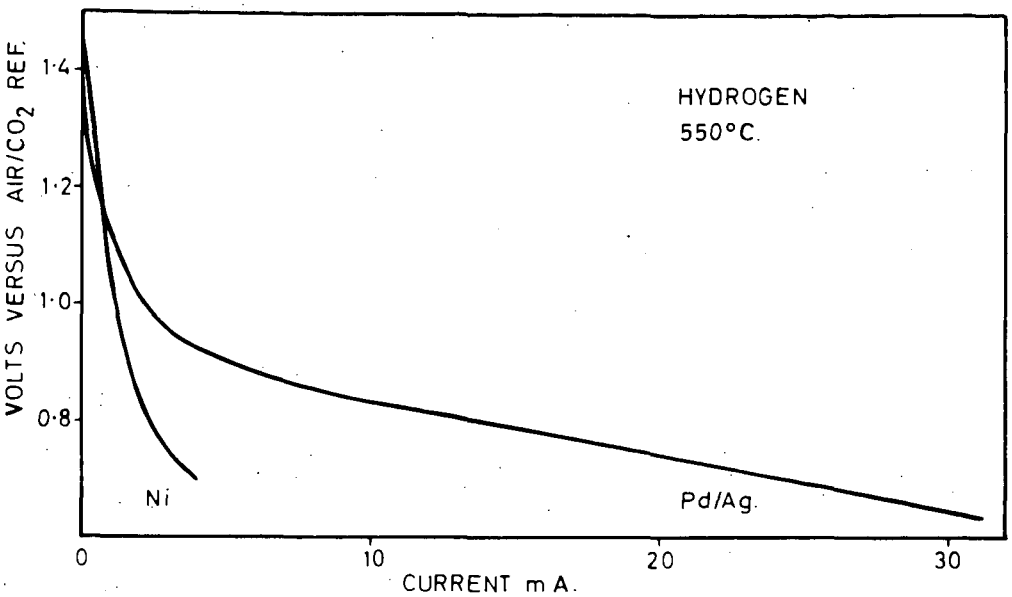

FIG. 16 COMPARISON OF Ni AND Pd/Ag FOIL ANODES.

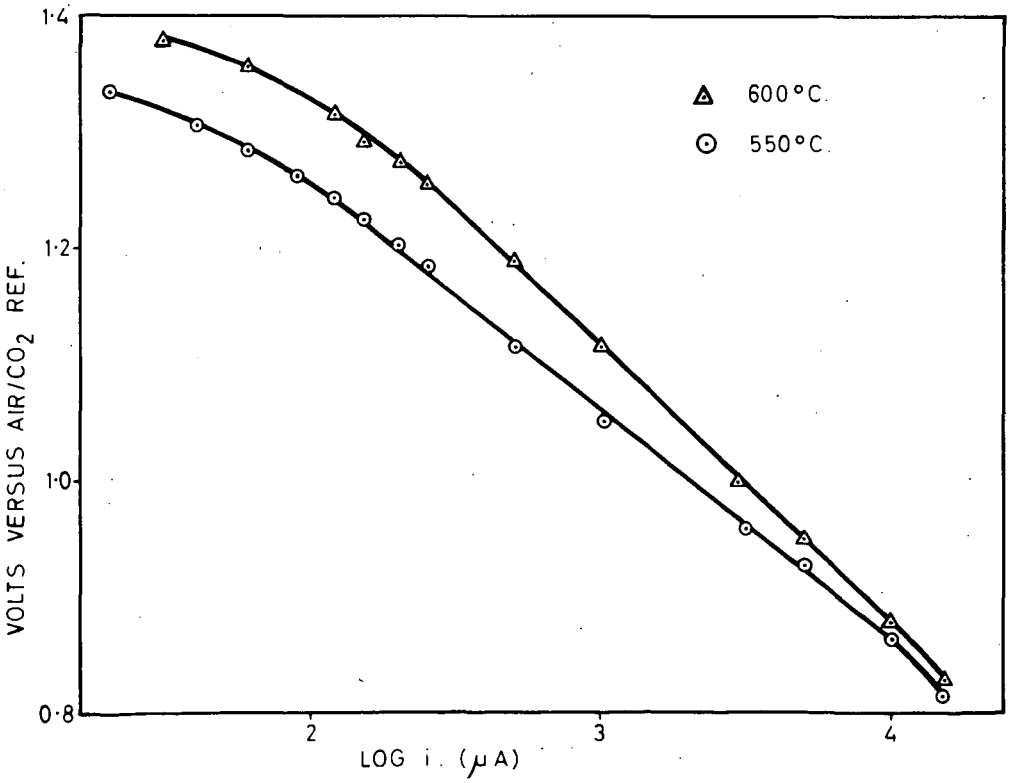

FIG. 17 E – LOG i PLOTS. H_2 ON Pd/Ag.

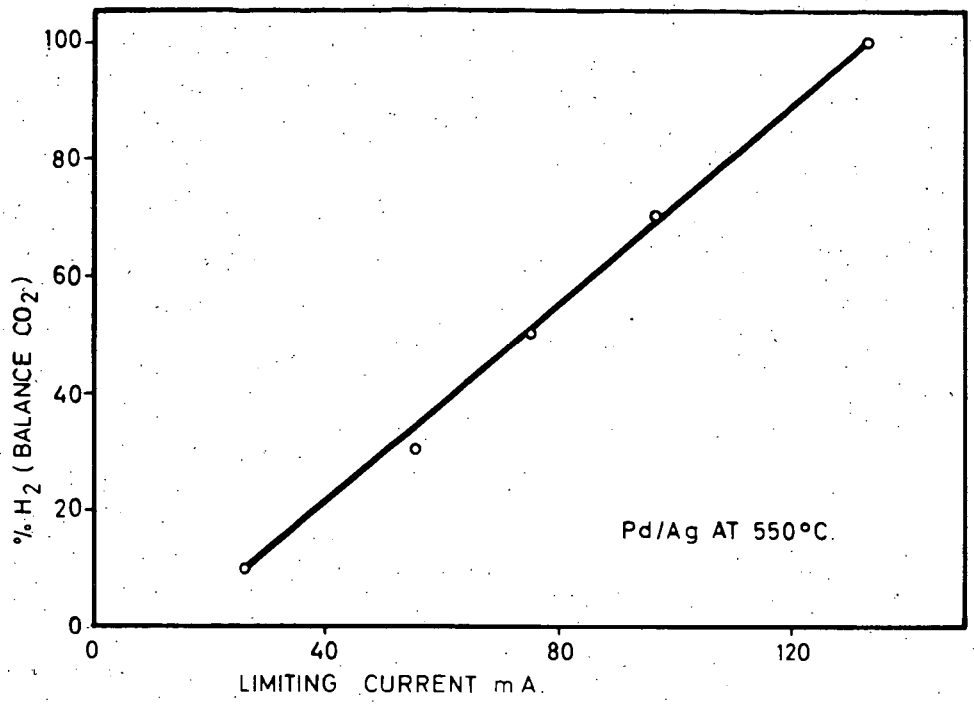

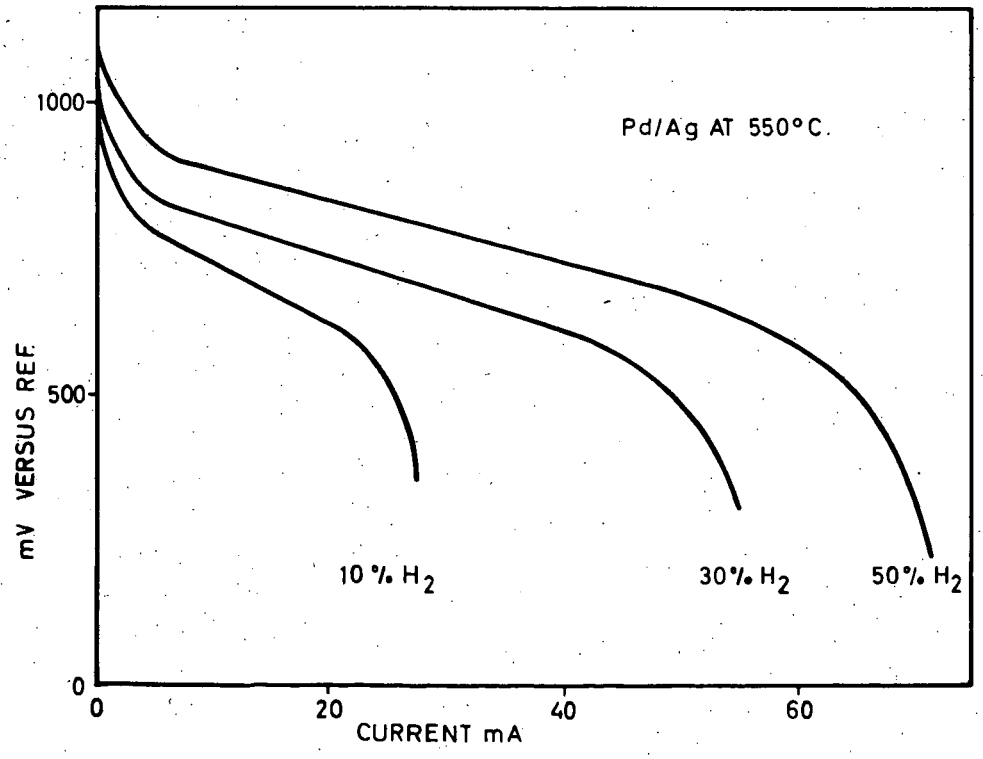

FIG. 18 LIMITING CURRENTS ON Pd/Ag.

THE DOUBLE-DUTY ANODE FOR MOLTEN-CARBONATE FUEL CELLS

R. W. Hardy, W. E. Chase, and J. McCallum

Battelle Memorial Institute
Columbus, Ohio

INTRODUCTION

One of the principal objectives of research on molten-carbonate fuel cells has been a battery which would operate on a carbonaceous fuel and air.[1-8] Natural gas has been of special interest because of its low cost and wide availability.[1,3,7,9] However, in the references cited it has been recognized that hydrocarbons do not supply much current when used directly in the fuel cell. There must be a preceding chemical step such as steam reforming or partial air oxidation to yield electrochemically active species, predominantly hydrogen and carbon monoxide. The requirements for effective steam reforming in a fuel cell were discussed in a previous paper,[8] and the advantages of carrying out the steam reforming on the anode were described.

Three advantages are realized by steam reforming natural gas directly on the anode:

(1) Good heat exchange between the exothermic electrochemical oxidation and the endothermic steam-reforming reaction.

(2) Less steam required because product steam from electrochemical oxidation of hydrogen is available.

(3) More extensive conversion of methane because products (H_2 + CO) are being consumed.

The possibility of realizing these advantages led to the first goal of electrochemical research. The goal was to obtain both reforming and electrochemical oxidation on the anode.

THE DOUBLE-DUTY-ANODE CONCEPT

The idea of carrying out steam reforming on the anode itself has been proposed by previous workers. Linden and Schultz suggest it in a patent,[10] and Schultz et al.[11] describe results of some reforming experiments with methane-steam mixtures on nickel battery plaques. Sandler[4] described results of experiments with mixtures of natural gas and steam reformed in a separate catalyst chamber in contact with the cell. Schultz's

data indicated that at 730 C, 15 mole percent hydrogen would be found in a mixture reformed on a nickel battery plaque, and 12 percent would be found when reforming on the electrode holder alone. The equilibrium composition is about 75 percent hydrogen. Thus, nickel battery plaques are not particularly effective. Sandler reported almost complete (i.e., equilibrium) conversion of methane to hydrogen on his unspecified catalyst at 580 C.

The performance of all-nickel porous bodies as steam reformers might be improved by forcing the steam-methane mixture through the pores of the coarse layer rather than simply passing the gas mixture along one face of the porous plaque and allowing the mixture to diffuse into the reaction zone. It was to obtain this "forced-by" operation that the double-duty anode shown in Figure 1 was designed. The term "forced-by" is used to distinguish this mode of fuel feed from other modes such as diffusion, "blow-through", and "dead-end".

The electrode is designed for use with a free electrolyte; therefore, it is a two-layer, double-porosity electrode. That is, there is a fine-pore layer which is flooded with electrolyte during operation, sealing one face of the coarse layer against gas leakage. By sintering the other face of the coarse layer to the electrode holder, a gas passage is formed so that fuel gas introduced at one edge of the electrode is forced through the coarse layer parallel to the electrolyte-gas interface and out the opposite edge. The use of forced flow requires that pressure drop be considered. For long flow paths, it would be impossible to maintain the meniscus in the fine layer near the exit edge without exceeding the bubble pressure near the inlet. A rule of thumb adopted for designing electrodes was that the pressure drop between the inlet and exit edges should not exceed 10 percent of the bubble pressure of the fine-pore layer.

To meet the pressure drop requirements for large-area electrodes, a holder was designed which provided short flow paths without restricting the overall dimensions of the electrode. This design is shown in Figure 2. The fuel inlet and outlet channels are interlaced to force the methane-steam mixture through a section of the coarse layer.

OPERATIONAL LIMITS FOR DOUBLE-DUTY ANODE

Most fuel batteries to be economically successful must convert a large percentage of the fuel to electricity. This requires both extensive conversion of fuel to products and high electrochemical efficiency. While much emphasis has been placed on the latter condition (i.e., voltage efficiency), many investigators seems to have neglected, so far, the first requirement (i.e., extensive conversion). When the products of the electrochemical reaction are gases, not only does dilution of the fuel occur, but the products reduce the reversible potential as their concentration increases.

This was well emphasized by Broers and Ketelaar[12] and by Chambers and Tantram,[3] who showed the effect of extent of conversion on the theoretical voltage of a cell.

Equilibrium gas compositions were calculated for each cell in a six-cell series-fed module (see Reference 8 for model). The calculated compositions for a 1:1 methane-steam mixture are given in Figure 3. It is apparent that most cells will be supplied with H_2 + CO if adequate reforming occurs. Double-duty anodes were operated on the composition corresponding to 70 percent electrochemical oxidation. This composition was designated "lean fuel gas". In the six-cell modules, the electrochemical consumption was projected as 84 percent; therefore, the last of the six cells must consume about half of the fuel value supplied to it. The goal established was 100 ma/sq cm at a potential more negative than -0.78 volt versus ORE* with 50 percent consumption of fuel. (The goal was also established on the basis of the design study.[8]) This potential was chosen because nickel is thermodynamically stable to oxidation according to the reaction

$$Ni + 1/2\ O_2 \rightleftharpoons NiO$$

at potentials more negative than -0.78 volt versus ORE when $a_{NiO} = 1$ (i.e., when the melt is saturated with NiO) and no other reactions occur.

The potentials calculated (assuming equilibrium) for the fuel mixture entering several cells are given in Table 1. Thus, the limitations imposed on the potential of the anode in the sixth cell by gas composition

TABLE 1. OPEN-CIRCUIT POTENTIAL OF FUEL GAS MIXTURES

Cell (of 6)	Open-Circuit Potential, at 1.4 Atm, vs ORE[(a)]
1 entering	-1.22
4 entering	-0.98
6 entering ("Lean Fuel Gas")	-0.91

(a) See footnote, page 5, for description of Oxygen Reference Electrode (ORE).

and by the nickel corrosion potential leave only 0.13 volt for polarization.

* Unpublished results. "ORE" is the Oxygen Reference Electrode, a reproducible, simple reference electrode for use in molten carbonates. It consists of a platinum wire spiral partially immersed in molten carbonate and bathed with a mixture of 70% CO_2 and 30% O_2. With proper construction and special attention to isolation of the electrolyte chamber from the bulk electrolyte, potentials are within 5 vf of the thermodynamically calculated values. It is reversible within the loading limits of a potentiometric recorder. In principle, this electrode is like those described by Stepanov and Trunov[13] and by Janz and Saegusa.[14]

OPERATION OF THE DOUBLE-DUTY ANODE ON A LEAN FUEL GAS MIXTURE

To establish that the proper flow pattern could be achieved, electrodes were operated on fuel mixtures containing hydrogen and carbon monoxide before using methane-steam mixtures. Experiments on stability of the forced-by mode were combined with experiments to determine the extent of the fuel utilization.

First experiments were performed with 2-sq-cm electrodes mounted in a holder of the type illustrated in Figure 4. The fuel gas was introduced at the arc-shaped recess on one side and was removed at the recess on the opposite side. Stability of the forced-by mode was established in several experiments where current densities up to 100 ma/sq cm were obtained at -0.78 volt versus ORE. Occasional flooding of the anode occurred when fuel pressure dropped accidentally or intentionally. Flooding was readily corrected by closing the exit line to force electrolyte out of the coarse-pore layer. No permanent loss of performance resulted from flooding. Thus, stable electrode operation is possible with the forced-by mode.

Most of the electrodes were operated for only a few hours at a given performance level to establish that the mode of operation was stable. Some failures occurred, resulting in loss of gas pressure. Failures were traceable to poor bonding of the electrode to the holder or of the coarse layer to the fine layer. But, satisfactory long-term performance was indicated by operating an anode for 11-1/2 days. Initially the electrode and associated tubing system showed little leakage, but at the end of 11-1/2 days the leakage of gas into the melt had become too great for further results to have practical significance. Performance remained the same throughout except during one purging required to remove a flooding condition. On lean fuel gas (18 percent H_2 + CO) the current density was 75 ma/sq cm at -0.80 volt versus ORE. Fifty to sixty percent of the fuel value was converted electrochemically throughout the 11-1/2-day operation. This established that good fuel utilization could be obtained along with adequate performance.

Cause of the gas leakage can be seen on the photograph in Figure 5. Two types of failure are apparent. The separation in the coarse layer seen in the section is responsible for the large bulge in the center. With active fuels which do not require steam reforming, separation has little effect on electrode performance. Separation is a mechanical problem and can be corrected by improved sintering technique and by the use of a mechanical support in the form of a honeycomb alumina separator between electrodes in a cell which reduces the unsupported span of the sintered structure.

Pockmarks and the small mounds of powder which appear predominantly at the edge of the electrode were the sites of gas leakage. The location of pits near the exit side and of powder deposits near the inlet side suggests that the gradient in reduction potential from inlet to outlet sides is the cause of this type of failure. A gradient in the reducing power of the gas phase will result in a similar gradient in the melt within the pores of the anode. In more oxidizing regions nickel dissolves; in more reducing regions it deposits. Small particles, released from the porous matrix at one point, are suspended in the melt and are incorporated in the surface where nickel ions deposit. Despite the potential seriousness of the loss of material, two measures can be proposed to reduce the transfer of nickel:

(1) Provide more uniform gas distribution to minimize the reduction gradient across the anode.

(2) Overlay the anode surface with a fine mesh screen to retain particles loosened by dissolution of nickel. Electroformed nickel screens of 1000 lines per inch are available and provide the equivalent of a specimen prepared by powder metallurgy with large particle-particle contact. Such screens have given satisfactory performance in short-time experiments where the screen was used as the fine-pore layer.

During the operation of this small (2-sq-cm) anode, a mass spectrometric analysis was made of a sample of exit gas. On a dry basis, 95 percent of the sample was carbon dioxide. The hydrogen-to-carbon monoxide ratio was 1 to 1.6, indicating that even without a special water-gas shift catalyst about one-third of the current was derived from carbon monoxide. This result means that it will not be necessary to convert all the methane to hydrogen, and the water-gas shift need not be complete.

A laboratory-model fuel cell having 18-sq-cm electrodes was used for several experiments with lean fuel gas. The anode holder of Figure 2 was used in the laboratory cell. Problems of sealing the cell against electrolyte loss were avoided by dipping both electrodes into a pot of molten carbonate. A reference electrode was included in the setup for recording single electrode potentials. The best performance obtained with one of these anodes on lean fuel gas was 25 ma/sq cm at -0.78 volt versus ORE for about two days. The performance of the 18-sq-cm electrode was somewhat low because of design and fabrication problems. Separation of the anode from the holder allowed fuel to bypass some sections of the electrode, resulting in a reduction of the effective area. Improvements in the design and fabrication are expected to bring the level of performance of the large anode up to that of the 2-sq-cm anode, or 100 ma/sq cm at -0.78 volt versus ORE.

STEAM REFORMING OF METHANE ON ANODE STRUCTURES

After demonstrating that the double-duty anode would operate satisfactorily in the forced-by mode and that the lean fuel gas reaching the last of a series of six cells could sustain adequate current densities, the next step was use of a methane-steam mixture in the double-duty anode. A few experiments with nickel double-duty anodes revealed little activity for steam reforming, in general agreement with the work of Schultz et al.

A suitable steam-reforming catalyst was sought for incorporation into the nickel matrix. A survey of the literature revealed that a suitable supported catalyst should be nickel on periclase (natural magnesium oxide). Near-theoretical conversions of methane-steam mixtures to hydrogen and carbon monoxide were reported.[15] Magnesium oxide is resistant to attack by molten alkali carbonates, as is nickel in the fuel atmosphere.

Several trial compositions lead to a suitable mixture of nickel and periclase powders which maintained structural integrity after pressing and sintering. The compact consisted of 15 weight percent periclase and 85 percent nickel. Both were in the form of 100-micron powders. After pressing and sintering under hydrogen, the compact was treated with nickel nitrate solution and dried on a hot plate. The nickel nitrate was decomposed and reduced simultaneously by heating in a hydrogen atmosphere to 760 C, slightly above the operating temperature of the cell.

Prior to making fuel electrodes, small-scale steam-reforming experiments were carried out with the catalyst-nickel powder mixture. The small-scale reformer consisted of a 1/8-inch Inconel pipe (0.269-inch ID) with brass tees silver soldered on each end. A 1/4-inch-OD Inconel tube with 200-mesh nickel screen over the end was inserted into the pipe. The pipe was oriented vertically in a 1-1/4-inch-diameter, 12-inch-long tube furnace, and 1.4-cm layer of unsintered nickel nitrate-treated mixture was packed onto the screen. The system was sealed well enough to keep the leak rate at only 1 ml of hydrogen in 13 minutes at 6 psig. The ends of the furnace were insulated, and heating tapes were used on the entrance line to keep the temperature above 100 C.

The usual test procedure was as follows: (1) purge this reactor with hydrogen, (2) heat to 760 C to decompose the nickel nitrate, (3) hold 1/2 to 1 hour at temperature to reduce the nickel oxide in the periclase, (4) adjust the temperature to the value shown in Table 2, and (5) purge from 4 to 6 hours with methane-steam mixture at the pressure shown before sampling the exit gas for analysis by mass spectrography.

The flow rate of the methane was adjusted to give a residence time of about 0.1 minute. A blank run was made with nickel powder in the reformer tube. Analytical results of these two experiments and the calculated equilibrium composition are given in Table 2.

TABLE 2. COMPOSITIONS OF MIXTURES RESULTING FROM STEAM REFORMING OF METHANE

Condition	Pressure, psig	Temperature, C	CH_4	H_2	CO	CO_2	Percentage Reaction(a)
Theoretical Equilibrium	5.9	727	7.8	69.2	20.8	2.2	74.6
Nickel Powder	5.5	732	97.5	0.3	0.8	0.3	1.1
Catalyst Mixture	5.6	727	9.4	68.8	17.9	3.9	70

(a) Calculated from:[16]

$$\% \text{ reaction} = \left[1 - \frac{\% \ CH_4}{\% \ CH_4 + \% \ CO + \% \ CO_2} \right] 100.$$

Percentage reaction, calculated by the equation of Arnold et al.,[16] is a measure of methane reacted. The extent of the water-gas shift reaction cannot be measured by the equation. The results demonstrate the efficacy of the catalyst mixture for steam-reforming methane. A number of other experiments with differing amounts of catalyst and somewhat different temperatures and pressures also gave reaction percentages in the region of the theoretical values. These other experiments support the validity of the conclusion that the catalyst mixture is effective. The short residence time permits use of a 0.05 to 0.06-inch-thick coarse layer in an anode operating at 100 ma/sq cm. A small double-layer anode containing 15 weight percent catalyzed periclase in the coarse layer was also prepared. It was a structurally integral disc after pressing and sintering.

SUMMARY

Experiments have shown the feasibility of obtaining good steam-reforming activity from a supported nickel steam-reforming catalyst. It has also been demonstrated that such mixtures can be incorporated in a structurally integral two-layer electrode.

Anodes were designed for dual-purpose operation in a free-electrolyte molten-carbonate fuel cell. The ability of the anode structure to function properly with the forced-by fuel flow mode was demonstrated. Stable operation at 100 ma/sq cm at -0.80 volt versus ORE was obtained with a fuel mixture containing only 18 percent hydrogen and carbon monoxide. Such operation demonstrates that adequate performance can be obtained while electrochemically oxidizing 85 percent of the fuel value in a methane-steam mixture as required for the battery model discussed in an earlier paper. Further work is needed to establish long-time performance of the double-duty anode with methane-steam mixtures.

The authors wish to thank members of the Fuel Cell Research Group, who sponsored this work, for permission to publish.

REFERENCES

(1) G.H.J. Broers, "High Temperature Galvanic Fuel Cells, Ph.D. Thesis from University of Amsterdam, 1958.

(2) E. Gorin and H. L. Recht, Chem. Eng. Prog., 55, 51 (1959).

(3) H. H. Chambers and A.D.S. Tantram, in "Fuel Cells" (G. J. Young, ed.), p. 94. Reinhold Publishing, New York, 1960.

(4) Y. L. Sandler, J. Electrochem. Soc., 109, 1115 (1962).

(5) I. Trachtenberg, J. Electrochem. Soc., 111, 110 (1964).

(6) V. S. Daniel'bek, M. Z. Mints, V. V. Sysoyeva, and M. V. Tikhonova, in "Soviet Electrochemistry", Vol. 3, p. 173. Consultants Bureau, New York, 1961.

(7) L. G. Marianowski, J. Meek, E. B. Schultz, Jr., and B. S. Baker, in "Proceedings of the 17th Annual Power Sources Conference" (PSC Publications Committee), p. 72. PSC Publications Committee, P.O. Box 891, Red Bank, New Jersey, 1963.

(8) R. W. Hardy and J. McCallum, in "Fuel Cells" (prepared by Editors of Chemical Engineering Progress), p. 45. American Institute of Chemical Engineers, New York, 1963

(9) G.H.J Broers, M. Schenke, and G. G. Piepers, Advanced Energy Conversion, 4, 131 (1964).

(10) H. R. Linden and E. B. Schultz, Jr., U.S. Patent 3,146,131, August 25, 1964.

(11) E. B. Schultz, Jr., K. S. Vorres, L. G. Marianowski, and H. R. Linden, in "Fuel Cells", Vol 2, (G.J. Young, ed.), p. 24. Reinhold Publishing, New York, 1963.

(12) G.H.J. Broers and J.A.A. Ketelaar, in "Fuel Cells" (G. J. Young, ed.), p. 78. Reinhold Publishing, New York, 1960.

(13) K. G. Stepanov and A. M. Trunov, Dokl. Akad. Nauk.SSSR, 142, 866 (1962).

(14) G. J. Janz and F. Saegusa, "The Oxygen Electrode in Fused Electrolytes", Technical Report No. 13 (September, 1961), AD263952.

(15) C. H. Riesz, H. A. Dirksen, and W. J. Pleticka, "Improvement of Nickel Cracking Catalysts", IGT Research Bulletin 20, Institute of Gas Technology, Chicago, 1952.

(16) M. R. Arnold, K. Atwood, H. M. Baugh, and H. D. Smyser, Ind. Eng. Chem., 44, 999 (1952).

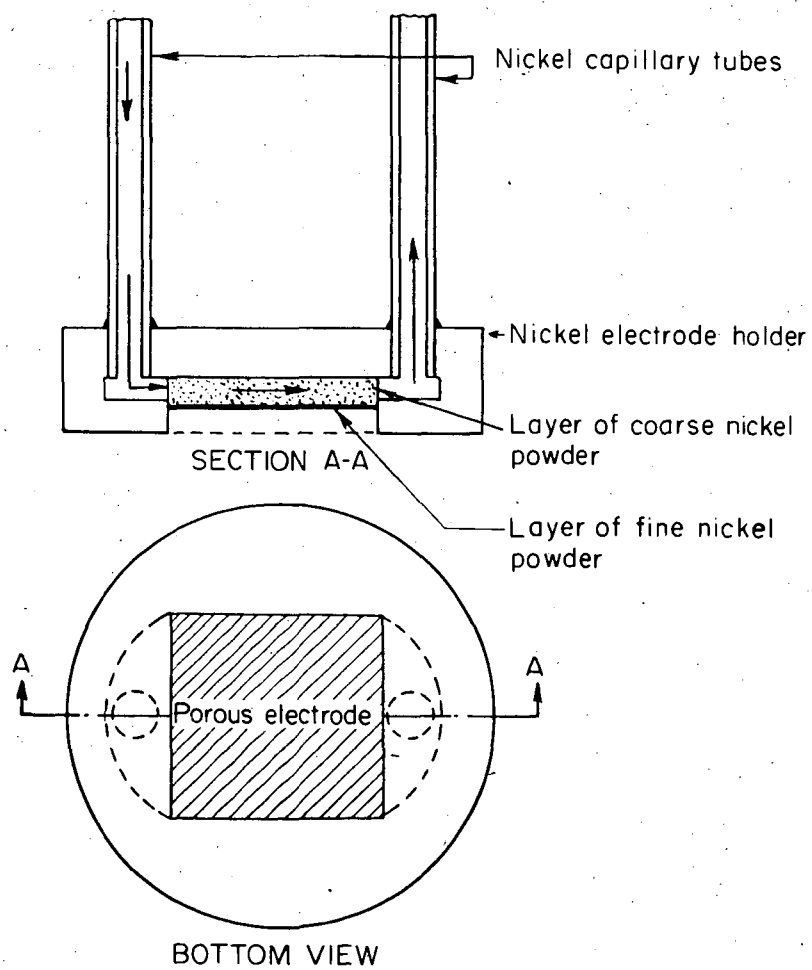

FIGURE 1. DOUBLE-DUTY ANODE DESIGN SHOWING FORCED-BY MODE. (WHEN COARSE LAYER CONTAINS CATALYST THE ELECTRODE PERFORMS BOTH FUNCTIONS, STEAM REFORMING OF METHANE AND ANODIC OXIDATION OF FUEL.)

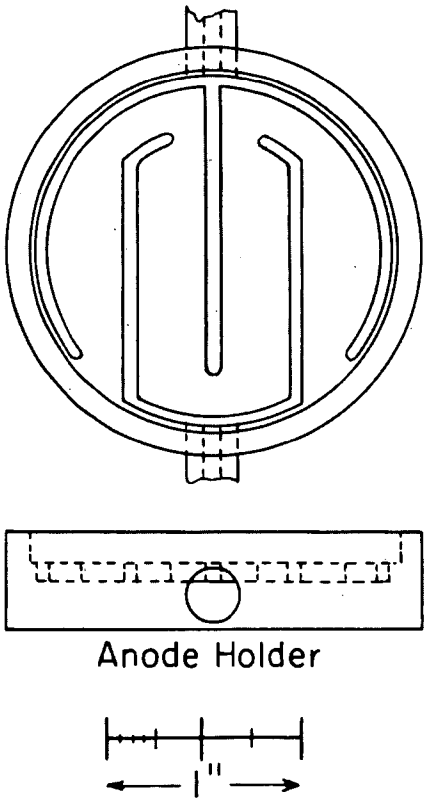

FIGURE 2. HOLDER FOR LARGE DOUBLE-DUTY ANODES. ELECTRODE AREA 18 SQ CM.

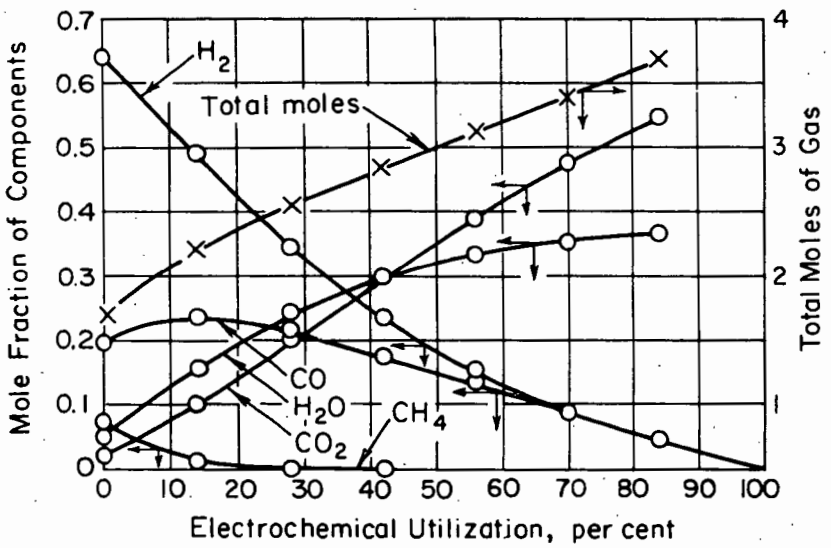

FIGURE 3. CALCULATED EQUILIBRIUM GAS COMPOSITION IN A FUEL BATTERY SUPPLIED WITH 1:1 METHANE:STEAM MIXTURE AT 1000 K AND 1.4 ATMOSPHERES.

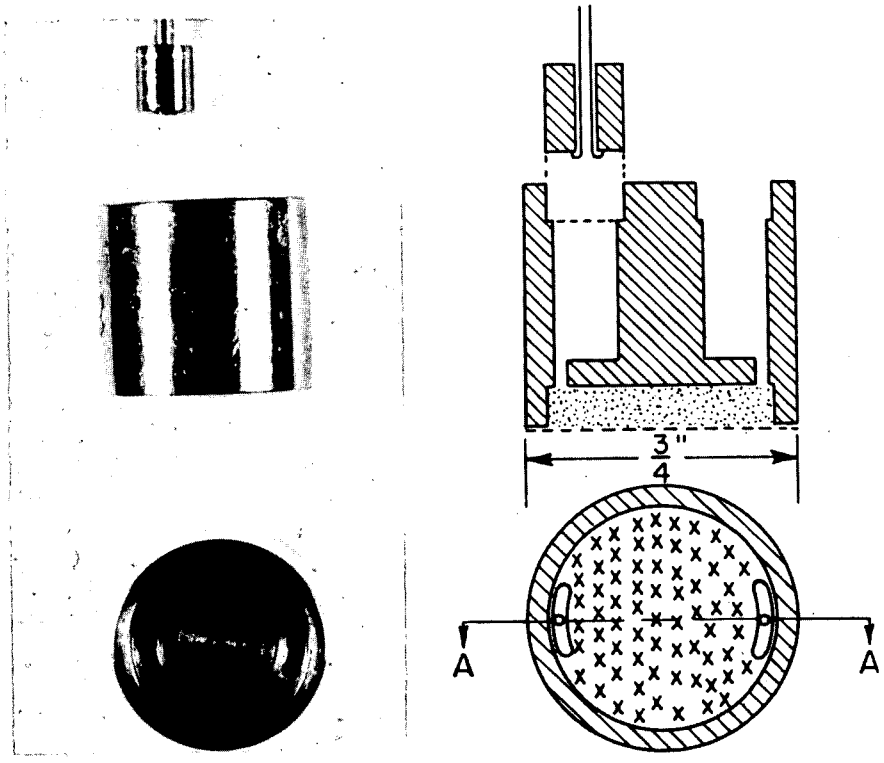

FIGURE 4. DETAILS OF 2-SQ-CM ANODES. ONE GAS INLET TUBE WITH FERRULE IS SHOWN.

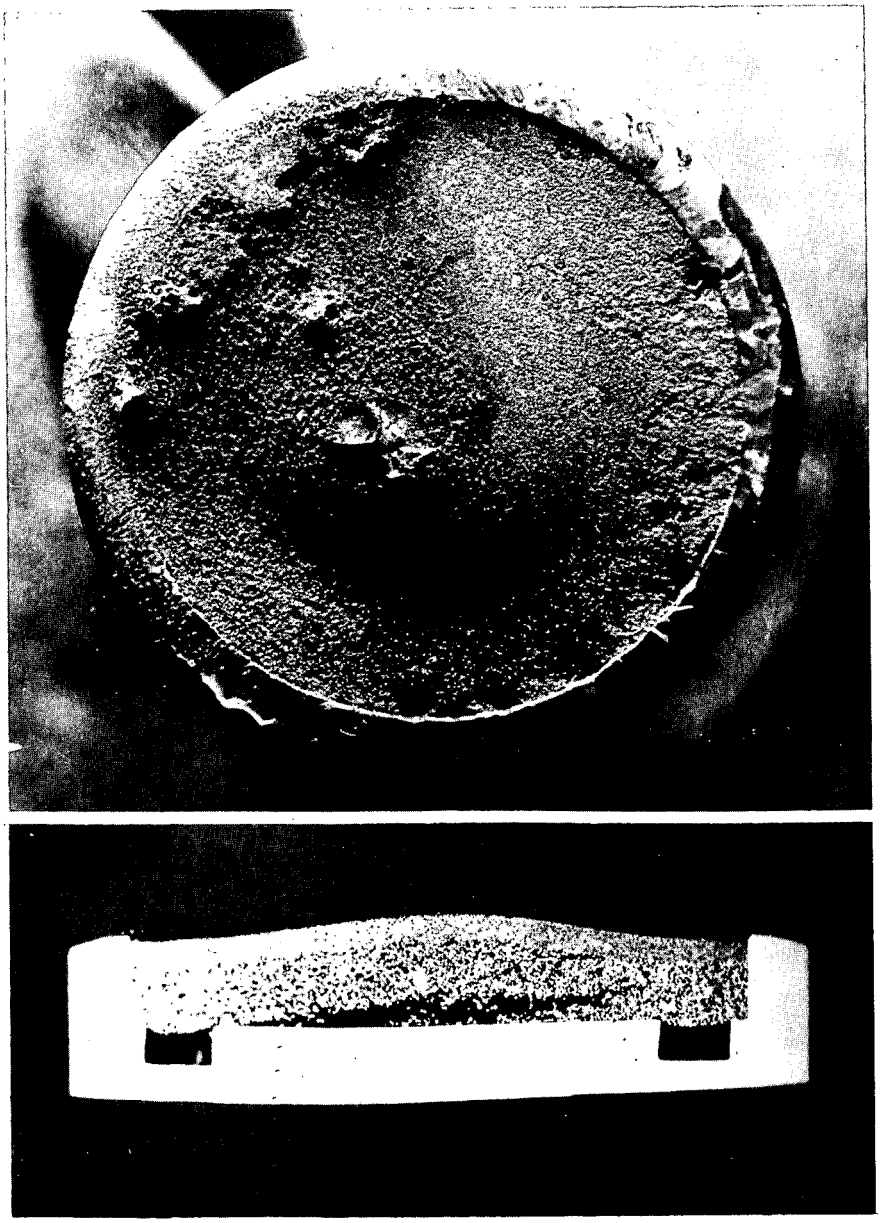

FIGURE 5. APPEARANCE OF A 2-SQ-CM ANODE AFTER 11-1/2 DAYS OF OPERATION ON LEAN FUEL GAS.

Long run experiments on high temperature molten carbonate fuel cells

G.H.J. Broers and M. Schenke

Central Technical Institute T.N.O., The Hague, Netherlands *)

1. INTRODUCTION

Research on high temperature fuel cells of the molten carbonate electrolyte type, by the Dutch organisation T.N.O., was taken up in 1950. The development of this work has been described in a series of publications [1] - [6]. Comments on the work can also be found in [7] and [8].

A significant step towards the realisation of the strictly necessary gastightness was made by the application of the so-called paste electrolyte [4], [5]. It is obtained by blending an inert powdered solid such as MgO with a given amount of binary or ternary alkali carbonate mixture (Li_2CO_3, Na_2CO_3, K_2CO_3).

Above the eutectic melting point of the carbonates (500°C for Li-Na; 396°C for Li-Na-K) a stiff and dense paste can be obtained when the inert solid to carbonates weight ratio remains above a certain critical value. This value depends on the particle size (and shape) of the solid constituent and the composition of the carbonate mixture. As a rough-and-ready rule, a 50 solid/50 liquid weight ratio will yield a rather stiff paste when the particle size of the solid (MgO) is below 1 micron; but closer readjustments have to be made in accordance with the basic materials used. A too high liquid content will cause plastic flow, a too low one causes an unnecessarily high electrolyte resistance. Under optimal conditions, the specific resistance of a typical MgO/ternary carbonate paste is about two times as large as the corresponding pure liquid resistance (paste resistance ~1.5 Ω cm at 700°C).

The experiments to be discussed here were all conducted on a laboratory scale. It was felt that technological development work was justified only if, in addition to leaktightness, the following demands could be satisfied:

1) a specific power output of at least 50 mW/cm² at 0.5 volt or better,
2) fuel and oxidant utilisation of at least 80%, at current densities of the order of 100 mA/cm²,
3) a cell life of at least several months at the just mentioned power output, with the aim of reaching a life of the order of three years [6], [9] in future developments.

2. CELL CONSTRUCTION, ELECTRODES AND FUELS

For purposes of fundamental research, a high temperature cell should meet the following demands: 1. perfect gastightness; 2. absence of any parasitic current paths, such as caused by metallic gaskets in contact with the electrolyte; 3. reliable contacts between the electrodes and the electrolyte; 4. presence of a suitable reference electrode, connected to the system by some form of electrolytic bridge; 5. no galvanic contacts with the surrounding heating furnace; 6. appriopriate means to know the degree of galvanic turnover, that is the ratio of the Faradaic current to the fuel and oxidant feed rate.

---

*) Correspondence on this subject to the laboratory address: 198, Hoogte Kadijk, Amsterdam-C, Netherlands.

2.1. Cells

The mentioned demands are satisfactorily met by the constructions shown in Fig. 1 and Fig. 2. In Fig. 1 the paste disc is pressed firmly against the inner wall of a high-purity Al_2O_3 tube at about 500°C. There is virtually no reaction between the alumina material and the carbonate melt when the former has been pretreated with a small quantity of molten carbonate for a few days. The working electrodes are pressed against the electrolyte by means of two additional Al_2O_3 tubes with a number of openings at the side of the electrodes, providing gas passages from inside to outside or conversely.

The pressing force on these tubes can be carefully controlled by means of springs with screw adjustments at their cold ends.

The reference electrode is a Pt or Au wire, dipping into a Al_2O_3 capillary filled with electrolyte paste. This "paste bridge" serves as a Haber-Luggin type connection to the disc surface. The phase boundary of the reference wire thereby is effectively screened from the electrolyte disc proper, and no ill-defined stray currents can pass through the reference wire, such as is most likely the case with so-called "idle electrodes". (The latter have their phase boundary situated direct in the current path between the working electrodes.) The reference is flushed with the same gas as the working electrode.

Two lead wires may be connected to each of the working electrodes, one serving as current lead and the other as potential lead. Resistance changes of each individual electrode can thus be measured too.

Fig. 2 depicts a simplified version of the cell of Fig. 1, being easier to assemble (as is evident from the figure). In this version, the reference electrode is a Pt wire wrapped around the outside of one of the gas sealing Al_2O_3 tubes. Use is made of the (in itself tedious) "creeping" effect of the carbonate melt along the wall of the tube. The "creeping film" stabilises within one or two days of cell operation (it comes to a stop at the colder parts of the tube) and forms a very effective electrolytic bridge between the wire and the ring-shaped periphery of the paste disc.

Whereas in Fig. 1 the reference potential is equal within $\pm$ 5 mV to the corresponding working electrode potential at open circuit, the reference potential in Fig. 2 depends on the gas atmosphere in the heating furnace. Addition of a small CO_2 flush to the air inside the furnace yields very stable potentials.

Great care must be taken to avoid direct contact between any hot parts of the cell and the (a.c. heated) furnace. The just mentioned "creeping" may otherwise lead to severe hum pick-up and electric leakage to either the a.c. mains or the ground.

2.2. Electrodes

The porous fuel electrodes discussed in this paper were all nickel specimens of various origin. Screens, sieve plates, sintered carbonyl nickel, nickel plates for secondary batteries* and "fiber nickel"** plates were used, as well as presintered nickel powder obtained by

---

* E.g. "Clevite" porous Ni; Clevite Corporation, Cleveland, Ohio, U.S.A.

** Huyck Corporation; Milford, Connecticut, U.S.A.

reduction of NiO with H_2. The commercially available types have no special advantages over Ni powder electrodes and are, at least at the present-day prices, by far too expensive to be used for anything else but research purposes.

The porous air electrodes were either of silver or copper oxide.

Silver electrodes were used in the form of wire screens and/or very thin layers of Ag powder (0.1 mm or less), adhered direct to the electrolyte surface.

The use of CuO as air electrode was reported by Justi and co-workers [7], [10], in connection with work on solid carbonate electrolyte fuel cells. In our case, commercially available CuO powder was mixed with some 10% of Cu powder. Small discs of about 1 mm thickness were pressed and subsequently sintered at 800°C in an air atmosphere. In the first few experiments, the discs were connected to all-copper current leads, in order to make sure that the electrochemical activity could be attributed solely to the CuO - Cu_2O system. In later tests, current leads of stainless steel or Pt wires were connected to the CuO material, thus avoiding gradual oxidation of the leads in long run experiments.

Whereas in low temperature cells the initially chosen porosity, pore size distribution and electro-catalytic activity of the electrodes is of crucial importance, a quite different situation exists in high temperature cells. Sintering effects, anodic dissolution and cathodic precipitation, and both surface- and bulk oxide formation under varying polarization strongly tend to alter the initial electrode structure. Figs. 3a and 3b show nickel anode specimens before and after use respectively. Initially, the commercially available material* had a porosity of 70% and a thickness of 1.0 mm. Fig. 3a is a microphoto of this material. Fig. 3b similarly shows the same material after 625 hours of continuous operation at 700°C and (nominally) 100 mA/cm^2, on an equilibrium mixture of H_2, CO, H_2O and CO_2. (iR-free polarization about +110 mV relative to open circuit.)

The thickness had shrunk to 0.6 mm (40% decrease) and a lateral shrinkage of about 15% was observed.

Evidently it is of no use to preselect electrode structures for high temperature cells on any basis different from long term operation experience. One might state that the high temperature cell tends to seek its own operating level, and not the one preferred by the investigator on the basis of initial electrode structures.

Also, conclusions about cell performances over periods of a few days have little meaning. Both overoptimistic and overpessimistic impressions may then result. An example of the latter will be shown in Sec. 3, Fig. 5.

2.3. Fuels

In most of the experiments a "standard fuel" of 1 mole of H_2 + 1 mole of CO_2 was used. The "standard oxidant" was 2.5 (vol.) air + 1 (vol.) CO_2. The feed rate was usually chosen in such a way that at 100 mA/cm^2, 10 per cent of the fuel and the oxidants were consumed. The cells were operated at atmospheric pressure.

*) Sintered nickel, type J.E.G.V.; Mond Nickel Company, London, England.

The overall cathodic and anodic reactions can be written as

cathode: $2\ N_2 + \frac{1}{2}\ O_2 + CO_2 + 2\ \lambda\ e^- \rightarrow$

$$\rightarrow 2\ N_2 + \tfrac{1}{2}\ (1-\lambda)\ O_2 + (1-\lambda)\ CO_2 + \lambda\ CO_3^{=} \qquad (1c)$$

anode : $H_2 + CO_2 + \lambda\ CO_3^{=} \rightarrow$

$$\rightarrow (1-\lambda)\ H_2 + (1+\lambda)\ CO_2 + \lambda\ H_2O + 2\ \lambda\ e^- \rightarrow \text{equilibrium fuel} \qquad (1a)$$

λ is the conversion degree of the reactants; the composition of atmospheric air is taken for convenience as $2\ N_2 + \frac{1}{2}\ O_2$.

Although the $1\ H_2 + 1\ CO_2$ fuel is not in thermodynamic equilibrium at the inlet of the cell, it turns out that at the Ni anode the equilibrium is indeed established. In the first place, the less convenient to handle fuel $1\ CO + 1\ H_2O$ yields the same open circuit potential as the forme one. Secondly, this open circuit potential E is virtually equal to the value calculated on the basis of the equilibrium fuel composition and the Nernst law (decadic logarithm):

$$E\ (\text{volts}) = E_o(H_2) + 0.992 \cdot 10^{-4}\ T \log \left[\frac{p_a(H_2)\ p_c^{\frac{1}{2}}\ (O_2)\ p_c(CO_2)}{p_a(H_2O)\ p_a(CO_2)} \right] \qquad (2)$$

where p_a and p_c refer to anodic and cathodic partial pressures respectively.

For $\lambda = 0$ in eqs. (1c) and (1a), the calculated E values are 968 mV at 1000°K and 980 mV at 700°C [6]. The observed values at 700°C are between 970 and 985 mV, apart from initial deviations due to "non-aged" Ni electrodes. It will be shown in Sec. 4 that the standard fuel can be considered as being oxidised already for 32% with regard to an "optimal fuel", just not depositing carbon at 1000°K.

In some of the experiments, $CH_4 + CO_2$ mixtures were used. Usually, equilibrium in that case is not established at the Ni electrodes, but insertion of a small amount of commercial Ni on MgO reform catalyst, in the anode space, is sufficient to yield equilibrium.

3. OPERATING CHARACTERISTICS AND POLARIZATION EFFECTS

The cells under discussion were all kept under a continuous current drain of 100 mA/cm^2 (whenever possible), unless current vs. voltage curves were measured. The latter measurements were carried out over time intervals of at least a full hour, so that a steady state was always achieved.

Individual electrode polarizations could be measured with the aid of the reference electrode, using a mercury-wetted relay for fast ($\approx$ 2 μsec) current interruption and a Tektronix type 535A oscilloscope to measure iR drops and potential/time transients. The method is essentially similar to the one described by Trachtenberg [11] and makes use of the "sweep delay" provision of the C.R.O. time base, to observe the magnitude of the iR break conveniently and quite sharply.

The principle of the measurement may be clear from Fig. 4a, where a typical course of the electrode potentials has been plotted on a linear time scale, for two different current densities before interruption.

Fig. 4b shows the corresponding cathodic and anodic transienst plotted on a $t^{\frac{1}{4}}$ scale. The meaning of the partial linearity of these plots will be discussed hereafter.

Fig. 5 shows the steady state (iR free) potentials and the iR drop, as functions of the current density, of a cell at 740°C with a "fiber nickel" anode and a silver powder cathode. The x x points refer to the third day of operation. It is seen that the Ni anode potential positivates "dangerously" at about 80 mA/cm^2, whereas the Ag cathode potential varies linearly with the current. Also, the open circuit voltage of the cell, 1035 mV, is too high, 960 mV being the true equilibrium value [6].

The open circle points, taken after 18 days of operation, reveal a rather striking improvement of the anode, now polarising linearly with the current up to 160 mA/cm^2, where the polarization is +105 mV*. The Ag cathode also shows some improvement, the polarization being -76 mV at 160 mA/cm^2. The open circuit voltage now shows the proper value, 960 mV, indicating that the fuel gas attains true equilibrium at the "aged" electrode. The iR drop obviously has not changed during the operation period of 18 days.

The figure clearly shows the relative importance of electrode polarizations and iR drop; at 160 mA/cm^2:

iR drop = 340 mV > anode polarization = 105 mV > cathode polarization = 76 mV.

Fig. 6a shows similar results for a cell with a CuO cathode on the 27th day of operation at 720°C. At 200 mA/cm^2:

iR = 325 mV > an.pol. = 102 mV > cath.pol. = 70 mV.

Both anodic and cathodic polarizations are linear with the current density.

Fig. 6b shows a number of terminal voltage vs. current density characteristics for the same cell, taken at different times and for different fuel feeds. The line 27 in Fig. 6b corresponds with Fig. 6a. Line 13, on $CH_4 + CO_2$, in the absence of a reform catalyst, reveals that in this case no equilibrium is established at the Ni electrode, otherwise a much higher open circuit potential would have been observed (about 1100 mV). Nevertheless, upon current drain a reasonable performance can be obtained. (Addition of a few tenths of a gram of reform catalyst in the anode space yields the calculated open circuit value and correspondingly improved results.)

The line 28, on pure hydrogen, was taken on the last day before deliberate termination of the test period, with the main purpose to test the leaktightness. The very high open circuit potential (1470 mV) shows the absence of any significant leakage after 4 weeks of operation. Also the capability of the CuO cathode to deliver current densities of 250 mA/cm^2 at about 90 mV polarization (on air + CO_2) could be demonstrated by this test.

The use of thinner electrolyte discs (9 mm in the case of Fig. 5 and 6.5 mm at Fig. 6) yields improved performances. The results shown in Fig. 4a, for instance, were obtained with a paste disc of 5 mm thickness. The terminal voltage in this case is 695 mV at 129 mA/cm^2 and still 540 mV at 212 mA/cm^2, with an iR drop of 282 mV in the latter case.

The given examples show that the purely resistive iR drop is always the predominant term in the total voltage drop of a current delivering cell. Nevertheless, the electrode polarization is by no means negligible, and therefore it is interesting to know whether it is mainly due to mass transport phenomena or to activation controlled processes (slow electron transfer, slow adsorption or desorption). A rather extensive study on this question has been

*) Polarization with respect to open circuit anode potential.

made by the present authors, but its details fall beyond the scope of this article and will be presented elsewhere [12].

Here it may be sufficient to note that d.c., a.c. and pulse methods, applied to both "flat" model electrodes (in the form of smooth wires or strips) and porous Ni and Ag electrodes, all point to mass transport controlled polarization (at least, above 600°C). Closer study reveals that the limiting factor is the presence of fluid electrolyte films on the surface of the electrodes, through which the reactant and product gases have to diffuse. At the Ni anode, the "off-diffusion" of the products CO_2 and/or H_2O through the film is rate determining, unless the H_2 partial pressure becomes very low (Sec. 4). At the Ag cathode the diffusion of either O_2 or CO_2 (depending on the relative partial pressures), is determining.

Evidence for the diffusion controlled character of the reactions at the porous electrodes is shown in Fig. 4b and Fig. 7. Though the porosity of the electrodes is ill defined, their properties may be approximated mathematically by the model of an "infinitely long" homogeneous transmission line [16].

Provided that the polarization tension at any spot on the phase boundary of the porous electrode is small enough as to yield an essentially linear relation between the instantaneous local tension and the corresponding current density, a mathematical analysis of the transmission line model yields the following results [12]:

1) Steady state. If the specific phase boundary resistance* of a planar electrode is R_b ($\Omega\,cm^2$), the corresponding effective resistance R_p of a porous electrode is proportional to $\sqrt{\rho\,\delta\,R_b}$, where ρ is the specific resistance of the electrolyte film and δ its thickness.

2) Alternating current impedance. Similar to 1), if the phase boundary impedance of a planar electrode is $Z_b = A - jB$, where A is the real and B the imaginary component of Z_b and $j = \sqrt{-1}$, then the corresponding impedance Z_p of a porous electrode is proportional to $\sqrt{\rho\,\delta\,Z_b}$.

3) Galvanostatic transient response. It is well known that for a diffusion controlled process at a planar electrode, the overtension v, resulting from a short constant current pulse Δi, changes proportional to the square root of time:

$$v = \text{const.}\ \Delta i\ \sqrt{t}.$$

For the transmission line model of the porous electrode the corresponding relation can now be written as:

$$v = \text{constant}\ \Delta i\ \sqrt{\rho\,\delta}\ \ t^{\frac{1}{4}}$$

Now Fig. 4b depicts the course of anodic (porous Ni) and cathodic (porous Ag) polarization tensions after current interruption**, as functions of $t^{\frac{1}{4}}$. It is seen that the curves for both 129 mA/cm^2 (geometrical current density) and 212 mA/cm^2 show linear portions, as predicted by the latter formula. Moreover, the slopes of these linear portions are proportional with the current density, both for the anodic and cathodic curves. The anodic and

---

* The phase boundary resistance is defined as the ratio of polarization tension to current density. The concept is valid for small polarizations only ($< RT/F$).

** In order to observe the polarization change accurately, oscilloscopic traces were photographed over time intervals of 10^{-4}, 10^{-3}, 10^{-2}, 10^{-1} and 1 second.

cathodic slopes for the same current density, however, are different. It is seen that the anodic response is considerably more sluggish than the cathodic one.

The deviating initial part of the anodic curves (the first 5 milliseconds) is probably due to the interference of double layer capacity effects.

Fig. 7 is a so-called Argand diagram of the impedance $Z_p = A_p - j\,B_p$ of a nickel brush electrode. In the diagram, the real part A of the observed electrode impedance has been plotted against the imaginary part B, for different a.c. frequencies between 10 c.p.s. and 50 kc.

For a purely diffusion controlled process at a planar electrode, the phase boundary impedance Z_b is the so-called Warburg impedance: $Z_b = W_o\,\omega^{-\frac{1}{2}} \exp - j\,\pi/4$; where W_o is a constant, ω the angular a.c. frequency and $\pi/4 = 45^o$ the phase angle (arc tan B/A). According to 2), the corresponding impedance Z_p of the porous electrode should now be proportional to $\sqrt{Z_b} = W_o^{\frac{1}{2}}\,\omega^{-\frac{1}{4}} \exp - j\,\pi/8$. In the Argand diagram of the impedance vector end points, the latter expression is represented by a straight line with a slope $\pi/8 = 22\frac{1}{2}^o$, and $|Z_p|\,\omega^{\frac{1}{4}}$ = constant. It is seen that the observed impedances satisfy these demands only approximately, with the greatest deviation at high frequencies. When, however, a correction is made for the influence of the double layer capacity (by standard vectorial subtraction methods) the cross-points are obtained, which satisfy the theoretical prediction very well. Similar results have been obtained for porous anodes with less ideal geometry than the brush form of the presented example.

The occurrence of the square root form $\sqrt{\rho\delta}$ in the various expressions for the polarization implies that the measured polarization always includes a purely resistive contribution from the electrolyte film. Moreover, since the true phase boundary resistance R_b only appears as $\sqrt{R_b}$ in the expression for the steady state polarization of a porous electrode, the latter will be relatively insensitive to small variations of R_b, such as can be expected for slightly non-linear voltage-current relations. And finally, because RT/F at 1000°K has the large value of 87 mV, it is not very surprising after all that the observed steady state polarizations (Figs. 5 and 6) are essentially linear with the current density.

4. FUEL AND OXIDANT UTILISATION

4.1. Oxidation of the fuel

In the experiments of Sec. 3, the fuel and oxidant utilisation was of the order of 10%, at about 100 mA/cm^2, relative to the feed. With regard to the fuel, the general course of its oxidation by $CO_3^=$ ions can be visualised conveniently in the triangular C-H-O diagram of Fig. 8.

The "standard fuel" 1 H_2 + 1 CO_2 is represented by P. Its oxidation (cf. reaction (1a), Sec. 2.3) proceeds along the straight line P - CO_3, and would be completed at point P_e. Considering P as the initial fuel, its conversion degree λ at P is zero, and λ = 1 at P_e on the line H_2O - CO_2. The "optimal fuel", however, which can be oxidised along the same path, is represented by P_o on the carbon deposition boundary (C.D.B.) curve [6], [13]. At 1000°K and 1 atm total pressure the composition of P_o is 0.17 C + 0.63 H + 0.20 O. Is is easy to show that, with respect to oxidation by $CO_3^=$ ions, the standard fuel P is already oxidised for 32% when P_o is taken as the initial fuel. If λ_o represents the conversion degree of P_o, then $\lambda_o = 0.32 + 0.68\,\lambda$ (λ = conversion degree of P).

It is possible to calculate the theoretical (Nernst) EMF for any value of λ or λ_o, by means of equation (2), Sec. 2.3 when the equilibrium compositions of the C-H-O gas phase on the line $P_o - P_e$ are known. The author (Broers) has found a simple method [14] to calculate curves of constant CH_4 partial pressure (Fig. 8) and curves of constant EMF (Fig. 9) in the triangular diagram, so that the theoretical EMF values for different points on the line $P_o - P_e$ can be read directly from it.

The CH_4 "isobars" of Fig. 8 show that at 1000°K, in the range of interest, $p(CH_4)$ is rather low, so that in good approximation only the equilibrium:

$$H_2 + CO_2 \leftrightarrows H_2O + CO$$

needsto be considered. This makes calculations of the equilibrium compositions along the path $P_o - P_e$ fairly simple.

A still more convenient method involves the use of the diagram of Fig. 9. The curves in this figure permit a direct reading of the "excess EMF", ΔE (in millivolts), which has to be added to $E_o(H_2)$, cf. equation (2), to obtain the E value with regard to anodic gases. The cathodic contribution in (2) can of course be calculated straight forwardly.

The course of the theoretical EMF along the path $P - P_e$, i.e. $\lambda = 0$ to $\lambda = 1$, is shown in Fig. 11, upper curve. The cathodic partial pressures $p_c(O_2)$ and $p_c(CO_2)$ are kept constant (0.14 atm and 0.28 atm respectively), in agreement with the experimental set-up to be described.

Now the course of the practical cell terminal voltage as a function of λ was determined as follows. Suppose we have a battery of n cells, of equal surface area, connected in series. The fuel is passed through this battery in series flow. Then each cell converts a fraction $\Delta\lambda$ of the fuel, at equal current density. When the current is i, and the feed rate of the combustible part of the fuel mixture is equivalent to n i, $\Delta\lambda = 1/n$. The overall conversion degree at the entrance of cell k will be $\lambda = (k - 1)/n$, and at its exit $\lambda = k/n$. Thus, in principle the conversion would be complete at the exit of cell n. In practice this cannot be realised, since progressive fuel depletion and product accumulation tend to increase the (mass transfer controlled) polarization, so that in some given cell of the battery the actual current density becomes the limiting one.

Since no practical battery was available, relevant experiments were carried out with a single cell at 720°C, by means of a simulator technique represented in Fig. 10. When the standard fuel has been oxidised to a degree λ, reaction (1a), Sec. 2.3 has occurred.

In order to realise this reaction, the necessary amount of "$CO_3^=$ ions" was supplied to the fuel in the form of gaseous O_2 and CO_2 (in the proper ratio), so that the latter gases reacted directly in the hot part* of the anode tube with the incoming fuel, before reaching the electrode.

The supposed number of cells n was chosen as 10. At a cell current i the H_2 feed was evolved electrolytically at a current 10 i, and the additional equal CO_2 feed (O_2 free) by accurate flow meter adjustment. O_2 simultaneously was evolved and supplied electrolytically at a current 10 λi, and mixed with an equivalent flow of 10 λi CO_2 (the double amount of CO_2 against O_2 when expressed in moles/second). Thus the conversion

---

* Compare Fig. 2, $O_2 + CO_2$ entering through auxiliary inlet.

of the fuel could be adjusted quite accurately, by ammeter readings.* The oxidant flow rate was held constant, at a large excess, in order to keep the cathode potential constant.

The results, at current densities of 62 mA/cm^2 and 125 mA/cm^2 are shown in Fig. 11. Since $\Delta\lambda = 0.1$ and e.g., at the entrance of cell no. 4, $\lambda = 0.3$, the voltage reading of cell 4 has been plotted at $\lambda = 0.35$. The actual voltages observed (full curves) have also been corrected for iR drop, yielding the dashed curves. It is seen that:

1. At 125 mA/cm^2 about 70% of the standard fuel (P in Fig. 8) can be utilised, or about 80% of the corresponding optimal fuel (P_o in Fig. 8; λ_o axis in Fig. 11). The partial pressure of the remaining fuel at $\lambda = 0.7$ is 0.11 atm.
2. At 62 mA/cm^2, 90% of the standard fuel, or 93% of the optimal fuel can be utilised. The partial pressure of the remaining fuel at $\lambda = 0.9$ is 0.034 atm.
3. The difference between the theoretical E curve and the dashed curves, that is the polarization, appears to decrease with increasing fuel conversion, till close to the point where the current density becomes the limiting one.

This rather surprising phenomenon may be explained by the already known fact that not the fuel, but the products CO_2 and H_2O are rate controlling (Sec. 3), and that the overall rate of gas flow increases with increasing conversion (equation 1a). Probably the effect of the increasing CO_2 and H_2O partial pressures is counteracted so much by the increasing flow rate, that the overall effect is in favour of a polarization decrease. But finally the mass transport of the H_2 + CO fuel, now at rather low partial pressure, takes over the role of the reaction products, and total depletion at the electrode surface starts very soon thereafter.

These observations clearly show that the attainable fuel utilisation is a pronounced function of the current density. In order to use the greatest possible fraction of the fuel feed, the current density in the "last cells" of the battery has to be decreased by increasing their surface area. Practically, this becomes a matter of optimising the increasing investment costs against the decreasing fuel costs. In this sense, the possibility of 90% fuel utilisation at (at least) about 60 mA/cm^2 seems a rather encouraging result.

4.2. Utilisation of O_2 and CO_2**

The conversion at the cathode is given by equation (1c), Sec. 2.3.

The experimental measurement of the terminal voltage as a function of λ in an imaginary 10 cell series battery was carried out as follows:

1. Excess fuel (1 H_2 + 1 CO_2) was used at the anode (about 10% conversion).
2. At cell current i, an electrolytically generated O_2 feed, 10 $(1-\lambda)$ i, was led into the cathode space of the cell, together with:
3. A CO_2 feed (O_2 free) of 10 $(1-\lambda)$ i, that is twice the O_2 flow rate in volume/sec.
4. A N_2 feed (O_2 free) held constant at 4 times the oxygen volume flow rate for $\lambda = 0$.

---

* Also to λ values not corresponding with integral cell numbers.

** The experiments described here and in Sec. 4.1 were carried out with one cell, with a Ag powder cathode and a "fiber nickel" anode. The measurements lasted 17 days in all.

The theoretical voltage as a function of λ was computed easily from the Nernst Law (equation (2), Sec. 2.3), using (1c) to calculate $p_c(O_2)$ and $p_c(CO_2)$. The results, at 720°C, are shown in Fig. 12, for current densities of 125 mA/cm^2 and 62 mA/cm^2. The dashed curves represent the iR free voltages. It is seen that:

1. At 125 mA/cm^2, about 85% of the "oxidant" $\frac{1}{2}\ O_2 + CO_2$ can be utilised. At this conversion, the remaining partial pressures are: $p(O_2) = 0.034$ atm; $p(CO_2) = 0.067$ atm.
2. Similarly at 62 mA/cm^2, about 95% utilisation is possible; $p(O_2) = 0.012$ atm; $p(CO_2) = 0.024$ atm.
3. By maintaining a slight excess of O_2 at 125 mA/cm^2, corresponding with $\lambda(O_2) = 0.80$, and studying the effect of $\lambda(CO_2) \geq 0.80$ solely, the dotted curve was found. Thus with regard to CO_2 conversion, about 90% can be utilised at 125 mA/cm^2.
4. Conversely, by keeping $\lambda(CO_2)$ at 0.80 and increasing $\lambda(O_2)$ beyond this value, about 93% O_2 utilisation could be reached. It seems therefore that in fact CO_2 is limiting when the stoichiometrical O_2/CO_2 ratio is used, but the match is rather close and may fall within the accuracy of the CO_2 flow meter calibration.
5. In contrast with Fig. 11, increasing conversion now brings about slightly increasing polarization, up till $\lambda \approx 0.75$. Since the overall flow rate in this cathodic case decreases with increasing λ, this is the result to be expected. Nevertheless, the polarization increase is enjoyably small.

From a purely theoretical standpoint, the maximum possible O_2 depletion from the air feed is not very important, though a great excess of air is definitely unwanted in connection with the heat balance of a battery system.

A quite different situation pertains to CO_2 depletion. Consider the (assumedly) complete combustion of a hydrocarbon C_nH_{2n+2}. The overall anode reaction is:

$$C_nH_{2n+2} + (3n+1)\ CO_3^{=} \rightarrow (4n+1)\ CO_2 + (n+1)\ H_2O + (6n+2)\ e^- \qquad (3)$$

Now the oxidation products are to be recycled to the cathode, and mixed with air in such an amount that at least $(3n+1)\ CO_3^{=}$ can be formed and also utilised. Since $(4n+1)\ CO_2$ is available, its conversion degree should be at least:

$$\lambda(CO_2)_{cath.} \geq (3n+1)/(4n+1)$$

Thus the cathodic conversion degree of CO_2 should be better than 80% for methane fuel, and still better than 75% for higher hydrocarbons ($n \gg 1$). The experiments depicted in Fig. 12 show that conversion degrees of this magnitude can indeed be attained at current densities up to 125 mA/cm^2.

To the knowledge of the authors, experiments of the kind discussed here have not been reported earlier. Only Chambers and Tantram [15] reported data on H_2 conversion percentages, but did neither specify the current density nor the actual terminal voltages observed.

5. LONG RUN EXPERIMENTS AT CONSTANT CURRENT DENSITY (100 mA/cm^2)

In earlier work [5], [6], it was not possible to draw current densities of the order 100 mA/cm^2 for more than about 1 week. Improvement of the electrolyte paste properties eliminated the instability effects at current densities > 25 mA/cm^2 virtually completely, so that a long run test at 100 mA/cm^2 could be carried out on a pair of small "twin cells" of 1 cm^2 surface area each.

Standard fuel and oxidant were used at 700°C, with 10% conversion relative to their feed rates. Both cells had "reinforced" Clevite porous nickel anodes (initially 70% porosity), which were used without any pretreatment. The cathodes were silver screens (0.5 mm wires with equally large spacings); cells constructed as shown in Fig. 1.

Fig. 13, upper section, shows the results over a 4600 hours period (after which the measurements were terminated deliberately), in terms of 1. terminal voltages, 2. iR free voltages, 3. open circuit voltages. The latter were observed only occasionally; see points indicated.

It is seen that:

1. The performances run rather similarly, the terminal voltages decreasing slowly from about 750 mV initially down to 470 mV at 4600 hours.
2. The iR free voltages become practically constant after 2-2½ months, so that the electrode polarizations also become constant after that period. The cathodic polarizations (not shown separately from the anodic ones) stabilise to about 50 mV, the anodic ones to about 150 mV.
3. Initially there is an increase in polarization, which has to be ascribed to alterations of the porous Ni anodes. (Sintering effects, compare Figs. 3a-3b, Sec. 2.2). With respect to these alterations, "ageing" of the electrodes by a heat pretreatment at 800°C, in reducing atmosphere, is rather favourable.
4. The open circuit voltages (initially too high) attain the calculated value 980 mV within about 2 weeks, up till the end of the test. This indicates that the cells were still gastight after 6 months.

Analysis of the electrolyte pellets revealed that about 50 mole % of the initial carbonate content was lost after the 6 months period. In Fig. 13, lower section, the conductivity of cell 3 (cell 2 gives similar results) has been plotted as a function of the operating time. It is seen that, roughly speaking, the decrease of the conductivity is proportional with time, and that from 500 to 4500 hours a 50% decrease has occurred. This suggests that the only cause of the performance decrease, after the "stabilising period" of the anode, is due to slow vaporisation of the carbonate melt.

In principle, carbonate losses may occur by "creeping" as well as by vaporisation. In the conditions of the experiment, however, creeping of the Li-Na-K carbonate melt comes to a stop at the cold parts of the alumina tubes, within one or two days. Moreover, it is very unlikely that losses through creepage would alter the ratio of Li to Na to K.

The chemical analysis of the used electrolyte pellets, however, proved that the mentioned ratio had changed considerably. Initially the alkali atom fractions were : 0.37 Li, 0.39 Na, 0.24 K,
whereas after 6 months they were : 0.47 Li, 0.36 Na, 0.17 K.

Thus the rate of K evaporation is the largest, that of Li the smallest one. Though the relative order of alkali carbonate stability is just the reverse with regard to CO_2 vapour pressure [1], it should be kept in mind that in the present experiments a relatively large CO_2 partial pressure was maintained all the time on both sides of the electrolyte pellet.

(A blank experiment with a liquid Li-Na-K carbonate mixture under CO_2 of 1 atm at 700°C, using a "cold finger" to condense the vapours, yielded qualitatively similar results. It took several weeks to collect a small quantity of condensed vapour.)

On the basis of the total amount of fuel and oxidant gases passed over the electrolyte pellets in the test period, it can be calculated that 1 mole of CO_3 was lost per (about) 10^5 moles of fuel, air and CO_2. Thus the vaporisation rate is quite small.

This in turn would mean that a (more or less) continuous supply of fresh melt in very small quantities would result in a practically constant performance over a period of several times the one observed here, that is in the order of at least a few years.

In conclusion, it may be stated that with regard to power output, attainable gas utilisation and life of the essential cell components, the prospects of the high temperature fused carbonate cell are far more favourable than thought hitherto.

Only work on a larger scale can show whether the construction of batteries is technically, and if so, also economically feasible. The authors fully appreciate that this still a long way to go.

ACKNOWLEDGEMENT

The authors would like to thank their colleagues Messrs. G.G. Piepers, J. Marchés, C. van der Harst, N. van Bezooyen, B.W. Treijtel, C. van der Laan, H.J.J. van Ballegoy and H.E. Huynink for their aid in carrying out the experiments and their inventivity in solving many of the practical problems.

REFERENCES

[1] G.H.J. Broers; "High temperature galvanic fuel cells"; thesis University of Amsterdam (1958).

[2] G.H.J. Broers; Dechema Monographien Bd. 38, 277 (1960), Verlag Chemie G.m.b.H., Weinheim, W. Deutschland.

[3] "Fuel Cells", Vol. 1, Chapt. 6. G.J. Young (Ed.), Reinhold, New York, (1960).

[4] "Fuel Cells", Vol. 2, Chapt. 2. G.J. Young (Ed.), Reinhold, New York, (1963).

[5] G.H.J. Broers; in "Fuel Cells, a C.E.P. Technical Manual", p. 90, Am. Inst. of Chem. Engineers, New York (1963).

[6] G.H.J. Broers, M. Schenke and G.G. Piepers; J.Advanced Energy Conversion 4, 131 (1964).

[7] E. Justi and A. Winsel; "Kalte Verbrennung - Fuel Cells", Chapt. 9.3. Steiner, Wiesbaden (1962).

[8] "Fuel Cells"; W. Mitchell Jr. (Ed.); Chapt. 5 and Chapt. 9; Acad. Press. New York and London (1963).

[9] R.W. Hardy and J. McCallum; in Reference [5], p. 45.

[10] K. Bischof and E. Justi; Jahrb. Akad. Wiss. Lit. (Mainz), 250 (1955).

[11] I. Trachtenberg; J. Electrochem. Soc. 111, 110 (1964).

[12] G.H.J. Broers and M. Schenke; J. Advanced Energy Conversion; to be published.

[13] E.J. Cairns, A.D. Tevebaugh and G.J. Holm; J. Electrochem. Soc. 110, 1025 (1963).
E.J. Cairns and A.D. Tevebaugh; J. of Chem. and Eng. Data 9, 453 (1964).

[14] G.H.J. Broers and B.W. Treijtel; submitted to J. Advanced Energy Conversion.

[15] H.H. Chambers and A.D.S. Tantram; in Reference [3], Chapt. 7, p. 105

[16] R. de Levie, Thesis, University of Amsterdam (1963); Electrochim. Acta 8, 751 (1963).

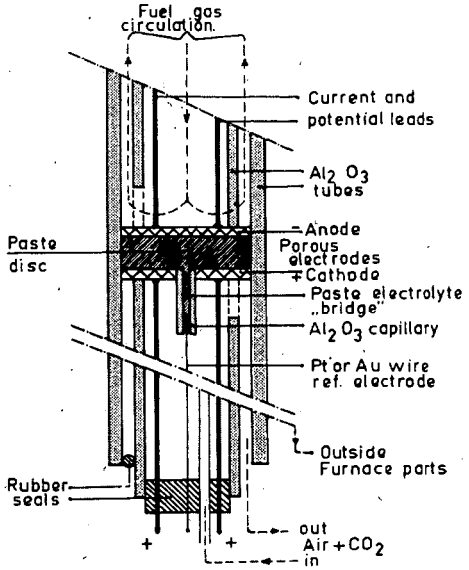

Fig.1 Disc cell with reference electrode for polarization and other fundamental studies.

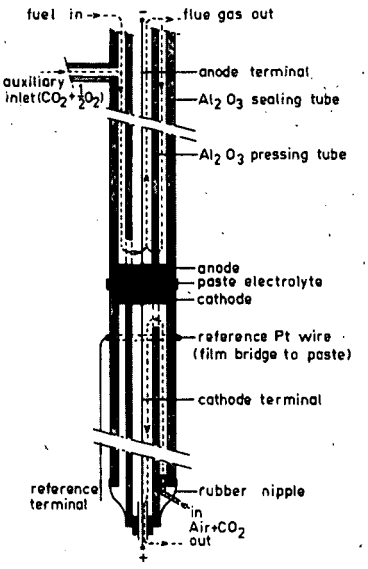

Fig.2 Simplified version of the cell cf. Fig.1.

Electrolytic bridge from reference wire to paste disc formed spontaneously by creeping of the molten salt.

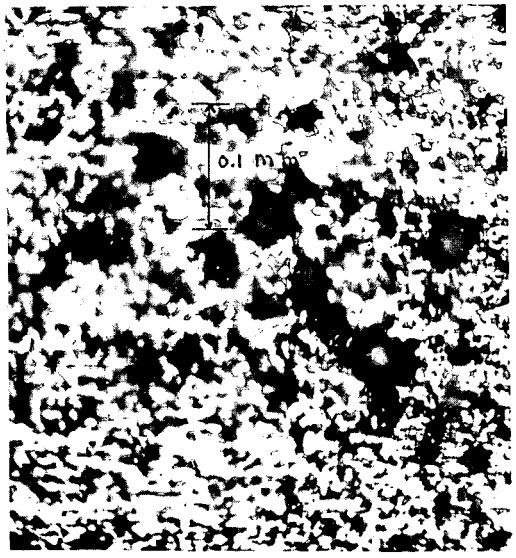

Fig.3a Porous Ni electrode (Mond Nickel Co.) before use. Magnification 125x, before final reproduction.

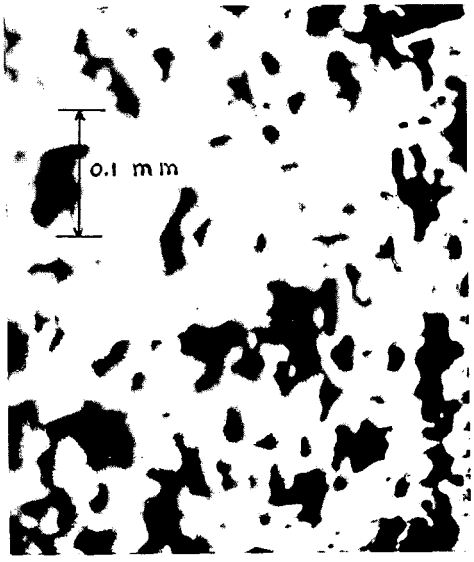

Fig.3b The same material after 625 hours of continuous anodic operation at 100 mA/cm^2, 700 °C.

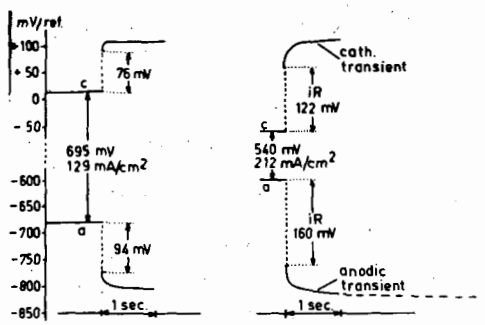

Fig.4a.
Determination of iR drop and electrode polarization by means of fast current interruption (< 2 µsec).

Linear time scale.

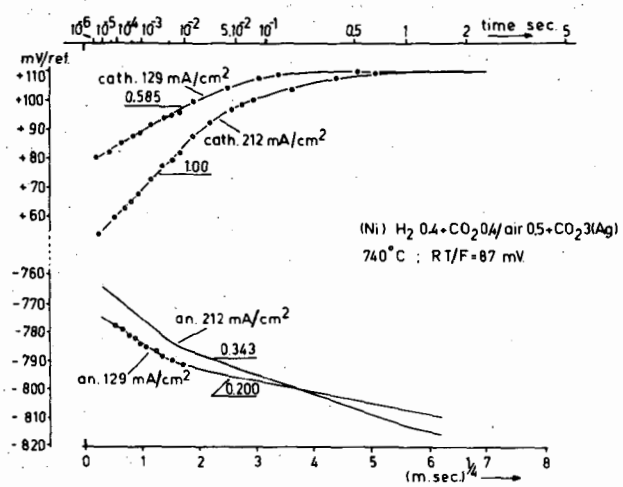

Fig.4b.

Cathodic and anodic potential transients cf. Fig.4a, but plotted on a $t^{\frac{1}{4}}$ time scale.

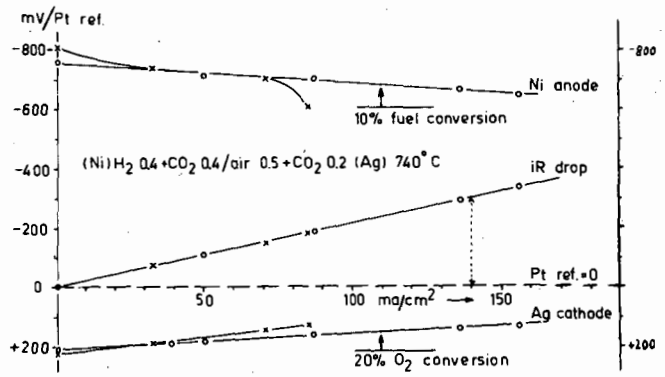

Fig.5. Steady state (iR free) potentials and iR drop of a cell cf. Fig.2, as functions of the current density. Cathode : Ag - powder, anode :"fiber nickel". x-x-x : 3rd day of operation; o-o-o-o :18th day of operation.

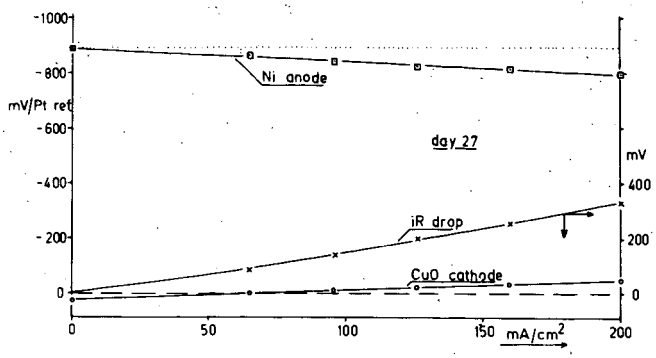

Fig. 6a. Steady state potentials and iR drop of a cell with CuO cathode and Ni anode, 27th day of operation.

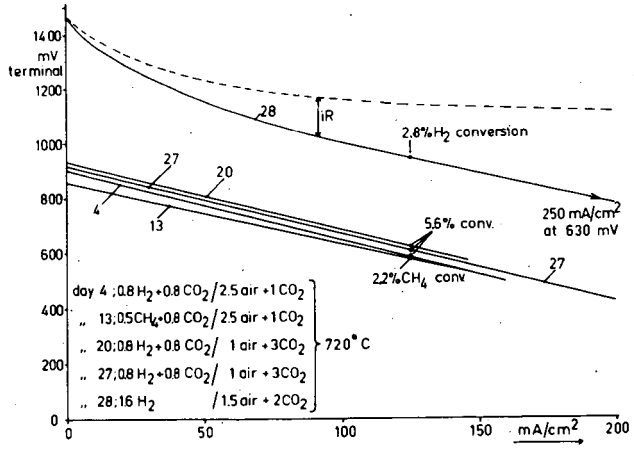

Fig.6b. Terminal voltage vs.current density characteristics of the cell cf. Fig.6a, over a 4 week period. No iR drop corrections, exept upper curve (dashed).

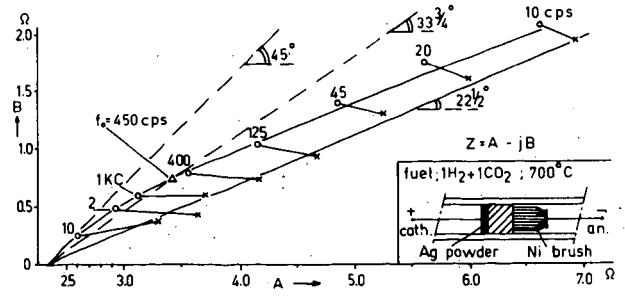

Fig.7. A.C.impedance vector diagram (Argand diagram) of a nickel brush electrode, simulating an ideally homoporous system. o-o-o : points observed; x-x-x : impedances corrected for influence of double layer capacity. Drawn straight line : theoretical prediction for pure diffusion control; $22\frac{1}{2}°$ slope, $|Z| \cdot f^{1/2}$ = constant.

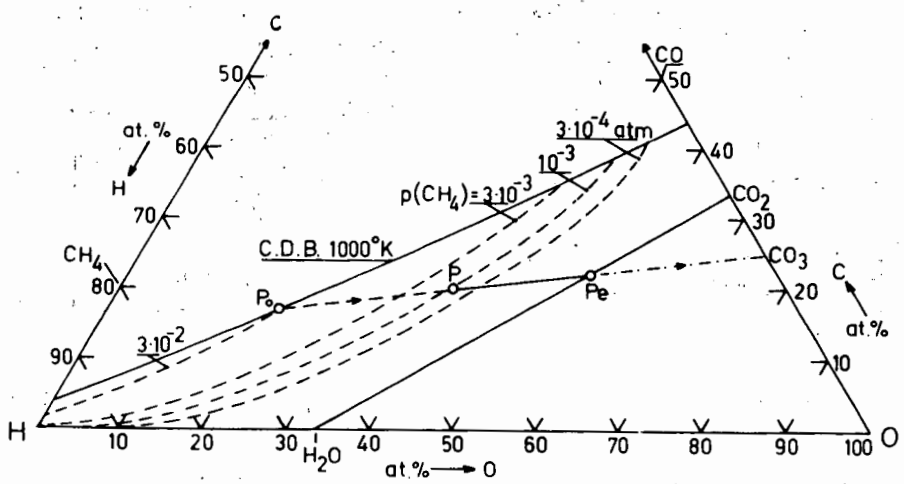

Fig.8. C-H-O triangular diagram, representing at 1000°K and 1 atm : 1) Carbon deposition boundary (CDB) ; 2) Equilibrium partial pressure "isobars" of CH_4 (dashed); 3) Oxidation path PP_e of the standard fuel P , reacting with $CO_3^{=}$ ions ; 4) Optimal fuel composition P_o that may be oxidised along the same path.
P corresponds with 32% oxidation of P_o .

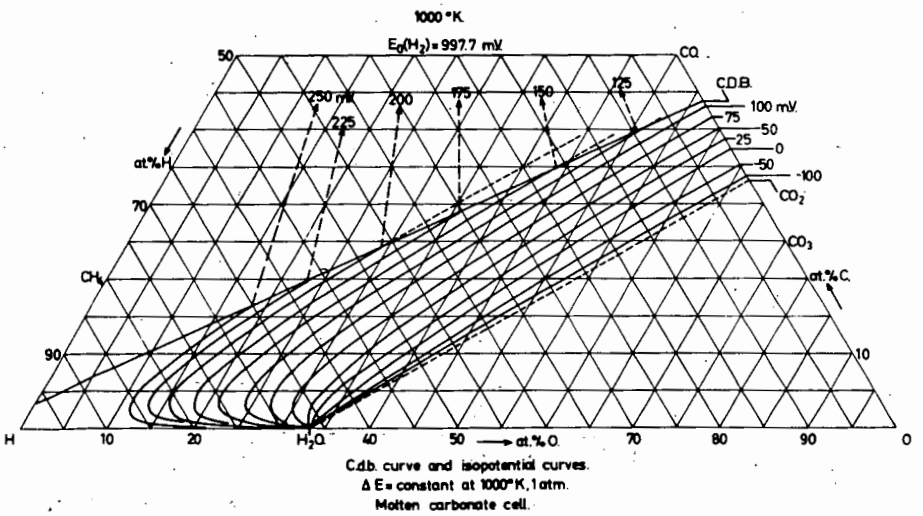

Fig.9. C-H-O diagram with CDB and curves of constant EMF with regard to fuel composition, for molten carbonate cells at 1000°K., 1 atm.
$E(cell) = E_o(H_2) + \Delta E(anodic) + \Delta E(cath.)$; cf. Eq.(2).
$\Delta E(anodic)$ can be read directly from the diagram, in mV.

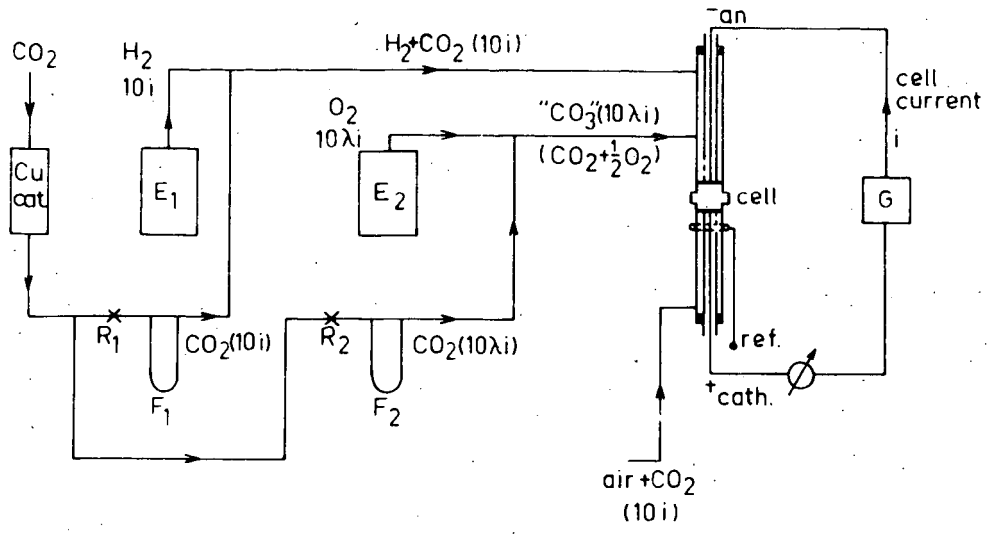

Fig.10. Determination of fuel utilization in an imaginary 10 cell series battery, by means of a single cell. E_1 : H_2 electrolyzer; E_2: O_2 electrolyzer; F_1 and F_2: CO_2 flowmeters with regulating valves R_1 and R_2 ; G : galvanostat. Cell cf. Fig.2.

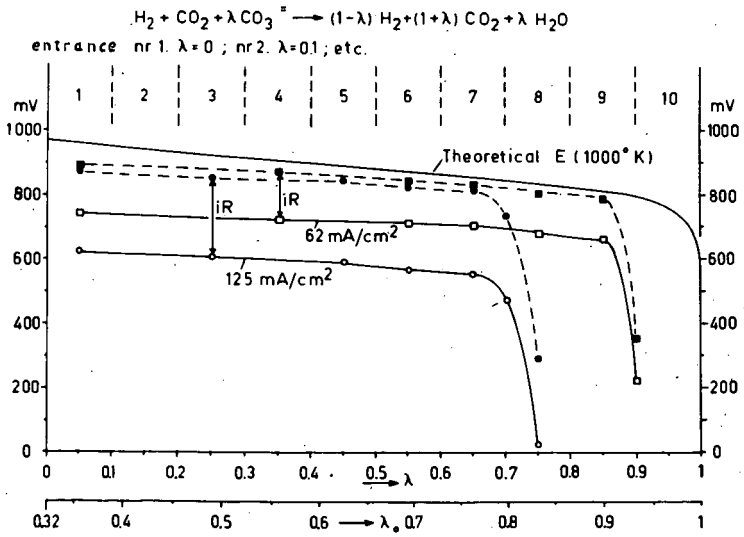

Fig.11. Results of fuel utilization experiments at 62 mA/cm² and 125 mA/cm². λ is the conversion degree relative to point P in Fig.8, λ_0 similarly to point P_0 in Fig.8. Anode: "fiber nickel", cathode: Ag screen. T=720°C. Theoretical E based upon equilibrium composition of the fuel mixture; derived from Fig.9 and Eqs.(1c)& (2).

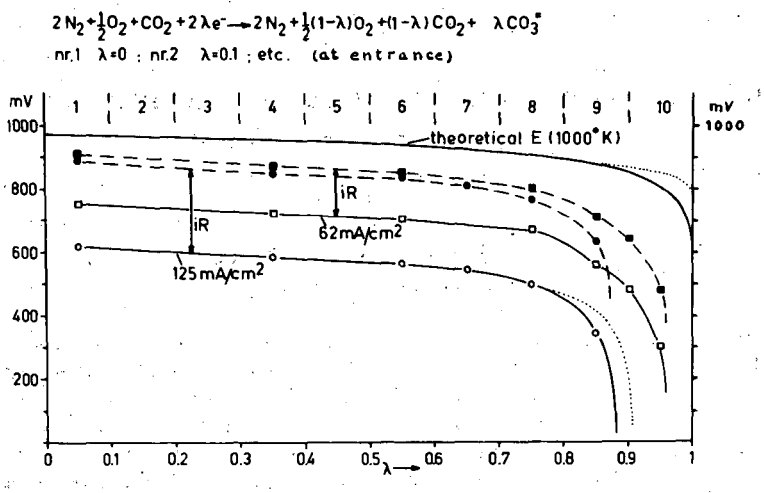

Fig.12. Results of oxidant utilization experiments. Points indicated: equal conversion degrees of O_2 and CO_2. Dot curve: $\lambda(O_2)$ held at 0.8 , $\lambda(CO_2) \geq 0.8$. (Similarly for the theoretical E curve.)

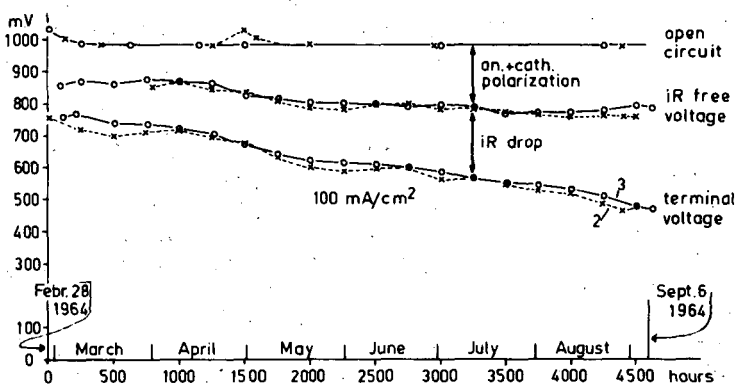

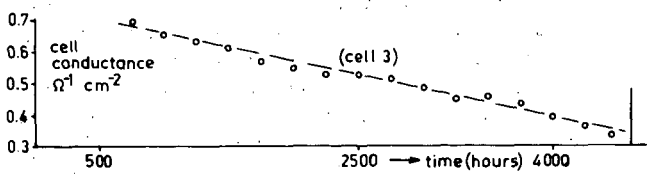

Fig.13. Long run (~6 months) output voltages of twin cells 2 (x-x-x) and 3 (o-o-o) at 700°C and 100 mA/cm², continuously. Fuel: 1 H_2 + 1 CO_2 , 10% conversion; oxidant: 2.5 air + 1 CO_2 , 10% conversion. Anode: "Clevite nickel"; cathode: Ag screen.
Lower section: decrease of cell conductance in the same period.

HYDROCARBON-AIR FUEL CELLS EMPLOYING SLURRIED MOLTEN CARBONATE ELECTROLYTES

Isaac Trachtenberg

Texas Instruments Incorporated, P. O. Box 5936
Dallas, Texas 75222

Fuel cells employing mixtures of molten alkali carbonates as the electrolyte have been described. These cells can be divided into three groups: those that employ a fixed ceramic matrix[1-3] impregnated with the electrolyte, a paste matrix[4-6] consisting of a mixture of fine ceramic particles and the electrolyte that is preformed, and a free electrolyte[7,8] with no matrix. In the first two groups, the ceramic-electrolyte body is the structural member and supports not only itself but also the electrodes. In the free electrolyte cells, the electrodes are the structural members and must to a great extent contain the very difficult to handle electrolyte. The slurried electrolyte cell described here takes advantage of the best of the cells mentioned above. There is no need for a pre-sintered or preformed ceramic-electrolyte body. The electrodes are the structural members. The ceramic particles serve as a separator and help contain the electrolyte. The electrolyte-ceramic slurry has no requirement for structural strength.

Cell Description

Figure 1 is a photograph of an actual test cell before operation. This unit consists of two cells connected electrically in parallel and is referred to as a 1 x 2 unit. The fuel gas supply flows between the two anodes. The unit is placed in a furnace chamber which contains the cathode gas supply. The cathodes are connected to the front plenum and the anodes to the rear plenum. The fuel gas plumbing is used for the current bus-bar, and cell voltage is measured between the leads coming from the top of the front and rear plenums. A silver wire used as a third idling electrode is placed in the ceramic electrolyte reservoir cup. Each electrode is 1 in. x 4 in. Since there are two such electrodes in parallel, there is a total geometric electrode area of 8 sq. in., or 51.6 sq. cm, of each electrode (anode and cathode) in these units. Figure 1 shows only one of the two working cathodes.

A cutaway perspective of the unit is shown in Fig. 2. The primary anodes are not only connected together at the plenum but also have a corrugated nickel screen welded between them to yield a stronger structure, provide better distribution of the gases, and to serve as a secondary electrode. In the experiments described here magnesia particles are used to form the electrolyte slurry. When the unit is assembled, dry MgO of selected particle size (depending on the electrode structure) is placed between the working cathodes and anodes. A mixture of 50 mol % Li_2CO_3 and 50 mol % Na_2CO_3 is prepared, fused, broken into pieces about 2 to 10-mesh, and placed in the electrolyte reservoir cup. The entire assembly is placed in a furnace and raised to operating temperature. At about 500°C the electrolyte begins to melt and is drawn by capillary action up the MgO-filled alumina feed tubes and into the MgO particles between the working anodes and cathodes. Once the electrolyte has saturated the MgO, the additional electrolyte in the reservoir cup merely remains there until it is needed to replace any electrolyte which may evaporate from the slurry. This feature of the unit permits very easy and rapid addition of electrolyte to the unit when it is operated continuously for extended time intervals.

Experimental

The following discussion will pertain to the performance of several of the 1 x 2 units in which the structure of the electrodes was changed. In these experiments the gas supplies were held constant. The fuel gas supply was a simulated natural gas (CH_4) reformate consisting of approximately 80% wet H_2 and 20% CO_2. Previous experience with the simulated natural gas reformate has shown that this mixture is water-gas shifted in the steel plumbing to a nearly equilibrium (> 90%) mixture of H_2, H_2O, CO_2, and CO at the operating temperature of the cell. The cathode gas supplied to the furnace chamber was 80% air and 20% CO_2.

The cells were under some load for more than 95% of the reported operating life. Operation of all the cells described was voluntarily terminated for postoperative examination while the cells were still performing at an acceptable level (>20 watts/ft^2).

The data presented here were obtained from current-voltage (E-I) curves recorded daily except for some of the week ends. These traces were obtained from the working cathode versus the working anode and from the anode and cathode individually versus the third idling electrode. The latter curves were recorded to determine total polarization of the individual electrodes. Traces were obtained using either an EAI 1110 Variplotter or a Varian F80 X-Y recorder.

Current interruption studies similar to those previously reported[1,3] for sintered matrix cells were performed. These studies continued to show that the total polarization is composed of two components, ohmic and concentration polarization. These interrupter studies also verified the 1000 cycle resistance measurements of the total internal cell resistance and determined the individual anode and cathode ohmic resistances.

Performance and polarization data as a function of operating time were presented to a 7040 computer to determine the best least mean square straight line, the standard error of the data points, and the standard error of the slope of the least means square line. The cell data treated in this manner include power density in watts/ft^2 at a fixed terminal voltage, open circuit voltage, total anode polarization, and total cathode polarization. Total anode and cathode polarization are defined as the difference between the potential versus the third idling electrode at open circuit voltage and that at the given current density. These data are discussed in detail in the following section.

Discussion of Results

Figure 3 shows two power versus hours of operation curves for 1 x 2 unit #47-47. This cell was operated at 600°C for 1100 hours before its operation was terminated voluntarily. It contains 120-mesh Ni screen primary and secondary anodes and silver-plated 120-mesh stainless steel cathodes. A secondary cathode of the same silver-plated material was also used on the cathode. (This secondary cathode can be seen on the cathodes in Fig. 10.) The MgO was sized so that it could be contained in the screens (> 120-mesh). The data points shown were selected randomly and are representative of all of the points. The solid lines are the best least mean square line at the two cell terminal voltages of 0.5 and 0.7 volt respectively. The dashed line indicates the standard deviation of the points from the line. Although the line at 0.5 volt shows a slight increase in power and that at 0.7 volt exhibits a slight decrease in power as a function of hours of operation, neither observation is statistically significant. The errors in both slopes are greater than the slopes themselves (see Table I at the end of this section). Similar treatments of the open circuit voltage,

anode and cathode polarization at current densities up to 75 ma/cm^2 also exhibit no significant slopes.

From these data it is concluded that within the limits of reproducibility of cell performance from day to day there was essentially no change in performance for 1100 hours of operation.

Cell #47-53 was another 1 x 2 unit operated at 600°C. It contained primary anodes made by sintering presieved, highly active nickel particles onto 120-mesh nickel screen. No secondary electrodes were used in this unit. The cathode consisted of sintered presieved silver particles on 120-mesh silver-plated stainless steel screen. The MgO was sized to be contained by the electrodes. Figure 4 illustrates the power at 0.5 volt as a function of hours of operation. Cell operation was voluntarily terminated after 828 hours. Notice that the initial power density of 50 watts/ft^2 is about twice that of the preceding unit. Power density remained 42 to 48 watts/ft^2 for more than 400 hours of continuous operation. The decline in performance started just after 400 hours of operation and continued to about 500 hours, when it leveled out for the next 200 hours before resuming a slower rate of decline until operation was voluntarily terminated.

Figure 5 illustrates the effects on the open circuit voltage and the total polarization of both the anode and cathode at 75 ma/cm^2. According to these data, the major cause of decline in power output of the cell was increased polarization of the cathode. There was essentially no change in the open circuit voltage during the entire operation. However, polarization on both electrodes did increase. Again notice that the cathode exhibits a distinct increase in polarization starting just after 400 hours and continuing to about 500 hours. The anode at the same time remained at worst unchanged, and at best it exhibited a slight decrease in polarization. However, the net result was a decrease in power output.

Postoperative examination of this cell showed that the sintered silver cathodes had undergone additional sintering sometime during their operating life with an accompanying decrease in surface area. The electrode appeared to be completely closed and the particles actually melted in spots. Little or no porosity remained. It is possible that a relay on the furnace temperature controller stuck, causing overheating so that the electrode continued to sinter. Some additional sintering was also observed on the nickel anodes, but these electrodes retained most of their original porosity.

Figure 6 illustrates the power at 0.5 volt versus hours of operation for cell #47-140. This cell contained 120-mesh nickel screen primary anodes and 50-mesh nickel screen secondary anodes. The cathodes were silver-plated 120-mesh stainless steel screens. The plating was heavier than that used in cell #47-47.

From 100 to 500 hours of operation power output was at a level of 35 to 40 watts/ft^2. Then it started to decline, reaching 22 watts/ft^2 at 1100 hours. The cell was terminated voluntarily after 1117 hours of operation.

The least mean square results are presented in Fig. 7 and Table I for open circuit voltage and polarization at 50 ma/cm^2 for both anode and cathode as a function of hours of operation. The order of contribution to the decline in power output of this unit are open circuit voltage, cathode polarization, anode polarization. Anode polarization, however, was higher from the start than is usually observed. This is attributed to the use of the 50-mesh nickel screen secondary electrode.

Examination of the electrodes after termination showed that the primary anode was flooded with electrolyte and had undergone appreciable oxidation. This oxidation is considered the cause for the decreased open circuit voltage, but is difficult to say which process occurred first. Previous experience with nickel anodes, however, has shown that nickel tends not to wet easily while nickel oxide does. The accompanying loss of active (for the fuel cell reaction) area may also account for the increase in anode polarization.

Several times during the operating life of this cell a small fire was observed on one of the cathodes. This fire was the result of fuel reaching the cathode. Although the fire did not cause the cell to fail, it did remove the silver plating in its vicinity. The redistribution of silver resulted in a loss of active cathode surface area, which could easily account for the increase in cathode polarization. Postoperative examination of these electrodes confirmed the silver redistribution. In many places the stainless steel screen was exposed to the electrolyte.

Silver migration on the electrodes and solubility in the electrolyte can be serious problems in any molten carbonate fuel cell. Migration can be retarded by preventing thermal and concentration gradients along the electrode. These gradients can be minimized by good heat management and gas distribution. The solubility aspects are a little more complicated. First, more silver must be present initially on the electrode than the amount required for good cathodes. Second, and more important, the solubility of silver can lead to dendrite formation, which can cause an electronic short and subsequent failure of the cell. In this respect the slurry-electrolyte system has an advantage over the other fixed matrix systems.[3,4] Fixed matrix cells provide a mechanical support for the silver dendrites through the electrolyte. The slurry system provides little, if any, mechanical support for such dendrites; consequently, it has considerably less tendency to form shorts. Reliability testing of more than 200 cells containing slurried electrolyte revealed no failures because of any type of electronic shorting. This was not the case in previous experience with fixed matrix cells.

Cell #33-1 was very similar to #47-140, but both secondary and primary anodes were constructed of 120-mesh nickel screen. Figure 8 presents the power output at 0.5 volt and the anode and cathode polarization as a function of hours of operation. The open circuit voltage was constant during this period of operation. All data points for the power output are shown. The least mean square line exhibits an increase in power output with time; however, this slope is not significant (see Table I). The cell operated at an average power density of 36-37 watts/ft^2. It should be noted that both anode and cathode polarization decreased with time and that these slopes are significant (see Table I). However, when their variations are added to the other cell variables, no significant slope for power output is obtained.

At 582 hours of operation additional electrolyte was added to the reservoir cup. The power declined in 3 hours from 42.5 watts/ft^2 to 34.5 watts/ft^2. At 602 and 625 hours of operation it had declined further to 31.0 and 29.8 watts/ft^2. At the same time the polarization at 75 ma/cm^2 for the cathode started to decrease, while that of the anode increased. These observations may be explained on the basis that the additional electrolyte increased the wetting at both electrodes. In the case of the cathode the original wetting was less than optimum, while at the anode it was more than optimum.

This cell was allowed to operate for a total of 2000 hours before it was voluntarily terminated. Power output remained above 24 watts/ft^2 for the entire 2000 hours.

These data all point to the composition and structure of the cathode as the weakest point in the present cell structure and system. Current exploratory work is aimed at appreciably reducing or overcoming this limitation. Figure 9 represents a step toward increased power performance. At 0.60 volt this cell was producing 60 watts/ft^2. At maximum power its output approached 70 watts/ft^2. The total anode polarization was 110 millivolts at 100 amps/ft^2, while the cathode polarization was 260 millivolts at the same current density. Even in this cell the cathode presents the greater problem and the more promising area for future research.

Research on new electrodes is continuing. The slurry-electrolyte cell design and construction is relatively new, and at this writing the investigations are still on the lower portion of the learning curve. In little over eight months, progress has been made from a sustained steady performance of 15 to 20 watts/ft^2 to 35 to 40 watts/ft^2. It is difficult to project what the power output of similar cells will be in the future.

Multicell Unit

A view of a 3 x 2 unit is shown in Fig. 10. This unit consists of 6 cells. Essentially, it is three 1 x 2 units connected electrically in series. These units and some similar 2 x 2 units have been operated on a mixture of H_2, CO_2, and N_2 which simulates partial oxidation of JP-4.[9,10] The CO_2 supply for the cathode is obtained by combusting the fuel gas effluent from the anodes in the furnace chamber. These units have had intermittent power output in the 40 to 60 watts/ft^2 range for short time intervals (6 to 24 hours), and 20 to 40 watts/ft^2 for hundreds of hours of operation. The cathodes employed in these units resemble those used in cell #47-47.

Figure 11 is a view of a 6 x 6 unit consisting of three parallel combinations of two 3 x 2 units in series.[9] This unit contains one square foot each of anode and cathode. Power output has been as high as 33 watts at 3.0 volt and has remained between 25 and 30 watts for longer than 500 hours of operation.

Conclusion

Fuel cells employing a magnesia alkali carbonate slurry as the electrolyte have been successfully operated for extended time intervals. Continuous operation for more than 2000 hours has been achieved. Power output in small units operating on a simulated natural gas reformate fuel has been maintained at 35 to 40 watts/ft^2 for longer than 1000 hours. Multicell units have been operated on a simulated fuel representative of partial oxidation of JP-4 at nearly the same level.

New electrode compositions and structures in the initial research stage at this time are yielding power densities equivalent to 60 to 70 watts/ft^2.

There appears to be no fundamental reason why slurried molten carbonate fuel cell systems should not achieve significantly higher power densities and longer operating periods than those reported here.

Acknowledgements

The author acknowledges the work of J. K. Truitt and T. N. Hooper, who are responsible for the design concept of the slurried electrolyte cell system, the 3 x 2 and 6 x 6 units, and for permission to use photographs of these units. The author is also indebted to J. F. Haefling for assistance on the metallurgical portion and Roy Deviney who assisted in the experimental portion of this work.

References

1. Trachtenberg, I., J. Electrochem. Soc. 111, 110 (1964).

2. Truitt, J. K., Peattie, C. G. and Frysinger, G., "Proceedings of the 18th Annual Power Sources Conference," Power Sources Conference Publication Committee, 1964, p. 14.

3. Trachtenberg, I., in Advances in Chemistry Series #47, Fuel Cell Systems (American Chemical Society, Washington, D. C., 1965), p. 232.

4. Broers, G. H. J., Schenke, M. and Piepers, G. G., Advanced Energy Conversion 4, 131, 1964.

5. Baker, B. S., Marianowski, L. G., Meek, John and Linden, H. R. in Advances in Chemistry Series #47, Fuel Cell Systems (American Chemical Society, Washington, D. C., 1965), p. 247.

6. Broers, G. H. J. and Schenke, M., in Fuel Cells, Vol. 2, G. J. Young Ed. (Reinhold Publishing Corp., New York, 1963), p. 6.

7. Hart, A. B., and Powell, J. H., in "Batteries Research and Development in Non-Mechanical Power Sources," D. H. Collins, Ed. (The MacMillan Co., New York, 1963), p. 265.

8. Trachtenberg, I. and Haefling, J. F., unpublished results.

9. Truitt, J. K., Proceedings of the 19th Annual Power Sources Conference, 1965, in press.

10. Texas Instruments Incorporated, Final Technical Report for Contract No. DA-44-009-AMC-54(T). Prepared for U. S. Army Engineer Research and Development Laboratories, Fort Belvoir, Virginia, 12 March 1965.

TABLE I

Computer Results

Least Mean Square Fit of Data Presented in Figures 3-8

Unit Number Dependent Variable*	Slope watts/ft^2/1000 hrs or volts/1000 hrs	Intercept watts/ft^2 or volts	Std. Error of Slope watts/ft^2/1000 hrs or volts/1000 hrs	Std. Error of Observation watts/ft^2 or volts
#47-47				
Power 0.7 v	-0.7	17.2	1.0	1.1
Power 0.5 v	1.5	25.8	1.5	1.7
#47-53				
Power 0.5v	-34.6	52	3.7	3.0
Open circuit voltage	-0.03	0.92	0.01	0.009
Anode-polarization 75 ma/cm^2	0.12	0.15	0.03	0.02
Cathode-polarization 75 ma/cm^2	0.22	0.05	0.09	0.07
#47-140				
Power 0.5v	-19.6	44	2.9	3.0
Open circuit voltage	-0.09	1.01	0.02	0.02
Anode-polarization 50 ma/cm^2	0.06	0.16	0.02	0.02
Cathode-polarization 50 ma/cm^2	0.07	0.13	0.01_5	0.01_5
#33-1				
Power 0.5v	1.0	36	3.1	4.8
Anode-polarization 75 ma/cm^2	-0.04	0.17	0.02	0.03
Cathode-polarization 75 ma/cm^2	-0.05	0.30	0.04	0.05

*Hours of operation is the independent variable.

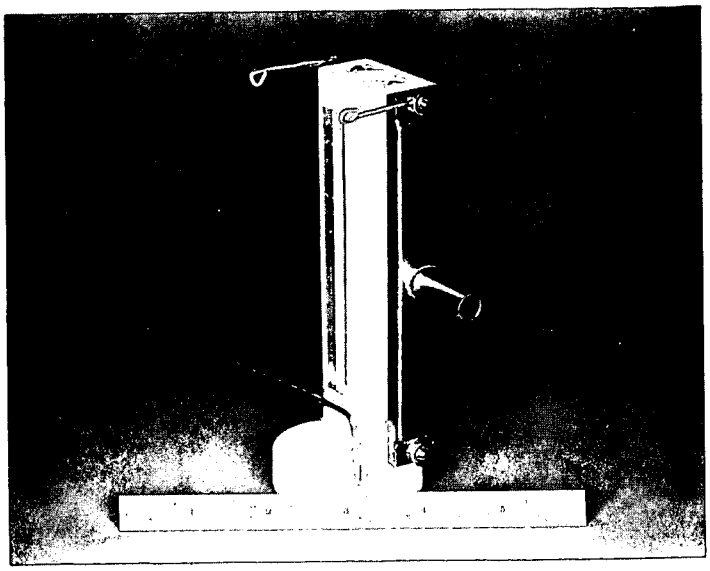

Fig. 1.-VIEW OF 1 x 2 UNIT SHOWING ONE WORKING CATHODE, THE IDLING ELECTRODE, AND THE ELECTROLYTE RESERVOIR.

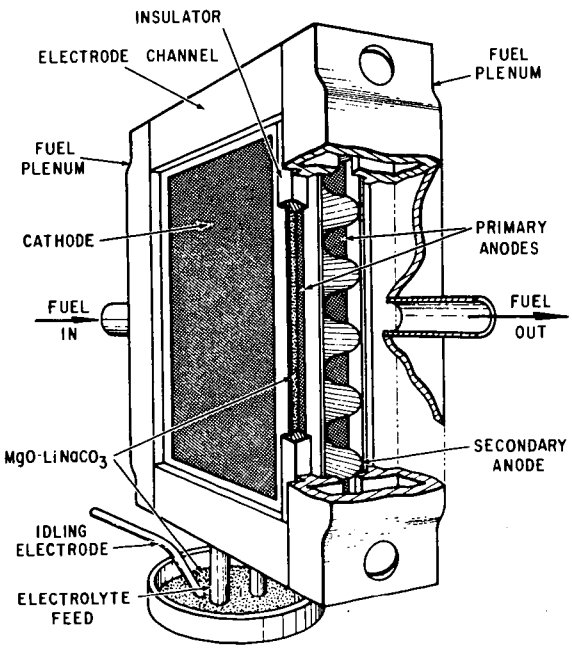

Fig. 2.-A CUT AWAY PERSPECTIVE OF A 1 x 2 UNIT.

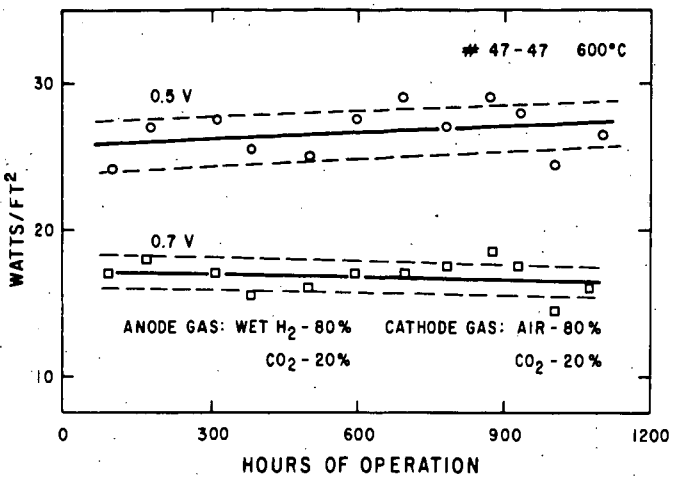

Fig. 3.-POWER OUTPUT AT CELL TERMINAL VOLTAGES (IR INCLUDED) OF 0.5 v. and 0.7 v. IS PLOTTED AS A FUNCTION OF HOURS OF OPERATION. SOLID LINES ARE THE BEST LEAST MEAN SQUARE FITS. DASHED LINES INDICATE THE STANDARD ERROR OF THE OBSERVATIONS FROM THE LINES.

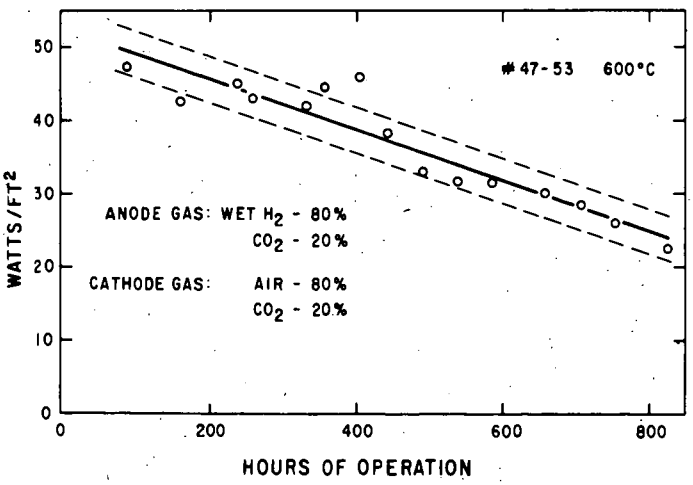

Fig. 4.-POWER OUTPUT AT A CELL TERMINAL VOLTAGE (IR INCLUDED) OF 0.5 v. IS PLOTTED AS A FUNCTION OF HOURS OF OPERATION. SOLID LINE IS THE BEST LEAST MEAN SQUARE FIT. DASHED LINES INDICATE THE STANDARD ERROR OF THE OBSERVATIONS FROM THE LINE.

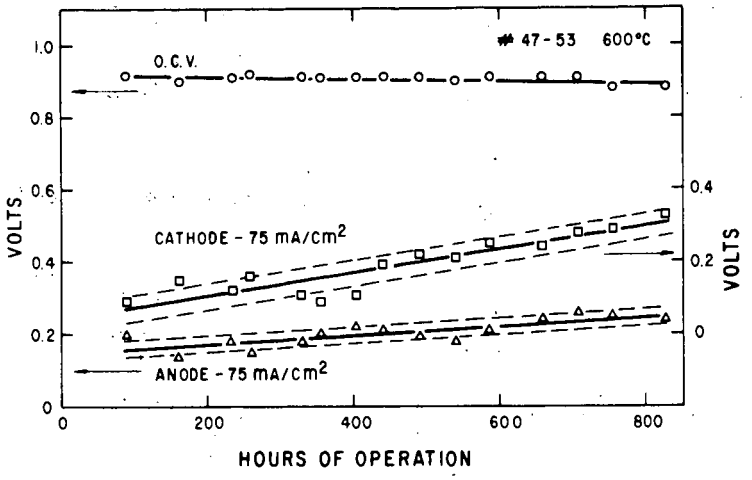

Fig. 5.-TOTAL CATHODE AND ANODE POLARIZATION INCLUDING IR AT 75 MA/CM^2 AND THE CELL OPEN CIRCUIT VOLTAGE ARE PLOTTED AS A FUNCTION OF HOURS OF OPERATION. SOLID LINES ARE THE BEST LEAST MEAN SQUARE FIT. DASHED LINES INDICATE THE STANDARD ERROR OF THE OBSERVATIONS FROM THE LINES.

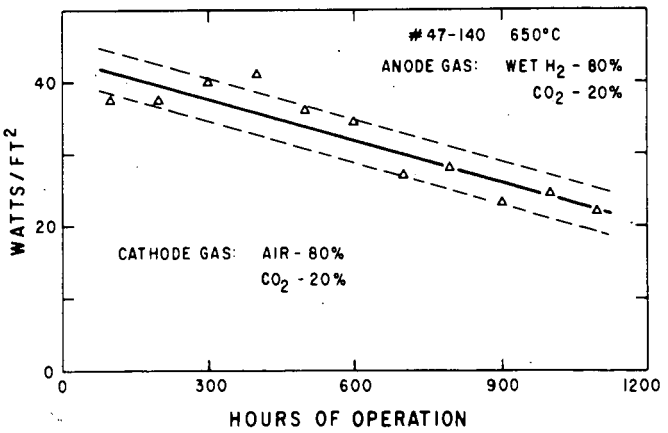

Fig. 6.-POWER OUTPUT AT A CELL TERMINAL VOLTAGE (IR INCLUDED) OF 0.5 v. IS PLOTTED AS A FUNCTION OF HOURS OF OPERATION. SOLID LINE IS THE BEST LEAST MEAN SQUARE FIT. DASHED LINES INDICATE THE STANDARD ERROR OF THE OBSERVATIONS FROM THE LINE.

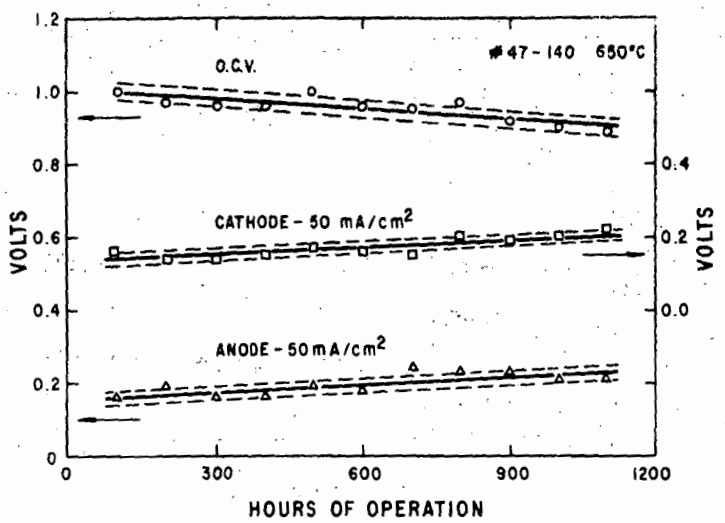

Fig. 7.-TOTAL CATHODE AND ANODE POLARIZATION INCLUDING IR AT 50 MA/CM² AND CELL OPEN CIRCUIT VOLTAGE ARE PLOTTED AS A FUNCTION OF HOURS OF OPERATION. SOLID LINES ARE THE BEST LEAST MEAN SQUARE FIT. DASHED LINES INDICATE THE STANDARD ERROR OF THE OBSERVATIONS FROM THE LINES.

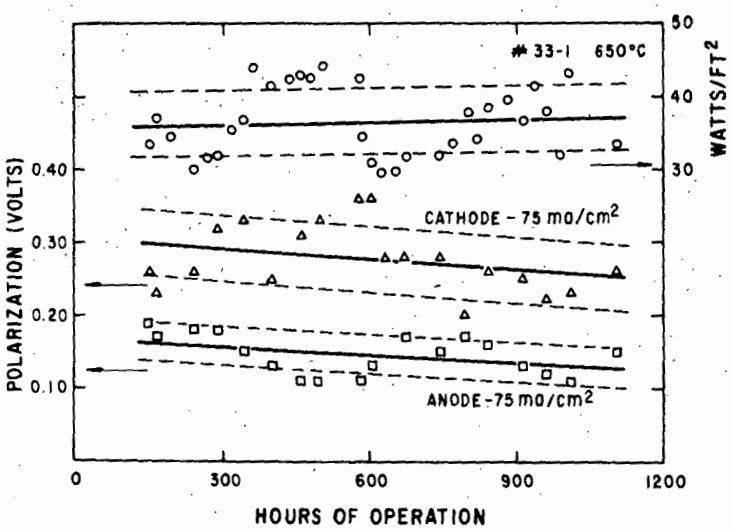

Fig. 8.-POWER OUTPUT AT A CELL TERMINAL VOLTAGE (IR INCLUDED) OF 0.5 v. AND TOTAL ANODE AND CATHODE POLARIZATION AT 75 MA/CM² ARE PLOTTED AS A FUNCTION OF HOURS OF OPERATION. SOLID LINES INDICATE THE STANDARD ERROR OF THE OBSERVATIONS FROM THE LINES.

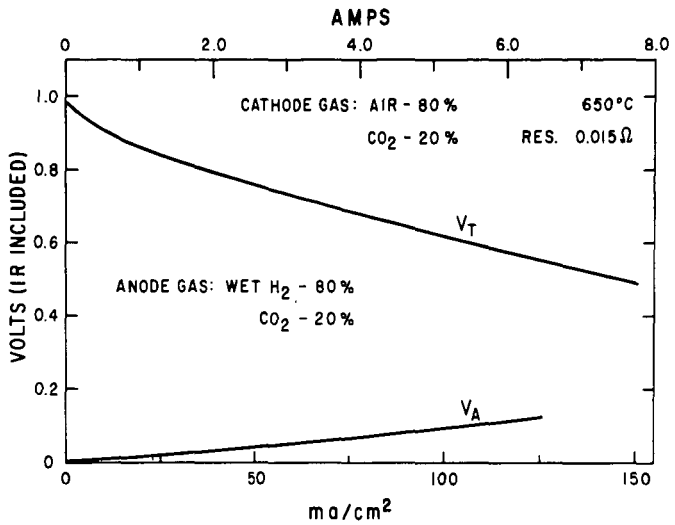

Fig. 9.-V_T IS THE CURRENT-VOLTAGE CURVE WITH IR INCLUDED. POWER OUTPUT IS 60 WATTS/FT^2 AT 0.6 v. CELL TERMINAL VOLTAGE. CURVE V_A INDICATES TOTAL ANODE POLARIZATION. AT 100 MA/CM^2 TOTAL ANODE POLARIZATION WITH IR IS 110 MILLIVOLTS.

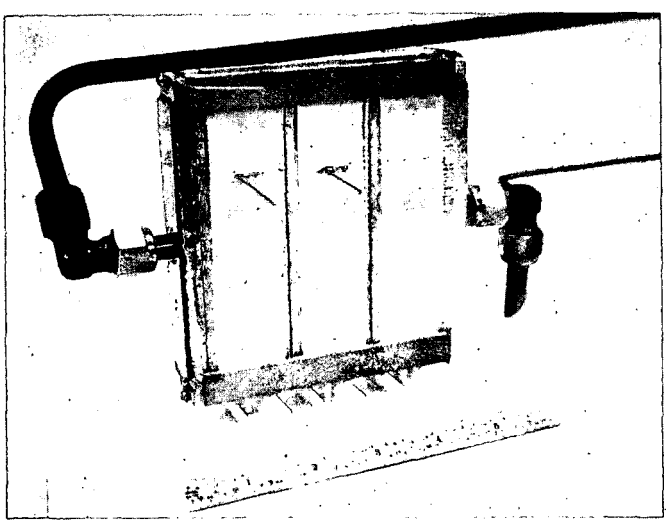

Fig. 10.-VIEW OF A 3 x 2 UNIT SHOWING HALF OF THE WORKING CATHODES.

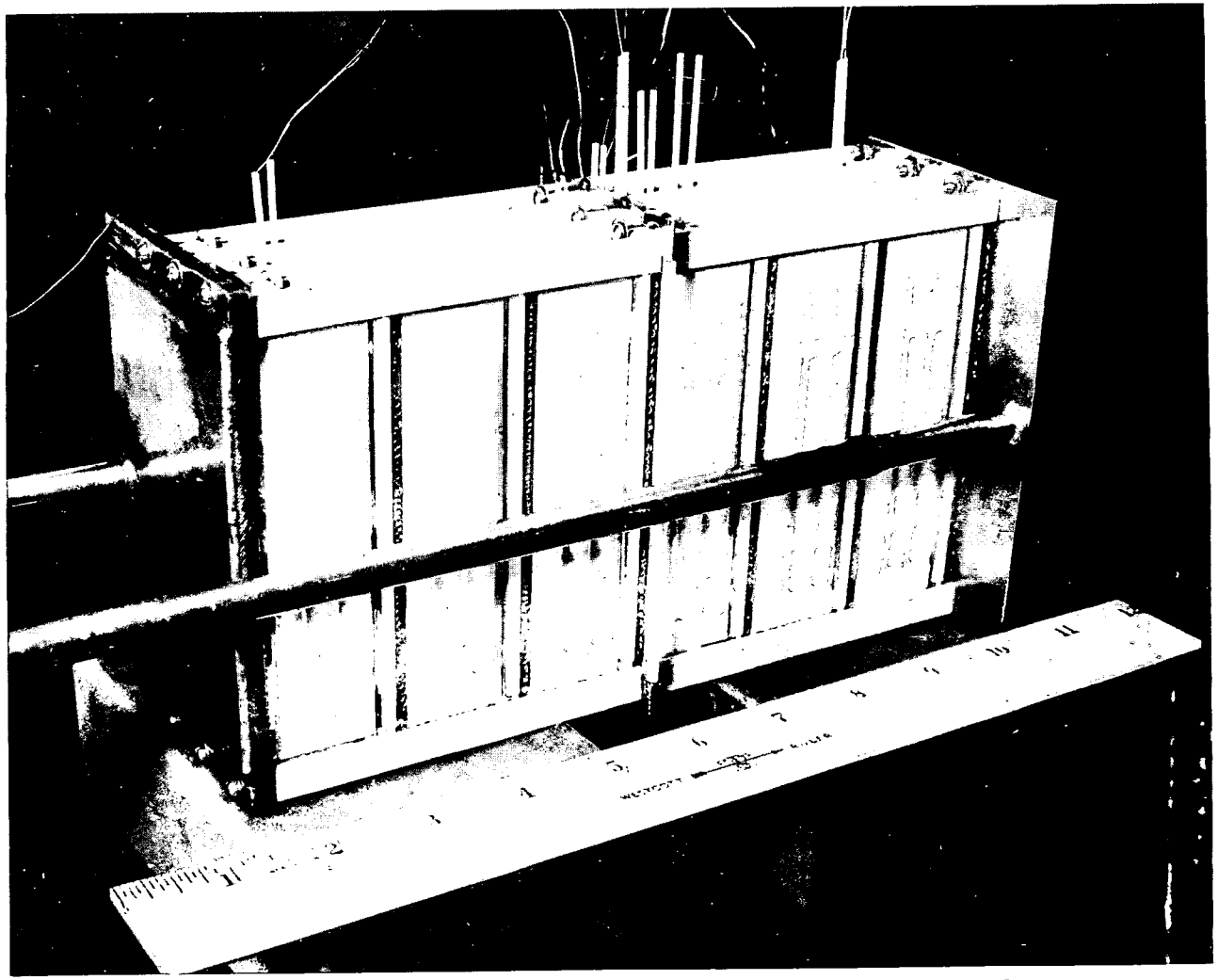

Fig. 11.-VIEW OF A 6 x 6 UNIT WITH THERMOCOUPLES ATTACHED TO SEVERAL OF THE WORKING ELECTRODES.

The Semi-Industrial Fuel Cell Element of the Gaz de France

A. Salvadori
Experimental and Research
Center No. 1 of the D.E.T.N. of
Gaz de France

INTRODUCTION

The studies undertaken by the laboratories of Gaz de France in the field of energy conversion have been carried out for almost four years in order to transform directly into electrical energy in a fuel cell the free energy of gases currently manufactured or distributed by this national service.

Massive quantities, relatively low prices and ease of transport of these raw materials encourage research towards perfecting industrial devices that would be simple, rugged, and inexpensive, but capable of yielding significant power. Relatively inert fuels are the usable gases: both natural gas either unreacted or catalytically steam reformed, and gas obtained by partial oxidation of gas and liquid hydrocarbons, nevertheless contain, although in small quantity, some impurities which seem to prohibit, to our knowledge, the use of sufficiently active, but sensitive catalysts which would allow functioning at moderate temperatures and in an aqueous environment. Under these conditions, it becomes necessary to counterbalance the catalytic effect by an increase in temperature and hence to operate in the presence of electrolytes made of molten salts. It seems better to make the best use of the notable advantages offered by the high temperatures providing the condition that the technological difficulties and the resulting corrosion problems can be solved.

The unavoidable heat release, provoked by any type of functioning cell, is all the more interesting to recover when the temperature of the system is high and when the dimensions of the battery are significant. The fuel cell then becomes a means of base production of electrical current which is located upstream in a complex. The other devices of this complex can use the thermal energy released by the cell.

1. PRINCIPLES OF OPERATION FOR AN INDUSTRIAL GENERATOR

Keeping these considerations in mind, the operating principle of an industrial generator can be defined in a general sense and thus serve as a constant objective towards which all investigations must be oriented.

The potential at the terminals of an elementary cell are low. For an installation to be of industrial interest it is necessary to group, in a unit well adapted to isothermal operation, the greatest possible number of elements. However, as these warm

each other, they must be spaced in the most judicious way so that the regulating fluid ensures as homogeneous a temperature as possible in all parts of the enclosure; for obvious reasons air used as an oxidant can be used for this role.

Two simple geometric forms may be considered a priori for the basic cells: the plane and the cylinder. We have deliberately set our choice on the latter for the following reasons: the thermal regulation of an assembly of bundles of the exchanger type is industrially well known; the practical construction of flat and thin electrodes of large area presents more difficulties than that of tubes; the high temperature construction in the shape of a filter press creates important sealing problems and prevents any possibility of replacing an element without a complete stop in the functioning of the battery; the phenomena of diffusion or creepage of the electrolyte at the joints or in any nonactive part of the cell may be easily eliminated in tubes by cooling of the involved extremity, at a temperature slightly below that of the melting point of the fused salts; the reacting gas supply is greatly simplified where all the cells have an electrode of the same sign in a unique enclosure containing the corresponding gas; the mechanical strength of a tube made by successive layers of the anode, of the electrolyte and of the cathode, is better than that of a plane surface made under identical conditions.

The construction of a cylindrical cell battery is advantageously made through a horizontal disposition of the elements inside a heated parallelepiped shaped container of which two opposite sides form supports and to which are fixed the ends of the cells bearing the different gas distribution systems and the current collectors. In order to determine orders of magnitude, the thickness of such an installation would be close to one meter, and its length and height would be a few meters. An unlimited number of cells may be used by placing them side by side separated by a passage large enough to conduct electric current of substantial size.

Figure 1 shows the sketch of an industrial unit which would function according to the above mentioned operating principles.

2. DESCRIPTION OF THE SINGLE CELL

The conception of an element must satisfy the technological constraints which have been enumerated and give an answer to the economic problems that the development of a new technology can create.

2.1 Choice of Materials

The materials with which the electrodes are made are generally expensive and rare, and it is necessary to use them in a small quantity and to build them by simple methods relying on industrial techniques that assure reproducible fabrication of several tens of thousand units. The three phase contact problem, gaseous (the reacting fluids), liquid (the electrolyte) and solid (the electrodes), has in the beginning of our work brought us to follow the method used very generally at the time, which consists of using porous metals and looking for their best operating conditions. Because, on the one hand, of the disadvantages that we have observed

in the utilization of a relatively thick layer, the accumulation in the pores either of products of combustion or nitrogen from the air, and on the other hand of the knowledge of the good diffusion at high temperature of gases through certain metals, we tried the use of these metals in thin compact sheets.

The diffusion of hydrogen through palladium and platinum is a phenomenon which has been known for a long time; further the systematic studies that we have made in this field have shown that the oxidant made of air to which carbon dioxide has been added passes sufficiently rapidly through thin silver sheets to give results at least as good as with the porous substances.

2.1$_1$ The Anode

In spite of above mentioned advantages, the utilization of palladium in a sheet cannot be considered for economical reasons, because it prohibits the use of any other fuel gas than hydrogen. For these reasons, the anode in our cells is always a graphite cylinder very lightly covered on the surface with palladium (close to 0.1 mg/cm^2).

Graphite has numerous advantages: good electronic conductance, very low expansion coefficient, relatively good mechanical strength and easy construction. Furthermore, in the reducing environment in which it is situated, it has never shown signs of deterioration.

2.1$_2$ The Cathode

Silver constitutes at the present state of our knowledge, the only metal usable as a cathode. But used as is and without preliminary precaution, in the presence of molten carbonates, it is subject to permanent corrosion. A systematic study has brought to light three principal aspects of the silver corrosion that can be summarized in the following manner; one of machanical nature due to a degradation of the structure and which favors grain formation; another of a chemical nature which can be defined by a limited dissolution in the electrolyte; finally the third of an electrochemical nature making some silver precipitates appear in the electrolyte, which, because of convection currents and variable potential lines in the functioning cells, can settle at different points between the two electrodes.

However, our observations on the inhibiting role of combining with refractory oxides either in the electrolyte bath or in the cathode itself, have lead us to use a film of these oxides in order to materialize the idea of protecting the silver surface.

The film itself is made in a thin layer (0.1 mm) by flame spraying and offers all the qualities of a sheet.

2.1$_3$ The Electrolyte

Only electrolytes made of molten salts are usable. Among the different possible solutions, carbonates in a mixture judiciously chosen in relation to the temperature have been employed for CO_2 as one of the reaction products and its presence is favorable in particular to their thermal stability.

2.2 Employment of Materials

To satisfy the conditions preceedingly developed: compactness, facility of assembling, good mechanical resistance, small quantities of materials, easy industrial operation, we have studied in the most comprehensive way the best method of construction based on the following principles:

2.2_1 The Active Substance of the Cell (Fig. 2)

On the anode graphite finger palladium is deposited. A layer of refractory oxide, preferably of magnesia or stabilized alumina is deposited on the anode by flame spraying. This very thin layer, just thick enough to assure a good electric insulation contains the carbonates and thus serves as a support for the electrolyte. A silver-based thin film (0.1 to 0.2 mm) which constitutes the cathode is then deposited on the assembly. This metallic film is too thin to insure by itself a sufficient means for current removal and this is achieved by a silver wire fixed along the electrode which can be joined in a battery, to a central conductor.

2.2_2 The Top of the Cell (Figure 3)

The open extremity of the graphite finger is fixed in a brass piece which contains: an axial nozzle that penetrates to the bottom of the anode, its role is to feed fuel to the cell and to collect the anodic current; a radial nozzle through which the excess fuel that has not reacted carries away the products of the reaction water vapor and carbon dioxide.

This part of the cell, is connected to the wall of the exterior enclosure and is maintained at a lower temperature than that of the melting point of carbonates; they solidify and the creepage phenomena that would provoke their disappearance is prevented.

3. CONSTRUCTION OF A LABORATORY BATTERY USING SEMI-INDUSTRIAL ELEMENTS

The experimentation with single cells of various dimensions and method of construction proceeds in different directions with two goals; first to increase electrical performances, and second to prolong their life.

The present conception of the cells would allow a unit of dimensions which are already substantial and the battery that we have made could easily be built on a larger scale. But current densities of the order of 40 mA/cm^2 at 600 mV, and limited longevities, do not permit such an extrapolation.

However, the necessity to come out with a development of gas cells as quickly as possible has lead us to deal with problems created by the grouping of several elements. The latter are many and the following enumeration mentions only the principal ones:

1. Regulation of the unit temperature

2. Effective collection of the current

3. Evacuation and recuperation of the reaction products.

4. Controlled feeding of oxidant and fuel

5. Current Efficiency

6. Starting and stopping of the batteries

7. Analysis of results and evaluation of true efficiency

Accordingly the study and construction of a unit of large laboratory proportions already using some elements at the semi-industrial scale, has been undertaken in parallel with research on single cells.

3.1 Description of the Installation

3.1_1 Choice of the Number of Elements

In order to correspond to the hexagonal disposition generally adopted for the bundles of tubes, we have chosen 7 elements of which one is centrally located. It is necessary to place them in an oven that will insure their heating at the start and to compensate for heat losses while in operation.

3.1_2 The Oven (Figures 4 and 5)

It permits heating to 1000°C the volume containing the seven elements and can be placed under an oxidant pressure of a few tenths of a bar. It contains three superposed resistances, the wiring and regulation of which are independent, the lid of the oven is fixed and supports the tubular cells; the oven can be lowered to give access to the electrodes. The lower part can also be taken apart and easily repaired in the case of electrolyte leakage; it is provided, with devices that secure the positioning and support of the cathodes. This oven is also provided with auxiliaries that include:

1. An elevator assembly made of a platform capable of moving vertically which supports the oven.

2. A lifting crane for the block of cells.

3. The regulation of the independent electrical connections to the three heat zones.

3.1_3 Auxiliaries Insuring the Functioning of the Battery

First let us mention the inlet and outlet circuits of the reactants which present a certain complexity since they must insure constant flows, pressures and mixtures (case of the carbonated oxidant). Furthermore, the products of the reaction are collected and accounted for.

The problem resulting from the utilization of a current produced at several tens of amperes under some hundreds of millivolts has been solved through the use of a rotating device.

The oven is surrounded by a platform of dimensions large

enough to allow the technicians to work directly on the tops of the cells: all the controlling and measuring instruments are grouped at this level.

Figure 6 shows a general view of the system, it shows:

1. In the foreground the platform.
2. At the left, the oven.
3. At the right the instruments for measuring, controlling and fuel supply assembled on the same board.

3.1$_4$ Measuring Instruments

The gas reactants are supplied via classical laboratory flow meters, the water produced is retained by collectors followed by weighings: the carbon dioxide is sampled by a mass spectrometer (Fig. 7).

The overall electrical characteristics of the battery and those of each single cell are recorded continuously in order to obtain the most information from each experiment.

To account for results and to calculate the electrical and electrochemical performances of the installation, suitable meters are employed. Let us add that these measurements are completed by taking temperature at numerous points in the installation and inside each cell.

3.2 Experimental Results

The assembling of the complete installation has just been completed but its auxilliary apparatus for production of reformed gas that is intended for use with it, is not yet functioning. This installation has been in operation for too short a time to make it possible to publish definite results that ought to be further substantiated. As an example we shall give the results obtained during the first experiment with a set of 7 cells made under identical but not optimum industrial conditions.

3.2$_1$ Characteristics of a Single Cell

Total Length, mm	Diam., mm	Active Surface, cm^2	Weight, gm/cm^2			
			Cathode	Anode	Electrolyte	Refractory Oxide
800	18	220	0.130	graphite 0.55 palladium 0.002	0.048	0.170

3.2$_2$ Operating conditions

Oxidant air + CO_2 (30%); flow, 300 l/h under 150 m bars. The flow of air is relatively important due to the oversized dimensions of the oven. Fuel industrial hydrogen flow, 50 l/h under 130 m bars. In this experiment the hydrogen is not recycled after use. Temperature of operation: 600°C.

3.2$_3$ Principal results obtained

This experiment was particularly aimed at determining the efficiency of series and parallel assemblies and in both cases the current potential curves shown on Figures 8 and 9.

The performances obtained with these cells made under poor conditions and for a relatively low test temperature are modest: 20A at 0.5v, which corresponds to a maximum power of 10w.

The duration of the experiment which was limited to approximately ten hours cannot be taken into consideration.

This experiment has shown, however, that the whole installation can satisfy all the technological objectives that we had defined. Furthermore, it will be possible to have twenty cells operate within the same dimensions and the same connections and the usable surface of each one of the cells may be further increased.

4. CONCLUSIONS

The conception of an elementary cell of semi-industrial dimensions which we have reached could, from the technological point of view, lead in the future, without major difficulty, to the construction of a pilot unit. Numerous problems for assembling and handling of materials were solved. They permit the construction of a battery which offers the possibility of studying the behavior of cells fabricated under various conditions, following operating methods apt to be used in industry.

Important progress has been made to considerably reduce the causes of corrosion (some silver cathodes preserved through combination with a coat of refractory oxide have shown no detectable sign of corrosion after operating for a few hundred hours). It is now necessary to ensure an industrial application that we consider, the construction of cells whose lifetime exceeds a year.

The current densities of some tens MA/cm^2 that we obtained from single cells are insufficient to make a powerful generator operate under advantageous conditions and compete with standard methods of power generation. We do not believe that this problem is impossible to solve in a reasonable period of time because it is difficult to imagine performance of high temperature cells being inferior to those of cold cells.

On the other hand the lifetime of gas cells which depends in particular, on many phenomena of corrosion, on the modification and the change with time of the properties of materials at various temperature, will require important efforts if the research is to be brought to the proper value.

For this purpose, Gaz de France is working in collaboration with specialized laboratories at universities or in industry and particularly with the Compagnie Generale d' Electricité. Gaz de France has obtained a research contract as a result of action of the committee for conversion of energy which is part of the General Delegation for Technical and Scientific Research.

Figure 1

Industrial scale plant
Flow sheet

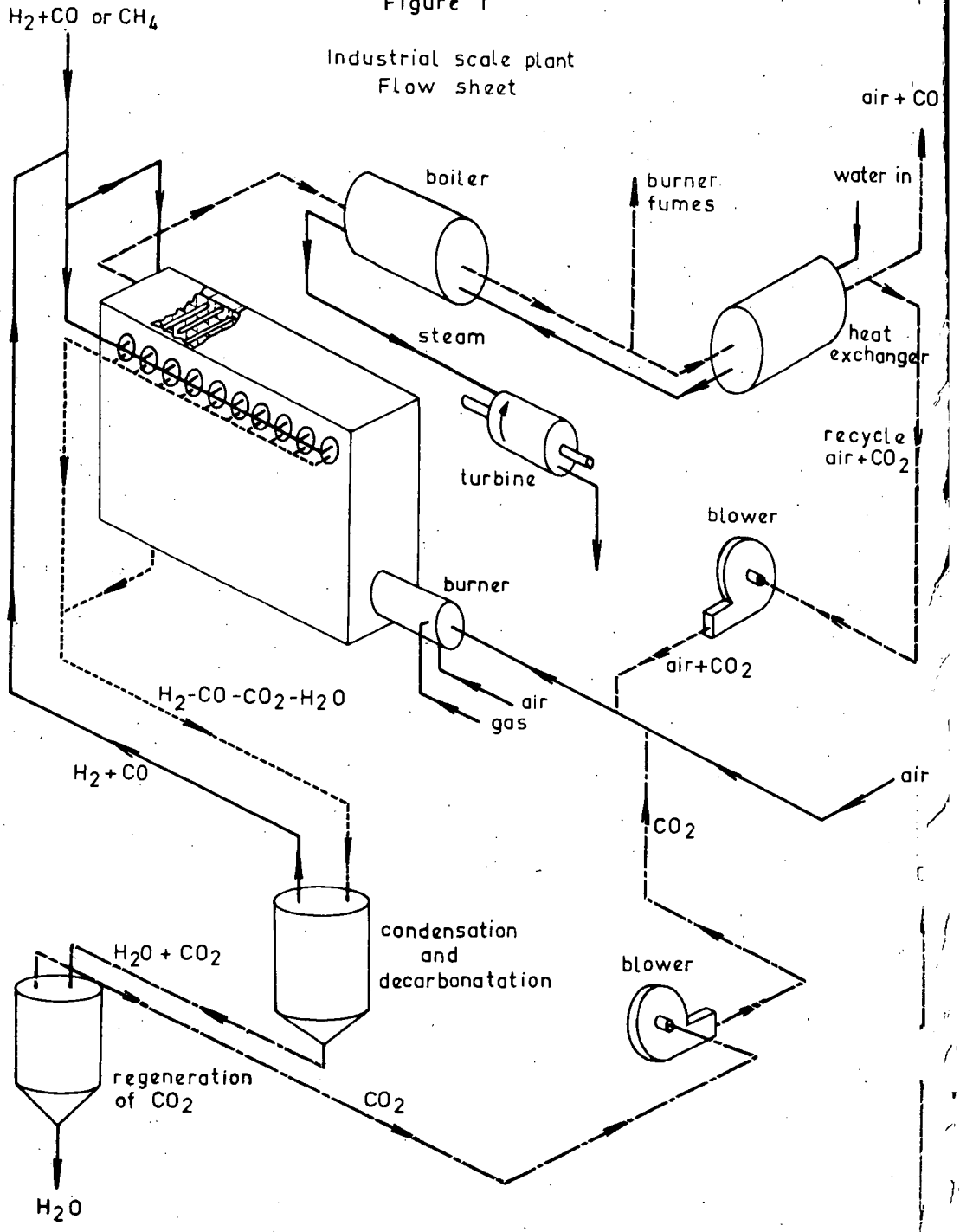

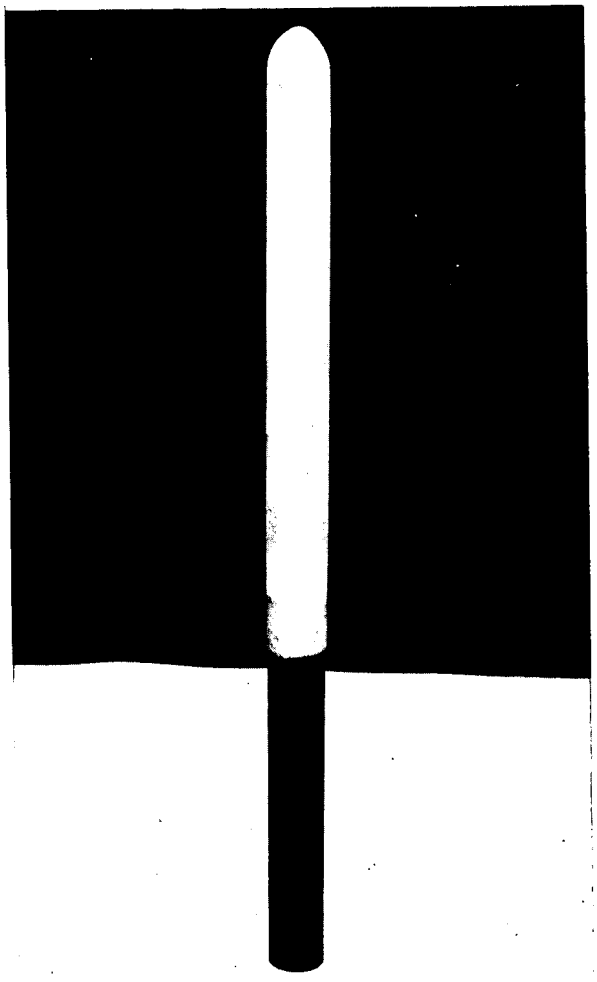

Figure 2: Main Section of a Single Cell

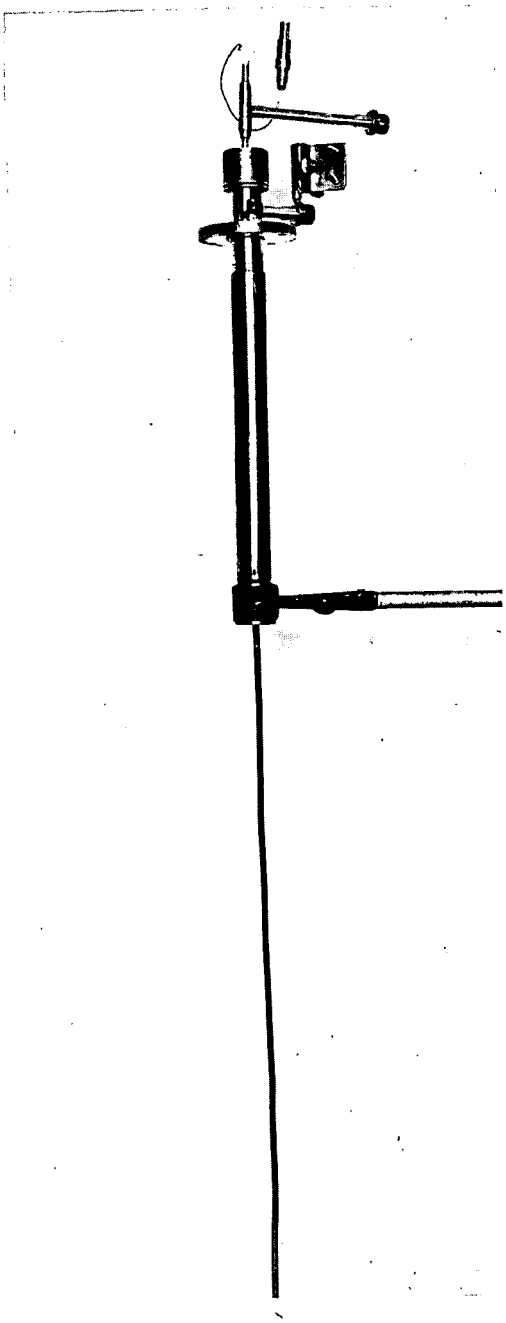

Figure 3: Top of a Single Cell

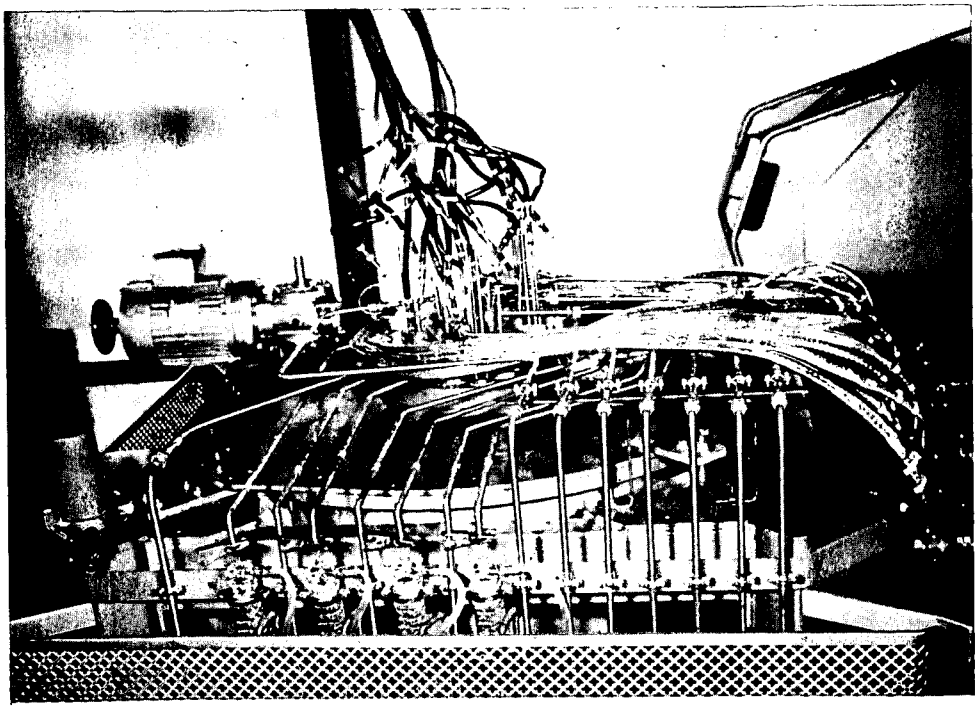

Figure 4: Seven-Element Battery, Top View

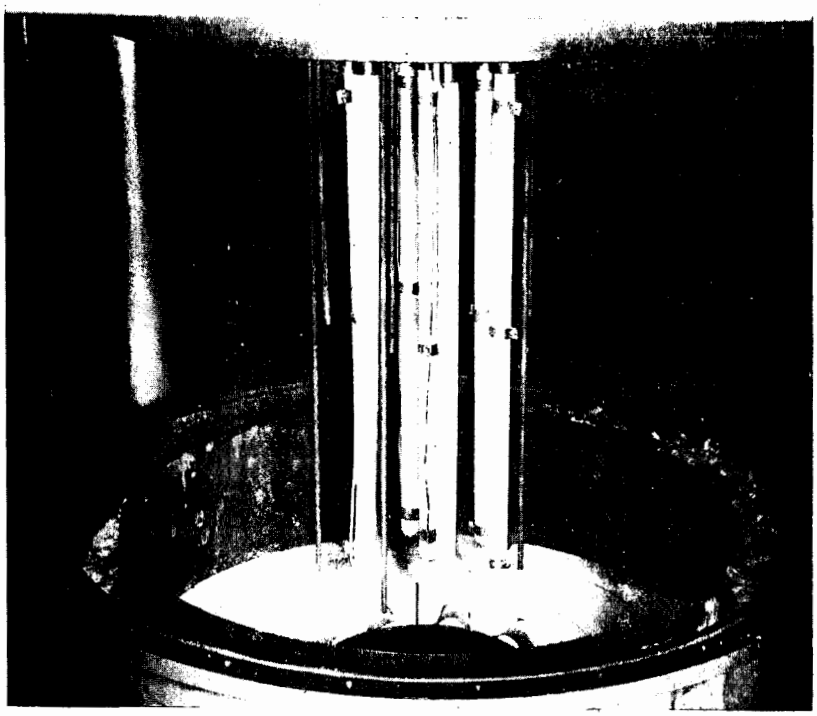

Figure 5: Seven-Element Battery, Bottom View

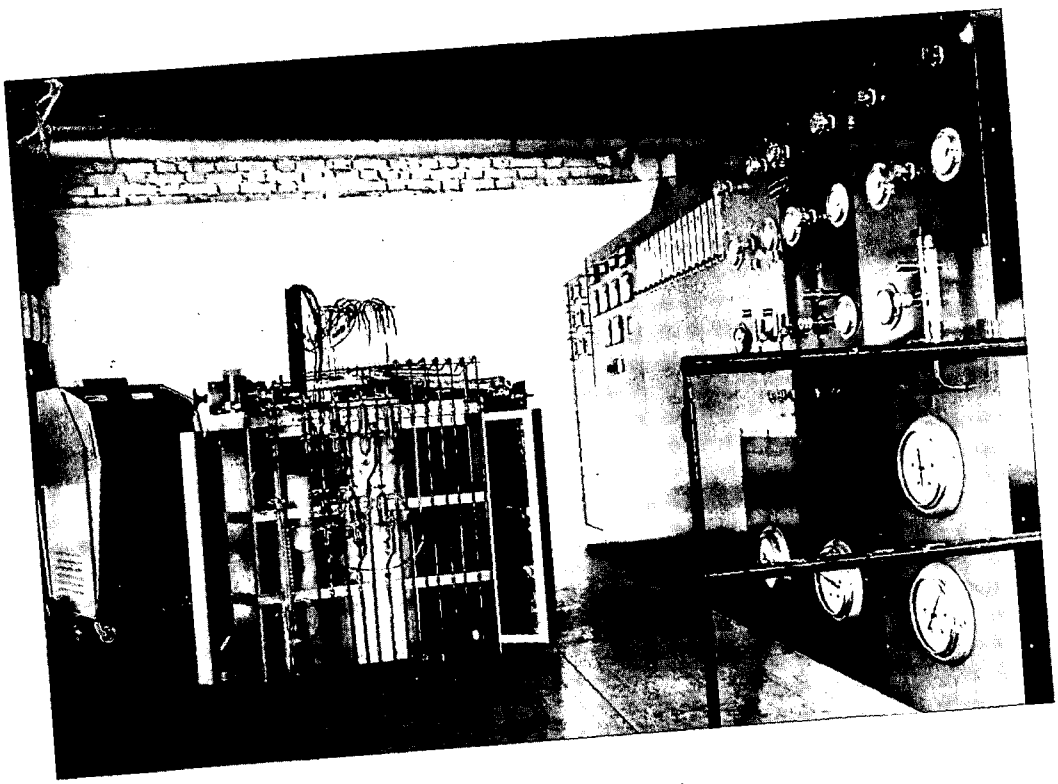

Figure 6: Total System

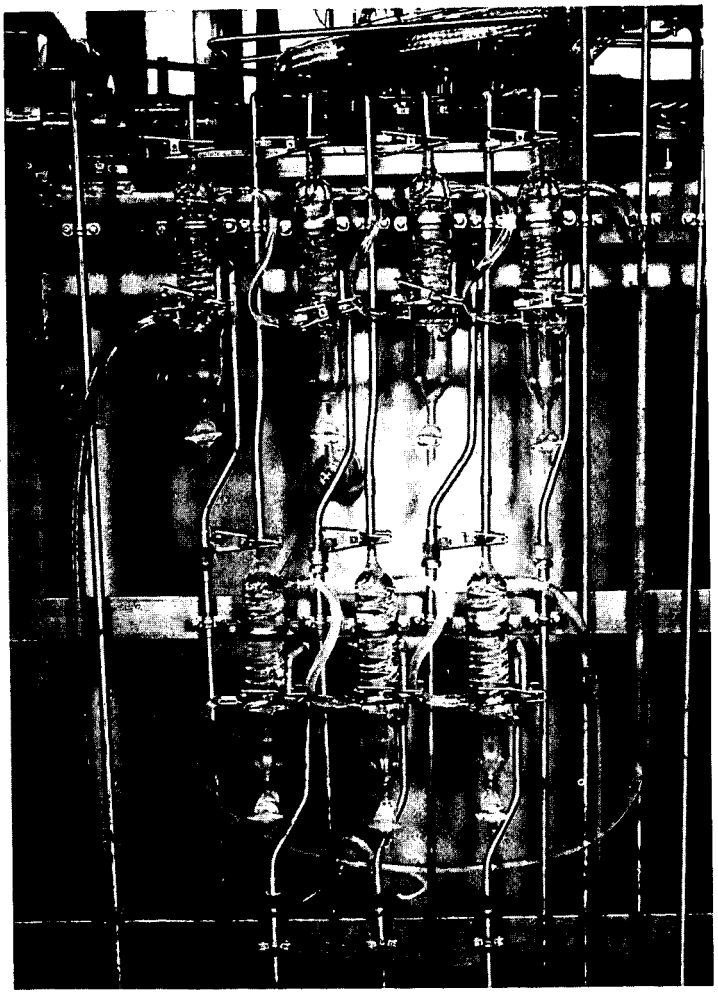

Figure 7: Recovery of the Reaction Products

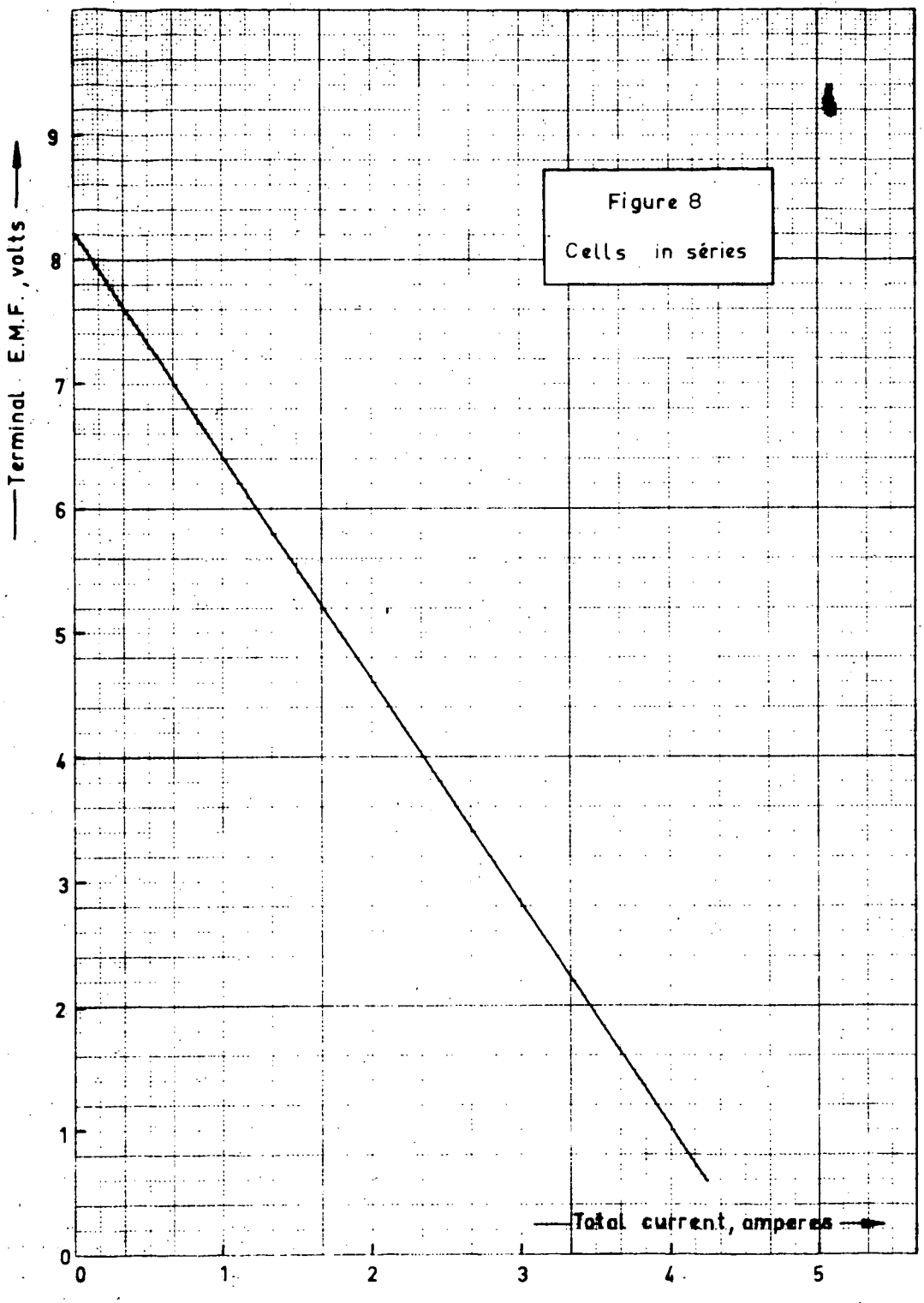
Figure 8
Cells in séries
Terminal E.M.F., volts
Total current, amperes
0
1
2
3
4
5
6
7
8
9

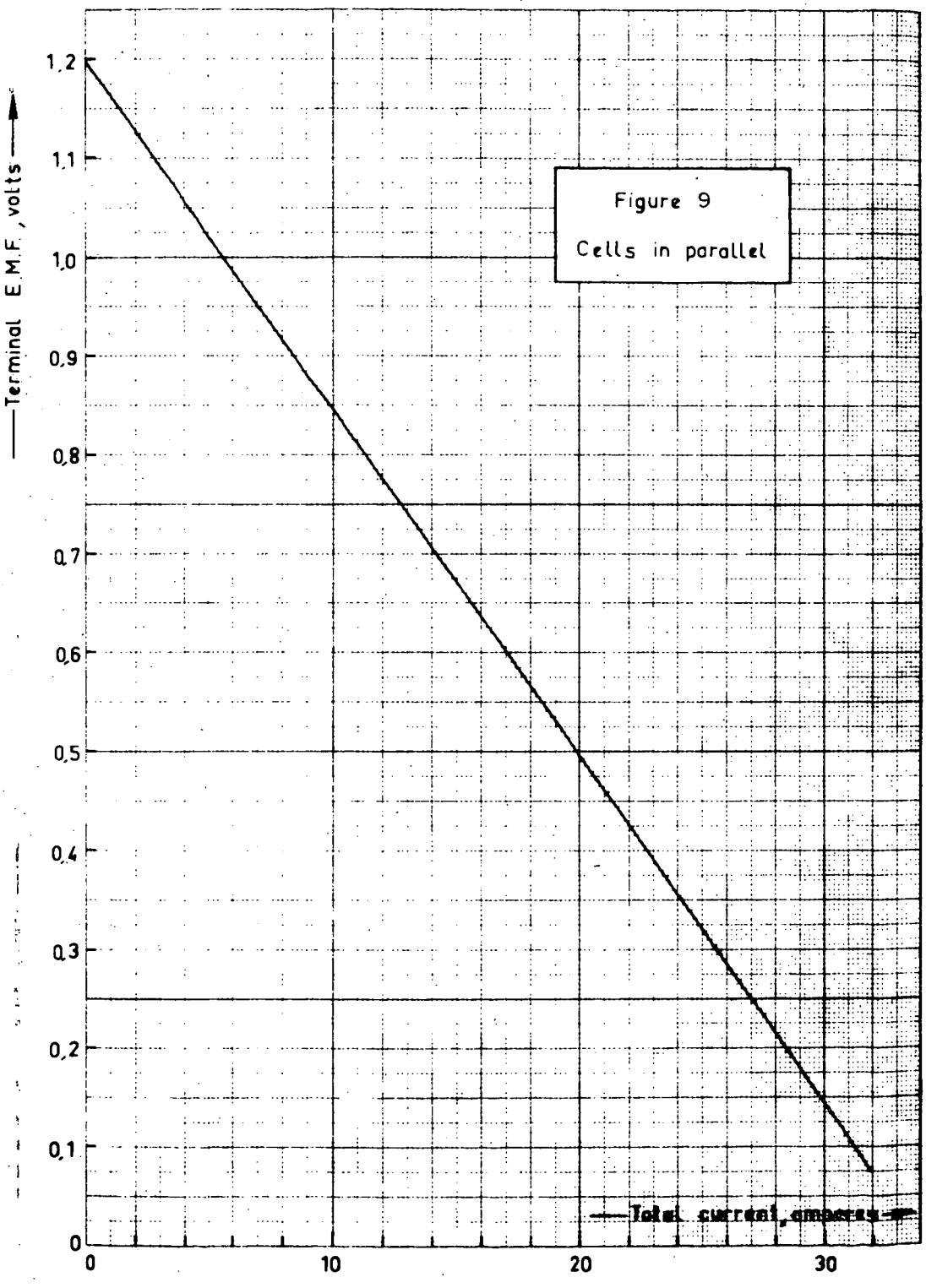
Figure 9
Cells in parallel
Terminal E.M.F., volts
Total current, amperes
1,2
1,1
1,0
0,9
0,8
0,7
0,6
0,5
0,4
0,3
0,2
0,1
0
0
10
20
30

ELECTRODE REACTIONS OF CO AND CO_2 IN MOLTEN CARBONATES

Alina Borucka
Cambridge University, Cambridge, England

ABSTRACT

Experiments have been made on the electrochemical reactions of CO/CO_2 gas mixtures at gold electrodes in molten ternary eutectic of lithium, sodium and potassium carbonates at temperatures up to 900°C. At zero applied current, the electrode potential depends on the partial pressures of CO and CO_2 according to the Nernst equation for the reaction: $CO + CO_3^{--2} \rightleftharpoons 2CO_2 + 2e^-$. Anodic current/potential relationships have been studied up to polarizations of 500 mV; similar measurements in the cathodic range have been made within the limits set by the Boudouard reaction.

MOLTEN CARBONATE FUEL CELL WITH WATER INJECTION

J. Millet R. Buvet

Direction Des Etudes Et Recherches
De L'Electricite de France

17 Avenue de la Liberation
Clamart, Seine, France

1. INTRODUCTION

Since the end of the 19th century, using the chemical oxidation energy of fossil fuels has been considered in order to produce electrical energy directly from fuel cells.

The fact that a cell is more easily supplied with a gas especially a carbon containing gas has lead engineers to be interested for a long time in molten carbonates as an electrolyte. The first works of Ostwald (1) then those of Baur (2) and his co-workers were concerned with cells using gases which contain hydrogen and carbon monoxide.

Davtyan (3) then Broers and Ketelaar (4) recommended a molten electrolyte fixed in a porous solid matrix. Gorin (5), Justi (6) and more recently many others such as Hart (7) and Salvadori (8) have also recommended the use of molten carbonates in fuel cells.

An important improvement has been brought forward these last few years, especially by Broers, in the performance of molten carbonate cells by adding carbon dioxide to oxygen feed.

2. USE OF AN ELECTROLYTE BUFFER

Several goals of our research group have been aimed at understanding the mechanism of exchange in the molten carbonates and the functioning of oxygen and hydrogen electrodes.

The carbonate solvent is entirely dissociated into the anion CO_3^{2-} and cations and the anion CO_3^{2-} is further dissociated according to the equilibrium:

$$CO_3^{2-} \rightleftharpoons CO_2 + O^{2-} \qquad [1]$$

The system CO_3^{2-}/CO_2 can thus be considered an acid-base system according to Lux (9) and Flood and Förland (10) with exchange of the O^{-2} ions.

To the equilibrium [1] there corresponds an equilibrium constant $K = C_{O^{2-}} \cdot P_{CO_2}$ that Dubois (11) has found equal to 10^{-6}.

The solubility of CO_2 in carbonates has been measured

$$\frac{C_{O^{2-}}}{P_{CO_2}} = 10^{-1}$$

In these formulas the pressures are expressed in atmospheres and the concentrations of solutions in molarities.

A more recent work of Busson and Palons (12) on the potential at zero current of the oxygen electrode in the carbonates has made it possible to establish with precision the constant of equilibrium to be K = 6.

A solution of molten carbonates can be defined by the pO^{2-}, the negative logarithm of the concentration of ions O^{2-}.

The function of the oxygen electrode in the molten carbonates produces some O^{2-} ions.

$$O_2 + 4e \rightleftharpoons 2\ O^{2-}$$

In the vicinity of the oxygen electrode, the concentration of O^{2-} ions increases and this increase, inasmuch as it is not counter-balanced by diffusion, produces a polarization of the cell which can be called acidity polarization.

To bring CO_2 to the oxygen electrode, is to counter-balance the production of O^{2-} through the contribution of the acid part of the solvent, which as the effect of maintaining the pO^{2-} at a high value. This is a buffer effect. This effect may be visualized thrcugh Fig. 1. The diagram represents potentials of the oxygen and hydrogen electrodes as a function of pO_2^-. The straight lines AC and BD are parallel and of slope $\frac{RT}{2F}$. The potential at zero current is the thermodynamic cell potential equal to AB and CD. If the hydrogen electrode operates at $pO^{2-} = 0$ and the oxygen electrode at $pO^{2-}6$, the potential of the cell is reduced to EB and the overpotential of acidity polarization is AE-A 600°. This overpotential is at the maximum of approximately 83 mV x 6 = 500 mV.

The pO^{2-} of the electrolyte of the cell can also vary at the fuel electrode through a contribution of CO_2 or of other products or where the pressure of CO_2 in the atmosphere rises abcve the electrolyte.

It is thus very important, in order to obtain a cell which operates in all circumstances, to maintain the pO^{2-} of the electrolyte constant on all parts of the cell.

Through association with the phenomena observed in aqueous solutions, we shall use weak acid systems relative to the solvent.

The orthosilicate metasilicate system fits very well:

$$_2Si\ O_4^{3-} \rightleftharpoons {}_2Si\ O_3^{2-} + O^{2-}$$

The same applies to other salts exchanging the O^{2-} ion.

Our research has brought us to a much more simple and industrially profitable system. It is the water system.

3. WATER IN MOLTEN CARBONATES

Water has the properties of a weak acid in molten carbonates.

The properties of water may be summarized by the two equilibrium reactions:

$$2OH^- + CO_2 \rightleftharpoons H_2O + CO_3^{2-} \qquad [3]$$

$$2OH^- \rightleftharpoons H_2O + O^{2-} \qquad [4]$$

The constants K_A and K_B are arranged to correspond respectively to these equilibria according to the relations:

$$\frac{P_{CO_2} \cdot C^2_{OH^-}}{P_{H_2O}} = K_A \qquad [5]$$

$$\frac{P_{H_2O} \cdot C_{O^{2-}}}{C^2_{OH^-}} = K_B \qquad [6]$$

These relations imply that the chemical potential of the solvent is constant, that is

$$C_{OH^-} \ll C_{CO_3^{2-}} \qquad [7]$$

In an acid environment, the pressure of CO_2 determines the equilibrium potential, K being the equilibrium constant [1].

$$E = E_o + \frac{RT}{4F} \log P_{O_2} + \frac{RT}{2F} \log P_{CO_2} + \frac{RT}{2F} pK \qquad [8]$$

In the presence of a water system, the potential of the oxygen electrode is given by the relation:

$$E = E_o + \frac{RT}{4F} \log P_{O_2} + \frac{RT}{2F} \log P_{H_2O} - \frac{RT}{F} \log C_{OH^-} + \frac{RT}{2F}\ p\,K_B \qquad [9]$$

By varing the OH^- concentration and the partial pressures of water and oxygen in the atmosphere in equilibrium with the molten carbonates, we have shown that $p K_B$ is close to 5. We conclude that $p K_A = p K - p'K_B = 1.5$ (by taking the reference states of gases at a pressure of one atmosphere).

There is a constant contribution of water vapor at the hydrogen electrode. On the oxygen electrode the contribution of water vapor has the effect of maintaining the basic electrolyte at a determined $p O^{2-}$ (below 6.2).

4. APPLICATION TO FUEL CELLS

The properties of a water system in carbonates have important consequences on the functioning of cells. They allow a reduction of the acidity polarization as does the carbon dioxide fed with oxygen. But as it was demonstrated by Hart (13), the use of carbon dioxide constitutes a heavy burden from an industrial point of view whereas the use of water would be much easier and cheaper.

In comparing the properties of similar elements of a cell fed on oxygen without any addition, with carbon dioxide and with water vapor, we were able to realize that the performances due to the addition of water are the best (Fig. 2).

The polarization is not only diminished by the contribution of water vapor (potential of zero current near 1 volt instead of 0.7 volt) but the current at the same cell potential is very superior to that obtained with the use of CO_2. This phenomenon seems to be comparable with the increase of fluidness of molten carbonates in the presence of water.

Finally, the action of water as a weak acid allows the use of fuel gas containing carbon dioxide with an hydrogen electrode of porous material. Indeed, let us consider a cell functioning with a water pressure of 0.3 atm, in an hydroxyl ion environment.

Equation [5] gives 0.015 atm as a value of $p CO_2$ in equilibrium. Consequently, any fuel gas containing a weaker carbon dioxide partial pressure may be used without the risk of modifying the $p O^{2-}$ of the electrolyte.

5. MAKING OF PROTOTYPES

The preceding studies have first lead to tests on elements of cells of a few watts.

We are presently constructing several prototypes of a power close to 1 kw which vary in their geometric conception (vertical or horizontal electrodes) but have the same electrochemical conception.

The materials used are steel (25% Cr, 20% Ni) and dense alumina for the containers, thin sheets of palladium (50 microns) of an alloy of 24% silver-76% palladium for the fuel electrodes and silver and porous steel for the air electrodes. The electrolyte is a ternary eutectic of lithium, sodium and potassium carbonates functioning at 600°C. The fuel is a gas obtained through the reforming of natural gas and the oxidant air contains from 10 to 30% of water vapor.

The gases are fed at a pressure slightly higher than atmospheric.

Figures 3 and 4 are photographs of prototype elements with horizontal and vertical electrodes.

Naturally, these prototypes must be placed in an oven because their dimensions are too small to be autothermic.

The prototypes will give rise to a technico-economical study aimed at searching for the place of this system in the industrial production of electrical energy.

ACKNOWLEDGEMENT

The results which we presented are based on the work of a group of researchers which includes, besides the authors:

Mmes: Busson

Jacquin

Palons

Messrs: Barde

Dubois

Heuze

Legrauche

Bibliography

1. W. Ostwald
Z. Elektrochem. 1894 1 122

2. E. Baur
Z. Elektrochem. 1921, 27 194-199

3. O. K. Davtyan
Direct Conversion of Chemical Energy of Fuel into Electrical Energy, Moscow, 1947.

4. G. H. J. Broers, J. A. A. Ketelaar
(Young) Fuel Cells. Reinhold, New York 1960.

5. E. Gorin, H. L. Recht
Chem. Eng. Progress, 1959, 55 51-58

6. E. Justi, F. H. Spengler
U. S. Patent No. 2,830,109 1958.

7. A. B. Hart
Private communication. 1963.

8. A. Salvadori
Rev. Just. Franc. Petrole 1964, 19 144.

9. H. Lux
Z. Elektrochem. 1939 45 303.

10. H. Flood, T. Förland
Acta. Chem. Scand. 1947, 1 592-604, 79-798.

11. J. Dubois
Thesis, Paris 1964

12. R. Buvet, N. Busson, J. Millet, S. Palons
C.R. Sc. Acad in preparation

13. A. B. Hart, J. H. Powell, C. H. DeWhalley
Third Intern. Battery Symp. Bournemouth 1962.

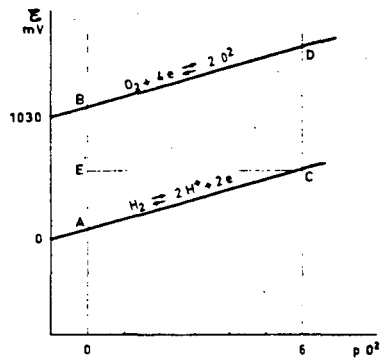

Fig.1 THERMODYNAMIC EQUILIBRIUM DIAGRAM IN MOLTEN CARBONATES

Fig.2 V/I CURVE OF A FUEL CELL H_2/O_2 IN MOLTEN CARBONATES

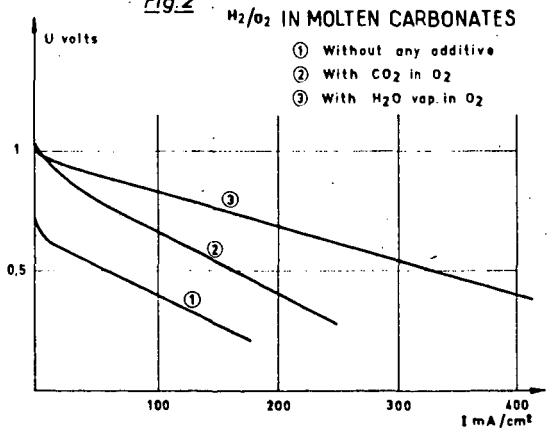

Fig. 3.-HORIZONTAL ELECTRODES PROTOTYPE

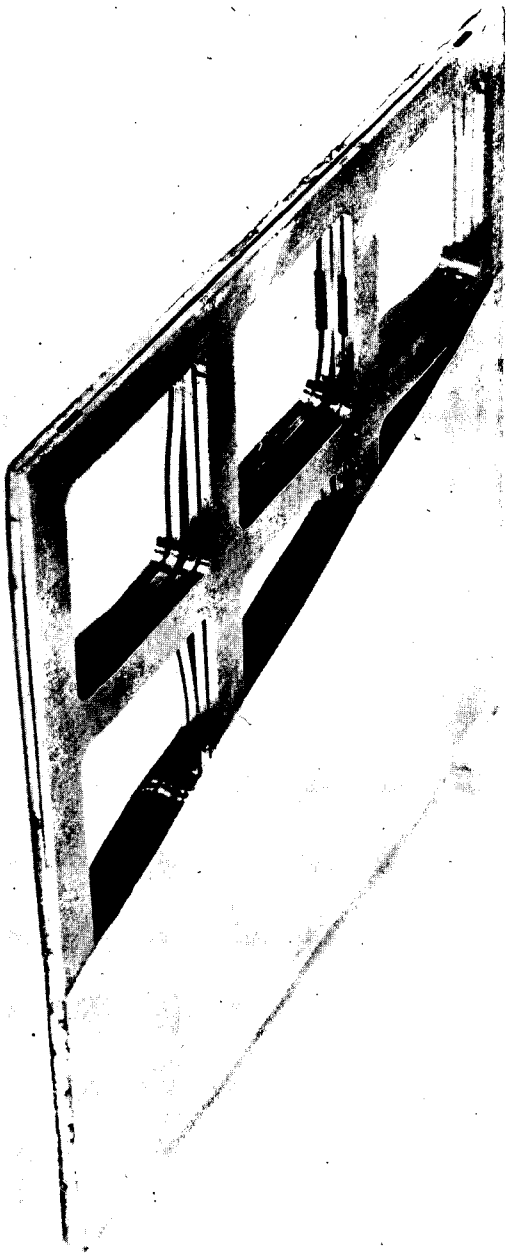

Fig. 4.-VERTICAL ELECTRODE PROTOTYPE

OPERATIONAL CHARACTERISTICS OF HIGH-TEMPERATURE FUEL CELLS

B. S. Baker
L. G. Marianowski
J. Zimmer
G. Price

Institute of Gas Technology
Chicago, Illinois

INTRODUCTION

High temperature fuel cells have not received as much attention in the United States as their low temperature counterparts. As a result, from the viewpoint of a total system, the high temperature fuel cell is far less developed. The reason for this is simple. High temperature fuel cells are not as attractive for most military and space applications as low temperature fuel cells.

In Europe, especially in France, England, and Holland, a much larger portion of fuel cell development is directed toward commercial applications. The high temperature fuel cell is being more extensively investigated because it has a much more attractive economic potential. At the Institute of Gas Technology, interest in fuel cells is very definitely directed toward commercial goals. Emphasis on both high and low temperature fuel cell research is aimed at the development of inexpensive systems. This paper on the High-Temperature Molten Carbonate Fuel Cell reports on work which has been in progress at IGT since 1960. Details of much of this work already appear in the literature.[1-5]

The principle advantages of the high temperature fuel cell are the elimination of expensive electrode catalysts from the system and the ability to operate with a variety of fuels and unpurified air.

However, raising the temperature to a typical figure of 900°F or above in a fuel cell which employs a water electrolyte would require a relatively high pressure system. This would be undesirable from both a technical as well as an economic viewpoint.

To avoid this difficulty, two solutions are possible. The electrolyte can be either 1) a salt that melts at a high temperature and which has a very low vapor pressure at this high temperature, or 2) an ion conducting solid used at still higher temperature (about 2000°F). Operating at this latter very high temperature requires the use of noble metals for stability rather than for catalytic purposes. This we want to avoid. For this reason, the fuel cell work at IGT is focused on the use of a molten salt electrolyte operating in the range of 900 to 1300°F.

The IGT molten carbonate fuel cell is patterned after the concept of Broers.[6] In this system, a eutectic mixture of two or three alkali metal carbonates is mixed with an inert material such as a metal oxide. This forms a ceramic tile-like structure at room temperatures which becomes a non-Newtonian fluid or paste at the operating temperature.

In the IGT system, the paste electrolyte is held between a silver film cathode about 10 microns thick and a porous fiber nickel anode. The cathode is supported by a stainless steel grid. A complete fuel cell element of this type with an active area of one square foot is shown in Figure 1. These elements can be stacked in various ways to produce batteries of any voltage desired.

At the present time, the fuel for the IGT cell is reformed natural gas which is prepared by steam reforming in the presence of commercially available catalysts.

PERFORMANCE CHARACTERISTICS

Performance characteristics of high temperature molten carbonate fuel cells are usually inferior to those obtained in low temperature systems. Since the elevated temperature should improve reaction rate kinetics, an explanation for the poorer performance must be sought in terms of electrode properties and mass transfer processes. Low temperature fuel cell electrodes can be prepared with very high real to geometric surface areas. This may be achieved using high surface area carbons, nickels and precious metal blacks. In the high temperature cells, such active surfaces are unstable. They tend to sinter to form relatively low surface area electrodes.

A second factor affecting performance levels is the nature of the gas-liquid-solid interface at the electrode. In low temperature cells, it has been possible to achieve a relatively effective interface in terms of mass transfer properties, for example, a thin film of electrolyte on the bulk of the electrode, using either a double porosity electrode structure, waterproofing, ion exchange membranes, or matrices. In molten carbonate fuel cells, there has always been evidence of macroscopic flooding on electrodes which have been in operation for some time – e.g. over several hundred hours.

Broers[7] and we at IGT[8] have observed evidence for diffusion control in the liquid film for this type cell. Quantitative measurements in terms of film theory have not been possible because of lack of information on the solubility of hydrogen, oxygen, carbon monoxide, carbon dioxide, and water vapor in carbonate melts. Nevertheless, more effective use of electrode surface is clearly warranted.

To see if improved interfacial characteristics could be achieved, experiments at IGT have been conducted with a variety of matrix materials with different surface areas and particle sizes. The use of high surface area metal oxides has led to the development of cells which show no evidence of macroscopic flooding after prolonged operation. They have yielded performance characteristics of the type shown in Figure 2. Earlier performance levels are also shown in this Figure for comparison.

All tests at IGT are performed on hot pressed electrolyte discs. Those discs are prepared by pressing electrolyte powders at 8000 lbs/in^2 and 950°F. To prevent extrusion of the electrolyte between sections of the dies, aluminum discs are inserted in the pressing unit. The discs are designed to take advantage of the difference in coefficient of thermal expansion between the steel and aluminum to insure a seal tighter than that which could be achieved by mechanical tolerances alone. A thin palladium-silver foil is placed between the electrolyte powders and the aluminum to facillitate release of the electrolyte discs from the die assembly.

A series of experiments on different density fiber nickel electrodes shown in Figure 3, have yielded polarization characteristics shown in Figure 4. Higher density electrodes, such as 43 and 62 percent nickel, show a high level of polarization and the appearance of limiting currents. Electrodes having a density of 15, 20, and 33 percent yield equivalent performance within experimental error. These data were taken with cells having an electrode area of three square centimeters. Results have since been duplicated with cells having surface areas of 32 square centimeters. Cell lifetimes of 850 hours at the indicated performance level is the best achieved so far. These cells are still being tested. From these results, it appears that further optimization of electrolyte and electrodes may yield even better performance levels, placing a whole new perspective on the use of this type fuel cell system.

In the next sections the impact of these new polarization curves on heat transfer and overall system efficiency will be outlined.

HEAT TRANSFER

Considering the voltage characteristic shown in Figure 2, it is apparent that the maximum voltage-current performance is desired. The volume, weight, and cost of the fuel cell system is decreased. It is of interest, however, to examine the engineering implications especially as to how heat transfer is affected by the different voltage-current characteristics.

At IGT, we have considered the three dimensional heat transfer problem in a fuel cell battery.[8] Figure 5, is a simplified diagram of the fuel cell. Heat transfer in such a cell depends mainly on such factors as battery dimensions, the voltage-current characteristic, the degree of fuel and air conversion, and the physical properties of the materials used to construct the cell. The complete problem is too broad to discuss here. However, in Figure 6 the temperature distribution within such a fuel cell is shown for the voltage-current characteristics of Figure 2. In all cases, the operating cell potential would be 800 millivolts.

It can be seen that the maximum temperature rise from the center of the battery to the assumed isothermal walls (in the case of the 1963 voltage-current characteristic) is only about 7°F. However, when the performance of the cell is improved (Best 1965), the maximum temperature rise increases to about 480°F. In practice, of course, the walls of the fuel cell would not be isothermal. Nevertheless, one can deduce from the experimental data that the low performance fuel cell would require the addition of heat to keep it at operating temperature. On the other hand, it would be necessary to remove heat from the system having the high performance characteristic.

This has been partly verified by constructing the 32-cell stack of elements shown in Figure 7. The performance of this battery was based on the 1963 characteristic. As expected, it was necessary to add heat to the system. The improved performance characteristics suggests another possibility. This is to incorporate reforming catalysts near the electrodes so that waste heat from the fuel cell can be used to sustain the endothermic reforming reaction. At the same time, this would provide a means for cooling the cell.

A further variation in cell performance is seen in Figure 8. Here the effect of conversion on temperature distribution is shown. In the direction of air flow (Z), it can be seen that as the conversion of oxygen is increased, two things happen. The first effect is a rise in the maximum temperature in the battery. This would be expected since less gas is available to remove heat. The second effect is somewhat less expected. The flow of gas through the cell causes a temperature distribution in the cell that is not symmetrical. Physically, this situation can be interpreted as follows: At a high rate of gas flow, heat is being removed from the section of the battery near the gas inlet and is being redistributed to the section near the outlet. In the case of a low rate of gas flow, complete symmetry in the Z direction can be expected.

The purpose of these heat transfer considerations was to determine some feeling for the size and shape of fuel cells which will be built at IGT within the next few years. More important, however, it permits assumptions on the nature of heat inputs in the system. It also establishes what the overall efficiency of such a system might be.

EFFICIENCY

In the high temperature molten carbonate fuel cell, a typical operating voltage that is compatable with the materials from which the cell is built is about 0.7 to 0.8 volts. From the previous discussion, we have seen that cells operating at this voltage level can be thermally self-sustaining. Thus, the overall efficiency of the system depends on the efficiencies of fuel and air conversion, and the reforming requirements. Air conversion is especially important in high temperature fuel cells where the heat content of the oxidant is substantial. In Figure 9, the overall efficiency of an external reformer-molten carbonate fuel cell is shown as a function of the efficiency of fuel and oxygen conversion. The oxidant is air.

For purposes of this example, it was assumed that 1) the external reformer was 60 percent efficient and 2) that no gas-to-gas heat exchange is possible but heat exchange from gas-to-boiling liquid is feasible. These assumptions are based on the need for unreasonably large gas-to-gas heat exchangers especially for low oxygen conversion. While such heat exchangers could be built, they would cost more than the fuel cell itself. However, from a practical viewpoint, steam generation is more feasible, and heat recovery for this purpose has been assumed.

It can be seen that at low oxygen conversion, the overall efficiency is not greatly affected by the efficiency of fuel conversion. It does become more important as the efficiency of the oxygen conversion improves. The reason for this is that when the fuel conversion is high, but the oxygen conversion is low, it is necessary to maintain a separate fuel supply to preheat the air. At low fuel conversion, the air can be preheated by burning spent fuel. The maximum efficiency for the external reforming system without gas-to-gas heat exchange will probably be between 35 and 39 percent.

In Figure 10, a similar analysis is made for an internal reforming system. In this case, the heat for the reformer is supplied by the polarization and entropic heats from the fuel cell. Again, the concept of gas-to-gas heat exchange for preheating feeds has been assumed to be impractical. The overall efficiency for this system is somewhat higher as might be expected. A figure of about 40-43 percent seems to be possible with present technology.

Finally, it should be noted that oxygen conversions higher than 60 percent may be possible in the future. In such a case, the efficiency of the overall system will be even higher. However, it is not likely to be greater than 50 percent unless low cost gas-to-gas heat exchangers can be developed.

ECONOMICS

The only real basis for economic evaluation of fuel cells at the present time is the cost of materials. Lack of knowledge and/or experience with manufacturing components and systems prohibits any more extensive analysis. To a certain extent, storage battery hardware can serve as a guide but this breaks down when confronted with a new component like the paste electrolyte in the high temperature fuel cell.

In an early publication[3] we estimated the material costs of molten carbonate fuel cells and related these costs to the performance of IGT cells. Applying a similar method, we have once again presented our performance data in this fashion, (Fig. 11). Material costs are essentially the same as in the earlier publication. It can be readily seen that progress has been made which gives rise to considerable optimism for the economics of this type fuel cell. Typical performance characteristics indicate that material costs of about $45 per kilowatt can be achieved and the best performance data reduces that figure to less than $20 per kilowatt.

With respect to further improvement, we might look to using copper in place of silver at the cathode and to reducing the amount of stainless steel used for the current collector in the cell. Lifetime remains the big factor in the case of the molten carbonate fuel cell. Only more intensive experimental work can find a solution to this problem.

ACKNOWLEDGMENT

The high-temperature fuel cell research program at IGT is sponsored by the American Gas Association under its PAR (Promotion-Advertising-Research) Plan. The authors wish to thank the A.G.A. for allowing results of the program to be discussed in this paper.

REFERENCES CITED

1. Shultz, E. B., Jr., Vorres, K. S., Marianowski, L. G. and Linden, H. R., "High Temperature Methane Fuel Cell," in Young, G. J. Ed., "Fuel Cells," Vol. 2, 24-36. New York: Reinhold Publishing Corp., 1963.

2. Marianowski, L. G., Meek, J., Shultz, E. B., Jr. and Baker, B. S., "New Concepts in High Temperature Hydrocarbon Fuel Cells," Power Sources Conference 17, 72-75 (1963).

3. Baker, B. S., Marianowski, L. G., Meek, J. and Linden, H. R., "Further Developments in High Temperature Natural Gas Fuel Cells," Advances in Chemistry Series No. 47, 247-261. Washington, D. C.: American Chemical Society, 1965.

4. Baker, B. S., Marianowski, L. G. and Zimmer, J., "Design and Construction of a Molten Carbonate Fuel Cell Battery System," Paper presented at Delegation Generale a la Recherche Scientifique et Technique Symposium on Conversion des Energies, Paris, France, February 1965.

5. Baker, B. S., and Marianowski, L. G. "Operating Characteristics of an Economical High Temperature Fuel Cell" paper presented at the International Conference on Energetics, ASME meeting, Rochester, New York, Aug. 18-20, 1965.

6. Broers, G. H. J., "High Temperature Fuel Cells," Ph.D Dissertation, University of Amsterdam, The Netherlands, 1958.

7. Broers, G.H.J., and Schenke, M., "High Temperature Galvanic Fuel Cells," Final Report. File No. DA-91-591-EUC-1701.

8. Baker, B. S., IGT unpublished data.

9. Gidaspow, D. and Baker, B. S., "Heat Transfer in a Fuel Cell Battery," Paper presented at the Eighth National Heat Transfer Conference of the ASME and A.I.Ch.E., Los Angeles, Calif., August 8-11, 1965.

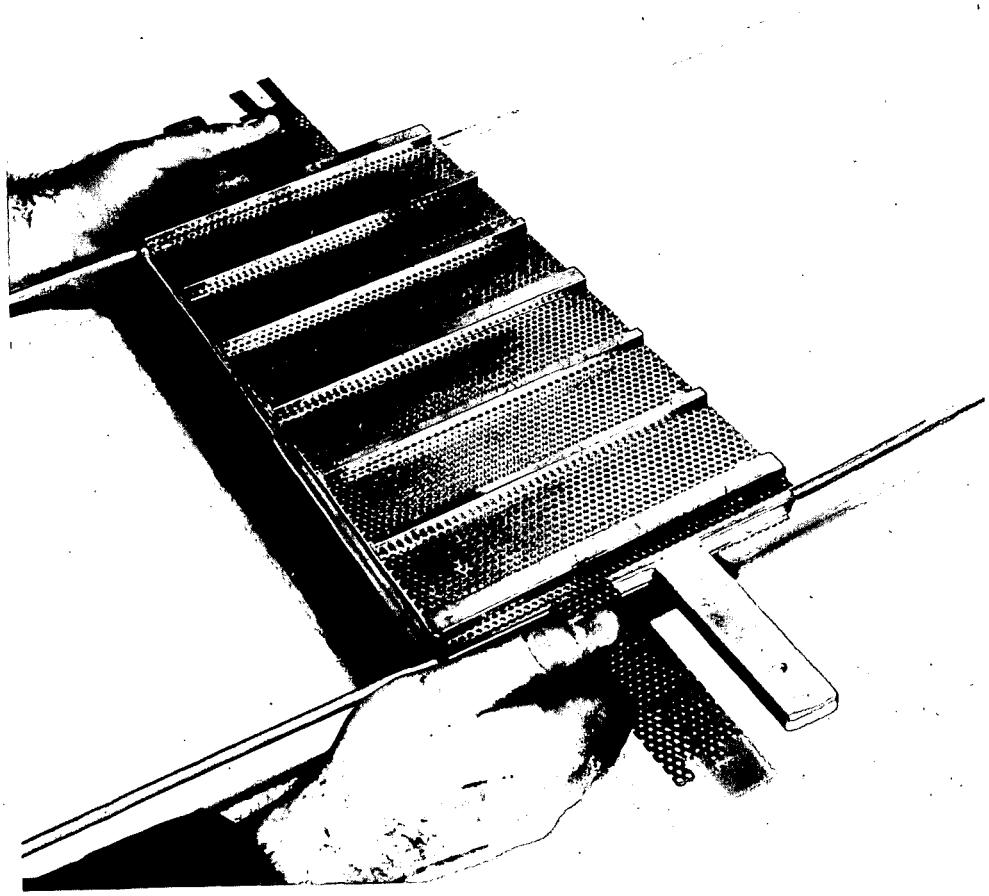

Fig. 1.-SINGLE ELEMENT OF IGT HIGH-TEMPERATURE FUEL CELL BATTERY

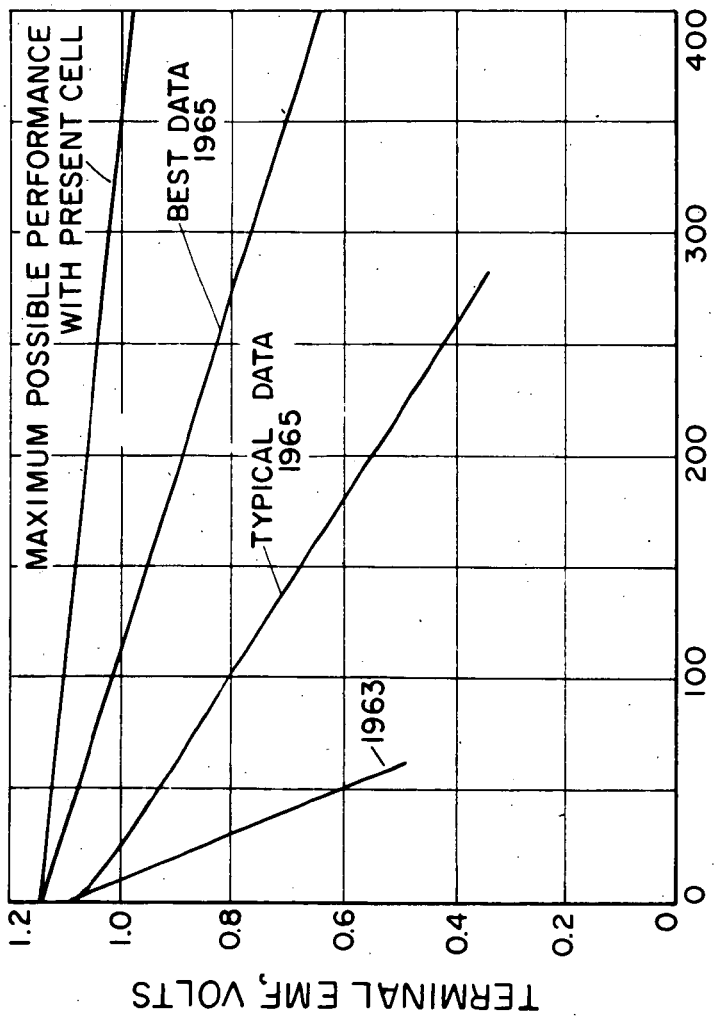

Fig. 2.-PERFORMANCE CHARACTERISTICS OF IGT MOLTEN CARBONATE FUEL CELL

15 %

20 %

33 %

43 %

62 %

Fig. 3.-DIFFERENT DENSITY FIBER NICKEL ELECTRODES USED IN IGT MOLTEN CARBONATE FUEL CELL (120X)

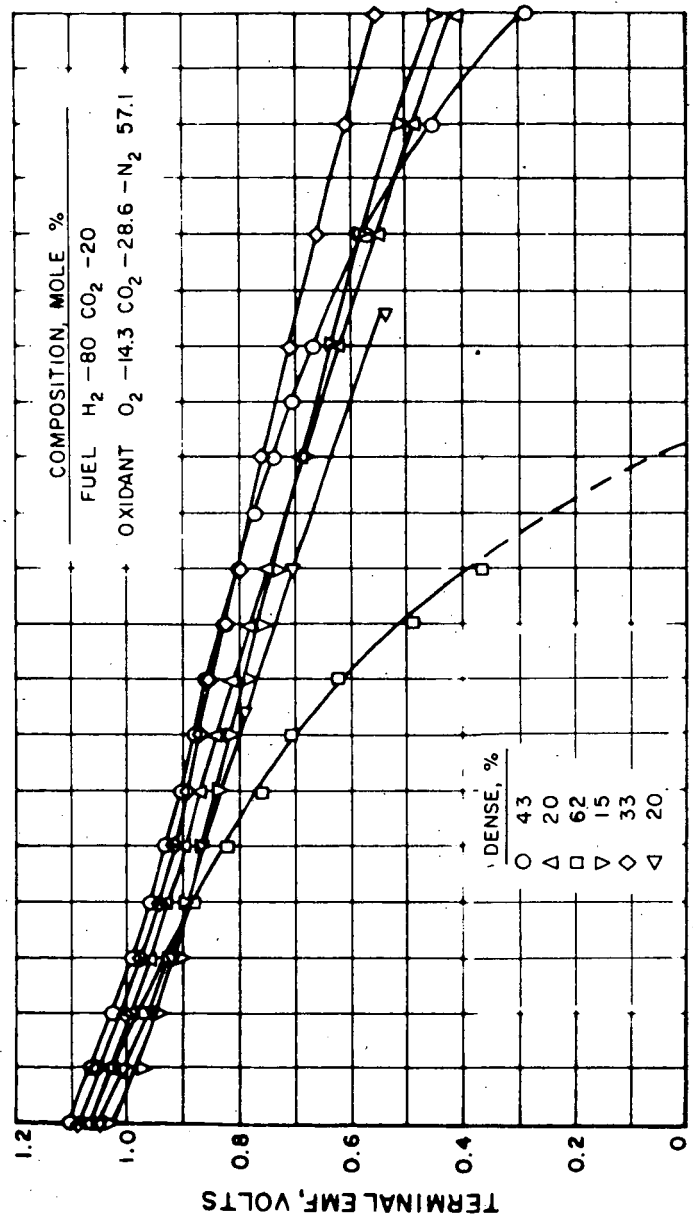

Fig. 4.-COMPARISON OF PERFORMANCE CHARACTERISTICS OF DIFFERENT DENSITY FIBER NICKEL ELECTRODES AFTER SEVERAL HUNDRED HOURS OPERATION

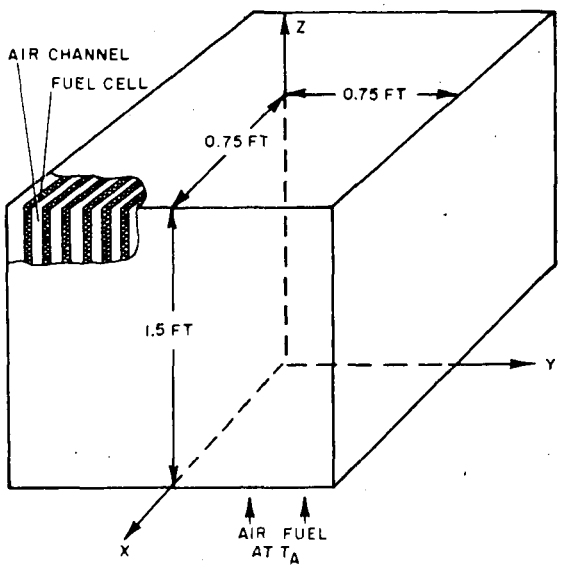

Fig. 5.-MODEL OF FUEL CELL BATTERY USED IN HEAT TRANSFER ANALYSIS

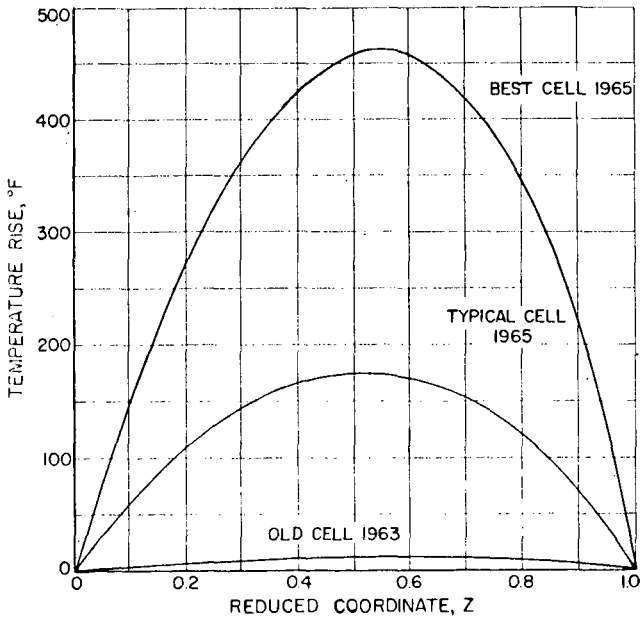

Fig. 6.-EFFECT OF POLARIZATION CHARACTERISTICS ON TEMPERATURE DISTRIBUTION. DIRECTION OF GAS FLOW.

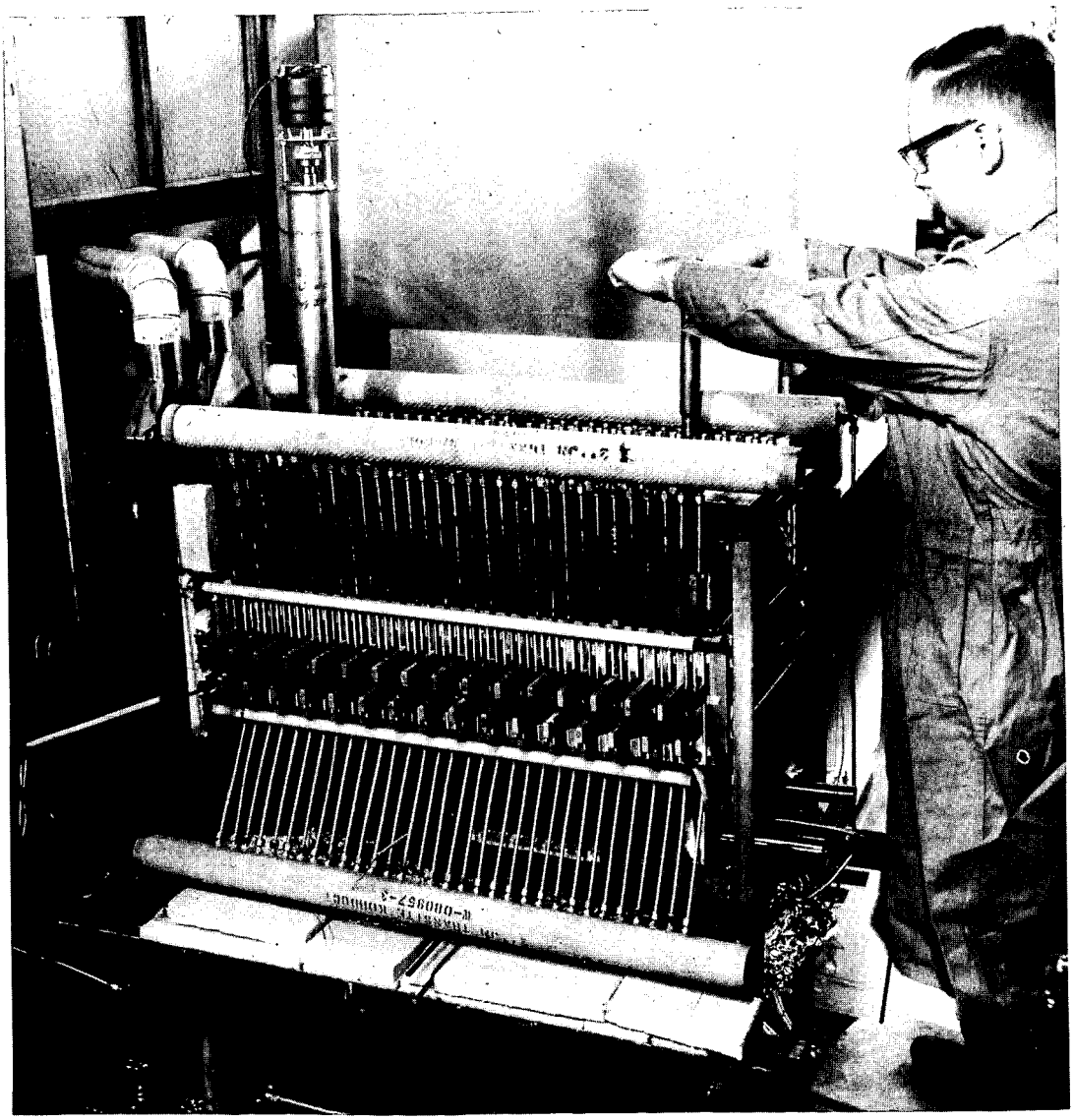

Fig. 7.-IGT 32-CELL HIGH-TEMPERATURE BATTERY

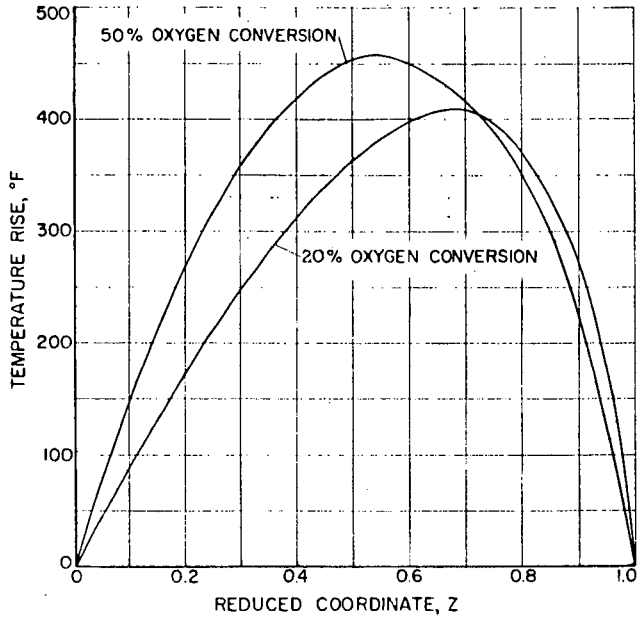

Fig. 8.-EFFECT OF AIR CONVERSION AT HIGH PERFORMANCE LEVELS ON TEMPERATURE DISTRIBUTION IN DIRECTION OF GAS FLOW

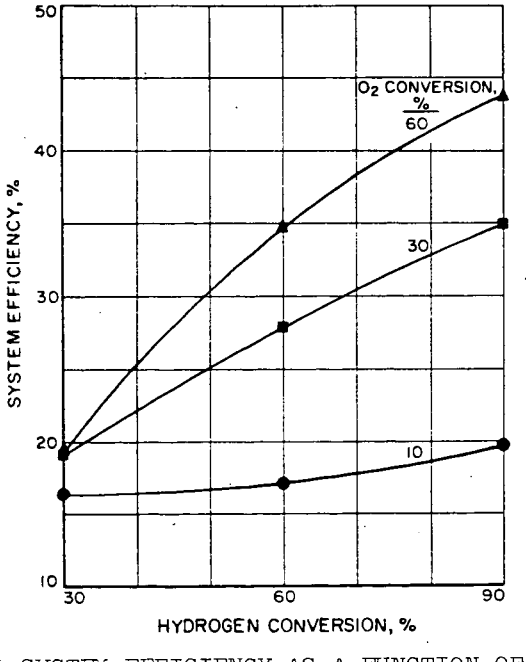

Fig. 9.-OVERALL SYSTEM EFFICIENCY AS A FUNCTION OF FUEL AND OXIDANT CONVERSION WITH AN EXTERNAL REFORMER

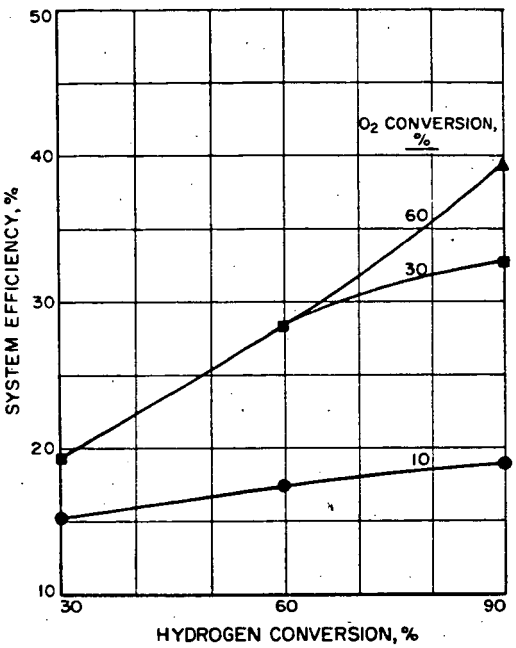

Fig. 10.-OVERALL SYSTEM EFFICIENCY AS A FUNCTION OF FUEL AND OXIDANT CONVERSION WITH AN INTERNAL REFORMER

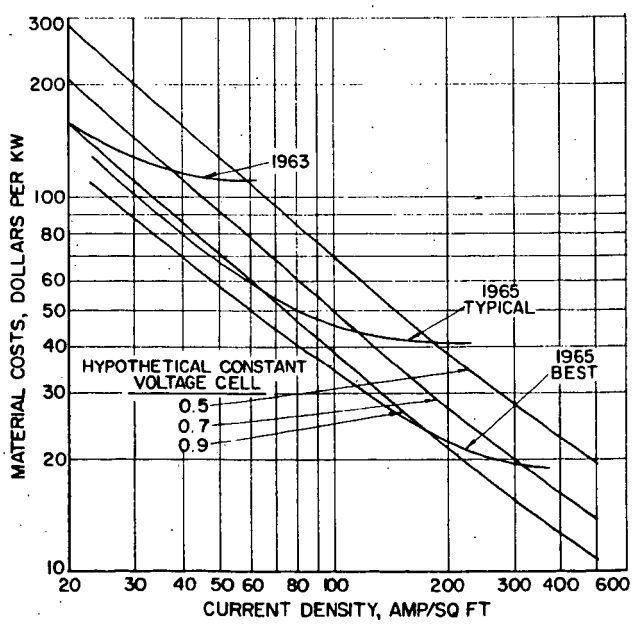

Fig. 11.-ECONOMICS OF MATERIALS USED IN HIGH TEMPERATURE MOLTEN CARBONATE FUEL CELLS